Technical University of Denmark

DTU

Anchorage of ribbed reinforcing bars

Andreasen, Bent Steen; Nielsen, Mogens Peter

Publication date:
1989

Document Version
Publisher's PDF, also known as Version of record

Link back to DTU Orbit

DTU Library
Technical Information Center of Denmark

Anchorage of Ribbed Reinforcing Bars

Bent Steen Andreasen

Anchorage of Ribbed Reinforcing Bars

Bent Steen Andreasen
Department of Structural Engineering
Technical University of Denmark
DK - 2800 Lyngby, Denmark

November, 1988

Preface

This report is prepared as a partial fulfilment of the requirements for obtaining the degree of "teknisk licentiat".

This thesis was carried out at the Department of Structural Engineering, Technical University of Denmark under the supervision of Professor, Dr.techn. M. P. Nielsen.

In the present report, theoretical considerations and treatment of tests from the literature are included. Tests carried out with connection to the project are to be found in another report.

I express my gratitude to all the persons, specially at the Department, who contributed to the completion of the Ph.D. study and this report.

Abstract

Anchorage of ribbed reinforcing bars is treated theoretically. The obtained expressions for the load carrying capacity are compared to test results reported in the literature.

The theory of plasticity is used as basis for the theoretical calculations. The material properties of the concrete do not fulfill the conditions of the theory and therefore modification factors are introduced. These factors are known as effectiveness factors. The effectiveness factor for tension is examined in particular.

The anchorage failure is divided into three parts: The local failure immediately around the reinforcing bar, the failure in the surroundings for one reinforcing bar, and the complete failure which includes all the bars in the section. The three parts are separated in the calculations.

The local failure is investigated by upper and lower bound calculations and correspondence between the load carrying capacities are obtained. The failure in the surroundings in an axisymmetrical specimen is also investigated using upper and lower bound calculations. Coinciding values of the load carrying capacity are obtained for part of the actual interval. From these calculations, it appears that upper bound solutions can be determined with satisfactory accuracy by using a failure mechanism, where the surrounding concrete is displaced away from the reinforcement as rigid bodies with a constant velocity. Upper bound solutions for the load carrying capacity are therefore in principle simple to determine.

Expressions based on upper bound calculations for anchorage at supports with one and more than one layer of reinforcement and lap splices are developed. The load carrying capacity from these expressions is compared to test results. In the light of the comparison with tests, simple expressions for calculations in practice are expounded for anchorage at supports with one layer of reinforcement and for lap splices.

ii

Resume

Forankring af forkammet armering er behandlet teoretisk. De fremkomne udtryk for bæreevnen er sammenlignet med forsøgsresultater refereret i litteraturen.

Som grundlag for de teoretiske beregninger er plasticitetsteorien benyttet. Da betons materialemæssige egenskaber ikke opfylder forudsætningerne til plasticitetsteorien indføres faktorer til korrektion af de fejl der begås. Disse faktorer benævnes effektivitetsfaktorer. Effektivitetsfaktoren for træk er undersøgt specielt.

Forankringsbruddet opdeles i tre dele: Det lokale brud umiddelbart omkring jernet, brud i omgivelserne fra et enkelt jern og det totale brud i hele tværsnittet. De tre dele adskilles fra hinanden rent beregningsmæssigt.

Ved øvre- og nedreværdiberegninger er det lokale brud undersøgt, og der er fundet sammenfaldende værdier for bæreevnen. Bruddet i omgivelserne af et rotationssymmetrisk legeme er ligeledes undersøgt ved øvre- og nedreværdiberegninger. Sammenfaldende værdier for bæreevnen er fundet for en del af det aktuelle interval. Det viser sig ved disse beregninger, at øvreværdier med god nøjagtighed kan bestemmes ved at benytte en brudmekanisme, hvor den omgivende beton flyttes væk fra armeringen som stive dellegemer med konstant hastighed. Øvreværdier for bæreevnen er derfor principielt simple at bestemme.

Udtryk, baseret på øvreværdiberegninger, for forankring ved vederlag af et og flere lag armering samt for overlapningsstød er opstillet. Disse udtryk er sammenlignet med forsøgsresultater. I tilfældet forankring ved vederlag af et lag armering og ved overlapningsstød er der på baggrund af forsøgssammenligningen opstillet simple udtryk til brug for beregninger i praksis.

Contents

List of Figures

xi

List of Tables

Notations

The most commenly used symbols are listed below. Exceptions from the list can appear, but this will then be mentioned in the text in connection to the actual symbol.

a	Distance between ribs.
a'	Distance between mid of rib to the middle of the next rib.
b	Width of beam section.
b_{eff}	Effective width of section.
b'	Width of beam for a single bar.
c	Cohesion of the concrete or concrete cover.
d	Diameter of the reinforcement.
d_s	Diameter of transverse/surrounding reinforcement (stirrups or spirals).
e	Number of end failure contributions ($e \in \{0, 1, 2\}$).
f_c	Uniaxial cylindrical compressive strength of concrete.
f_{cc}	Compressive strength of concrete measured on cubes.
f_t	Uniaxial tensile strength of concrete.
f_{ts}	Splitting tensile strength of concrete.
f_y	Yield strength of reinforcement.
f_{ys}	Yield strength of transverse/surrounding reinforcement.
h	Total depth of beam section.
h_d	Depth of ribs on the reinforcement.
k	Material constant, $k = 4$ for concrete.
ℓ, l	Anchorage length, support length, lap length.
n_ℓ	Number of layers of reinforcement.
n_s	Number of stirrups or spirals over the anchorage length.
n_{ss}	Number of stirrups or spirals crossed by the horizontal yield line in the plate mechanism.
n_m	Number of main bars in a section.
n_{sp}	Number of lap splices in a section.
r	Reaction stress, $r = \frac{R}{b\ell}$.
r_i	Distance.

r_1, r_2, r_3	Distance.
$r_{\ell 1}, r_{\ell 2}, r_{\ell 3}$	Distance.
s	Vertical distance from the bottom of the beam to the center of the reinforcement.
s_ℓ	Vertical distance between two layers of reinforcement measured from the center to the center.
s_t	Vertical distance from the top of the beam to the center of reinforcement placed in the top.
t	Horizontal clear distance between bars in a lap splice.
u	Dimension of ribs on the reinforcement in the direction of the bar axis.
v	Increment in displacement (velocity).
v_c	Increment in displacement (velocity) of the concrete.
$v_{ci}, v_{c1}, v_{c2}, v_{c3}$	Increment in displacement (velocities).
v_s	Increment in displacement (velocity) of the reinforcement.
A	Area.
A_s	Cross sectional area of reinforcement.
A_{ss}	Cross sectional area of surrounding reinforcement.
C	Dimensionless internal work from the surroundings, $C = \frac{W_i}{\pi d l f_c}$.
C_T	Total dimensionless internal work in the case of more than one layer of reinforcement.
D	Dimensionless rib parameter, $D = \frac{h_d(d+h_d)}{2d(a+u)}$.
E_e	Special dimensionless end failure contribution.
F	Dimensionless rib parameter, $F = \frac{a}{a+u}\left(\frac{h_d}{d} + \frac{1}{2}\right)$.
R	Total support reaction, $R = rb\ell$.
T	Tensile force in a single bar, $T = \pi d\ell\tau$.
W_e	External work.
W_i	Internal work.
W_{ic}	Internal work from the concrete (yield lines).
W_{ei}	Internal work from the end surface.
W_{ir}	Internal work from the reaction.
W_{is}	Total internal work from the surroundings.
W_{it}	Internal work from transverse reinforcement (stirrups, spirals).

α	Direction of displacement relative to yield line.
β	Angle.
γ	Angle between bar axis and failure surface in front of ribs.
δ	Dimensionless parameter.
ϵ	Strain.
ζ	Anchorage factor.
κ	Dimensionless parameter.
κ_1, κ_2	Angles.
η	Dimensionless parameter.
θ	Angle.
λ	$\lambda = \nu - \rho(k-1)$.
λ_e	$\lambda_e = \nu - \rho_e(k-1)$.
μ	$\mu = \nu - \rho(k+1)$.
μ_e	$\mu_e = \nu - \rho_e(k+1)$.
ν	Effectiveness factor for compression.
ξ	Dimensionless parameter, ξs- horizontal cover.
ρ	Effectiveness factor for tension.
ρ_e	Effectiveness factor for tension in the end failure surface.
σ	Normal stress.
σ_n	Radial stress from the reinforcement.
σ_θ	Stress in the ring direction around a bar.
τ	Average shear stress along a reinforcing bar, $\tau = \frac{T}{\pi d\ell}$.
φ	Angle of friction for concrete, $\tan\varphi = \frac{k-1}{2\sqrt{k}} = \frac{3}{4}$.
χ	$1 - \frac{1}{2}\frac{d}{s}$.
ψ	Stirrup reinforcement degree, $\psi = \frac{A_{ss}f_{ys}n_s}{d\ell f_c}$.
ω	Angle.
Γ	$2n_{sp}\frac{d}{s} + (n_{sp}-1)\frac{t}{s}$.
Ω	$\frac{h}{s} - n_\ell\frac{d}{s}$.

Chapter 1

Introduction

To be able to utilize reinforced concrete for structures, a transfer of forces between the concrete and the reinforcement must be possible. If this transfer of forces is not possible, one of the two, the concrete or the reinforcement, must carry the applied load alone, which is probably impossible. Hence the anchorage of reinforcement in concrete has interested designers for as long as reinforced concrete has been used as a composite material for supporting constructions.

The anchorage of a reinforcing bar in concrete is the resistance which prevents the bar from being pulled out of the concrete. Bond or anchorage stresses develop between the bar surface and the surrounding concrete so that the stress in the bar is maximal at the loaded end and zero at the other end.

Anchorage will take place in different ways, depending mainly on the load level and the type of reinforcement. Anchorage is often divided into the following:

- adhesion resistance
- friction resistance
- mechanical resistance

The adhesion is a weak effect and is due to the chemical or micro-mechanical interlocking of the steel-concrete interface. The effect is negligble when talking about the load carrying capacity because large displacements occur before failure.

1

The friction resistance appears as a result of the small indentations, the surface roughness, in the steel appearing in the production. When the reinforcement moves at failure, the surroundings offer resistance and friction forces arise at the surface of the reinforcement. However, compared to mechanical resistance, the friction is negligible.

Mechanical resistance is obtained as a result of deformations or ribs on the reinforcement. The deformations hold on to the concrete, by which the failure appears between the concrete holding on to the reinforcement and the rest of the concrete. This type of failure is satisfactory because the failure occurs in the weaker of the two materials, and the interface between them does not yield any weakening. In this report only the mechanical resistance is considered. The failure in the interface between steel and concrete is not taken into account; only failure between concrete and concrete is included. Consequently the reinforcement is assumed to be deformed reinforcement.

The reinforcement is here denoted as deformed bars or ribbed bars. In both cases it is the same type of reinforcement. The deformations or ribs are not appeared by cold working.

Many parameters influence the anchorage strength. Hence it is very difficult to treat the problem theoretically, and it is even more difficult to develop a simple method for calculations in practice, which include the influence from the various parameters with satisfactory accuracy. However, anchorage theories have been developed over many years. The most important theory is certainly the one presented by Tepfers [73.1] for lap splices with deformed reinforcing bars. Some have taken the consequences of the complicated conditions and have developed empirical expressions based on test results. Anchorage problems have also been dealt with numerically by means of finite element calculations. Regardless of the way in which the anchorage problem is solved, the result strongly depends on the basic assumptions. Nevertheless two methods with different assumptions can yield almost the same result. Unfortunately no workable rational method, which can be used to treat various types of anchorage problems exists. However, Hess [84.2] has started the development of such a theory, where the theory of plasticity has been used as foundation for the calculations. The main ideas evolved

by Hess will be used in this report.

In the literature many results of anchorage tests are reported. The test methods vary from one test series to another, so it is difficult to compare the results directly. However, there is general agreement that the anchorage strength, expressed by the shear stress along the surface of the reinforcement, primarily depends on the type of reinforcement and the resistance from the surroundings. For increasing rib height and decreasing distance between the ribs, the strength increases, other things being equal. The resistance from the surroundings depends mainly on the concrete strength, the concrete cover, the diameter of the reinforcement, the anchorage length, lateral pressure on the concrete, and possible surrounding reinforcement. The stronger the surroundings are, the stronger the strength of the anchorage will be, all other things being equal.

The failure in the concrete at an anchorage of ribbed reinforcing bars is normally accompanied by the development of cracks and splitting of the concrete. The cracks often appear rather close to the failure load, but it is possible to increase the load even after cracks have developed. The final failure can be very sudden and violent.

In this report the anchorage of deformed reinforcing bars is treated theoretically by means of the theory of plasticity. The concrete does not satisfy the conditions of the theory of plasticity; hence modification factors on the concrete strengths are introduced. The factors are multiplied by the uniaxial concrete strengths and are usually named effectiveness factors. The product between an effectiveness factor and the respective uniaxial strength is a measure of the effective stress occurring in the actual section at failure.

The anchorage failure is divided into three parts:

- the local failure

- failure mechanisms

- complete failure mechanism.

The three types of failure are in principle treated separately.

The local failure is the failure in the concrete immediately around and along the reinforcement. The local failure is assumed to be axisymmetrical.

A failure mechanism is the failure in the concrete surrounding the reinforcement. A failure mechanism is composed of yield lines radiating out from the reinforcement, the yield lines being perpendicular to the longitudinal direction of the reinforcement. Normally only one bar is included in a failure mechanism, but exceptions occur.

The complete failure involves all bars in the section. The optimal complete failure mechanism is composed of the failure mechanisms for one bar.

The failure mechanisms and, accordingly, the complete failure mechanisms, are in principle independent of the local failure. The failures in the surroundings can be considered without knowing anything about the local failure.

The local failure is treated by lower and upper bound calculations and coinciding solutions are obtained. The surroundings are not specified in details; it is only stated that they can offer some resistance. The developed expressions for the local failure are functions of dimensionless rib parameters, the effectiveness factors, and a quantity which is a function of the resistance from the surroundings. Assuming that the reinforcement and the effectiveness factors are known, it is only the value of the resistance from the surroundings which needs to be determined before the anchorage strength can be calculated. It appears that the failure in the surroundings can be determined with sufficient accuracy by means of simple upper bound calculations which have therefore been made.

The failure in the surroundings is treated in the case of anchorage at supports and lap splices. Expressions for various failure mechanisms are developed. It is possible to use the results to treat related anchorage problems, for instance development length problems.

In the case of anchorage at supports and lap splices, the theoretical expressions are compared to test results, and the value of the effectiveness factors is determined. It was possible to find tests in the literature and those which

were appraised to be applicable are included in the analysis. Because the expressions are too complicated for practical use, they have been simplified on the basis of the comparison with the test results.

All test results used, are from tests on specimens loaded by static load; no tests with varying load, dynamic load, are included.

The dowell action is not taken into account in the theoretical considerations, but the action is indirectly included in the determined values of the effectiveness factors.

In chapter 2 the basic assumptions for the calculations are specified. A short summary of the theory of plasticity is given. The effective plastic tensile strength for the concrete is investigated and the results are used in the subsequent chapters.

Some of the theories and methods found in the literature to determine the anchorage strength, are in main points expounded in chapter 3.

Lower and upper bound calculations for the local failure around a deformed reinforcing bar are carried out in chapter 4. Moreover, the failure in the surroundings of an axisymmetrical specimen is treated. The results are used as argumentation for the fact that the failure in the surroundings can be treated by implementing upper bound calculations and using simple mechanisms.

In chapters 5, 6, and 7, expressions for various failure mechanisms in the case of anchorage at supports with one layer of reinforcement, anchorage at supports with more than one layer of reinforcement, and for lap splices are developed. These expressions are compared with test results in chapter 8, 9, and 10. In the light of this, simple expressions for the load carrying capacity are expounded.

The most important expressions from the preceding chapters are summarized in chapter 11. The expressions are valid for anchorage at supports with one layer of reinforcement and for lap splices.

Concluding comments appear in chapter 12.

Chapter 2

Basic Assumptions

This chapter contains a summary of the basic assumptions upon which the subsequent calculations will be based. Firstly a brief survey of the theory of perfectly plastic materials is given. Then the assumptions about the concrete are discussed and the problems arising when applying the theory of plasticity to concrete structures are discussed. Finally the assumptions about the reinforcement are mentioned.

2.1 The Theory of Plasticity

A *rigid-plastic material* is defined as a material in which no deformations occur for stresses up to a certain limit, which is called the *yield point*. For stresses at the yield point, arbitrarily large deformations are possible without any change in the stresses. A rigid-plastic material does not exist in reality, but it is possible to use the model when the plastic strains are much larger than the elastic strains. In the following only rigid-plastic materials will be dealt with here.

The yield strength of a material can be described by *the yield condition*. The yield condition is a mathematical description of the combinations of stresses in which yielding may occur.

In a stress-coordinate system the yield condition describes a surface, which is called *the yield surface*. The yield surface is assumed to be *convex*. For stresses within the yield surface no yielding can occur. Stresses outside the yield surface are not possible.

The ratios between the plastic strains at yield can be determined by *the*

associated flow law. The associated flow law is also known as *Von Mises's Flow Rule* or *the normality condition,* because the plastic strains are an outwardly directed normal to the yield surface. The strains obtained using the flow law are actually the rates of the strains. Because we are only concerned with the instant of failure, the strains are understood to be incremental and it is therefore not necessary to distinguish between strains and strain rates.

The yield condition, together with the flow law, forms the constitutive equations for a perfectly plastic material.

As mentioned above no deformation occurs in a structure of rigid- plastic material when the stresses are below the yield point. Increasing the load to a point, where it can be carried only by stresses at the yield point, unlimited deformations are possible without changing the load, if the strains correspond to a geometrically possible displacement field. A structure in this condition is said to be subjected to *collapse by yielding.* The load corresponding to this state is called *the collapse load, the yield load, the failure load, or the load-carrying capacity* of the structure.

The following extremum principles are useful when the load carrying capacity of rigid-plastic bodies is to be determined.

- *The Lower Bound Theorem:* A load for which it is possible to find a safe and statically admissible stress distribution is less than or equal to the load carrying capacity.

- *The Upper Bound Theorem:* A load for which it is possible to find a kinematically admissible failure mechanism is greater than or equal to the collapse load.

- *The Uniqueness Theorem:* When the lowest upper bound and the highest lower bound coincide, the load obtained is equal to the exact load carrying capacity of the structure.

In the theorems mentioned above different terms have been used. A *statically admissible stress distribution* is a distribution which satisfies the equilibrium equations and the statical boundary conditions and a *safe stress distribution* is a distribution which corresponds to stresses within or on the

yield surface. A *kinematically admissible failure mechanism* corresponds to a displacement field which is in agreement with the geometrical boundary conditions and which satisfies the conditions of compatibility.

A lower bound solution can be determined by finding out how the load can be transferred through the structure to the foundations, without exhausting the strengths of the materials. The principle in lower bound calculations is simple, but nevertheless it often causes problems in finding good lower bound solutions. An upper bound solution can be found by applying the work equation to a geometrically possible strain field. The external work done by the load in the failure mechanism is equated to the internal work dissipated in the structure. It is often easy to carry out upper bound calculations and in many cases the obtained results are satisfactory.

Gvozdev [38.1] was the first to give a complete formulation of the limit analysis theorems, but Prager [52.1], Drucker et al. [52.2], [52.3] formulated the theorem independently of Gvozdev. A more thorough summary of the theory can be found in these publications or in, amongst others, Prager [59.1] and Prager & Hodge [68.1]. Summaries can also be found in Jensen [76.2] and Nielsen [84.1].

2.2   Concrete

Concrete cannot be characterized as an elastic or a plastic material for all stress levels. For small stresses the elastic theory can normally be used, but for stresses near to the material strengths this theory is not useful. As is well known, concrete has a limited ductility. Therefore it does not immediately appear that the theory of plasticity can be used to treat the case of failure in concrete structures. In the case of reinforced concrete structures, where the behavior is governed primarily by the reinforcement, the theory of plasticity has been shown to be workable and has been used for many years. The theory of plasticity is useful in this case, because the properties of the reinforcement can be identified with those of a perfectly plastic material. In the case of unreinforced structures and structures with high ratios of reinforcement, the load carrying capacity is governed mainly by the properties of the concrete. Employing the theory of plasticity in these

cases does not result in a satisfactory agreement between test and theory. This is probably because of the limited concrete ductility. Therefore when using a rigid plastic material model for the concrete, modification factors must be used for taking into account the lack of plasticity.

The modification factors can be introduced in such a way that the concrete is considered to be a material having *plastic strengths*, instead of the normal strengths. The plastic strengths are reduced in proportion to the normal strengths by *effectiveness factors*. The plastic uniaxial compression and tensile strengths can then be written as

$$f_{cp} = \nu f_c \tag{2.1}$$

$$f_{tp} = \nu_t f_t = \rho f_c \tag{2.2}$$

where f_c is the uniaxial compressive strength measured by a standard compression test on a cylinder and f_t is the uniaxial tensile strength measured by a standard procedure. The dimensionless quantities ν, ν_t and ρ are the effectiveness factors. The concrete strengths and the effectiveness factors are discussed later in this section.

As a failure criterion for the concrete, the *frictional hypothesis* of Coulomb together with a limitation of the tensile strength is used. The yield condition corresponding to this hypothesis is called the *modified Coulomb failure condition*. For determining the modified failure condition three material constants must be known. This can for instance be the uniaxial compression strength f_c, the uniaxial tensile strength f_t, and the angle of friction φ. The angle of friction can, with sufficient accuracy, be taken as a constant corresponding to $\tan \varphi = \frac{3}{4}$, see below.

The condition for sliding failure in a section can be written as

$$|\tau| = c - \sigma \tan \varphi \tag{2.3}$$

where τ is the shear stress, σ is a stress measured positive as tension, c is the cohesion and φ is the above-mentioned angle of friction. Using principal stresses σ_1, σ_2 and σ_3, where $\sigma_1 \geq \sigma_2 \geq \sigma_3$, the condition for sliding failure can be reformulated as

$$k\sigma_1 - \sigma_3 = 2c\sqrt{k} \tag{2.4}$$
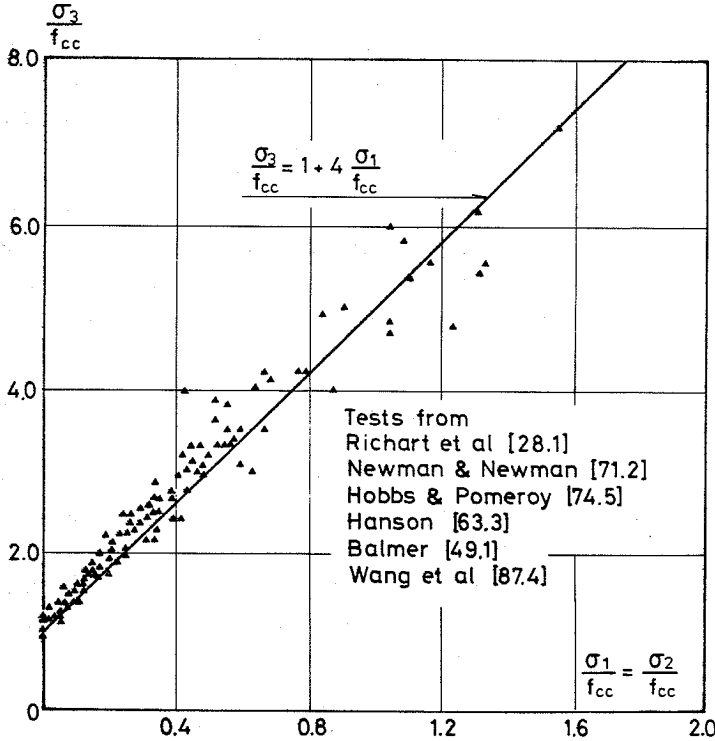
Figure 2.1: *Test results from triaxial compression tests on cubes. Expression (2.7) is shown using $k = 4 \sim \tan\varphi = 3/4$, and $f_c = f_{cc}$ which is the uniaxial cube strength. The figure is more or less taken from Wang et al. [87.4]. The stresses are shown positive as compression.*

where

$$k = \frac{1 + \sin\varphi}{1 - \sin\varphi} \qquad (2.5)$$

A compression test with $\sigma_1 = \sigma_2 = 0$ and $\sigma_3 = -f_c$, will always result in sliding failure, therefore

$$f_c = 2c\sqrt{k} \qquad (2.6)$$

Using (2.6), expression (2.4) can be rewritten as

$$-\frac{\sigma_3}{f_c} = 1 - k\frac{\sigma_1}{f_c} \qquad (2.7)$$

(2.7) is shown in figure 2.1 together with test results.

As can be seen in figure 2.1, expression (2.7), with $k = 4$, fits in very well with the test results. However, Wang et al. [87.4] have carried out
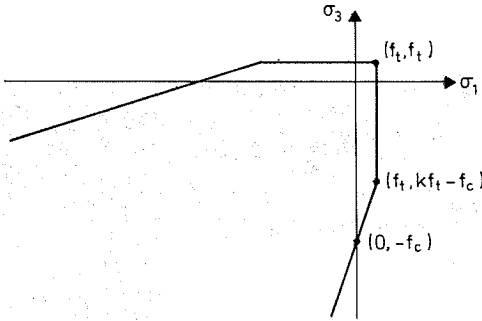
Figure 2.2: *The modified Coulomb failure condition in plain strain in the principal stress space.*

two tests with $\frac{\sigma_1}{f_{cc}} = \frac{\sigma_2}{f_{cc}} \simeq 3.1$, f_{cc} being the uniaxial compression strength measured on cubes, which are not shown in the figure. The correspondence between (2.7) and these tests is not as good as for the tests shown in the figure. However, these two tests represent a very high stress level which is unusual in practice. Jensen [76.2] and Nielsen [84.1] have also compared the expression for the sliding failure with test results and they find satisfactory agreement using $k = 4$. The frictional hypothesis can therefore probably be used for concrete for stress levels occuring in practice. Other failure conditions are used in the literature, but they are all more complicated than Coulomb's failure condition. Amongst others, Sandbye [65.2], Ottosen [77.1], Chen [78.1], and Boswell & Chen [87.2] have presented proposals to different descriptions of the yield surface. Ottosen [77.1] and Chen [78.1] also presents surveys of the failure conditions which have been used in the literature.

The modified Coulomb failure condition is shown in figure 2.2 in the case of plane strain.

In figure 2.3 photos taken from different positions of the modified Coulomb failure condition are shown. The arrows represent the principal stress space.

Figure 2.3 I to III shows the transition in the figure, when the position of the camera is changed from $(0, 0, a)$ to (a, a, a), a being a positive constant. It must be noticed that the large hexagon in the background in figure III does not represent one section, but three.
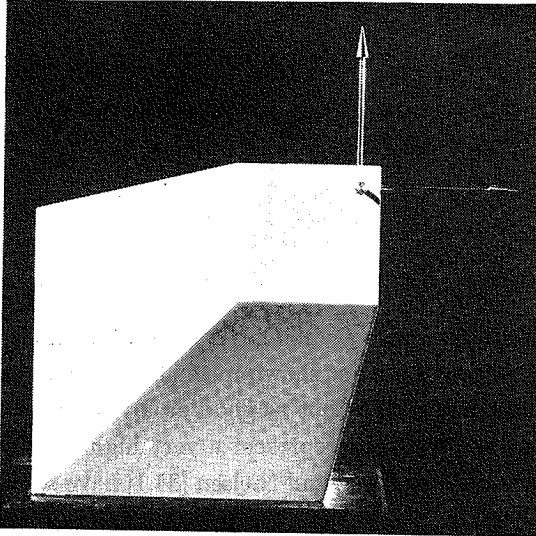
I
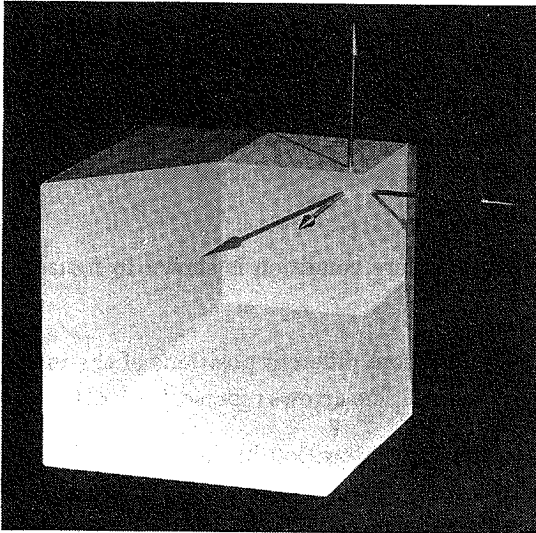
II
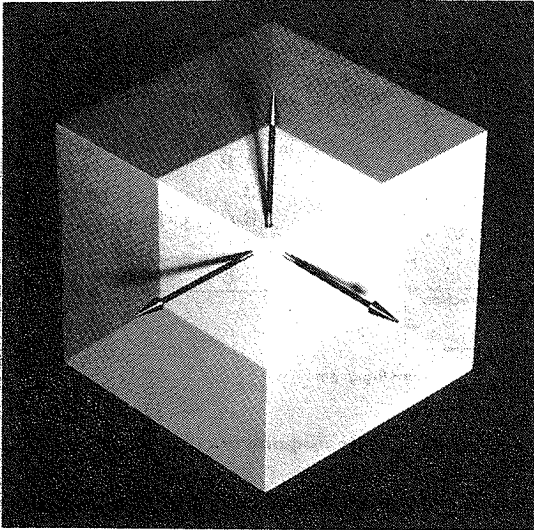
III
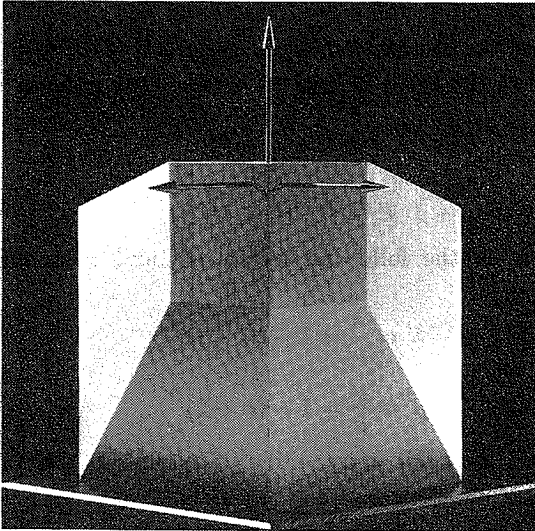
IV

Figure 2.3: *The modified Coulomb failure condition in the principal stress space.*

Reference point on the failure condition	Angle α	Dissipation D
A-B	$\frac{\pi}{2}$	$\rho f_c v$
B	$[\varphi; \frac{\pi}{2}]$	$\frac{1}{2} f_c (\lambda - \mu \sin \alpha) v$
B-C & C-D	φ	$\frac{1}{2} \nu f_c (1 - \sin \varphi) v$
C	$[-\frac{\pi}{2}; \varphi]$	$\frac{1}{2} \nu f_c (1 - \sin \alpha) v$
C-E	$-\frac{\pi}{2}$	$\nu f_c v$
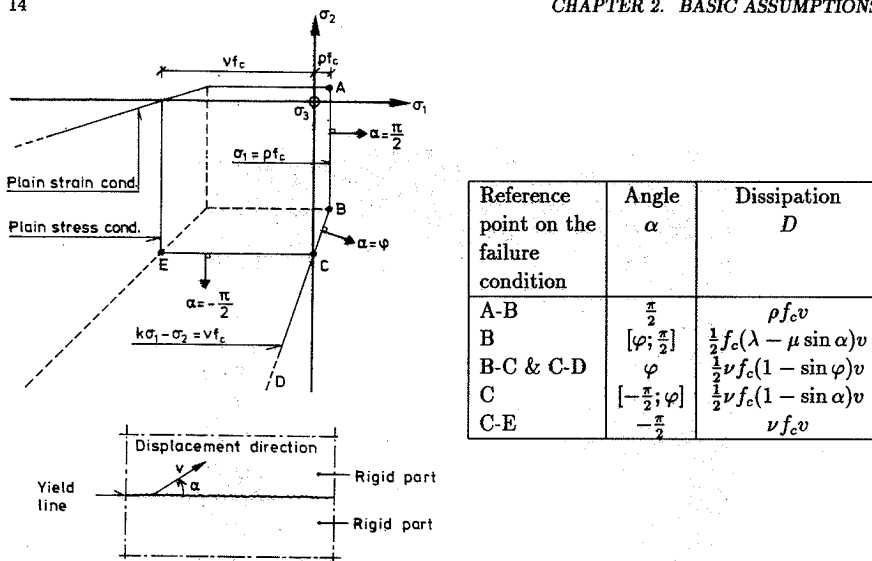
Figure 2.4: *Yield condition and equations for the dissipation in a yield line for a modified Coulomb material.*

In figure 2.4 the modified Coulomb failure condition for plane strain and equations for the *dissipation, D,* in a yield line are shown.

The effectiveness factors ν and ρ are included in the yield condition and in the expressions for the dissipation in the concrete. Two quantities, λ and μ, are introduced in the table in figure 2.4. They are defined as

$$\lambda = \nu - (k - 1)\rho \qquad (2.8)$$

$$\mu = \nu - (k + 1)\rho \qquad (2.9)$$

In the calculations in the following sections λ and μ are in some cases modified to

$$\lambda' = \frac{\lambda}{\nu} = 1 - (k - 1)\frac{\rho}{\nu} \qquad (2.10)$$

$$\mu' = \frac{\mu}{\nu} = 1 - (k + 1)\frac{\rho}{\nu} \qquad (2.11)$$

The dissipation in a yield line of a modified Coulomb material as a function of the *angle between the yield line and the displacement, α,* is illustrated in figure 2.5.
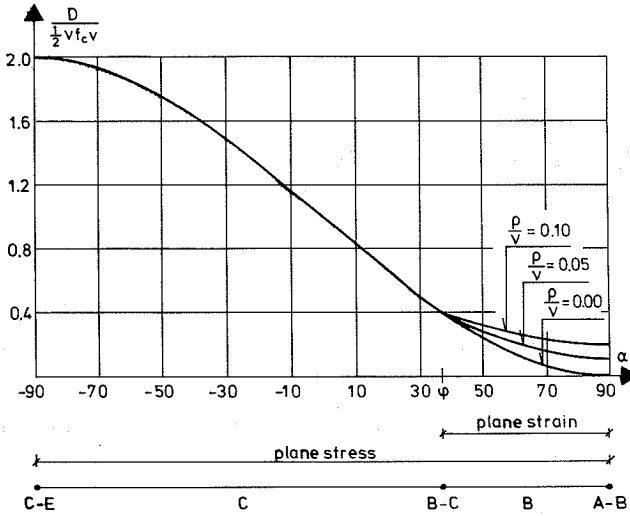
Figure 2.5: *The dissipation in a yield line as a function of the angle between the yield line and the displacement.*

As can be seen, the dissipation, D, decreases for increasing α, when $\frac{\rho}{\nu}$ is less than $\frac{1}{k+1}$. In the case of plane strain the dissipation in the yield line will always be less than $\frac{1}{2}\nu f_c v \frac{2}{k+1}$ for $\frac{\rho}{\nu} \le \frac{1}{k+1}$.

Jensen [75.2] and [76.2] shows how the expressions for the dissipation in a yield line can be formulated.

The compression strength of the concrete is defined as the peak value on the stress-strain curve appearing from a standard compression test on a cylinder, see figure 2.6.

The stress-strain relationship for concrete in uniaxial compression, curve I in the figure, does not fulfil the requirements of a rigid-plastic material. After the peak, the stress decreases for increasing strain. In the case of uniformly distributed strains, the stresses at failure will be equal all over the section. If the strains are not uniformly distributed at failure it is not certain that the stresses are equal over the whole section. This can be taken into account by reducing the uniaxial compressive strength by the effectiveness factor, ν, given in (2.1). The effective plastic strength can
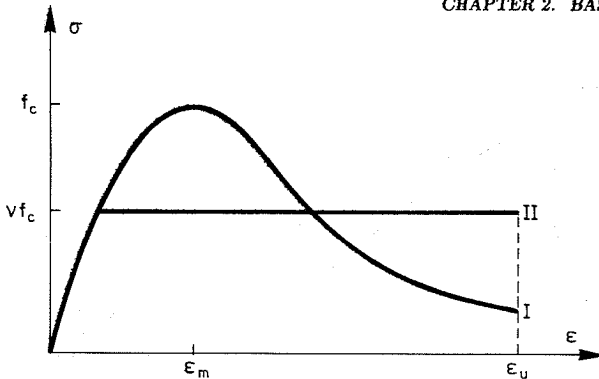
Figure 2.6: *Example of a uniaxial stress-strain relationship for concrete in compression, curve I, and an elastic- plastic relationship with the yield strength νf_c, curve II.*

be considered as a uniform stress over the section with a value of νf_c, see figure 2.6, curve II.

The value of the effectiveness factor can be determined in such a way that the area under the stress-strain curve is equal for the real and the elastic-plastic relationship. Such calculations have been carried out by Exner [79.5] using stress-strain curves measured by Wang et al. [78.5]. These calculations show that the effectiveness factor will be a function of the compression strength f_c and the strain at rupture ε_u, and it has been found that the effectiveness factor decreases with increasing concrete strength and strain at rupture. This is in agreement with the empirical fact that the falling branch of the uniaxial stress-strain curve is steeper for high concrete strengths than for small strengths. In practice the effectiveness factor therefore depends on the concrete strength and the strains in the structure at failure.

Exner [79.5], [83.1] has compared the load carrying capacity of two structures, the one having a concrete like stress-strain curve (curve I in figure 2.6) and the other having an elastic-plastic stress-strain curve (curve II in figure 2.6). It is found that the load carrying capacity of structure I is greater than or equal to the load carrying capacity of structure II, when the strain in the plastic structure II does not exceed the rupture-strain ε_u.

The effectiveness factor was first introduced in 1969 by Nielsen [69.2] in the case of shear strength of beams. The name *effectiveness factor* and the symbol ν was not used but the plastic uniaxial concrete strength was

introduced as $f_c^* = 0,85f_c$. The term 'effectiveness factor' and the symbol ν were introduced in Brœstrup [74.3] and Nielsen & Brœstrup [75.3] in the case of shear strength of beams. The arguments for using the effectiveness factor are the same as in Nielsen [69.2]; the concentrated forces from the bars are transferred to the concrete, whereas the entire web width of the beam will not be active. The value of the effectiveness factor ν was taken as a constant equal to 0.88, found by comparing the theory with test results. In the case of shear problems, Jensen [75.2], [76.2] has also used the effectiveness factor. He mentions that only a part of the section is active at failure and therefore the failure section is multiplied by the effectiveness factor. In the case of monolithic concrete, ν was found by test results to be equal to $\frac{2}{3}$, but other constant values are given for other cases.

Brœstrup et al. [76.4] have treated punching shear strength by means of the theory of plasticity. They concluded that the theoretical load carrying capacity is generally higher than the test results, because of the strain-softening and the limited deformability of the concrete. Therefore the stress is probably not equal to the uniaxial concrete strength in all points of the failure section. Hence the effectiveness factor $\nu = \frac{f_c^*}{f_c}$ is introduced. The effectiveness factor for tension, ρ in (2.2), is also used because the failure surface has no limit for $\rho = 0$. It is observed that ν decreases for increasing concrete strength, but ν is taken as a constant equal to 0.835, where $\rho = \frac{1}{400}$ is used.

Shear tests are carried out in Bach et al. [77.2]. It is stated that the tests does not show precisely, which of the varying parameters influence the effectiveness factor. However, there is a tendency that ν increases for decreasing concrete strength and cover. The effectiveness factor is taken as a constant between 0.64 and 0.75 in the different cases which are dealt with.

The theoretical expressions for the punching strength set up in Brœstrup et al. [76.4] are used by Hess et al. [78.3] to compare test and theory. It is found that the effectiveness factor can be determined as a constant divided by the square root of the uniaxial concrete compression strength. The effectiveness factor for tension, ρ , is taken as a constant equal to $\frac{1}{400}$.

All the results mentioned above have been compiled in Nielsen et al. [78.4]. In the case of shear in beams with stirrups it is proposed that the effectiveness factor, ν, can be determined as a constant minus the uniaxial concrete compression strength divided by another constant. In the case of shear in beams without shear reinforcement, which is also treated in Roikjær et al [79.6], it is found that the effectiveness factor decreases for increasing concrete strength and beam height and increases for increasing reinforcement ratio. It is also found that ν decreases for increasing shear span, for the shear span less than a certain value and increases when the shear span is larger than this value. This effect is due to the fact that the tensile strength is not included in the theoretical considerations.

A theoretical explanation of the effectiveness factor is given in Exner [79.5] as mentioned above. It is the first time that the concrete strength f_c and the effectiveness factor ν are connected in a figure, similar to those shown in figure 2.6. By using stress-strain curves measured by Wang et al. [78.5] it is shown that ν decreases for increasing f_c and ε_u. It is concluded that the only problem in a special case is finding the strain at rupture in the failure section.

More shear tests on beams with shear reinforcement are conducted in Bach et al. [80.1]. It is concluded that the effectiveness factor can be determined using the same expression used in Nielsen et al. [78.4].

The only now known case, where it is possible analytically to find the effectiveness factor, is in the case of pure bending. Exner [83.2] has dealt with this problem, again using stress-strain curves from [78.5]. The main result is that the effectiveness factor in the case of pure bending can be determined with sufficient accuracy as a function of the concrete strength f_c and the yield strength of the reinforcement f_y, but the geometrical reinforcement ratio also has an influence. Increasing f_c and f_y results in decreasing and increasing ν-values, respectively. From the analysis it appears that ν is rather close to 1 for low reinforcement ratios and low concrete strengths. The function for ν expounded by Exner is simplified in Nielsen & Feddersen [83.3] in such a way, that the expressions for ν can be used in practice. The theoretical expressions for the bending strength, where ν is determined from

the simplified expressions, are compared with test results. The agreement is quite good.

Pure torsion is dealt with by means of the plastic theory in Feddersen & Nielsen [83.4]. It is concluded that the effectiveness factor can be determined as a constant with acceptable accordance. However, it is mentioned that the concrete strength, the diameter of the main reinforcement, the ratio between the edges of the section, and the yield strengths for the reinforcement probably have an influence on the effectiveness factor. The results from the bending and the torsion analysis are also mentioned in Feddersen & Nielsen [84.4].

Anchorage is treated in Hess [84.2], Andreasen [84.3], [86.7], and Andreasen & Nielsen [86.8]. The effectiveness factors are inversely proportional to the square root of the uniaxial compression concrete strength.

Amongst other things, the results discussed above are mentioned in Nielsen [84.1]. Membrane action in reinforced concrete slabs is dealt with in Andreasen [85.4] and Andreasen & Nielsen [86.3], [88.4], [88.5], and [88.6]. ν is here found to be equal to a constant divided by the square root of the uniaxial compression concrete strength. Combined bending, shear and torsion are currently being dealt with by B. Feddersen and bending and shear in corbels, high beam and normal beams by Chen [88.7].

In the cases dealt with in the literature up till now, the effectiveness factor has been considered as a certain quantity. However, Ditlevsen [87.5] has suggested that the effectiveness factor approach can be extended to a model uncertainty approach in random vector form for system reliability analysis.

The effectiveness factor ν is a quantity which takes into account the lacking plasticity with respect to compression where a rigid plastic material model is used for concrete. In practice the effectiveness factor considers the strain conditions and the load history in the case under consideration. Pure bending is up till now the only case where it has been possible to determine the effectiveness factor ν analytically. Normally ν must be found by comparing the theory with test results. In general the magnitude of ν will be different from case to case, but usually described by a simple function. In the
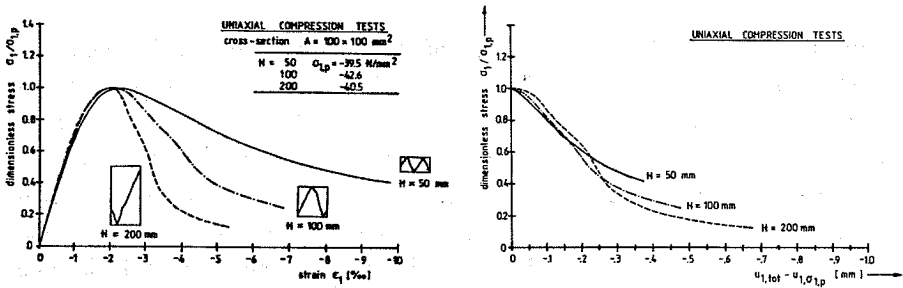
Figure 2.7: *Reprints of figure 1.17 and 1.18 in Van Mier [86.1].*

cases dealt with in the literature, ν is found to be a function of at least the uniaxial concrete compression strength f_c, where ν decreases for increasing concrete strength. Two types of functions are used

$$\nu = \frac{k_1}{\sqrt{f_c}} \tag{2.12}$$

$$\nu = k_2 - \frac{f_c}{k_3} \tag{2.13}$$

where k_1, k_2 and k_3 are positive constants.

Using the effectiveness factor in the way described above it is presupposed that the stress-strain relationship is independent of the size of the specimen, which is being tested. ν is simply calculated as the ratio between the effective plastic strength and the peak value. However, it is not the case in tests carried out by Van Mier [86.1], [86.2] . In figure 2.7 some of the test results are shown.

In the tests shown in figure 2.7 the friction between the concrete specimen and the applied load is eliminated using a special loading system. As can be seen from the figures, the stress-strain and the stress-displacement curves in compression are similar to those found in tensile tests; there is a size effect in the falling branch on the stress-strain relationship. The stress-strain curves are equal in the pre-peak region and the stress-displacement curves are almost equal in the post-peak region.

These tests indicate that it should be impossible to use the theory of plasticity for concrete structures where the strength is covered mainly by the concrete. However, the theory of plasticity has been used for many years to design many different concrete structures and the results are generally remarkably good, when the concrete is modified to have the plastic compression strength νf_c. The reason for this is probably that in a practical problem the dimensions do not change to such a degree that the size effect has a large influence. Furthermore in most cases it is very likely that the load carrying capacity is reached for a strain not very much larger than the strain corresponding to the peak value f_c. Therefore the difference in the descending part of the stress-strain curves does not have much influence. A reason why the size effect has not been remarked on earlier is probably because of the normal scatter on the uniaxial strengths of the concrete. If the strengths are encumbered by a scatter, the stress-strain curves, including the falling branch, must also be encumbered by a scatter. The scatter on the stress-strain curves is included in the values for the effectiveness factors, which have been found in such a way that the size effect is indirectly included in the theory. In many of the cases dealt with in the above mentioned literature, the scatter on the ratio test/theory is less than or equal to the scatter on the uniaxial concrete strength. The theory of plasticity seems in the way it is used here for concrete structures to work satisfactorily. The limitations for the theory must of cause not be forgotten and the use of the plastic principle must not be used without considering the problem and the solution critically.

Studying the failure patterns in figure 2.7 on the left, it can be seen that the observed failure lines correspond to what should be expected according to the theory of plasticity.

In some cases it is necessary to include the tensile strength of the concrete in the calculations. This can be done by introducing the plastic tensile strength as given in (2.2). The tensile strength of the concrete is included in many theoretical solutions expounded in the literature, but only in a few cases when comparing the theory with test results is the tensile strength considered to be other than zero. In Hess et al. [78.3] and Hess [84.2] the tensile strength of the concrete is included both in the theoretical calcula-

tions and in the comparison with test results.

In the case of anchorage the tensile strength is also included in the theoretical expressions and in the comparison with test results. In an anchorage the deformations at failure are small compared to other problems in concrete structures, wherefore it in this case is reasonable to take the tensile strength into account.

In the case of uniaxial compression in concrete little or no size effect has been recognised, but the test by Van Mier [86.1], [86.2] shows this is not the case. In the case of uniaxial tensile in concrete it was for a long time believed that the failure was brittle, but the test by Rüsch & Hilsdorf [63.1] shows that the stress-strain relationship for tension is similar to the one for compression. The difference between compression and tension is therefore mainly the absolute value of the stresses at failure. However, it is absolutely not correct to determine the effectiveness factor for tension, ρ , in a similar way as for the effectiveness factor for compression ν by requiring the same area under the stress-strain curve for the real and the plastic relationship. A tension failure is concentrated in a few cracks and therefore the measured strains depend on the measurement length. This is for instance shown by Hillerborg et al [76.3] and Hillerborg [78.2]. The falling branch of the stress-strain curve becomes steeper when the size of the test specimen is increased. Using the area principle as with ν, a tension failure in a small specimen will result in a large value for ρ and a failure in a large specimen will give a small ρ value.

The compression strength of concrete is influenced by various parameters, but it seems that the tension strength is even more sensitive to the test conditions than the compression strength. The tension strength and the stress-strain curve are very much influenced by the test set up and the size and shape of the test specimen, see figure 2.8.

Figure 2.8 shows that the observed stress-strain curves for tension in concrete are similar to those observed for compression. More test results are, amongst others, given in Petersson [81.2], Gopalaratman & Shah [85.2], and Cedolin et al. [87.3].

CURVE No.	AGGREGATE		AGE in months
	TYPE	SIZE	
1	GRANITE	3/8"- 3/16"	2
2	GRAVEL	3/8"- 3/16"	2
3	GRAVEL	3/16"-B.S.7	3
4	GRAVEL	3/8"- 3/16"	2
5	GRAVEL	3/8 -3/16"	1

rate of straining = 1% in 2500 min.
approx. water / cement = 0.54 (by wt.)
approx. aggregate / cement = 2.0
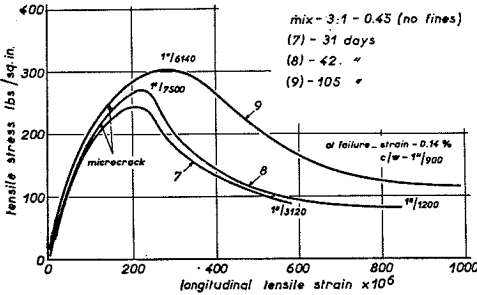
FIG. 2c. — Complete stress strain curves in direct tension (Contd).

FIG. 4. — Resulting tensile stress-strain curves.

Figure 2.8: *Complete stress-strain curves in direct tension. Reprints of figure 2c in Evans & Marathe [68.2] and figure 4 in Hughes & Chapmann [66.2].*
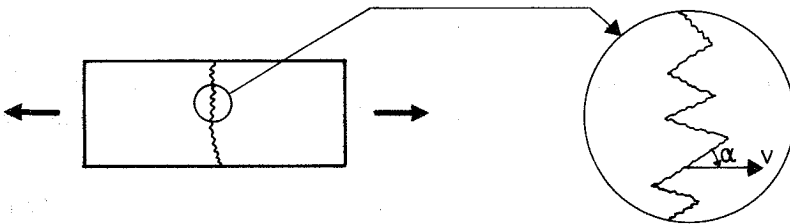
Figure 2.9: *Tensile failure in a specimen.*

It is an empirical fact that the uniaxial tensile strength of concrete f_t can be determined as a function of the uniaxial compression strength f_c. This can be due to the fact that the tension failure is in reality a lot of small sliding failures, see figure 2.9.

The strength of failure by sliding depends on the compression strength of the concrete, therefore the tension strength can very likely be described as a function of the compression strength. The empirical relation between the tension and the compression strength is often given by

$$f_t = k_{tc}\sqrt{f_c} \tag{2.14}$$

where k_{tc} is a positive constant.

As previously mentioned, the effectiveness factor ν is, in different problems, found to be a function of the uniaxial compression strength and the relation can be written as

$$\nu = \frac{k_c}{\sqrt{f_c}} \tag{2.15}$$

which is also given in (2.12).

If it is assumed that the effectiveness factor for tension, ρ, can be calculated in the same way as ν, but as a function of f_t instead of f_c, the relation between ρ and f_t can be given as

$$\rho = \frac{k_t}{\sqrt{f_t}} \tag{2.16}$$

Using (2.14), (2.15), and (2.16) the following expressions are found

$$\rho = \frac{k_t}{\sqrt{k_{tc}}} \frac{1}{f_c^{\frac{1}{4}}} \tag{2.17}$$

$$\frac{\rho}{\nu} = \frac{k_t}{k_c\sqrt{k_{tc}}} f_c^{\frac{1}{4}} \tag{2.18}$$

In theoretical calculations the ratio between ρ and ν often appears. If $\frac{\rho}{\nu}$ therefore can be assumed to be constant the theoretical considerations will be more simple. The following is therefore introduced

$$\frac{\rho}{\nu} = k_r \tag{2.19}$$

where k_r is a positive constant. In this case the following expressions are found by (2.14), (2.15), and (2.19)

$$\rho = \frac{k_{tc}k_ck_r}{f_t} \tag{2.20}$$

$$\rho = \frac{k_ck_r}{\sqrt{f_c}} \tag{2.21}$$

It is not immediately clear whether assumptions (2.16), (2.19), or a third one should be used to describe the plastic tensile strength of the concrete. Test results are therefore used to clarify which of the two models set-up are to be used here. In the following (2.16) - (2.18) are denoted as model A and (2.19) - (2.21) as model B.

Gravesen & Krenchel [72.2] have carried out bending tensile strength tests, where the compression strength is measured for every specimen. The stress
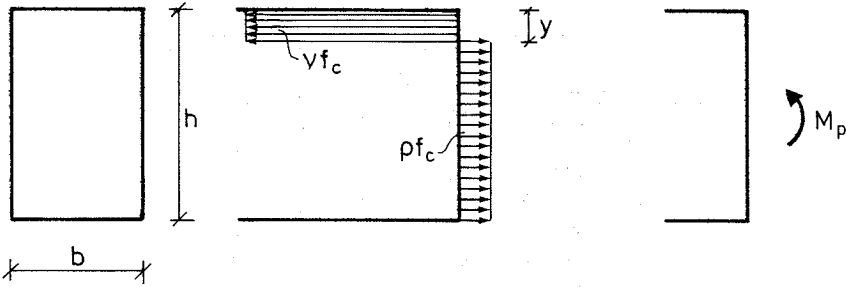
Figure 2.10: *Stress distribution according to the theory of plasticity in a rectangular plain concrete section subjected to pure bending.*

distribution in a section according to the theory of plasticity is shown in figure 2.10.

The unreinforced beam has a rectangular cross section with depth h and width b and is stressed to pure bending. The yield moment in pure bending can be determined by

$$M_p = \frac{1}{2}bh^2\rho f_c\frac{\nu}{\nu + \rho} \qquad (2.22)$$

Assuming the extension of the compression zone to be equal to zero, the moment can be written as

$$M_{p,y=0} = \frac{1}{2}bh^2\rho f_c \qquad (2.23)$$

which corresponds to $\nu \to \infty$.

In Gravesen & Krenchel [72.2] the bending tensile stress f_{tb} is defined as the maximum stress appearing if the stress distribution is linear, according to the elastic theory

$$M_{ell} = \frac{1}{6}bh^2 f_{tb} \qquad (2.24)$$

Equating equations (2.22) and (2.24), the following expression is arrived

$$\rho = \frac{\nu f_{tb}}{3\nu f_c - f_{tb}} \qquad (2.25)$$

If $\nu \to \infty$ the expression can be rewritten as

$$\rho = \frac{f_{tb}}{3f_c} \qquad (2.26)$$

(2.26) is a good approximation to (2.25) because f_{tb} in the denominator in (2.25) is small compared to $3\nu f_c$. This indicates that the analysis is not

No.	f_{tb}	f_c	$\nu = \frac{3}{\sqrt{f_c}}$		$\nu = \infty$	
	[Mpa]	[Mpa]	ρ from (2.25)	$\frac{\varrho}{\nu}$	ρ from (2.26)	$\frac{\varrho}{\nu}$
1	2.16	11.2	0.069	0.077	0.064	0
2	2.34	11.6	0.073	0.083	0.067	0
3	4.12	22.0	0.069	0.108	0.062	0
4	4.12	23.3	0.065	0.105	0.059	0
5	4.62	32.8	0.051	0.098	0.047	0
6	4.68	33.2	0.052	0.099	0.047	0
7	4.66	33.6	0.051	0.098	0.046	0
8	5.20	42.4	0.045	0.097	0.041	0
9	5.48	44.8	0.045	0.100	0.041	0
10	5.80	45.0	0.047	0.106	0.043	0
11	5.68	46.4	0.045	0.102	0.041	0
12	7.02	55.6	0.047	0.117	0.042	0
13	7.38	56.0	0.049	0.123	0.044	0

The specimens are made of rapid cement (14 days old) and are stored in water in a horizontal position. The depth $h = 100mm$, width $b = 150mm$, and the length $\ell = 800mm$.

Table 2.1: *Bending tensile strength tests from Gravesen & Krenchel [72.2].*

sensitive regarding the value of ν. In table 2.1 the results from the tests are shown.

In table 2.1 results from two analyses are also given. The first analysis is carried out using (2.25) and (2.15) with $k_c = 3$ and in the second expression (2.26) is used. Comparing ρ obtained in the two analyses, it can be seen that the difference is small, which was also to be expected. In figure 2.11 the ρ values obtained from (2.26) are shown as a function of the uniaxial concrete strength f_c.

Curves from the previously mentioned two models A and B are also shown in figure 2.11. The constants are determined in such a way that the correspondence between the curves and the test results is the best possible. It is not obvious from this analysis to say which of the two models, A and B, is the best.

The values obtained for $\frac{\varrho}{\nu}$ using expression (2.25) are shown in figure 2.12, together with curves representing models A and B.
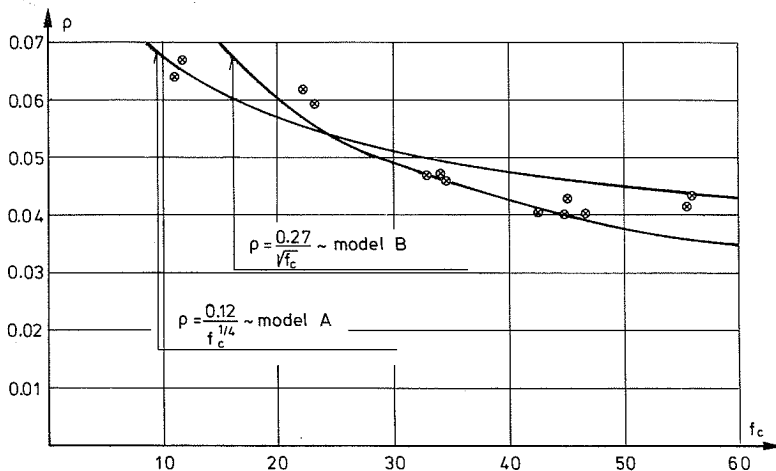
Figure 2.11: *Values of ρ obtained from (2.26), see table 2.1. The two curves represent model A and model B, respektively.*

As can be seen from the figure model A describes the test results indeed very satisfactorily. For concrete strengths appearing in practice the constant description, model B, is acceptable, but for all possible strengths model B does not seem to be as good as model A.

The mean value of $\frac{\ell}{\nu}$ from the analysis using (2.25) in table 2.1 is 0.101, the standard deviation is 0.012 and the coefficient of variation is 0.120. For $k_c = 2$ the corresponding values are 0.160, 0.020, and 0.126, and for $k_c = 5$ the values are 0.058, 0.007, and 0.114. This indicates that the coefficient of variation on the ratio $\frac{\ell}{\nu}$ is nearly independent of the value of ν, but the values for $\frac{\ell}{\nu}$ are of course influenced by ν. In practice the constant k_c is in the interval 2 to 5, therefore $\frac{\ell}{\nu}$ in practice will probably be in the interval of 0.01 to 0.150 depending on the absolute dimensions of the failure zone in a special case. The specimen used by Gravesen & Krenchel [72.2] is small compared with structures in practice, therefore the lower limit for $\frac{\ell}{\nu}$ is reduced in proportion to the value obtained in the analysis.

In table 2.2 the functions obtained from the analyses are shown. ρ as a function of f_c can be seen to be almost equal for the two analyses with different values of ν.

From the previous calculations it can be concluded that model A, expres-
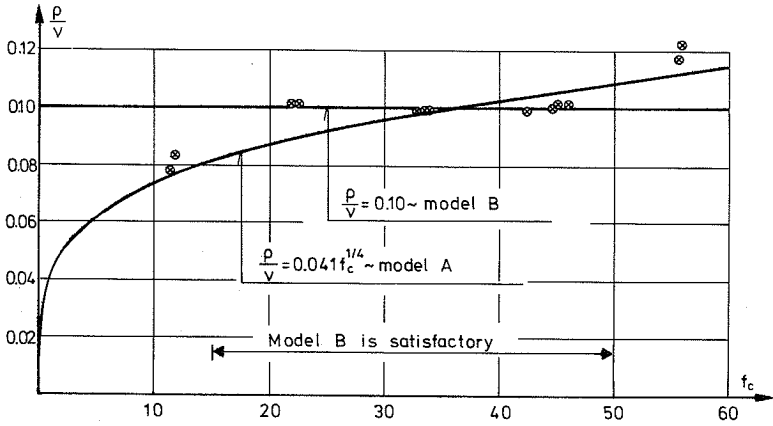
Figure 2.12: *Values of $\frac{\rho}{\nu}$ obtained from (2.25), see table 2.1. The two curves represent model A and model B, respectively.*

	$\nu = \frac{3}{\sqrt{f_c}}$		$\nu = \infty$	
	model A	model B	model A	model B
$\frac{\rho}{\nu}$	$0.041 f_c^{\frac{1}{4}}$	0.10	-	-
ρ	$\dfrac{0.125}{f_c^{\frac{1}{4}}}$	$\dfrac{0.30}{\sqrt{f_c}}$	$\dfrac{0.12}{f_c^{\frac{1}{4}}}$	$\dfrac{0.27}{\sqrt{f_c}}$
ρ	$\dfrac{0.069}{\sqrt{f_t}}$	$\dfrac{0.095}{f_t}$	-	$\dfrac{0.085}{f_t}$

Table 2.2: *Expression (2.16) – (2.21) for the cases in table 2.1.*

No.	f_c [MPa]	f_{ts} [MPa]	f_t [MPa]
1†	11.0	1.46	0.98
2†	11.6	1.24	1.08
3†	12.4	1.38	1.08
4†	28.8	3.12	2.14
5†	29.8	2.80	2.00
6†	33.0	2.60	1.92
7†	43.2	3.60	2.18
8†	43.2	4.10	2.30
9†	45.2	4.14	2.42
10†	56.2	4.66	2.58
11‡	16.6	2.04	1.54
12‡	16.6	2.64	1.46
13‡	21.8	2.28	1.64
14‡	22.2	2.56	1.74
15‡	27.2	2.50	1.86
16‡	27.6	2.44	2.08
17‡	31.6	3.38	2.12
18‡	38.6	3.40	2.16
19‡	38.8	4.00	2.24
20‡	42.0	3.50	2.12
21‡	48.8	4.00	2.62

Specimen stored in water and air.

†: standard cement, 28 days.

‡: rapid cement, 14 days.

Dimensions:

diameter $d = 150mm$,

length of cylinder $\ell = 300mm$,

loading plate $b = 15mm$.

The splitting tensile strength is defined as

$$f_{ts} = \frac{2P}{\pi d \ell}$$

where P is the load, see figure 2.13.

Table 2.3: *Related values of the compression strength f_c, the tensile strength f_t and the splitting strength f_{ts} from Gravesen & Krenchel [72.2].*

sions (2.16) - (2.18) results in the best description of these tests. Model B fits in very well with the test results, but if the interval for the concrete compression strength is limited to 15 - 50 MPa, the agreement is even better than for model A.

Gravesen & Krenchel [72.2] have also carried out some tests, where the uniaxial compression strength f_c the uniaxial tensile strength f_t, and the splitting strength f_{ts} are measured for the same concrete. The main varying parameter was the strength of the concrete. The results from a test series where the concrete was stored in water for the first half period and in air for the last period, are shown in table 2.3.

In figure 2.13 the cylinder used in the splitting tension tests is shown.
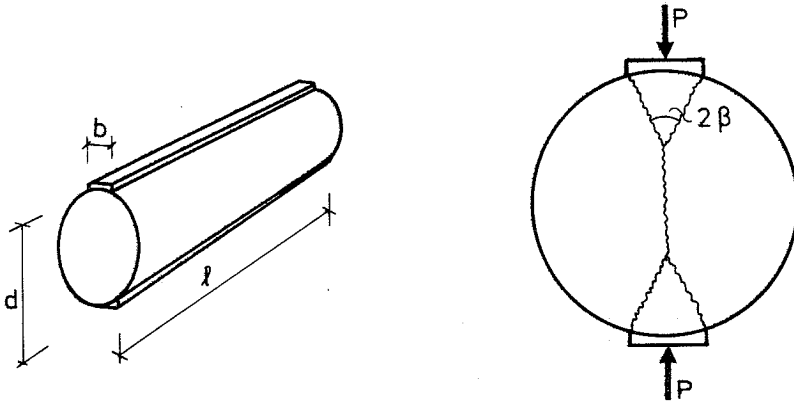
Figure 2.13: *Cylinder used to the splitting tensile tests given in table 2.3.*

Applying the upper bound theorem to the failure mechanism shown in figure 2.13, the load carrying capacity can be found to be

$$\frac{P}{b\ell\rho f_c} = \frac{d}{b}\tan(2\beta + \varphi) - 1 \tag{2.27}$$

where

$$\cot\beta = \tan\beta + \frac{1}{\cos\varphi}\sqrt{1 + \frac{\frac{d}{b}\cos\varphi}{\frac{1}{2}\frac{\nu}{\rho}(1 - \sin\varphi) - \sin\varphi}} \tag{2.28}$$

which has been set up by Chen & Drucker [69.3]. If $\cot\beta > \frac{d}{b}$ in (2.28) then $\cot\beta = \frac{d}{b}$ should be used in (2.27).

The exact plastic solution for the splitting problem was developed by Izbicki [72.3]. According to Exner [83.1] the upper bound solution corresponds very well to the exact solution in some cases. For $\frac{b}{d} > 0.05$ and $\frac{\ell}{\nu} > 0.1$ the difference between the correct solution and the upper bound solution is less than 6% .

(2.27) and (2.28) do not give the load carrying capacity directly. The angle β should first be found from (2.28) and the obtained value then inserted into (2.27). However, it is possible to combine the expressions in such a way that one can find the load carrying capacity by using only one expression. It is seen that

$$\tan(2\beta + \varphi) = \frac{2\cot\beta + \tan\varphi\cot^2\beta - \tan\varphi}{\cot^2\beta - 1 - 2\tan\varphi\cot\beta} \tag{2.29}$$

Inserting (2.28) into (2.29) and inserting this expression into (2.27), the following expression for the load carrying capacity is found

$$\frac{P}{b\ell\rho f_c} = \frac{d}{b}\left[\tan\varphi + 2\cot\beta\frac{\frac{1}{2}\frac{\nu}{\rho}(1-\sin\varphi)-\sin\varphi}{\frac{d}{b}\cos\varphi}\right] \qquad (2.30)$$

(2.28) can be inserted into (2.30) directly. Having done this and using (2.5), the expression can be reformulated as

$$\frac{P}{b\ell\rho f_c} = \frac{\frac{\nu}{\rho}-(k-1)}{2k}\left[\sqrt{k}\frac{(k-1)\frac{d}{b}-2\sqrt{k}}{\frac{\nu}{\rho}-(k-1)}+(k-1)+(k+1)\sqrt{1+\frac{2\sqrt{k}\frac{d}{b}}{\frac{\nu}{\rho}-(k-1)}}\right]$$
$$(2.31)$$

For the case $k=4$ (2.31) can be written as

$$\frac{P}{b\ell\rho f_c} = \frac{1}{8}\left[3\frac{\nu}{\rho}+6\frac{d}{b}-17+5(\frac{\nu}{\rho}-3)\sqrt{1+\frac{4\frac{d}{b}}{\frac{\nu}{\rho}-3}}\right] \qquad (2.32)$$

Using the test results in table 2.3 to find the plastic tensile strength of the concrete at least two methods can now be used. In the first method $\frac{\nu}{\rho}$ is assumed and inserted into (2.32); ρ can now be calculated. In the second method ρ is assumed and $\frac{\nu}{\rho}$ is then calculated by isolating this parameter in (2.32). The value of the assumed parameter is determined so that the value is in accordance with one of the models A or B, expressions (2.16) - (2.21). Calculations have been carried out using these two methods and some of the results are shown in figures 2.14 and 2.15.

Calculations using constants in the functions other than in figures 2.14 and 2.15 and using the second method (ρ is assumed) have also been carried out. These calculations indicate that the main result is not so sensitive regarding the assumed values. Of course the absolute value of the calculated parameters changes when the constants are changed, but the general view is the same as shown in the figures. The functions, the standard deviation around the used curve, and the corresponding coefficient of variation are shown in table 2.4.

As can be seen by comparing figures 2.14 and 2.15 and the results in table 2.4 it seems as if the correspondence between the tests and model A is somewhat better than with model B, but it is only a slight difference. The same was
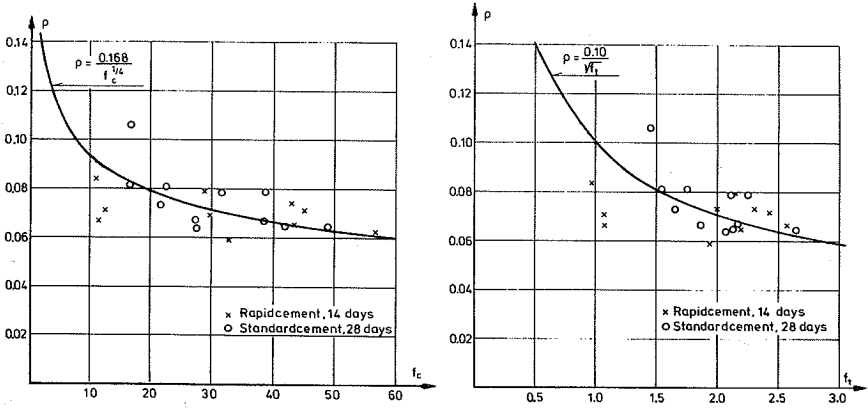
Figure 2.14: ρ calculated by (2.32) assuming $\rho/\nu = 0.040 f_c^{\frac{1}{4}}$ (model A) for the tests in table 2.3. The curves represent the best fit for the assumed functions.
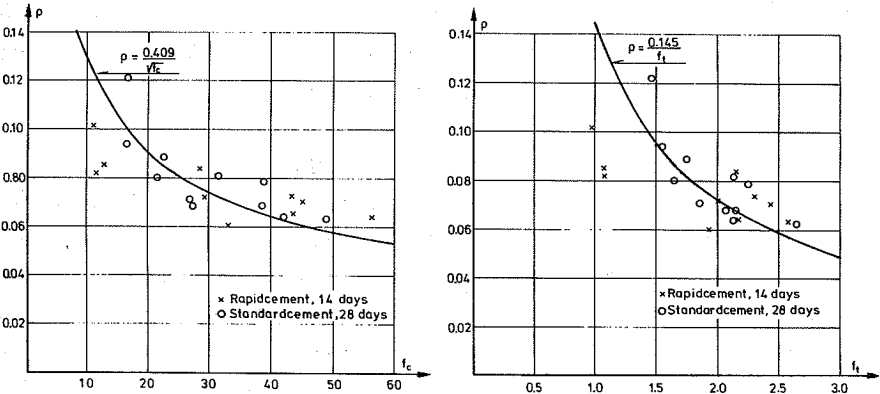
Figure 2.15: ρ calculated by (2.32) assuming $\frac{\rho}{\nu} = 0.100$ (model B) for the tests in table 2.3. The curves represent the best fit for the assumed functions.

	Model A			Model B		
	functions	standard deviation	coefficient of variation	functions	standard deviation	coefficient of variation
$\frac{\ell}{\nu}$	$0.040 f_c^{\frac{1}{4}}$	-	-	0.100	-	-
ρ	$\frac{0.168}{f_c^{\frac{1}{4}}}$	0.022	0.132	$\frac{0.409}{\sqrt{f_c}}$	0.062	0.152
ρ	$\frac{0.100}{\sqrt{f_t}}$	0.015	0.151	$\frac{0.145}{f_t}$	0.028	0.191

Table 2.4: *Functions, the standard deviation around the curves, and the corresponding coefficient of variation using the two models A and B for the splitting tensile tests in table 2.3.*

found previously in the case of bending of an unreinforced beam. It is not possible in the light of the test results and the analysis used here to say if one of the models is significantly better than the other.

It must be observed that the results obtained in using the assumptions in model A are not as inaccurate as might be expected. As can be seen from (2.15) and (2.16), model A, the effectiveness factor for tension, ρ, depends on the uniaxial tensile strength, f_t, as the effectiveness factor for compression, ν, depends on the uniaxial compression strength. From (2.15) and (2.19) it can be seen that in the case of model B, ρ depends on f_c in the same way as ν depends on f_c.

Model B, the constant model, is the easiest to use in practical calculations, because the ratio between ν and ρ often appears in the theoretical expressions for the geometrical parameters and the load carrying capacity. If $\frac{\nu}{\rho}$ can be taken as a constant, it is easier to make simplifications from the theoretically correct expressions, which in some cases are too complicated to be used directly. Concerning practical calculations it is therefore probably the best to use the constant model. Because the analysis carried out here does not show any significant difference between the two models, the simplest one, the constant model (model B), will be used in the calculations in the following chapters.

Other tests similar to Gravesen & Krenchel's tests can amoungst others be found in Torrent & Brooks [85.3]. These tests will not be discussed here.

If the simple models used here to describe the plastic tensile strength of con-

crete show to be incorrect or inconsistent when comparing theory with test
results, another model and certainly a more complicated one must be used.
It is probably possible to use some of the results obtained from fracture
mechanics analysis for concrete structures[1]; particularly the bending tests
to determine the fracture energy, but also the simple tensile tests, which
are carried out to find out which parameters are decisive in determining
the stress-strain and stress-deformation curves. This will not be discussed
in detail here, but it should be mentioned that the size of the aggregates is
found to influence the stress-deformation curve in the post-peak region.

In most cases it is not possible to determine the effectiveness factors ν and ρ
analytically. They must be found by comparing the theory with test results.
The value of the effectiveness factors is determined in such a way that the
correspondence between the theory and the test results is the best possible.

When the tensile strength of the concrete is not zero, there is a problem
in determining the two unknown parameters, ν and ρ. In plastic calcula-
tions the load carrying capacity is the only thing, which is unambiguously
determined. The theoretical load carrying capacity should be equal to the
test result which yield one equation. The theoretical load carrying capacity
is in general a function of at least ν and ρ, therefore there is one equation
with two unknown parameters. This indicates that one of the parameters
must be determined in another way or a two dimensional statistical analysis
must be used. In some cases it will be simpler to use ν and $\frac{\rho}{\nu}$ as parameters
instead of ν and ρ. An estimate for the value of $\frac{\rho}{\nu}$ can then be found by
considering the obtained failure mechanism in the tests, if these are not
fixed by geometrical conditions. Doing this it must be remembered, that a
crack is not necessarily a yield line, therefore this method should be used
with caution. A way of solving the problem is to assume a value for $\frac{\rho}{\nu}$, for
instance in accordance with model A or B, inserting this into the theoreti-
cal expressions and then finding ν. If the result is not satisfactory another
value for $\frac{\rho}{\nu}$ is assumed.

If there are two possible failure mechanisms in a concrete case using the
upper bound theorem, the best one can be found by comparing them theo-

---

[1]Amongst others Olson [85.6], [86.4], Gustavson [85.5], and Petersson [81.2] have dealt with this.
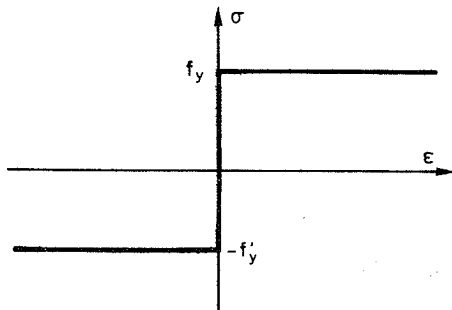
Figure 2.16: *The stress-strain relationship for the reinforcement.*

retically and selecting the smaller one (the one with the smaller load-bearing capacity). Doing this, it is assumed that the effectiveness factors are equal for the two mechanisms. This is not necessarily the case. Another possibility is to find the values for the effectiveness factors for all the tests[2] and observe which of the two mechanisms results in the largest values. This mechanism will be the best upper bound solution if the effectiveness factors are equal in both cases. As with the method above, this is not necessarily the case here either. It is not immediately possible to give a general guide-line on how to solve the problem under specific circumstances; in all considered situations there is a problem in finding the best mechanism when the effectiveness factors are not known.

2.3 Reinforcement

The reinforcement is assumed to be a rigid-plastic material and to be capable of carrying longitudinal tensile and compressive stresses only. Thus the dowel effect is neglected, which cannot always be considered inferiorly according to Nielsen [69.4] and [84.1]. The stress-strain relationship for the reinforcement is shown in figure 2.16.

---

[2]The values of the effectiveness factors are found by making the theoretical load carrying capacity equal to the load obtained in the tests, i.e. if the ratio $\frac{f}{\nu}$ is determined ν can be found as the ratio between the test value and the theoretical value using $\nu = 1$

Chapter 3

Anchorage Theories

Anchorage of reinforcing bars in concrete is a complicated problem because of the influence of many parameters. Until now only a few attempts to create a theory for the problem have been made. Many design rules are therefore empirical methods. Some of the theories presented in the literature will be discussed here. Moreover different methods of calculation of the anchorage strength will be given. This review should be considered only as a survey of the theories and methods. For a more thorough description the reader is referred to the actual reports and papers.

Ferguson & Briceno [69.1] have made theoretical considerations on the lap splice strength of deformed reinforcing bars. They state that besides the longitudinal cracks along the reinforcing bars, there will also be internal cracks radiating from each rib on the bar. It is assumed that the force in the bar develops inclined compressive forces in the concrete with the same inclination as the radiating cracks. The inclination is assumed, in the light of photos from Goto, see [71.3], to be *45 degrees*. Because of this, the longitudinal and the radial component of the stress are equal. Tests indicate that close to ultimate load the variation in steel stress along the splice is approximately linear from zero at one end to maximum at the other. The shear stress along the anchorage are therefore determined as a *constant*

$$\tau = \frac{A_s \sigma}{\pi d l} = \frac{d\sigma}{4l} \tag{3.1}$$

where A_s is the cross sectional area of the bar, σ is the steel stress, d is the diameter of the bar and l is the splice length.

Three kinds of failure patterns shown in figure 3.1 are considered.
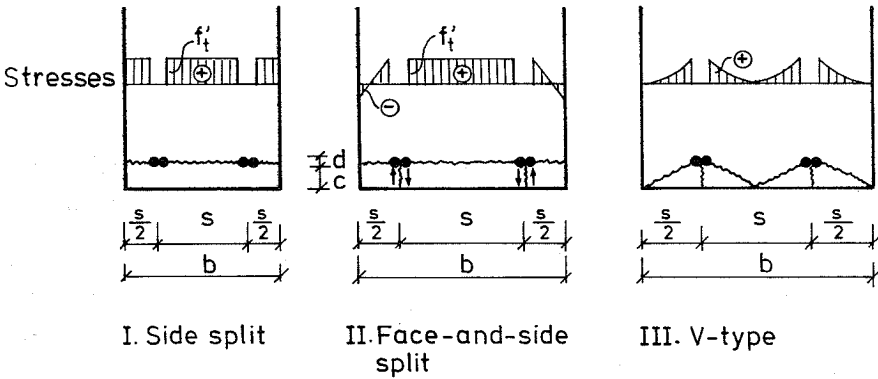
Figure 3.1: *Failure patterns used by Ferguson & Briceno [69.1]. The stresses in the concrete in a horizontal section through the bars at failure are indicated.*

The failure pattern I in figure 3.1, side split failure, will be treated here. It is assumed that if the splice is placed in a region with *varying moment*, the load carrying capacity is determined from the average value of the stresses in the bars. This is done by introducing a factor $k' = \sigma_{min}/\sigma_{max}$. The total outwarded force from two bars (one splice) can then be written as, using (3.1)

$$2(1 + k')\tau d = \frac{(1 + k')d^2\sigma}{2l} \tag{3.2}$$

The tensile stress f'_t (average splitting stress) shown in figure 3.1 should be in equilibrium with the outwarded forces from the bars, i.e.

$$f'_t = \frac{(1 + k')d\sigma}{2(\frac{b}{d} - 4)l} \tag{3.3}$$

where b is the width of the beam.

The face–and–side split failure is treated in a similar manner, but the calculations and the expressions are not as simple as for the side split failure. It is assumed that the vertical cracks can transmit shear stresses by aggregate interlock and that the stress distribution in the horizontal cover can be determined by Navier's expression. It is found that the expression for f'_t results in smaller values than (3.3), because the corner bodies are less efficient than for the side split failure.

The V-type failure will appear if the beam is very wide. This type of failure is not dealt with theoretically, but it is expected that this failure forms an upper limit for the values of f'_t found from the side split and the face-and-side split failure.

The values of f'_t obtained from splice tests are compared with splitting tensile cylinder tests and it is concluded that the agreement is quite reasonable.

Ferguson & Krisnaswamy [71.1] have used the same failure patterns as Ferguson & Briceno [69.1]. The longitudinal and the radial component of the stresses from the reinforcement are at first assumed not to be equal, but in the final expressions the inclination between them is 45 degrees. The tensile stress in the concrete f'_t is taken as the splitting cylinder strength multiplied by a factor α. The splitting strength is calculated as a function of the uniaxial compression strength f_c as $f_{t,split} = 0.53\sqrt{f_c}$ ($f_{t,split}$ and f_c in MPa). α takes into account that the stresses are not evenly distributed in the longitudinal direction and across the splice and that the inclination of the compressive stresses in the concrete changes with varying confinement or cover. The outward force from two bars is then $2dl\tau$, which referring to (3.1) can be written as $\sigma d^2/2$. This force is taken by an average tensile stress in the concrete $f'_t s'l = \alpha(0.53\sqrt{f_c})s'l$, where $s' = b/2 - 2d$, from which it is found that the splice length can be calculated using

$$l = \frac{0.94\sigma d^2}{s'\alpha\sqrt{f_c}} \tag{3.4}$$

Comparing (3.4) with test results it is found that α can be determined from

$$\frac{1}{\alpha} = 0.9(1 + 0.5\frac{s'}{c}) \tag{3.5}$$

for σ less than approximately $400MPa$. The splice length can then be determined from (3.4) assuming the steel stress σ to be equal to the yield stress. Design rules are established for tension lap splices based on (3.4) and (3.5). Special cases such as staggered splices, splices in a variable moment region, interior splices in walls and slabs and splices with transverse reinforcement are also treated.

In Orangon et al. [75.1] and [77.3] the work done in the previously men-
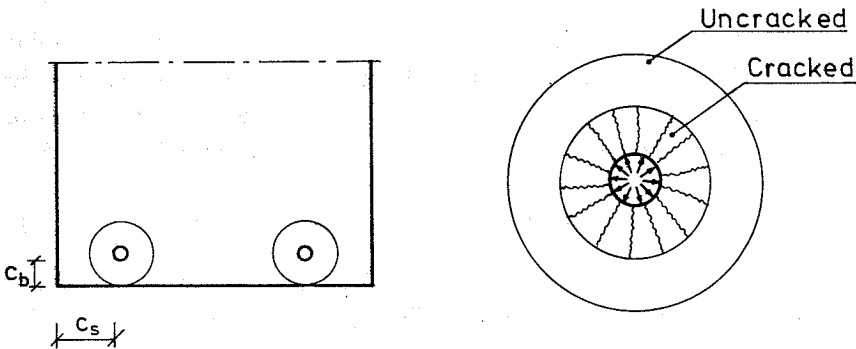
Figure 3.2: *Circle to take the radial stress from the bar to the concrete according to Orangon et al. [75.1] and [77.3].*

tioned reports [69.1] and [71.1] and the huge work done by Tepfers[1] [73.1], are discussed. It is mentioned that the transfer of stresses from a deformed reinforcing bar to the concrete is mainly derived from the mechanical locking of the lugs (the deformations) into the surrounding concrete. The resultant stress from the lugs is inclined at an angle β to the axis of the bar. The radial component of the stresses causes a splitting of the surrounding concrete at failure. The radial stress component is assumed to be carried by the surrounding concrete inside the circle indicated in figure 3.2 on the left.

The circle is determined from the minimum value of the side cover, c_s, and the bottom cover, c_b, in figure 3.2. For two bars lying next to each other – the lap splice case – similar conditions occur, but the circle is now an oval ring. Tepfers [73.1] has analysed the stresses in the circle by water pressure analogy. No attempt has yet been successful in analysing the stresses in the oval ring concrete cylinder analytically, but the problem is treated numerically in the literature.

Orangun et al. consider the main problem to be the determination of the angle β between the tangential and radial stress component from the lugs on the bar to the concrete. Tepfers' [73.1] theory for a partly cracked concrete circle, shown on the right in figure 3.2, is used to analyse the problem. It is found that the value of $\tan \beta$ can vary from 0.77 to 1.32, depending on the assumptions used. It is concluded that dealing with the anchorage problem

---

[1]Tepfers' work will be described below

analytically will be very difficult, because of the large variations. Therefore, it was decided to give up a theoretical approach in favour of an empirical one. Nonlinear regression analysis was carried out using various functions and test results from the literature. The best fitting curve has been found to be

$$\frac{\tau}{\sqrt{f_c}} = 0.10 + 0.27\frac{c_{min}}{d} + 4.40\frac{d}{l} + \frac{1}{41.5}\frac{A_{tr}f_{ys}n_s}{ld} \qquad (3.6)$$

where τ is the shear stress defined in (3.1), f_c is the uniaxial concrete compression strength measured in MPa. c_{min} is the minimum of c_b and c_s, d is the nominal bar diameter, l is the anchorage length, A_{tr} is the cross sectional area of the transverse reinforcement, which has an angle of 90 degrees with the failure surface, f_{ys} is the yield strength for the transverse reinforcement, and n_s is the number of transverse reinforcing bars over the anchorage length.

The contribution from the transverse reinforcement $\frac{A_{tr}f_{ys}n_s}{41.5ld}$ should always be less than or equal to 0.25.

The large amount of test results from Tepfers [73.1] is not included in the development of expression (3.6), but the expression is compared with the test results. It is found that the ratio between τ_{test} and τ_{theory} has a mean value and standard deviation of 1.18 and 0.32, respectively. The formula is somewhat conservative in this case. For the other tests included in the analysis the correspondence is satisfactory.

As previously mentioned the theoretical considerations on the strength of lap splices by Tepfers [73.1] and [82.4] will be discussed. The local stresses around a reinforcing bar anchored in a concrete body with the cover c_y is discussed first. c_y is the thinnest of the concrete covers appearing around the bar. Three different *stages* are considered:

I Uncracked elastic stage (ES)

II Partly cracked elastic stage (PCES)

III (Uncracked) plastic stage (PS)

The three situations are shown schematically in figure 3.3.
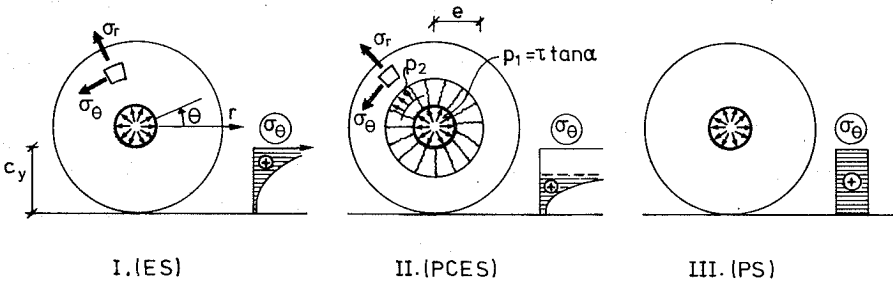
Figure 3.3: *The three stages in the local stresses around a reinforcing bar according to Tepfers [73.1].*

The shear stress τ is assumed, in the light of tests, to be evenly distributed over the anchorage length. The stresses from the reinforcement are assumed to be transferred to the concrete by a uniaxial compression which is inclined with an angle α to the axis of the bar in stages II (PCES) and III (PS). The radial component of the stresses is therefore $\tau \tan \alpha$. In stage I (ES) the concrete is uncracked and the properties of the concrete in tension and compression are equal and the angle α is therefore 45 degrees.

In the elastic stage the stresses in the concrete ring surrounding the reinforcement are calculated assuming the concrete to be elastic. According to Tepfers the solution in this case first appeared in the paper by Lamé & Clapeyron [1833]. The stress distribution in the ring direction is shown in principle in figure 3.3. The expressions for the stresses will not be given here.

In the second stage, the partly cracked elastic stage, it is still assumed that the concrete is an elastic material, but the concrete near the bar is assumed to be cracked, because the tensile strength is exceeded in the ring direction. The radial stresses from the bar are transferred through the cracked part of the concrete without redistribution of the stresses, i.e. $d\pi p_1 = 2e\pi p_2$, see figure 3.3. The ring stress σ_θ in the uncracked part is determined from the expressions appearing in the elastic stage, assuming σ_r equal to p_2 for $r = e$. The maximum value of σ_θ must be less than the tensile strength f_{ts}, which appears for $r = e$. Using this, the ratio $\frac{\tau \tan \alpha}{f_{ts}}$ can be written as a function of e, amongst others, and the maximum load carrying capacity is

then found by differentiating this expression with respect to e. Doing this, it is found that the optimal crack depth $e - d/2$ can be determined by

$$e = 0.486(c_y + \frac{d}{2}) \tag{3.7}$$

In the third stage, the plastic stage, the concrete is assumed to be a fully plastic material. The radial stress component of the stresses from the reinforcement is assumed to be $\tau \tan \alpha$ and the stress in the ring direction is assumed to be constant, and can be determined by

$$2c_y \sigma_\theta = d\tau \tan \alpha \tag{3.8}$$

The load carrying capacity according to the elastic stage corresponds to the cracks starting at the reinforcement and the partly cracked elastic stage corresponds to the cracks going right through the total concrete cover. It is mentioned that the full plastic stage is not to be expected. The load will probably be between the partly cracked elastic stage and the plastic stage, because the concrete will have some plastic deformations. Tests show that the cracking load in fact lies between these two stages and can be given by

$$\frac{\tau_{max} \tan \alpha}{f_{ts}} = 0.15 + 1.3\frac{c}{d} \tag{3.9}$$

where τ_{max} is used in the theory to distinguish between in which way the total load carrying capacity is to be determined.

Finite element calculations have been carried out to analyse the stress conditions and the variation of the angle α around the bar. The calculations were carried out, assuming the problem to be plane and the material to be fully elastic and without limitations in the tensile strength. It is concluded that α is approximately equal to 45 degrees at a line touching the top surface of the ribs in the cases which are dealt with. It is mentioned that the action would probably change if the tensile stresses were limited to the tensile strength; the angle α must be determined from tests.

In the case of surrounding reinforcement two stages are considered. The first stage covers the elastic, partly cracked elastic and plastic action of the surrounding concrete. In the second stage the concrete around the anchored bar has external longitudinal cracks.
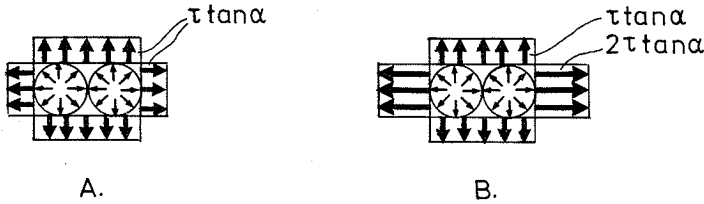
Figure 3.4: *Resultant bond stresses perpendicular to the axes of the bars in the splice for the two cases.*

In the first stage the force in the surrounding reinforcement is proportional to the expansion of the concrete. In the elastic stage the deformations of the concrete are very small, therefore the surrounding reinforcement has only little influence on the load carrying capacity. It is therefore concluded that at least internal cracking must appear. In the partly cracked elastic and plastic stage the strains are assumed to be $\varepsilon_{tu} \simeq 0.00015$ at the surface of the anchorage bar, which corresponds to the fact that the concrete in the cover is stressed up to ultimate tensile stress at cracking. The strain increases with the radius of the concrete ring. The strain in the surrounding reinforcement can be written as $\varepsilon_s = \varepsilon_{tu} \frac{2r}{d}$ assuming a complete bond between the steel and the concrete. The load carrying capacity is found by adding the contribution $\frac{2\varepsilon_s E_s A_{st} n}{l}$ from the reinforcement to the concrete contribution; the right hand side in equation (3.9).

In the second stage (external longitudinal cracks) the load is carried by the surrounding reinforcement and the concrete cantilevers. In this case the deformations are also small, otherwise the ribs on the reinforcement could not maintain the connection between the concrete and the steel. The surrounding reinforcement does not yield. Therefore it is the cross sectional area which is decisive and not the yield strength.

In the case of lap splices the concrete ring model used for one bar can not be used directly. Two cases, denoted A and B, respectively are considered, assuming the radial stress component $\tau \tan \alpha$ from the two bars in the splice to be equal. The two situations are illustrated in figure 3.4.

The difference between case A and B is that in A it is assumed that the
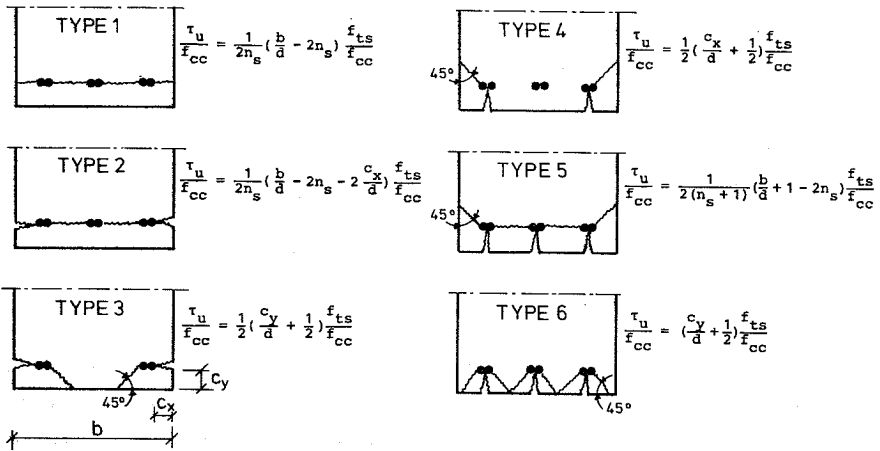
f_{cc}: cube compression strength for the concrete

f_{ts}: splitting strength for the concrete

n_s : number of splices in the section

Figure 3.5: *Failure patterns in beam sections with lapped splices without surrounding reinforcement according to Tepfers [73.1].*

stresses between the two bars have opposite directions, are equal and have the same inclination to the respective bar. Therefore they carry each other. In situation B it is assumed that no stresses carry one another and the horizontal stresses in figure 3.4, on the right, are therefore multiplied by 2.

The conclusion of the considerations and calculations is that B must be considered to be the most critical and is therefore used in the calculations. According to Tepfers these calculations and the conclusion are not as well founded as one could wish for.

Failure patterns in beam sections with lapped splices without surrounding reinforcement are then treated. By studying the failure patterns observed in tests, it is found that six types of failure patterns are to be considered, see figure 3.5. It is assumed that the angle α is constant, that the shear stress τ is evenly distributed and that the shear stresses in the two bars in a lap splice are equal.

In failure type 1 the stresses are evenly distributed over the beam width and equal to the splitting tensile strength of the concrete f_{ts}, see figure 3.6,
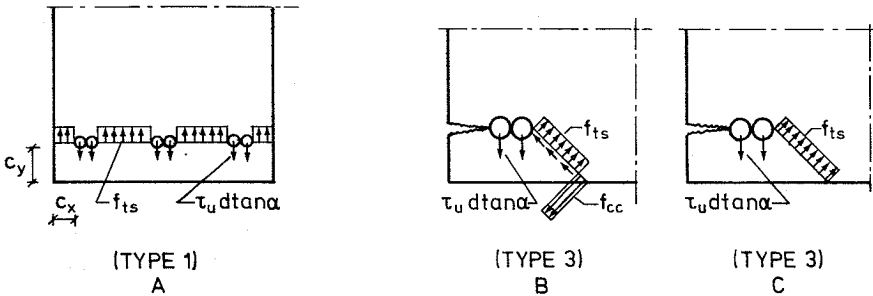
Figure 3.6: *Stress distribution in the failure lines*

which is also the case in failure type 2, except in the covers, where the stresses are assumed to be zero. The stress distribution in the skew failure lines in failure types 4 to 6 is first assumed to be as shown in figure 3.6.B

It is assumed that the stresses from the bars act vertically and that the cover acts like a cantilever. Tension, compression and shear stresses will therefore appear in the concrete cover. However, it is observed that the load carrying capacity for τ_u obtained from these assumptions is too low compared with test results. Furthermore, the expressions are too complicated for practical use. A uniform stress distribution as shown in figure 3.6.C is therefore used instead. Expressions for the ultimate load carrying capacity τ_u are set up for the six failure patterns. The expression for failure type 5 appears as the sum of failure types 2 and 4. For the cover ratio $\frac{c_x}{c_y}$ less than one, failure types 1, 2 or 3 are decisive and for $\frac{c_x}{c_y}$ larger than one, failure types 1, 4, 5, or 6 are decisive. The expression for the failure patterns can be used only if the concrete cover is cracked, because the concrete can then be considered to be in a plastic stage and accordingly it can be assumed that the shear stress is evenly distributed over the anchorage length. It must therefore be required that $\tau_u > \tau_{max}$, where τ_{max} is determined from (3.9), corresponding to the shear stress giving cracks in the concrete cover.

In the case of splices with surrounding reinforcement two models are used. In the first model the concrete is assumed to be active and the surrounding reinforcement is in an elastic or plastic stage. In the second model the concrete is assumed to be inactive and the surrounding reinforcement yields. The load carrying capacity is found by using the failure patterns from splices

without surrounding reinforcement with some modifications. The *largest* load obtained from the two models is used as the load carrying capacity.

In the first model the surrounding reinforcement has the same strain as the concrete when it is uncracked. When the concrete is cracked the surrounding reinforcement and the concrete act together until the cracks open. The stress in the surrounding reinforcement is therefore determined according to the following two principles: The surrounding reinforcement passes through a

- closed crack: The surrounding reinforcement follows the concrete, i.e. the stress in the reinforcement σ_{ss} can be determined as $E_s\varepsilon_{tu}$, which is valid just before the failure patterns develop. E_s is the modulus of elasticity for the reinforcement and ε_{tu} is the ultimate tensile strain for the concrete, which is taken as $\simeq 0.00015$

- open crack: The stress in the surrounding reinforcement is calculated by an equilibrium condition of moments. This situation is also assumed to be valid for the case where the reinforcement yields.

The expressions for the six failure patterns are almost like these for splices without surrounding reinforcement. The only difference is that an extra term, taking the surrounding reinforcement into account, is included.

In the second model it is assumed that no forces are absorbed by the concrete; the surrounding reinforcement alone carries the forces. The surrounding reinforcement is assumed to yield. The yield force in the surrounding reinforcement can be both less and larger than the force from the concrete and surrounding steel acting together.

Tests show that the strains in the main reinforcement are approximately linear just before failure when the concrete cover is cracked. This indicates that the stress approximately increases linearly from the unloaded end, which means the shear stress τ along the anchorage must be approximately uniformly distributed close to failure.

When the concrete is uncracked it is not certain that the shear stress is evenly distributed over the anchorage length. This situation is analysed by

the use of *Modulus of displacement theory*. Relatively simple expressions for the tensile stresses in the two bars, the shear stresses and the stresses in the concrete are shown to be valid. The stresses in the bars increase from zero in the unloaded end to their maximum value in the other end. The shear stress has a value other than zero in the unloaded end and, depending on the actual parameters, it will decrease, more or less, until a point before or equal to the middle of the anchorage length and it increases again in the loaded end.

Using the simple formulas to determine the stresses, yields a distribution of the stress in the reinforcement as described above. The shear stress distribution is more simple because it is symmetrical about the middle point of the anchorage length.

A combined theory for lapped splices, partly cracked with longitudinal cracks, is set up. The anchorage length is separated into different parts. In those parts where the concrete cover is cracked, the concrete is assumed to be in a plastic stage and the expressions for the failure patterns, shown in figure 3.5, are used to determine the load carrying capacity. The modulus of displacement theory is taken to be valid, in those parts of the splice, where no longitudinal cracks appear in the concrete cover. The load carrying capacity is therefore in general the sum of a plastic and an elastic part. The different parts can be found by assuming that the concrete is uncracked and the distribution of the stresses is found according to the modulus of displacement theory. If the shear stress is larger than the shear stress producing cracks in the concrete cover, given by expression (3.9) multiplied by $\frac{1}{2}$ [2], the length in which the concrete is assumed to be elastic is limited, so that the shear stress does not exceed this value. According to the simple expressions for the stresses appearing from the modulus of displacement theory, the shear stress has its maximal value at the ends of the splice. The cracks in the concrete cover are consequently initiated here, if they do appear.

This means three different situations can arise, as illustrated in figure 3.7

---

[2]Expression (3.9) is valid for one bar. In the case of lapped splices the expression must be multiplied by $\frac{1}{2}$ in accordance with the discussion in relation to figure 3.4.
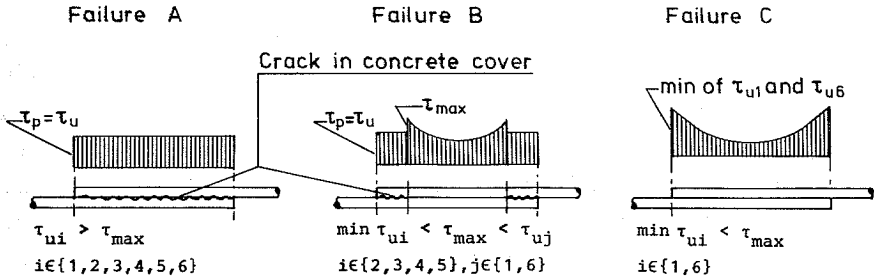
Figure 3.7: *The distribution of the shear stress along the anchorage length in a lap splice according to Tepfers [73.1].*

Failure A: The shear stresses in each of the six failure patterns, τ_{ui}, $i\epsilon\{1,2...6\}$, are all larger than τ_{max}. The concrete cover is cracked and the shear stress is assumed to be evenly distributed. The load carrying capacity is found to be the smallest load of the six failure patterns, i.e. $\tau_p = \min \tau_{ui}$ where $i\epsilon\{1,2...6\}$.

Failure B: The load carrying capacity τ_u from failure patterns 2, 3, 4 and 5 is less than τ_{max}, and τ_u from failure patterns 1 and 6 is larger than τ_{max}. The concrete is cracked at the ends of the splice and uncracked in the middle. In the cracked parts $\tau_p = \min \tau_{ui}$ where $i\epsilon\{2,3,4,5\}$ and in the uncracked part the expressions from the modulus of displacement theory are used with the maximal shear stress equal to τ_{max}.

Failure C: The shear stress from each of the six failure patterns, τ_{ui}, $i\epsilon\{1,2...6\}$, is in each case less than τ_{max}. The concrete cover will be uncracked and the modulus of displacement theory is used. The maximal shear stress is determined as the smallest of τ_u from failure patterns 1 and 6.

In the case of failure B stress distribution, the shear stress in the plastic cracked parts τ_p is less than the maximal shear stress in the elastic uncracked part $\tau = \tau_{max}$. This is because the stresses redistribute when the cover cracks and the average value is less than the peak value.

The theory for the strength of lapped splices is compared with a large amount of test results. Reasonable agreement between test and theory is found. The stress distribution in failures A and B is observed in the tests,

while failure C does not seem to appear, not in these tests at any rate. Design recommendations are set up in the light of the theory and the test treatment.

Many other problems than those discussed here are treated in Tepfers [73.1]. It will be too comprehensive to go through all these subjects, so for more details the reader is referred to Tepfers [73.1]. Tepfers' work is probably the largest step forward to a understanding of how the anchorage between concrete and deformed reinforcing bars takes place and how the stresses from the bars can be carried by the surroundings.

In the case of anchorage of supports Nielsen [74.1] has set up a simple formula to determine the load carrying capacity. It is assumed that the relationship between the shear stress along the anchorage length τ and the axial stress at the support r is a straight line. The axial stress at the support is defined as the reaction force divided by the support area. The connection between τ and r is written as

$$\tau = c' + \mu' r \tag{3.10}$$

where the constant c' can be considered to be the cohesion and μ' the coefficient of friction of the surface between steel and concrete. μ' must not be confused with μ' defined in chapter 2.

By comparing test results it is found that c' is mainly a function of the quality of the concrete and the type and diameter of the reinforcement. μ' is found to be a function of the number of bars over the support and the type of reinforcement. In the light of this, the relationship between the total tensile force in the reinforcement T_t and the reaction force R is obtained by

$$T_t = n\pi dl c' + n\pi \frac{d}{b}\mu' R \tag{3.11}$$

where n is the number of bars, d is the diameter of the bars, l is the anchorage length and b is the width of the beam.

Values for c' and μ' are given for different types of reinforcement. Using the values for Danish Kam steel and using τ and r instead of T_t and R, respectively, (3.11) can be rewritten into

$$\frac{\tau}{f_c} = \frac{0.95}{\sqrt{f_c}} + 0.7\frac{r}{f_c} \tag{3.12}$$

which is valid for n equal to 2. The concrete compression strength f_c is measured in MPa. For n equal to 1 the expression yields

$$\frac{\tau}{f_c} = \frac{0.95}{\sqrt{f_c}} + 1.4\frac{r}{f_c} \qquad (3.13)$$

These expressions are very simple, especially when the speak is about anchorage at supports, but they must be used with circumspection because only one test series is used to check their validity.

The anchorage problem has been dealt with by many authors using the *finite element method*. Amongst others Lutz [66.1] and [70.1], Eligehausen [79.2], Bodén [85.7], Nagatomo & Kaku [85.1], Tsubaki et al. [85.8], Furuuchi & Kakuta [86.5], Kærn [87.1], and Sorouschian et al. [87.6] have used it. One of the problems when using the finite element method is that only one case is treated for every calculation. When changing the geometri or the material properties, an entirely new calculation must be carried out. However, the method is very useful in supporting analytical calculations as a means of controlling whether the results obtained by the analytical calculations are satisfactory. In the writings of the authors mentioned above the concrete is assumed to be an elastic, elastic-plastic or plastic material. The results are of course influenced by this. Therefore the assumptions for a calculation must be examined before using the results.

The anchorage problem is treated as a *fracture mechanics* problem in Olsson [85.6] and [86.4]. The finite element method is also used here; several times for one calculation. An extension of the fictitious crack model is used as the basis for the calculations. Calculations are carried out for the specimen shown in figure 3.8.

The relative stress distribution in a horizontal section is illustrated in the figure for the two specimens, which are dealt with. As can be seen, the stress is practically evenly distributed in the case of small bar spacing and $\frac{\sigma}{f_t} \simeq 1$. In the case of large bar spacing, the stress σ is almost equal to f_t at the symmetrical line and decreases towards the bars. The fracture mechanics method is probably very useful, but it requires a large computer capacity[3].

---

[3]To get the stress distribution in the specimen with large bar spacing a finite element program was used 37 times.

I. Small bar spacing   II. Large bar spacing
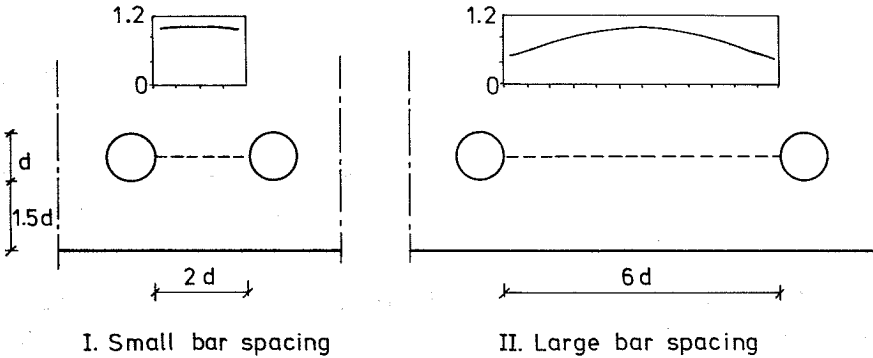
Figure 3.8: *Specimen and results from Olsson [85.6] and [86.4] The diagram shows the relative stress distribution in the section emphasized by a dotted line.*

In the Danish code of practice for the structural use of concrete, DS 411 [84.5], the anchorage length of deformed reinforcing bars is determined by

$$\frac{l}{d} \geq \begin{cases} \frac{0.09}{\zeta}\frac{f_y}{f_t} \\ \frac{30}{\zeta} \end{cases} \tag{3.14}$$

where the greater of the two values of l/d is taken. d is the diameter of the bar, ζ is the so called anchorage factor, f_y is the yield or 0.2 per cent proof-stress of the reinforcement and f_t is the tensile strength of the concrete. Assuming yielding in the reinforcement, expression (3.14) can be rewritten into

$$\frac{\tau}{f_c} \leq \begin{cases} \frac{\zeta}{0.36}\frac{f_t}{f_c} \\ \frac{\zeta}{120}\frac{f_y}{f_c} \end{cases} \tag{3.15}$$

A connection between f_t and f_c in DS411 is given by

$$f_t = \sqrt{\frac{f_c}{10}} \tag{3.16}$$

where f_t and f_c are measured in MPa. For $f_t \leq 0.003 f_y$ the upper expression in (3.15) will be decisive. Observing this and using (3.16) the expression for the shear stress can be written as

$$\frac{\tau}{f_c} = \zeta \frac{0.88}{\sqrt{f_c}} \tag{3.17}$$

The anchorage factor ζ is for ribbed, hot-rolled high yield bars in DS411 given to be between 0.8 and 0.9. Using $\zeta = 0.85$ and inserting this into (3.17) the expression for the anchorage load carrying capacity for deformed

bars can be written as

$$\frac{\tau}{f_c} = \frac{0.75}{\sqrt{f_c}} \tag{3.18}$$

If the stress σ_s in the reinforcement is less than f_y, the anchorage length may be reduced in the ratio $\frac{\sigma_s}{f_y}$. The anchorage length may be reduced further if a favourable effect from a reaction or from increased transverse reinforcement is shown to be present.

The theories and methods used to determine the anchorage strength of deformed reinforcing bars, which have been discussed here, are all valid for single cases or have been checked to be valid only in special cases. Hence it would be valuable to extend these theories to be valid in more cases or to develop a theory, taking into account the influence from the various parameters.

Chapter 4

Local Failure

The local failure around a deformed reinforcing bar is defined as the failure in the concrete immediately around the bar. The surroundings are not specified in detail, except for the assumption that they can deliver a certain resistance against failure and that they are axisymmetric in respect to the axis of the bar. In chapter 1 it is explained how the anchorage failure in a real structure is divided up into different failure types, and the names for the different types are given.

A model of a deformed reinforcing bar shown in figure 4.1 will be used in the calculations.

The ribs are assumed to be perpendicular to the longitudinal direction of the bar, and the angle between the bar axis and the surface of the ribs; κ in figure 4.1, is assumed to be 90 degrees. The consequence of this assumptions are discussed in section 4.4.

The adhesion and friktion between concrete and steel is disregarded. Be-
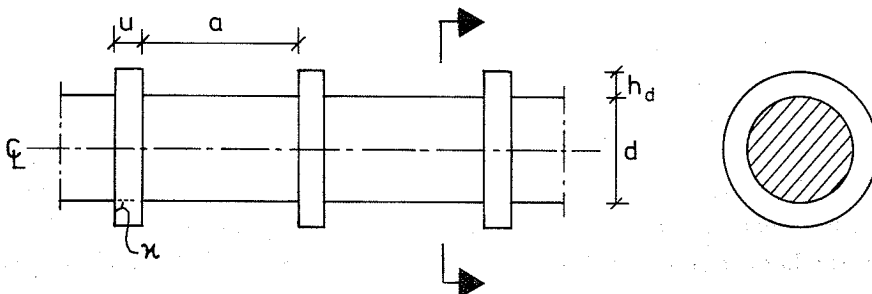
Figure 4.1: *Model of a deformed reinforcing bar.*
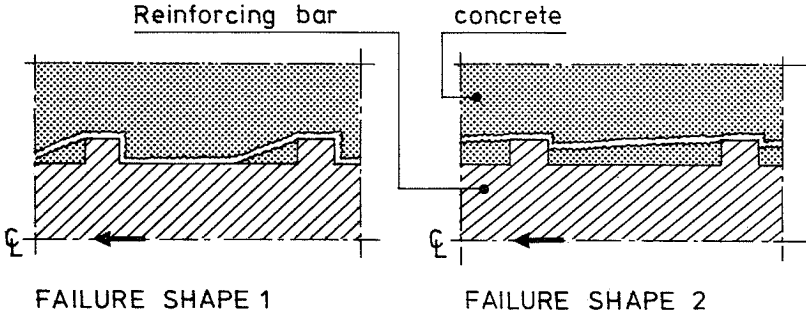
Figure 4.2: *Possible failure shapes at an axisymmetric failure around a deformed bar.*

cause of the deformations, there is a mechanical interaction between the concrete and the reinforcing bar. The local failure around a bar is considered to be axisymmetrical to the bar axis and, as previously mentioned, the surroundings are also considered to be axisymmetric to the bar axis.

An upper bound calculation for the local failure is given in section 4.1. In section 4.2 the corresponding lower bound solution is shown. Failure in the surroundings is treated in section 4.3 and in section 4.4 the different assumptions are discussed, amongst other things.

4.1 Upper Bound Solutions

The local failure depends on the strength of the surroundings. The strength of the surroundings is a function of the cover thickness, the concrete strength, the surrounding reinforcement, and stresses acting on the concrete surface, but many other parameters influence the strength. Possible failure shapes around a reinforcing bar are shown in figure 4.2.

The two types of considered failures are named *failure shape 1* and *failure shape 2*, see figure 4.2. In both failure types, concrete will be fixed to the bar in front of or between the ribs. There is a contribution to the dissipation only from the failure zones between concrete and concrete, not from the zones between concrete and steel. The displacement in the failure surfaces comes from a displacement of the bar in the direction of the force in the bar acting in the direction of the bar axis, and a displacement of the surrounding concrete in the direction perpendicular and axisymmetrical to
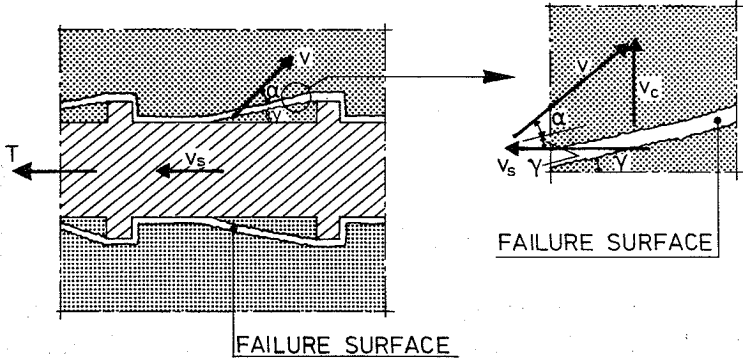
RELATIVE DISPLACEMENTS: v_s, $v = \dfrac{v_s}{\cos(\alpha+\gamma)}$, $v_c = v_s \tan(\alpha+\gamma)$

Figure 4.3: *Failure shape 1. Displacements of bar and surrounding concrete. The angle between the relative displacement v and the truncated cone is denoted by α (see chapter 2).*

the bar axis. The two failure types are treated separately. Firstly failure shape 1 is considered.

The displacement of the bar and the surrounding concrete, and the relative displacement in the yield surface are shown in figure 4.3.

The upper bound theorem is used. The external work can be found to be

$$W_E = T v_s \tag{4.1}$$

where T is the force in the reinforcement and v_s is the (increment of the) displacement of the reinforcement.

The internal work consists of two contributions, one from the concrete and one from the surroundings. The internal work can be written

$$W_i = \frac{1}{2} f_c (\lambda - \mu \sin\alpha) \frac{v_s}{\cos(\alpha + \gamma)} \frac{h_d}{\sin\gamma} \frac{\ell}{a + u} \pi(d + h_d) + W_{is} v_s \tan(\alpha + \gamma) \tag{4.2}$$

where W_{is} is the internal work from the surroundings, ℓ is the anchorage length and d, h_d, a and u are geometrical parameters for the bar, see figure 4.1. (4.2) is valid for $\cot\gamma \in [0; \frac{a}{h_d}]$ ($\gamma \in [\arctan(\frac{h_d}{a}); \frac{\pi}{2}]$).

From (4.1) and (4.2) the load carrying capacity for failure shape 1 can be obtained

$$\frac{\tau}{f_c} = D \frac{\lambda - \mu \sin\alpha}{\sin\gamma \cos(\alpha + \gamma)} + C \tan(\alpha + \gamma) \tag{4.3}$$

where

$$\frac{\tau}{f_c} = \frac{T}{\pi d \ell f_c} \tag{4.4}$$

$$C = \frac{W_{is}}{\pi d \ell f_c} \tag{4.5}$$

$$D = \frac{(d + h_d)h_d}{2d(a + u)} \tag{4.6}$$

τ can be considered as an evenly distributed shear stress over the anchorage length ℓ and around the diameter d. (4.3) must be minimized with respect to α and γ. It is first assumed that the optimum value for α is φ, the angle of friction for concrete. (4.3) is then differentiated with regard to γ, and the expression obtained is equated to zero. The optimum value for γ is found to be

$$\cot\gamma = \frac{1}{2\sqrt{k}} \left((k-1) + (k+1)\sqrt{1 + \sqrt{k}\frac{C}{D\nu}} \right) \tag{4.7}$$

where $k > 0$.

Differentiating (4.3) with respect to α and inserting $\alpha = \varphi$, yields the following expression

$$\frac{\partial}{\partial \alpha}\left(\frac{\tau}{f_c}\right)_{\alpha=\varphi} = \frac{D(\lambda\cos\varphi + \cot\gamma(\lambda\sin\varphi - \mu)) + C}{\cos^2(\varphi + \gamma)} \tag{4.8}$$

By inserting (4.7) into (4.8) it can be shown that (4.8) is always positive for possible values of the other parameters included in the expression.

The optimum expression for the load carrying capacity is then found by inserting $\alpha = \varphi$ and (4.7) into (4.3), which gives

$$\frac{\tau}{f_c} = \frac{D\nu}{k}\left[(k-1)\left(1 + \frac{\sqrt{k}}{2}\frac{C}{D\nu}\right) + (k+1)\sqrt{1 + \sqrt{k}\frac{C}{D\nu}}\right] \tag{4.9}$$

where $k > 0$.

Failure shape 2 is now considered. The failure pattern and the displacements are shown in figure 4.4.
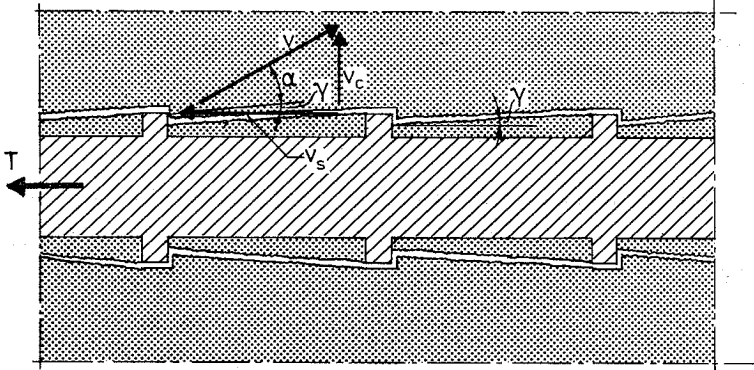
Figure 4.4: *Failure shape 2. Displacements of bar and surrounding concrete.*

The external work is again given by (4.1). The internal work can be found to be

$$W_i = \frac{1}{2}f_c(\lambda - \mu\sin\alpha)\frac{v_s}{\cos(\alpha+\gamma)}\frac{a}{\cos\gamma}\frac{\ell}{a+u}\pi(d+2h_d-a\tan\gamma)+W_{is}\tan(\alpha+\gamma)$$

(4.10)

valid for $\gamma \in [0, \arctan(\frac{h_d}{a})]$.

Using the upper bound theorem in (4.1) and (4.10) gives the following expression for the load carrying capacity for failure shape 2

$$\frac{\tau}{f_c} = (F - \frac{a}{2d}\tan\gamma)\frac{\lambda - \mu\sin\alpha}{\cos\gamma\cos(\alpha+\gamma)} + C\tan(\alpha+\gamma)$$

(4.11)

where

$$F = \frac{a}{a+u}\left(\frac{1}{2}+\frac{h_d}{d}\right)$$

(4.12)

(4.11) must be minimized with respect to α and γ. (4.11) is differentiated with respect to γ and γ is set equal to zero in this expression

$$\frac{\partial}{\partial\gamma}\left(\frac{\tau}{f_c}\right)_{\gamma=0} = \frac{\left(F\sin\alpha - \frac{a}{2d}\cos\alpha\right)(\lambda - \mu\sin\alpha)+C}{\cos^2\alpha}$$

(4.13)

It can be shown that (4.13) is larger than or equal to zero if

$$\frac{\rho}{\nu} \leq \frac{1}{k+1}\left(1 - \frac{1}{\sqrt{k}}\frac{a}{2Fd}\right)$$

(4.14)

which is satisfied for realistic values of the included parameters. (4.11) therefore has a minimum for $\gamma = 0$. Inserting $\gamma = 0$ into (4.11) and differentiating the expression with respect to α, the following applies

$$\sin\alpha = \frac{\mu - \frac{C}{F}}{\lambda}$$

(4.15)

α must be greater than or equal to φ. Using (4.15) this demand can be rewritten into

$$C \leq F(\mu - \lambda \sin \varphi) = \frac{2F\nu}{k+1}\left(1 - 2k\frac{\rho}{\nu}\right) \tag{4.16}$$

If (4.16) is not satisfied, the optimal expression for the load carrying capacity for failure shape 2 is found by inserting $\alpha = \varphi$ and $\gamma = 0$ into (4.11), giving

$$\frac{\tau}{f_c} = \frac{F\nu}{\sqrt{k}} + \frac{k-1}{2\sqrt{k}}C \tag{4.17}$$

This failure is named *failure shape 2a*. When (4.16) is satisfied, α is determined from (4.15). Inserting (4.15) and $\gamma = 0$ into (4.11) yields

$$\left(\frac{\tau}{f_c}\right)^2 + (C - F\mu)^2 = (F\lambda)^2 \tag{4.18}$$

from which τ can be found. This failure is named *failure shape 2b*.

In a diagram showing $\frac{\tau}{f_c}$ as a function of C, failure shape 2a consists of parallel straight lines for different values of $F\nu$, when k is taken as a constant. Failure shape 2b will, in the same diagram, consists of circles with center $(F\mu, 0)$ and radius $F\lambda$. The circles and the straight lines intersects for a value of C, which can be found using the equal sign in (4.16).

As can be seen from (4.9), (4.17) and (4.18) the effectiveness factor for the tensile strength ρ directly influences only the load carrying capacity in failure shape 2b. However, the intersection between failure shape 2a and 2b is also influenced by ρ.

In figure 4.5 the dimensionless shear stress $\frac{\tau}{F\nu f_c}$ is shown as a function of the dimensionless work from the surroundings $\frac{C}{F\nu}$. The intersection points between the failure shapes are also illustrated in the figure.

In the example in figure 4.5 failure shape 2b will not occur. This is the case when the intersection point between failure shape 1 and 2a, C_{1-2a}, is larger than the intersection point between 2a and 2b, C_{2a-2b}. This demand can be written as

$$\frac{\rho}{\nu} > \frac{1}{k+1}\left(1 + \frac{1}{4\sqrt{k}}\left(4\frac{D}{F} - \frac{F}{D}\right)\right) \tag{4.19}$$

Failure shape 1

$$\frac{\tau}{F \nu f_c} = \frac{1}{4} \frac{D}{F} \left(3 \left(1 + \frac{F}{D} \frac{C}{F\nu} \right) + 5 \sqrt{1 + 2 \frac{F}{D} \frac{C}{F\nu}} \right)$$

Failure shape 2a

$$\frac{\tau}{F\nu f_c} = \frac{1}{2} + \frac{3}{4} \frac{C}{F\nu}$$

Failure shape 2b

$$\left(\frac{\tau}{F\nu f_c} \right)^2 + \left(\frac{C}{F\nu} - \frac{\mu}{\nu} \right)^2 = \left(\frac{\lambda}{\nu} \right)^2$$

Intersection between 1-2a

$$\frac{C}{F\nu} = \frac{2}{25} \left(\frac{F}{D} - 4 \frac{D}{F} - 3 \right)$$

$$\frac{\tau}{F\nu f_c} = \frac{3}{50} \left(\frac{F}{D} - \frac{D}{F} - \frac{16}{3} \right)$$

Intersection between 2a-2b

$$\frac{C}{F\nu} = \frac{2}{5} \left(1 - 8 \frac{\rho}{\nu} \right)$$

$$\frac{\tau}{F\nu f_c} = \frac{4}{5} \left(1 - 3 \frac{\rho}{\nu} \right)$$
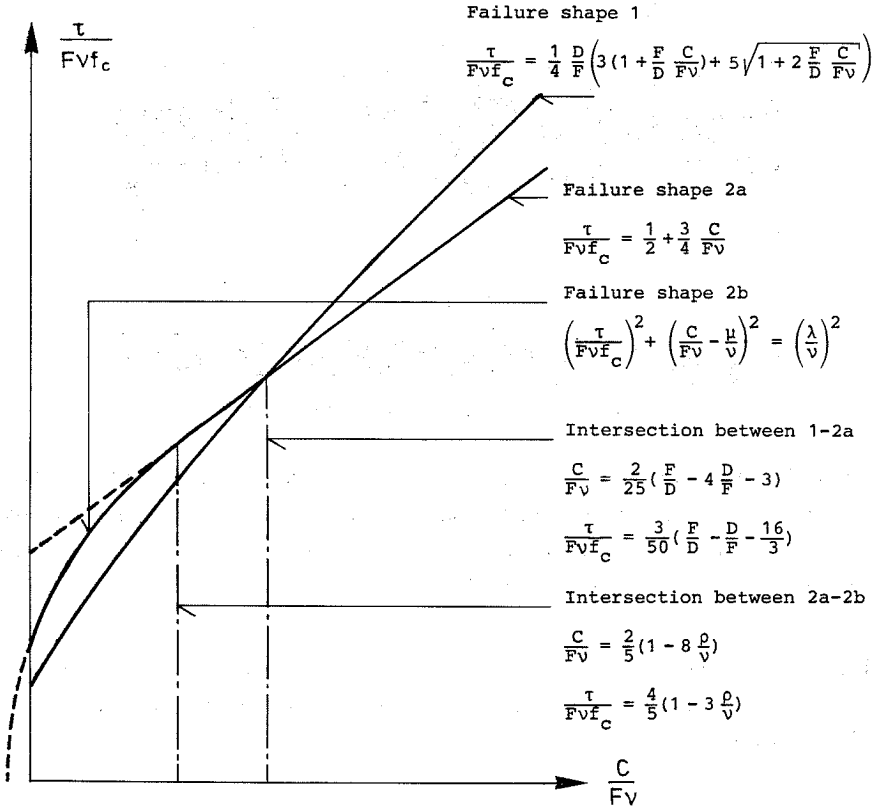
Figure 4.5: *The load carrying capacity as a function of the work from the surroundings.*
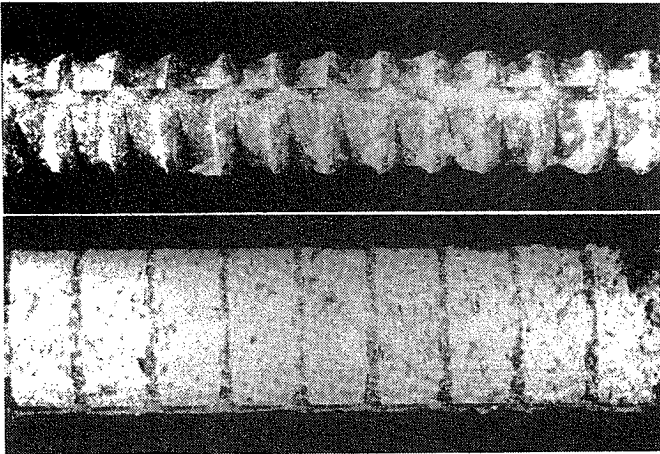
Figure 4.6: *Examples of failure around a deformed bar.*

Using failure shape 1, $\cot \gamma \in [0; \frac{a}{h_d}]$ must be satisfied, where $\cot \gamma$ is determined from (4.7). It can be shown that failure shape 1 not will be decisive in the situation where $\cot \gamma$ exceeds the limits, wherefore it is not neccessary to check if the requirement is fulfilled.

Examples of the two types of failure shapes are shown in figure 4.6. In the case of failure shape 2, it is impossible to say whether failure shape 2a or 2b has been active.

The local failure around a deformed reinforcing bar is now solved by means of an upper bound calculation. As can be seen from the expressions for failure shapes 1 and 2, (4.9), (4.17) and (4.18), the only problem left, if the load carrying capacity is to be determined, is to find the value of C, which is a measure of the work done in the surroundings. However, before going on to the problem of finding the value of C, the local failure will be treated by means of the lower bound theorem.

The expressions for the local failure found by using the upper bound theorem are also given in Hess [84.2] and Andreasen [84.3].
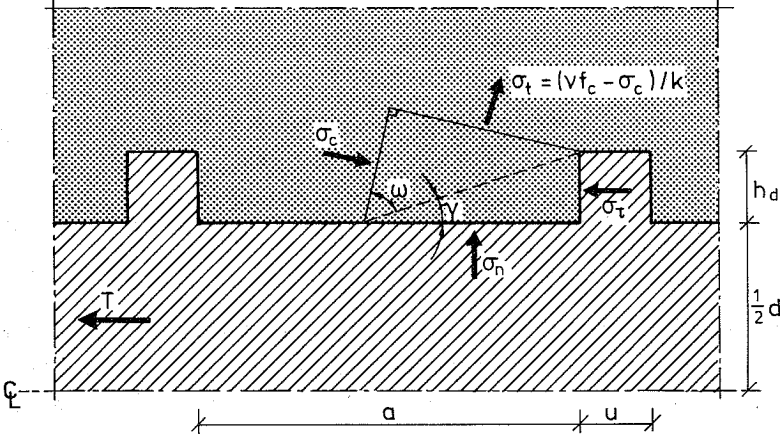
Figure 4.7: *Stress distribution for failure shape 1.*

4.2 Local Lower Bound Solutions

The same assumptions as those used in the upper bound calculations will also be used here. This means that only the local conditions around the bar are considered. The increase in area (volume) from the surface of the bar to the top of the ribs is taken into account, and the increase in area only immediately outside this peripheri is included. Therefore the formulas are valid only locally around the bar; thus the name *local failure*. The stresses in the surroundings have to be considered before the complete lower bound solution can be found.

A stress distribution as shown in figure 4.7 is considered. This stress distribution is shown to correspond to failure shape 1 from the previous section.

It is assumed that the stresses in the concrete are given by σ_c and σ_t, as shown in figure 4.7. The stresses in the reinforcement are given by σ_n and σ_r, as shown. The stresses are taken as positive in the directions indicated in the figure. In the calculation the evenly distributed shear stress τ will be used instead of σ_r. σ_t in the concrete is determined as a function of σ_c according to Coulomb's yield condition.

The connection between τ and σ_r is $\tau = 2D\sigma_r$, wherefore it is easy to transform the one stress to the other.

Horizontal and vertical equilibria for the triangle near the bar result in the following equations

$$\frac{1}{2}\frac{\tau}{D} - \sigma_t \frac{\sin\omega\cos(\gamma+\omega)}{\sin\gamma} - \sigma_c \frac{\sin\omega\sin(\gamma+\omega)}{\sin\gamma} = 0 \qquad (4.20)$$

$$\frac{1}{2}\frac{\sigma_n}{D} + \sigma_t \frac{\sin\omega\sin(\gamma+\omega)}{\sin\gamma} - \sigma_c \frac{\sin\omega\cos(\gamma+\omega)}{\sin\gamma} = 0 \qquad (4.21)$$

where D is given by (4.6).

These equations are similar to the normal transformation formulas when Mohr's circle is used, except that the increase in area has been taken into account. Inserting $\sigma_t = \frac{\nu f_c - \sigma_c}{k}$ into (4.20) and (4.21) and eliminating σ_c from these expressions gives

$$\frac{\tau}{D\nu f_c} = \frac{\frac{\sigma_n}{D\nu f_c}\left((k-1)\cot\gamma\tan\omega + \tan^2\omega + k\right) + 2\tan\omega\left(1 + \cot^2\gamma\right)}{\cot\gamma\left(\tan^2\omega + k\right) - (k-1)\tan\omega} \qquad (4.22)$$

This expression must be maximised with respect to the two parameters γ and ω. (4.22) is differentiated with regard to $\tan\omega$ and the expression obtained is equated to zero. The optimum value for $\tan\omega$ is found to be

$$\tan\omega = \sqrt{k} \qquad (4.23)$$

Differentiating (4.22) with respect to $\cot\gamma$, inserting (4.23) and equating the coefficient of differentiation to zero yields

$$\cot\gamma = \frac{1}{2\sqrt{k}}\left((k-1) + (k+1)\sqrt{1 + \sqrt{k}\frac{\sigma_n}{D\nu f_c}}\right) \qquad (4.24)$$

Inserting (4.23) and (4.24) into (4.22) gives

$$\frac{\tau}{f_c} = \frac{D\nu}{k}\left[(k-1)\left(1 + \frac{\sqrt{k}}{2}\frac{\sigma_n}{D\nu f_c}\right) + (k+1)\sqrt{1 + \sqrt{k}\frac{\sigma_n}{D\nu f_c}}\right] \qquad (4.25)$$

Comparing (4.25) with (4.9), shows that the lower and upper bound analyses result in the same expression for the load carrying capacity for the local failure around a deformed bar for failure shape 1 if $C = \frac{\sigma_n}{f_c}$.

The concrete compression stress σ_c, see figure 4.7, corresponding to (4.25) is given by

$$\frac{\sigma_c}{\nu f_c} = \frac{1}{2}\left[1 + \sqrt{1 + \sqrt{k}\frac{\sigma_n}{D\nu f_c}}\right] \qquad (4.26)$$
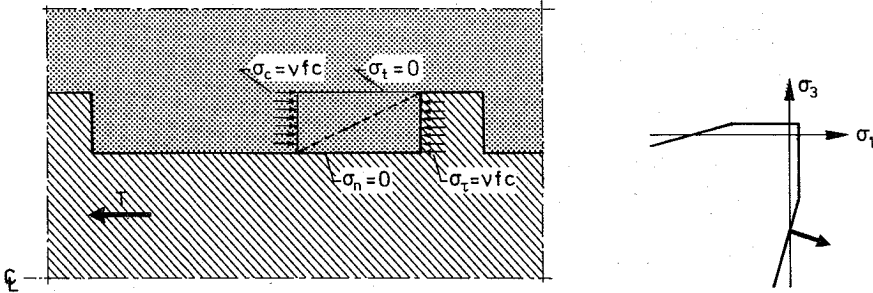
Figure 4.8: *Stresses in the concrete and the bar for $\sigma_n = 0$ in failure shape 1.*

As can be seen from (4.26), σ_c will always be larger than νf_c for $\sigma_n > 0$. Consequently σ_t will always be less than ρf_c.

For $\sigma_n = 0$, σ_c will be equal to νf_c and σ_t is equal to zero. $\cot \gamma$ is equal to $\sqrt{k}$ and the load carrying capacity is given by

$$\tau = 2D\nu f_c \tag{4.27}$$

(4.27) might be given the alternative form

$$\sigma_\tau = \nu f_c \tag{4.28}$$

This means that in the case of $\sigma_n = 0$ a uniaxial compression state appears. This is illustrated in figure 4.8.

In the previous calculations the stress in the ring direction, σ_θ, is not included. The equilibrium conditions used in setting up the formulas are correct, even when the ring stress has not been taken into account. The developed formulas are therefore theoretically correct. The ring stress σ_θ has to be considered, when the failure in the surroundings is to be treated, see section 4.3.

The stress distribution shown in figure 4.9, corresponding to failure shape 2 in section 4.1, is now considered.

Horizontal and vertical equilibria for the stresses shown in figure 4.9 give

$$\tau' - (\sigma_t + \sigma_c) \sin\omega \cos\omega = 0 \tag{4.29}$$

$$\sigma_n' + \sigma_t \cos^2 \omega - \sigma_c \sin^2 \omega = 0 \tag{4.30}$$
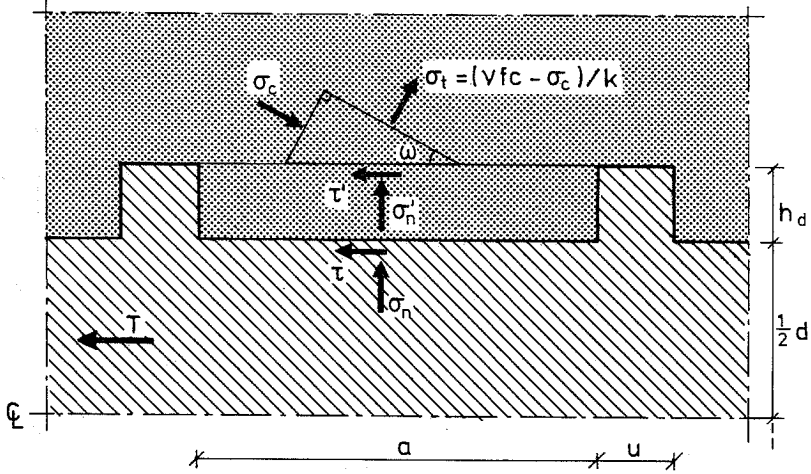
Figure 4.9: *Stress distribution for failure shape 2.*

The tensile stress σ_t has to satisfy

$$\sigma_t \leq \rho f_c \tag{4.31}$$

The stresses τ' and σ_n' can be transferred to the stresses τ and σ_n by

$$\tau = 2F\tau' \tag{4.32}$$

$$\sigma_n = 2F\sigma_n' \tag{4.33}$$

where F is given by (4.12).

Inserting (4.32), (4.33) and $\sigma_t = \frac{\nu f_c - \sigma_c}{k}$ into (4.29) and (4.30) and eliminating σ_c from the arrived expression gives

$$\frac{\tau}{2F\nu f_c} = \left((k-1)\frac{\sigma_n}{2F\nu f_c} + 1\right)\frac{\sin\omega \cos\omega}{\cos^2\omega + k\sin^2\omega} \tag{4.34}$$

(4.34) is differentiated with respect to ω and the expression obtained is equated to zero. The following is obtained

$$\omega = \frac{\pi}{4} - \frac{\varphi}{2} \tag{4.35}$$

Inserting (4.35) into (4.34) gives

$$\frac{\tau}{f_c} = \frac{F\nu}{\sqrt{k}} + \frac{k-1}{2\sqrt{k}}\frac{\sigma_n}{f_c} \tag{4.36}$$

which is identical with expression (4.17), failure shape 2a, for $C = \frac{\sigma_n}{f_c}$. (4.36) is valid when (4.31) is satisfied, which can be rewritten into

$$\frac{\sigma_n}{f_c} \geq \frac{2F\nu}{k+1}\left(1 - 2k\frac{\rho}{\nu}\right) \tag{4.37}$$

When (4.31) or (4.37) is satisfied by the equal sign, ω is not necessarily determined by (4.35). For $\sigma_t = \frac{\nu f_c - \sigma_c}{k} = \rho f_c$, ω can be calculated by inserting the expression for σ_c, found from (4.30), into the expression for σ_t. This results in the following expression

$$\sin^2\omega = \frac{1}{\lambda}\left(\frac{\sigma_n}{2Ff_c} + \rho\right) \tag{4.38}$$

Inserting (4.38) into (4.34) gives

$$\left(\frac{\tau}{f_c}\right)^2 + \left(\frac{\sigma_n}{f_c} - \mu F\right)^2 = (\lambda F)^2 \tag{4.39}$$

which can be seen to be similar to (4.18), failure shape 2b, if $C = \frac{\sigma_n}{f_c}$. (4.39) is valid for

$$\frac{\sigma_n}{f_c} < \frac{2F\nu}{k+1}\left(1 - 2k\frac{\rho}{\nu}\right) \tag{4.40}$$

The concrete compression stress σ_c corresponding to (4.36) and (4.39) can be found to be

$$\frac{\sigma_c}{\nu f_c} = \frac{1}{2}\left(1 + (k+1)\frac{\sigma_n}{2F\nu f_c}\right) \tag{4.41}$$

$$\frac{\sigma_c}{\nu f_c} = 1 - k\frac{\rho}{\nu} \tag{4.42}$$

(4.42) is valid for failure shape 2b, i.e. $\frac{\sigma_n}{\nu f_c} < \frac{2F}{k+1}(1 - 2k\frac{\rho}{\nu})$. The value of σ_c for failure shape 2b corresponds to $\sigma_t = \rho f_c$. The compression stress increases for increasing values of σ_n for failure shape 2a, and for $\frac{\sigma_n}{\nu f_c} = \frac{2F}{k+1}(1 - 2k\frac{\rho}{\nu})$ σ_c is equal to σ_c for failure shape 2b. This is illustrated in figure 4.10.

The load carrying capacity τ as a function of σ_n and Coulomb's failure condition are shown in figure 4.10. The correspondence between failure type and the value of the stresses in the concrete σ_c and σ_t are illustrated. Failure type 2b can be called a tensile failure, while type 2a can be called a compression failure. For $\frac{\sigma_n}{\nu f_c} > \frac{1}{k+1}$ failure shape 2a is decisive and there must be a three dimensional compression stress distribution in the concrete, because the failure condition has to be fulfilled. In fact σ_c and σ_t are
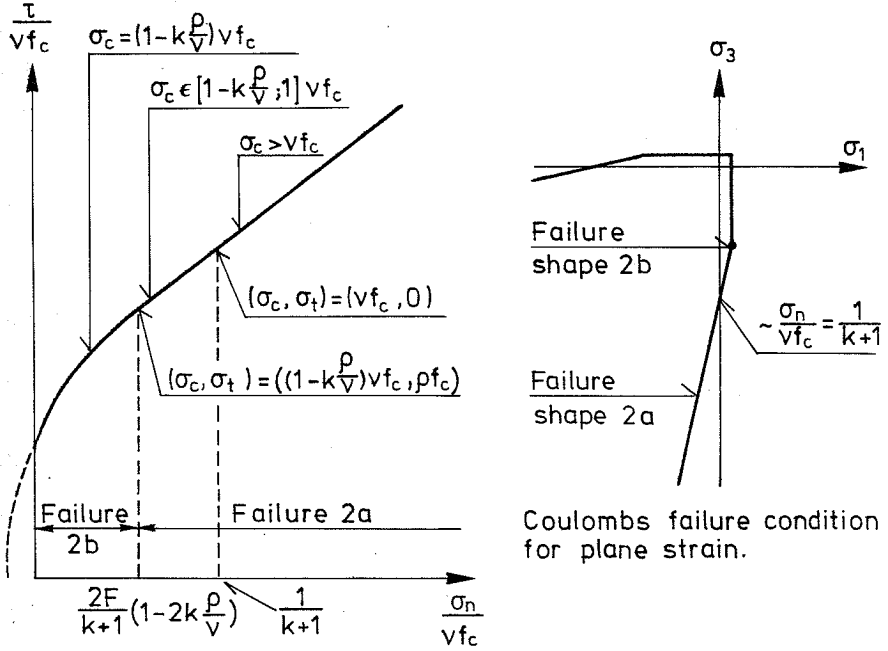
Figure 4.10: *The load carrying capacity $\left(\frac{\tau}{\nu f_c}\right)$ as a function of $\left(\frac{\sigma_n}{\nu f_c}\right)$ and Coulomb's failure condition for plane strain.*
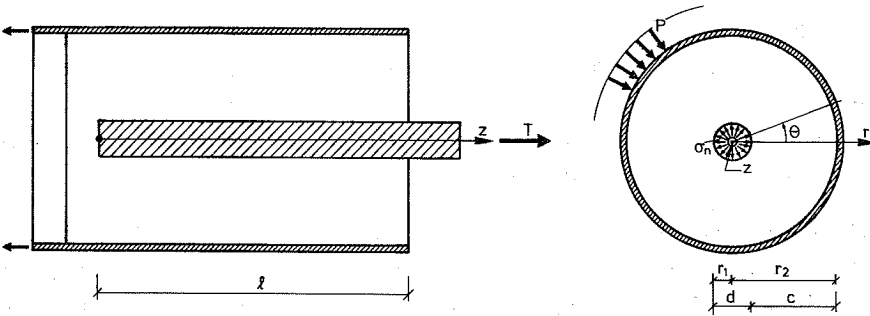
Figure 4.11: *Anchorage of a bar in a circular concrete body surrounded by a steel ring.*

compression stresses. The third primary stress σ_θ is not now known, but in this case it has to be a compression stress.

In failure shape 1 there will also be a three dimensional stress condition in the concrete near the bar. Hence σ_θ is also, in this case, a compression stress. The problem concerning the ring stress will be discussed in the following section 4.3.

As previously mentioned, there is agreement between the expressions for the load carrying capacity found from the upper and lower bound calculations, if the dimensionless internal work C from the surroundings is equal to $\frac{\sigma_n}{f_c}$. This indicates that the dimensionless internal work C and the internal dimensionless pressure $\frac{\sigma_n}{f_c}$ in principle are equal quantities. This is investigated in the next section.

4.3 Failure in the surroundings

Anchorage of a deformed reinforcing bar in an axisymmetrical body will be considered first. Afterwards the application of the theory for the axisymmetrical local failure in practical cases is discussed, because anchorage of a bar in a structure appearing in practice is not necessarily an axisymmetrical problem.

The problem considered is shown in figure 4.11.

A reinforcing bar is anchored in an axisymmetrical concrete body surrounded by a steel ring. The diameter of the bar is named d, the concrete cover c and the anchorage length ℓ. The anchorage length is assumed to be so long that it is not necessary to consider the special conditions at the end section, near the force. The steel ring delivers a radial stress p at failure where it yields in the ring direction.

Cylinder coordinates r, θ, z are used as shown in figure 4.11. According to the assumption made, the stresses are independent of z; wherefore polar coordinates r, θ can be used. In the case of axisymmetrical surroundings, the equilibrium conditions can be written

$$\frac{\partial \sigma_r}{\partial r} + \frac{\sigma_r - \sigma_\theta}{r} = 0 \tag{4.43}$$

$$\frac{\partial \tau_{rz}}{\partial r} + \frac{\tau_{rz}}{r} = 0 \tag{4.44}$$

assuming that the mass density of the body is zero. The stresses $\tau_{r\theta}$ and $\tau_{\theta z}$ are zero. The geometrical conditions, the strain-displacement relations, are in this case given by

$$\varepsilon_r = \frac{\partial u_r}{\partial r} \tag{4.45}$$

$$\varepsilon_\theta = \frac{u_r}{r} \tag{4.46}$$

$$\gamma_{rz} = 2\varepsilon_{rz} = \frac{\partial u_z}{\partial r} \tag{4.47}$$

and $\varepsilon_z = \varepsilon_{r\theta} = \varepsilon_{\theta z} = 0$ (because $\frac{\partial ()}{\partial z} = 0, \frac{\partial ()}{\partial \theta} = 0$ and $u_\theta = 0$).

As can be seen from the equilibrium condition (4.43), the ring stress σ_θ has to be taken into account.

The constitutive equations can be written

$$k\sigma_t + \sigma_c - \nu f_c = 0 \quad \sigma_t \geq \sigma_\theta \geq -\sigma_c \tag{4.48}$$

$$k\sigma_\theta + \sigma_c - \nu f_c = 0 \quad \sigma_\theta \geq \sigma_t \geq -\sigma_c \tag{4.49}$$

σ_t and σ_θ are positive as tension and σ_c is positive as compression. σ_t and σ_c are the main stresses in the r, z plan, see figure 4.7. Because the concrete is assumed to be a modified Coulomb material, the stresses σ_t and σ_θ must be less than the tensile strength of the concrete, ρf_c.

Using the normality condition in (4.48) and (4.49) gives the following strains (strain rates)

$$\varepsilon_t = k\lambda_1 \ , \ \ \varepsilon_\theta = 0 \ , \ \ \varepsilon_c = -\lambda_1 \ \ (\lambda_1 \geq 0) \tag{4.50}$$

$$\varepsilon_t = 0 \ , \ \ \varepsilon_\theta = k\lambda_2 \ , \ \ \varepsilon_t = \lambda_2 \ \ (\lambda_2 \geq 0) \tag{4.51}$$

The yield surface has an edge where (4.48) and (4.49) intersect. In this case a condition for the strains can be found from (4.50) and (4.51)

$$\varepsilon_t + \varepsilon_\theta + k\varepsilon_c = 0 \tag{4.52}$$

In the calculations below it is assumed that the local failure is failure shape 2, and that F, given by (4.12), is equal to $\frac{1}{2}$. Expressions for the load carrying capacity of the surroundings, using the lower bound theorem, will be set up first.

For an arbitrary point r, θ, z equations (4.29) and (4.30) can be written

$$\tau_{rz} - (\sigma_t + \sigma_c)\sin\omega_r \cos\omega_r = 0 \tag{4.53}$$

$$- \sigma_r + \sigma_t \cos^2\omega_r - \sigma_c \sin^2\omega_r = 0 \tag{4.54}$$

The angle ω_r is in general a function of r. For $r = r_1 = \frac{1}{2}d$, ω_r must be equal to ω obtained in section 4.2.

Inserting (4.48) into (4.54) gives

$$\sigma_c = \frac{-k\sigma_r + \nu f_c \sin^2\omega_r}{\cos^2\omega_r + k\sin^2\omega_r} \tag{4.55}$$

Inserting this expression into (4.49) gives an expression for σ_θ

$$\sigma_\theta = \frac{\sigma_r + \nu f_c \sin^2\omega_r}{\cos^2\omega_r + k\sin^2\omega_r} \tag{4.56}$$

(4.43) can now be rewritten by inserting (4.56)

$$\frac{\partial\sigma_r}{\sigma_r - \frac{\nu f_c}{k-1}} = -K_r \frac{\partial r}{r} \tag{4.57}$$

where

$$K_r = \frac{(k-1)\sin^2\omega_r}{\cos^2\omega_r + k\sin^2\omega_r} \tag{4.58}$$

Assuming that K_r is independent of r and using the fact that $\sigma_r = -\sigma_n$ for $r = r_1 = \frac{1}{2}d$ gives

$$\sigma_r = -\left(\sigma_n + \frac{\nu f_c}{k-1}\right)\left(\frac{r_1}{r}\right)^{K_r} + \frac{\nu f_c}{k-1} \tag{4.59}$$

Using the fact that $\sigma_r = -p$ for $r = r_2 = c + \frac{1}{2}d$ gives the following expressions for σ_n

$$\frac{\sigma_n}{\nu f_c} = \left(\frac{p}{\nu f_c} + \frac{1}{k-1}\right)\eta^{\frac{k-1}{2k}} - \frac{1}{k-1} \tag{4.60}$$

where K_r is determined by setting ω_r equal to ω (see section 4.2) and assuming that failure shape 2a is decisive, i.e. $\omega_r = \omega = \frac{\pi}{4} - \frac{\varphi}{2}$. η in (4.60) is given by

$$\eta = \frac{r_2}{r_1} = 1 + 2\frac{c}{d} \tag{4.61}$$

Inserting (4.60) into (4.59) and inserting this expression into (4.56) gives

$$\frac{\sigma_\theta}{\nu f_c} = \frac{1}{k-1}\left(1 - \frac{k+1}{2k}\left(1 + (k-1)\frac{p}{\nu f_c}\right)\left(\frac{\eta}{\frac{r}{r_1}}\right)^{\frac{k-1}{2k}}\right) \tag{4.62}$$

$\frac{\sigma_\theta}{\nu f_c}$ is shown as a function of $\frac{r}{r_1}$ for different values of $\eta = \frac{r_2}{r_1}$ and $\frac{p}{\nu f_c}$ in figure 4.12.

As it is seen in figure 4.12 σ_θ is in some cases negative in a zone near the bar and increases with the distance to the bar. If the tensile strength ρf_c is less than $\frac{\nu f_c}{2k}$ the expressions may be wrong, because σ_θ must be less than or equal to the tensile strength. Requiring $\sigma_\theta \leq \rho f_c$ for $\frac{r}{r_1} = \eta = 1$ gives

$$\frac{p}{\nu f_c} \geq \frac{1}{k+1}\left(1 - 2k\frac{\rho}{\nu}\right) \tag{4.63}$$

For $\frac{\rho}{\nu} = 0.1$ and $k = 4$ (4.63) gives $\frac{p}{\nu f_c} \geq 0.04$. In this case σ_θ will not exceed the tensile strength.

It is possible to set up the correct solution taking account of the limited tensile strength, combined with the solution given above, but this will not be done here. Instead, a solution will be given in the case where σ_θ is equal to the tensile strength ρf_c, for all values of r.

Inserting $\sigma_\theta = \rho f_c$ into (4.43) and requiring $\sigma_r = -\sigma_n$ for $r = r_1$ gives

$$\frac{\sigma_r}{\nu f_c} = \left(-\frac{\sigma_n}{\nu f_c} - \frac{\rho}{\nu}\right)\frac{r_1}{r} + \frac{\rho}{\nu} \tag{4.64}$$
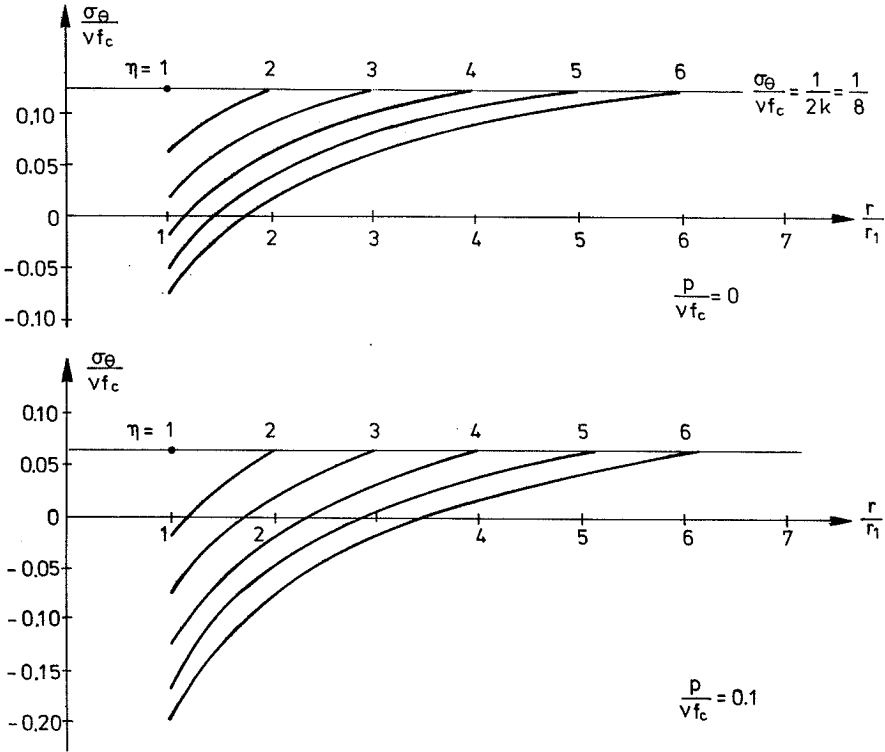
Figure 4.12: $\frac{\sigma_\theta}{\nu f_c}$ (4.62) as a function of $\frac{r}{r_1}$ for different values of η and $\frac{p}{\nu f_c}$. The material parameter k is taken as 4.

Using that $\sigma_r = -p$ for $r = r_2$ gives the following expressions for σ_n

$$\frac{\sigma_n}{\nu f_c} = \left(\frac{p}{\nu f_c} + \frac{\rho}{\nu}\right)\eta - \frac{\rho}{\nu} \tag{4.65}$$

The following symbols are introduced

$$\mathbf{T} = \frac{\frac{\tau}{\nu f_c}}{1 - (k-1)\frac{\rho}{\nu}} \tag{4.66}$$

$$\mathbf{P} = \frac{\frac{p}{\nu f_c} + \frac{\rho}{\nu}}{1 - (k-1)\frac{\rho}{\nu}} \tag{4.67}$$

Inserting (4.65) into the expression for failure shape 2b (4.18) or (4.39) using (4.66) and (4.67) gives

$$\mathbf{T} = \sqrt{\eta \mathbf{P}(1 - \eta \mathbf{P})} \tag{4.68}$$
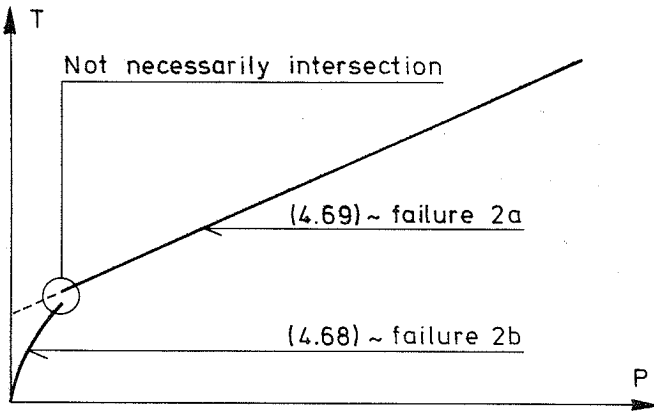
Figure 4.13: $\mathbf{T}$ *as a function of* $\mathbf{P}$ *for the lower bound solution.*

where $F = \frac{1}{2}$ has been used.

Similarly (4.60) is inserted into the expression for failure shape 2a (4.17) or (4.36) which returns the following expression

$$\mathbf{T} = \frac{1}{2\sqrt{k}}\eta^{\frac{k-1}{2k}}(1 + (k-1)\mathbf{P}) \qquad (4.69)$$

Figure 4.13 shows the principle in expression (4.68) and (4.69).

As is seen in the figure, the two curves do not in all cases intersect. This is certainly because (4.69) is not valid in the cases where σ_θ exceeds the tensile strength.

It must be mentioned that it is not necessary to insert the expressions for σ_n into the expressions for the local failure, if different solutions are to be compared. σ_n can be compared directly.

An upper bound solution will now be given. It is assumed that the displacement of the surrounding concrete at the edge of the reinforcement is δ. The external work can then be written as

$$W_e = 2\pi r_1 \sigma_n \delta \qquad (4.70)$$

The internal work in the concrete is generally given by

$$W_i = \int_0^{2\pi} \int_{r_1}^{r_2} (\sigma_t \varepsilon_t + \sigma_\theta \varepsilon_\theta + (-\sigma_c)\varepsilon_c) r \, d\theta \, dr \qquad (4.71)$$

Using (4.48), (4.49) and (4.52), this can also be written as

$$W_i = 2\pi \frac{\nu f_c}{k} \int_{r_1}^{r_2} (\varepsilon_t + \varepsilon_\theta) r \, dr \tag{4.72}$$

the fact that ε_t and ε_θ are independent of θ, is used here.

The following displacement is used

$$u_r = \delta \tag{4.73}$$

which by (4.45) and (4.46) gives the strains

$$\varepsilon_r = 0 \quad , \quad \varepsilon_\theta = \frac{\delta}{r} \tag{4.74}$$

Assuming $\varepsilon_t = \varepsilon_c = 0$ and $\sigma_\theta = \rho f_c$ the internal work is found using (4.71)

$$W_i = 2\pi \rho f_c (r_2 - r_1)\delta + 2\pi p r_2 \delta \tag{4.75}$$

Using the upper bound theorem on (4.70) and (4.75) gives the following expression for σ_n

$$\frac{\sigma_n}{\nu f_c} = \left(\frac{p}{\nu f_c} + \frac{\rho}{\nu} \right) \eta - \frac{\rho}{\nu} \tag{4.76}$$

Comparing (4.76) with (4.65) shows that the upper and lower bound solutions are equal in this case. Therefore the same solution is obtained when (4.76) is inserted into (4.18) or (4.39), as with the lower bound solution, i.e.

$$\mathbf{T} = \sqrt{\eta \mathbf{P}(1 - \eta \mathbf{P})} \tag{4.77}$$

Inserting (4.76) into (4.17) or (4.36) gives

$$\mathbf{T} = \frac{1}{2\sqrt{k}}(1 + (k-1)\eta \mathbf{P}) \tag{4.78}$$

The intersection point between (4.77) and (4.78) can be found from the intersection point between failure shape 2a and 2b, see section 4.1 and 4.2

$$\mathbf{P} = \frac{1}{\eta(k+1)} \tag{4.79}$$

$$\mathbf{T} = \frac{\sqrt{k}}{k+1} \tag{4.80}$$

$\mathbf{T}$ given by (4.80) is a constant. For $k = 4$, $\mathbf{T}$ is equal to $\frac{2}{5}$.

The displacement u_r is now given by

$$u_r = \delta \left(\frac{r_1}{r}\right)^{\frac{1}{k}} \tag{4.81}$$

The internal work is found by using (4.45), (4.46) and (4.72) to

$$W_i = 2\pi r_1 \delta \nu f_c \left[\left(\frac{p}{\nu f_c} + \frac{1}{k-1}\right)\eta^{\frac{k-1}{k}} - \frac{1}{k-1}\right] \tag{4.82}$$

The upper bound solution is then found to be

$$\frac{\sigma_n}{\nu f_c} = \left(\frac{p}{\nu f_c} + \frac{1}{k-1}\right)\eta^{\frac{k-1}{k}} - \frac{1}{k-1} \tag{4.83}$$

Comparing (4.83) with (4.60) shows they are almost identical. The only difference is a factor $\frac{1}{2}$ in the exponent on η.

Using the displacement (4.81), the strain rate ε_r is found to be negative and ε_θ is found to be positive. Compared with the lower bound solution given by (4.60), it can be seen from (4.62) and figure 4.12 that σ_θ is negative near the bar, especially when p is large, which is the case when (4.83) is decisive. This means that, if the lower or upper bound solutions are assumed to be correct with respect to these conclusions, there is a negative stress and a positive strain, which is in agreement with the yield condition and the associated flow rule. The principle in this part of the solution is therefore probably correct.

Inserting (4.83) into the expression for failure shape 2a gives

$$\mathbf{T} = \frac{1}{2\sqrt{k}}\eta^{\frac{k-1}{k}}(1 + (k-1)\mathbf{P}) \tag{4.84}$$

In figure 4.14 the load carrying capacity found by the upper bound theorem is illustrated.

The displacements given in (4.73) and (4.81) have also been used by Exner [83.1]. Exner has not divided the failure into a local failure and a failure in the surroundings, but the principle in the calculations is the same as used here. Exner has also treated the same problem using the slipline theory and he has found a correct solution to the problem using this method.

In figures 4.15 – 4.18 the upper and lower bound solutions given here are shown together with Exner's [83.1] correct solution for different values of $\eta = \frac{r_2}{r_1}$.
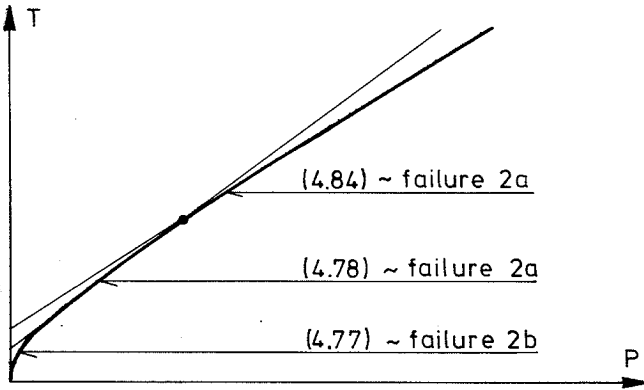
Figure 4.14: **T** *as a function of* **P** *for the upper bound solution.*

Exner's correct solution is composed of an ellipse and a straight line connected by a curve. The ellipse is given by the same expression as found here by the lower and upper bound calculations. The straight line goes through $(\mathbf{P}, \mathbf{T}) = (-\frac{1}{k-1}, 0)$. Unfortunately no analytical expressions is given for the straight line and the curve.

From the figures 4.15 – 4.18 it can be seen that the lower and upper bound solutions describe the correct load carrying capacity fairly well. The absolute error increases with increasing value of $\eta = \frac{r_2}{r_1}$ and **P**, but the relative error is constant for **P** larger than approximately 0.5. For small values of **P** the lower and upper bound solutions are equal and therefore correspond to the correct load carrying capacity in this area. For the special case $\eta = 1(\eta = 1^+)$, the lower and upper bound solutions are equal for all values of **P**, wherefore the given expressions in this case represent the correct load carrying capacity.

The lower bound solution (4.60) can probably be improved by allowing the angle ω_r to vary with r, and not considering it to be a constant. The difference between the upper bound solution and the correct solution is certainly due to the fact that the expressions for the local failure do not include a displacement in the concrete in the direction of the bar axis, u_z. The concrete is assumed to move perpendicularly and axisymmetrically away from the bar. Including u_z in the calculations for the local failure shows that in
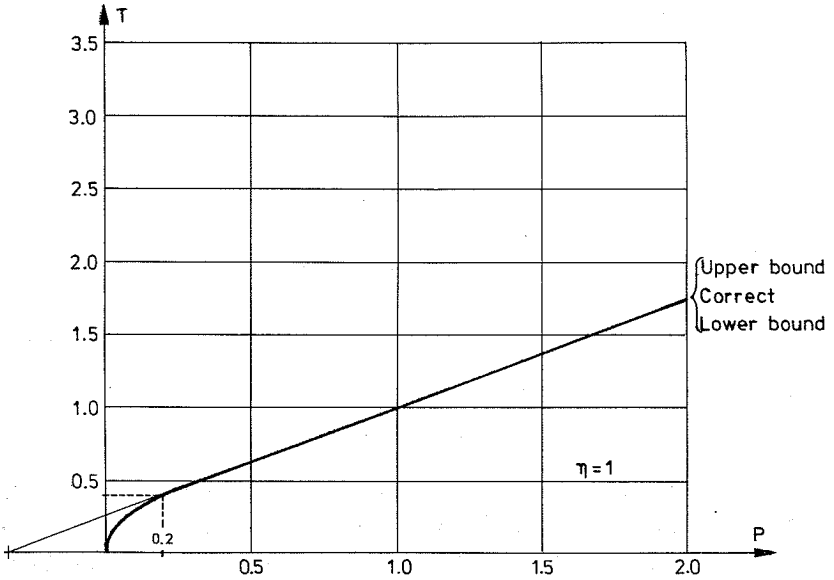
Figure 4.15: *The lower bound, the upper bound and the correct solution for $\eta = 1$ $(\eta \to 1)$.*
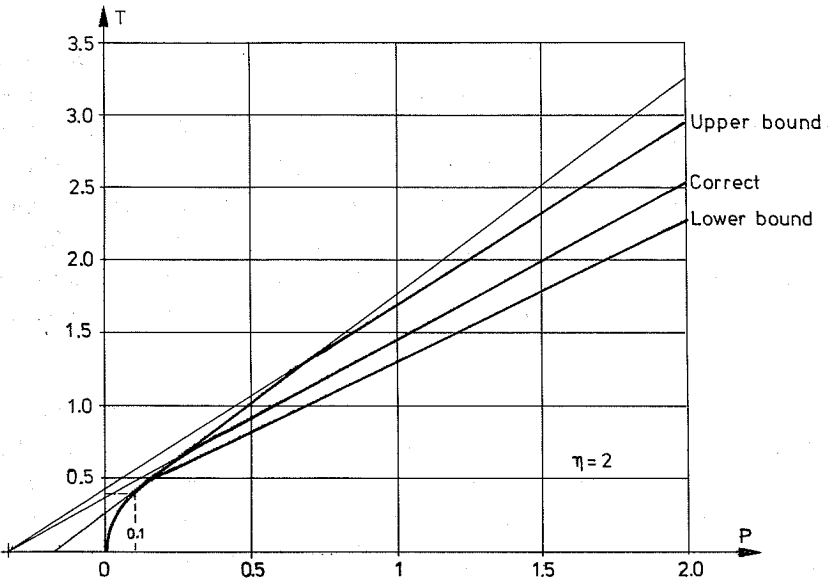
Figure 4.16: *The lower bound, the upper bound and the correct solution for $\eta = 2$.*
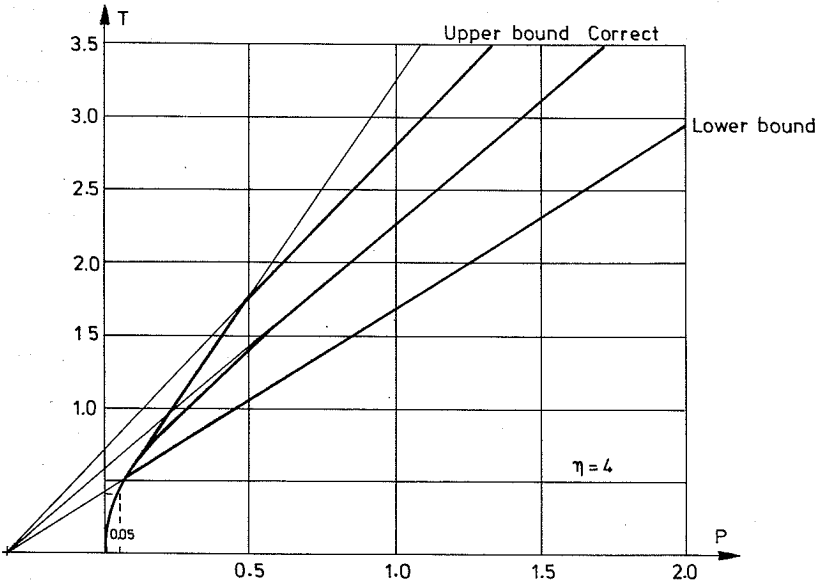
Figure 4.17: *The lower bound, the upper bound and the correct solution for $\eta = 4$.*
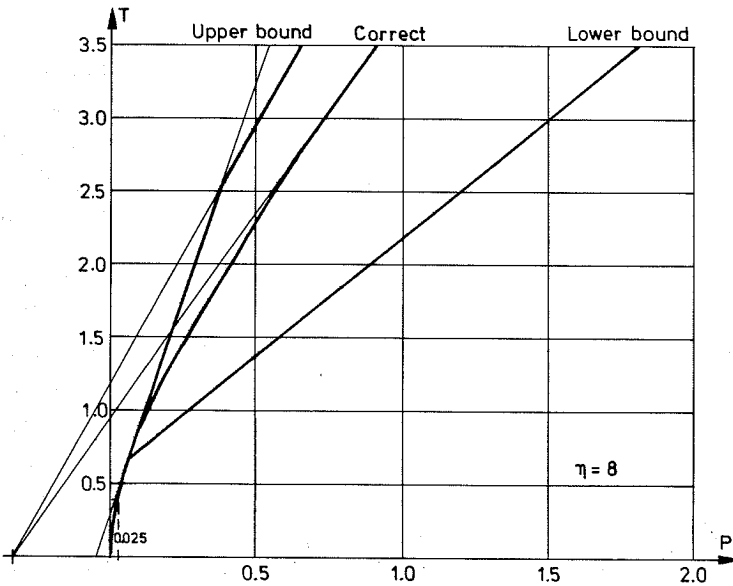
Figure 4.18: *The lower bound, the upper bound and the correct solution for $\eta = 8$.*

the case of failure shape 2b, the optimal displacement condition appear, to be the one where the concrete is displaced axisymmetrically and perpendicularly to the bar axis. As can also be seen in figures 4.15 - 4.18, the correct solution is obtained in the case where failure shape 2b is used.

Taking into account the displacement u_z in the concrete will probably improve the upper bound solution, but the calculations and the expressions will be more complicated than they are already. Hence more details will not be given.

Considering figures 4.15 - 4.18, it can be seen that the correspondence between the upper bound solution and the correct solution is fairly good, especially for small values of **P** and **T**. In practice **T** is less than approximately 1.5 and as can be seen, it is normally the constant displacement field (4.73) which is decisive for **T** fulfilling this. This indicates that upper bound solutions for the load carrying capacity can in practice be found by using a constant displacement field, i.e. a displacement field where the concrete is displaced axisymmetrically and perpendicularly to the bar axis with a constant displacement.

In most of the calculations and expressions in this section a value for the rib parameter F equal to $\frac{1}{2}$ has been used. This is not always satisfied in practice but it is a good approximation. The main conclusion from the calculations will not be changed, even if F is not taken to be equal to $\frac{1}{2}$, because the values for F obtained in practical cases are close to this value.

As presented previously, failure shape 1 is not included in the calculations for the failure in the surroundings. This must of course be done if the purpose is to find the exact solution for the problem. The correct solution, including all kinds of failure, is probably very complicated and is useful only in theoretical calculations. This section shows only that the upper bound theorem can be used in a very simple way with sufficient accuracy. In the following calculations the upper bound theorem will therefore be used to determine the load carrying capacity. The expressions for failure shapes 1 and 2 will be considered and the one giving the lowest value for the load carrying capacity will be used.

The resistance of the surroundings against anchorage failure can therefore be found by considering the section perpendicular to the longitudinal direction of the bar, where the reinforcing bar is replaced by the outward stress σ_n, see figure 4.11. The surrounding concrete is displaced axisymmetrically away from the bar by a constant velocity and the internal work from the surroundings is determined. Using C given in (4.5), the calculations are carried out as when using σ_n, but the surrounding concrete moves away from the bar with the constant velocity $v = 1$. It must be observed that the relation between C and σ_n is given by $C = \frac{\sigma_n}{f_c}$. The load carrying capacity is found by inserting the value for C or $\frac{\sigma_n}{f_c}$ into the expression for the local failure, failure shapes 1 or 2, which gives the lowest value.

In the preceeding discussion a reinforcing bar anchored in a axisymmetrical concrete body, surrounded by a steel ring (a cylinder) has been considered. The steel ring was assumed to yield in the ring direction, and to give an inward stress p in the radial direction. Supposing that the cylinder instead was a stirrup reinforcement placed in the same position and strong enough to deliver an inward radial stress p, the connection between p and the force in the longitudinal direction of the stirrup can be found from the ring stress formula

$$2r_2 p = 2A_{ss} f_{ys} \frac{n}{\ell} \tag{4.85}$$

where A_{ss} is the cross sectional area of the stirrup reinforcement, f_{ys} is the yield stress, and n is the number of stirrups over the anchorage length.

The stirrup reinforcement degree is introduced by

$$\psi = \frac{A_{ss} f_{ys} n_s}{d\ell f_c} \qquad (d = 2r_1) \tag{4.86}$$

Using (4.86), expression (4.85) can be rewritten as

$$2\psi = \eta \frac{p}{f_c} \tag{4.87}$$

Inserting (4.87) into (4.65) or (4.76), the expression for σ_n can in this case be given by

$$\frac{\sigma_n}{\nu f_c} = 2\frac{c}{d}\frac{\rho}{\nu} + 2\frac{\psi}{\nu} \tag{4.88}$$

where it has been used that $r_1 = \frac{1}{2}d$ and $r_2 = c + \frac{1}{2}d$.

The increase in the load carrying capacity appearing for increasing $\eta = \frac{r_2}{r_1}$ is primarily due to the way p is defined. Expressing the load capacity, τ, as a function of ψ, the increase will be less pronounced. Using p or ψ will of course produce the same final result. In the following calculations ψ will be used.

The way the local failure here is distinct from the failure in the surroundings, raises the possibility of estimating the load carrying capacity without involving the expressions for the local failure in the optimizing procedure. Using the upper bound theorem, the optimal solution is found by taking the mechanism producing the lowest value of $C = \frac{\sigma_n}{f_c}$. The optimal value for C is then inserted into the expression for the local failure giving the lowest value for the load carrying capacity, $\frac{\tau}{f_c}$. This means that it is the expressions for $C = \frac{\sigma_n}{f_c}$ which are minimized in an actual case and not the expression for $\frac{\tau}{f_c}$. This has been done once and for all in section 4.1.

4.4   Discussion

The assumptions on which the theory for the anchorage failure are based are of course very important for the results obtained. If the assumptions are not correct it is obvious that one will probably not get the correct results. If the anchorage has a free edge perpendicular to the longitudinal direction of the bar, see figure 4.19, it is very likely that the assumptions and therefore the obtained expressions are not correct.

In this case the conditions at the free edge of the concrete will be different from the conditions at the end of the bar in the concrete, which is not included in the theory. An anchorage having a free edge will probably produce a kind of a punching shear failure, especially if the anchorage length is very short. It is very likely that an increase in the anchorage length will yield a punching shear failure at the section near the free edge and an anchorage failure, as assumed here, near the end of the bar. Under all circumstances it will be very difficult to treat this problem theoretically and it is improbable that the solution will be simple and easy to use.

Nagatomo & Kaku [85.1] have carried out anchorage tests using reinforcing bars with only a single transverse rib. In figure 4.20 some of the test
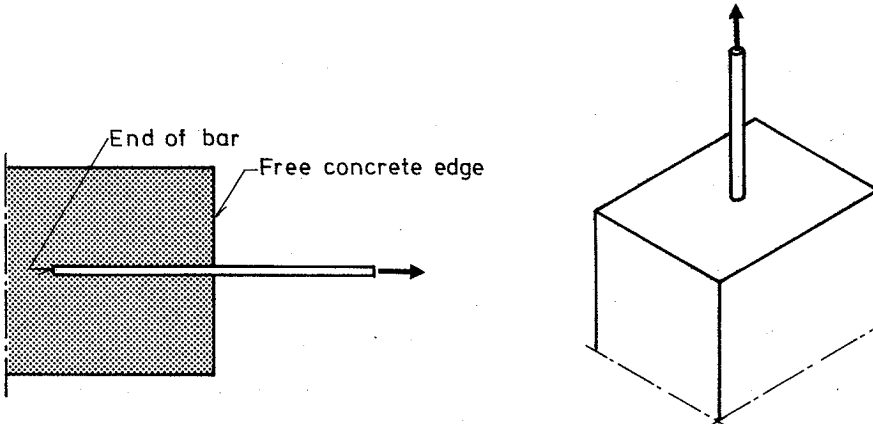
Figure 4.19: *Anchorage of a bar in a concrete specimen with a free edge.*

(a) Funnel Cracking   (b) Splitting   (c) Corner Shear
Fig.2 Failure Patterns
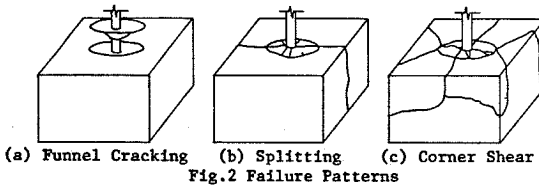
Figure 4.20: *Anchorage test with reinforcing bars having only a single transverse rib from Nagatomo & Kaku [85.1].*

specimens after failure are shown.

Lutz [66.1] has carried out similar tests. Some of the specimens after failure are shown in figure 4.21.

The distance from the free concrete edge to the transverse rib is increased from case I to case II and III both in figures 4.20 and 4.21. As can be seen from the figures, the failure pattern changes when the distance from the edge to the rib is increased. For small distances the failure looks like a punching shear failure, and for larger distances the failure is a sort of a splitting failure. This problem will not be treated in more detail here, but it should be noticed that the expressions set up previously may not be valid in some cases. This is especially so in situations with short anchorage length and free concrete edge as shown in figure 4.19.
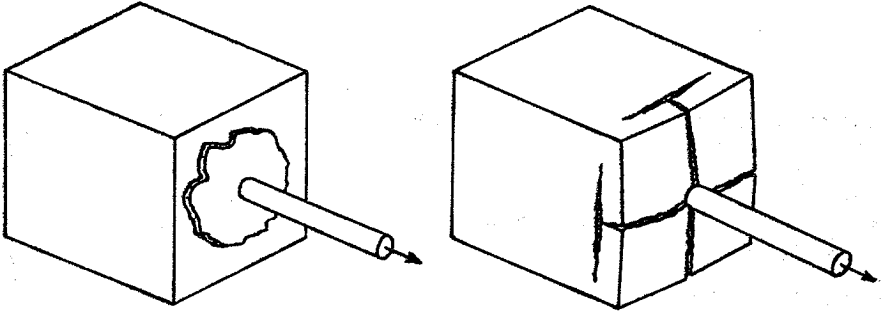
Figure 4.21: *Anchorage test with reinforcing bars having only a single transverse rib from Lutz [66.1].*

As described in chapter 2 the modified Coulomb criterion is used as yield condition for the concrete. The sliding failure resistance τ can be expressed as

$$\tau = c + \mu\sigma \tag{4.89}$$

where c is the cohesion, μ is the coefficient of friction and σ is a stress counted positive as compression. c and μ are positive constants. The angle of friction φ and the coefficient of friction μ are connected by

$$\mu = \tan\varphi = \frac{k-1}{2\sqrt{k}} \tag{4.90}$$

and the cohesion c is connected to the uniaxial concrete strength by

$$\nu f_c = \frac{2c\cos\varphi}{1-\sin\varphi} = 2c\sqrt{k} \tag{4.91}$$

In Nielsen [74.1] (4.89) is used to describe the strength of an anchorage. The cohesion c and the coefficient of friction μ are not taken as the values used normally, but are found from a test series carried out by Rathkjen [72.1], see chapter 3.

The expression for the local failure $2a$ (4.17) or (4.36) can be written as

$$\tau = \frac{2F\nu f_c}{2\sqrt{k}} + \frac{k-1}{2\sqrt{k}}\sigma_n \tag{4.92}$$

where $\sigma_n = Cf_c$.

The cohesion c is here given by

$$c = \frac{2F\nu f_c}{2\sqrt{k}} \tag{4.93}$$

and the coefficient of friction is given by

$$\mu = \frac{k-1}{2\sqrt{k}} \tag{4.94}$$

if σ_n is equal to σ in (4.89).

The similarity between (4.89) and (4.92) must be noticed.

In Nielsen [74.1] the cohesion is found primarily to be a function of the concrete strength, the type of reinforcement and the diameter of the bar. As can be seen from (4.93), this is in good agreement with the expressions set up here. The coefficient of friction is found to be a function of the type of reinforcement and the number of bars which have to be anchored in the section. This is not in accordance with (4.94) but this must be due to the fact that σ_n can not be made equal to σ. Comparing Nielsen's conclusion with the calculations in the previous section where expressions for σ_n were found, it seems very likely that the result here is in harmony with the result obtained in [74.1], se chapter 3.

The expressions for the local failure set up in sections 4.1 and 4.2 correspond to at least a two dimensionless stress condition in the concrete surrounding the reinforcing bar. As can be seen from the calculations, the main stress, σ_c, acts at an angle, α_c, between 0 and $\frac{\pi}{4} - \frac{\varphi}{2} (\simeq 26.6^\circ)$, depending on the kind of local failure which is decisive. α_c is the angle from the axis of the bar to the compression stress σ_c. In failure shape 1 the angle α_c is placed between 0 and $\frac{\pi}{4} - \frac{\varphi}{2}$, which is also the case for failure shape 2b. In the case of failure shape 2a, the angle α_c will be equal to $\frac{\pi}{4} - \frac{\varphi}{2}$. As can be seen, α_c will always be equal or less than $\frac{\pi}{4} - \frac{\varphi}{2}$ in the expressions set up here. This does not agree in all cases with the values given for α_c in the literature[1]. Tepfers [73.1] made finite element calculations to determine α_c, see chapter 3. The problem is treated as a two-dimensional case and the concrete is assumed to be linear elastic. In the case of small stresses (the adhesion case) it is found that the angle α_c is close to 45 degrees for the structure considered. For larger stresses α_c is found to be close to 31 degrees in the boundary line between the two materials and 45 degrees for the line touching the top surface of the ribs. Rehm [61.1] and Lutz &

---

[1]α_c is normally denoted by α in the literature.

Gergeley [67.1] claim that the angle α_c is equal to 50 degrees and Losberg &
Olsson [79.1] say that $\alpha_c \simeq 45^o$. These calculations are all based on elastic
asumptions. Eligehausen [79.2] carried out finite element calculations where
he used elastic assumptions, but the relationship between the strains and
the stresses in the concrete is given by three different linear expressions
in such a way that the stiffness decreases for increasing strains. For a lap
splice it is found that α_c is about 25 degrees. Kærn [87.1] has made finite
element calculations using a plastic material model for the concrete. For
the anchorage problem it is found that the angle α_c in the middle of the
anchorage is about 28 degrees for the case being dealt with. Using the slip
line theory, Exner [83.1] has found that α_c is determined by $\frac{\pi}{4} - \frac{\varphi}{2}$ for strong
surroundings and that α_c lies between 0 and $\frac{\pi}{4} - \frac{\varphi}{2}$ for weak surroundings.

The results obtained for α_c in the literature and here are in satisfactory
agreement when the assumptions about the material properties are similar.
In the calculations where the concrete is assumed to be an elastic material,
the value for α_c is larger than the value obtained when the concrete is
assumed to be a plastic material.

The rib parameters D (4.6) and F (4.12) must be known before the strength
of an anchorage can be found. Often it is not possible to obtain the actual
values for the parameters to determine D and F, i.e. the diameter d, the
rib height h_d, the distance between the ribs a and the dimension of the rib
in the direction of the bar axis u, see figure 4.1. Another problem is that
the parameters d, h_d, a and u can change for the same kind of reinforcement
produced on different days. This is because the rolls to make the reinforce-
ment are worn down in time. If it is impossible to obtain the actual values
for the parameters, they must be determined in such a way that the values
of D and F are at a minimum. This can be done by using the national
standard specifications for deformed bars where the minimum requirements
are given. The different reinforcing bar manufacturers normally set up their
own minimum requirements and they can of course be used, if it is certain
that the reinforcement was produced by them.

If it is not possible to find any information at all about the parameters, min-
imum values for D and F must be used. By examining different standard

specifications and reinforcing bar manufacturers specifications, minimum values for D and F on 0.030 and 0.50, respectively, are found for normal deformed bars. Because the dimension of the rib in the direction of the bar axis u is not normally given, this parameter is not included in the values given above. The distance between the ribs, a, is therefore taken as the distance from middle of the rib to the middle of the next rib. Using this, the value for D is correct according to (4.6), while the value for F is larger than it should be. The error which is made, does probably not have a large significance. In appendix D values for D and F are given for different types of reinforcement.

As shown in figure 4.1, the ribs on the reinforcement are assumed to be perpendicular to the longitudinal direction of the bar, and the angle between the bar axis and the surface of the ribs, the rib face angle κ, is assumed to be 90°. The influence on the anchorage from the rib face angle has been examined. Menzed [39.1] made tests with bars where the rib face angle was 45 and 57 degrees. Menzed concluded that there was only a small difference in the way they responded. Clark [46.1] observed that there is a large difference in the effect when the rib face angle is 30 or 90 degrees.

Rehm [61.1] also studied this problem by changing the rib face angle. Lutz [66.1] concluded that a bar with rib having a face angle less than 30 to 40 degrees will slip relative to the adjacent concrete, while bars with ribs having a face angle of 40 to 45 degrees or more crush the concrete in front of the ribs. The resistance is not increased when the rib face angle is more than 45 degrees. The same conclusion is found in Soretz & Hölzenbein [79.3]; the strength does not increase when the rib face angle is increased from 45 to 90 degrees.

Soretz & Hölzenbein [79.3] also studiet the influence from the inclination of the ribs relative to the longitudinal direction of the bar. They conclude that the angle between 45 and 90 degrees only influence the strength slightly. The influence from the rib area is far more important. However, in Clark [46.1] and Tepfers [73.1] it is observed that an inclination of the ribs relative to the bar which is not 90 degrees decreases the strength. From these references it is difficult to say if there is an influence from the inclination

of the ribs with respect to the bar axis. However, the observations indicate that the expressions set up previously can be used when the rib face angle and the inclination of the ribs relative to the bar axis are larger than 45 degrees.

In sections 4.1 and 4.2, the local failure around a reinforcing bar is treated. The failure in the surroundings is discussed in section 4.3, where it is assumed that the surroundings are axisymmetrical to the bar axis. In practice the surroundings are not axisymmetrical, wherefore the expressions for the local failure and the principles in the determination of the work from the surroundings can not be used. However, this will be done. Using the upper bound theorem, the failure in the surroundings must then look like the axisymmetrical failure as far as possible. The surrounding concrete is displaced axisymmetrically away from the bar by a constant velocity and the internal work from the surroundings is determined. The method is used in the next chapter, where it can be seen how the calculations are carried out.

Chapter 5

Anchorage at Supports

Failure mechanisms for anchorage of one layer of reinforcement at beam supports will be dealt with in this chapter. A *failure mechanism* in the surroundings is defined as the failure consisting of yield lines in a section perpendicular to the bar axis where only a single bar is involved. The total failure involving all bars in the actual beam section perpendicular to the beam axis, is named *the complete failure mechanism*. To achieve the optimal complete failure mechanism the failure mechanisms are combined in such a way, that the total load carrying capacity is minimized. These terms are used generally, not only in the cases treated here.

The failure mechanisms which are dealt with in this chapter, can all be characterized as simple mechanisms. The number of unknown parameters and the complexity of the expressions are attempt kept to a minimum. In some cases the expressions are not clear and simple, because there seems to be a limit for how simple they can be and yet still reflect what happens in reality. More complex failure mechanisms in the case of anchorage at supports are treated in a later chapter.

In figure 5.1 a beam end support is shown.

As can be seen in figure 5.1, it is assumed that the support is placed at the end of the beam. The anchorage length ℓ is assumed to be equal to the length of the support in the direction of the beam and bar axis. The total force in the n bars, nT, just in front of the support must therefore be transferred to the concrete over the anchorage (and support) length. The total reaction force R is assumed to be evenly distributed over the area ℓb,
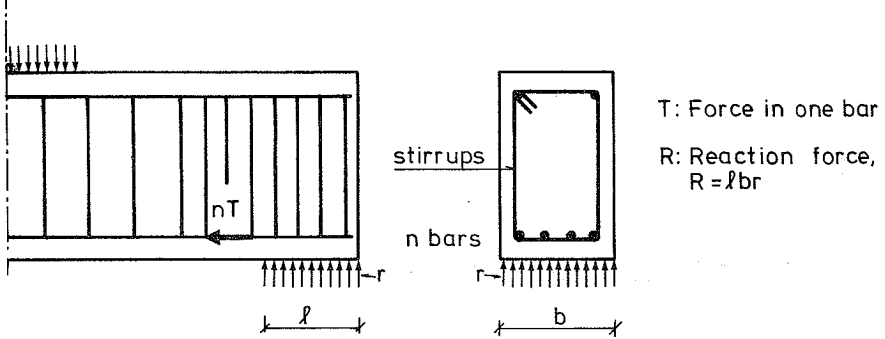
Figure 5.1: *Beam end support and cross section at the support.*

where b is the width of the beam. Stirrups at the support will be taken into account.

The expressions for the load carrying capacity, which will be set up are based on upper bound calculations. This produces unsafe expressions. But the final expressions are as safe as if they had been developed from lower bound calculations because of the effectiveness factors, which must be included and found from tests. The values for the effectiveness factors based on upper bound expressions will be lower than or equal to the values from lower bound expressions. Hence it is always safe to use values for the effectiveness factors when they are found from upper bound expressions. However, under all circumstances it is best to use effectiveness factors and expressions which are linked.

5.1   Failure Mechanisms

As previously mentioned, a failure mechanism is the failure in the surroundings, where only a single bar is involved. Expressions for the most important mechanisms in the case of anchorage at supports will be set up in this section. Because the local failure around a reinforcing bar has been treated and solutions are found, see chapter 4, the failure mechanisms can be separated from the local failure. Hence the only problem is finding expressions for C, which, in the equations for the local failure found from the upper bound calculations, is denoted as the internal work from the surroundings.

The work from concrete, stirrups, and support reaction is included in the expressions.

The work done by the *reaction* is an external work, but generally it is negative. Therefore it can be taken as a positive internal work. Since the total external work in upper bound calculations must be positive, it ought to be checked that this is the case. However, in the case of anchorage at supports, the internal work without the contribution from the reaction will always be positive and thus the work from the reaction has to be less than the work from the anchorage shear stress.

In the expressions for the internal work the contribution from *stirrups* is included. In accordance with the assumptions in section 2.3 it is assumed that the stirrups carry longitudinal stresses only. Moreover, it is assumed that the stirrups follow the main reinforcement in the movements in the failure mechanism. When the problem concerns anchorage of one layer of reinforcement at a beam support, this assumption will be close to reality, but as shown in a later chapter, it is probably not always correct to use this assumption. The expressions are developed assuming normal stirrups, but it is easy to extend the expressions so that other kinds of surrounding reinforcement can be taken into account. This is, for instance, done in chapter 7.

The failure in the *surrounding concrete* must look like the failure in an axisymmetrical specimen as far as possible. As shown in section 4.3 the surrounding concrete can be assumed to move away from the bar at a constant velocity of $v = 1$. In the case of anchorage in a beam with the bar placed close to the concrete surface, it is assumed that the beam does not move at anchorage failure. Hence the bar will move away from the beam at a velocity of $v = 1$ and the concrete cover will move away from the bar by $v = 1$. This means that the velocity in a radial yield line adjacent to the bar will generally be $v = 2$. Therefore, an upper bound solution can be found, assuming that the bar moves away from the beam at the velocity of $v = 2$.

The yield lines in the failure mechanism must end in some way. The failure mechanism has to be geometrically possible; therefore the failure surface
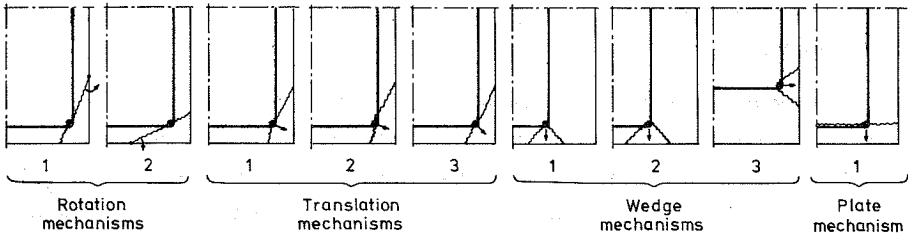
Figure 5.2: *Failure mechanisms for anchorage at supports of one layer of reinforcement.*

cannot just finish at the ends of the anchorage length. The failure surface has to pass the concrete surface. This will in general result in an additional contribution to the internal work, which will be named as the *end failure contribution*. Cracks in the concrete just behind the support will in some cases disturb the end failure surface. Thus it is very difficult to formulate a theoretically correct expressions for this contribution. Assuming that no cracks influence the end failure, it is possible to develop expressions for this contribution. These are of course theoretical solutions, but they indicate the influence from the different parameters. When dealing with anchorage along a beam support, the end failure contribution will be of less importance due to the work done by the reaction, the yield lines, and the stirrups. Therefore expressions for this contribution will not be set up in this chapter. Splices are treated theoretically in chapter 7 and expressions for the end failure, are included here. It is not difficult to combine the expressions for the end failure set up in chapter 7 with the expressions set up in this chapter, so the end contribution can be taken into account in the case of anchorage at supports.

The various mechanisms will be treated separately. A figure showing the geometri, the yield lines, and the displacements in a section, perpendicular to the bar axis is shown first. The different contributions to the internal work are listed and the total internal work is determined. If necessary and if it is possible, the expression for the total internal work is minimized with respect to the free parameters. The mechanisms and their names are shown in figure 5.2.
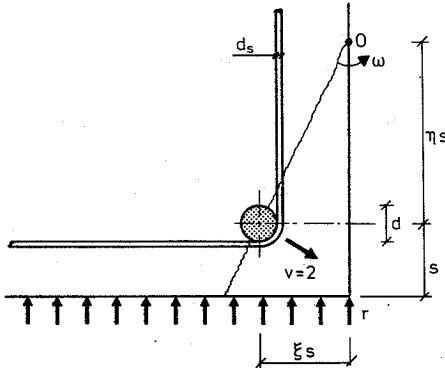
Figure 5.3: *Rotation mechanism no. 1, geometri and yield line pattern.*

The first five mechanisms in figure 5.2, the rotation and the translation mechanisms, can be characterized as corner mechanisms. The last two types of mechanisms, the wedge and the plate mechanisms, take place both in the corners and inside the section. If there is more than one bar, the plate mechanism will involve all bars placed in the same (horizontal) section as the yield line.

5.1.1 Rotation mechanisms

The rotation mechanism is treated using the symbols in figure 5.3. The failure pattern consists of a straight yield line, going from one concrete edge through the center of the bar to the other edge, so that the corner of the beam breaks off. The displacement consists of a rotation, $\omega = \frac{v}{s\sqrt{\xi^2+\eta^2}}$, about a point, 0, on the face of the structure. At the reinforcing bar the velocity is $v = 2$ in the concrete, in accordance with the discussion held previously. As mentioned above, the transverse reinforcement, the stirrups, are assumed to follow the reinforcement in the movements; therefore the angle of rotation is $\frac{\omega}{2}$.

The different contributions to the total internal work are given by

$$W_{ic} = \omega\rho f_c l\left(\frac{1}{2}s^2\left(\frac{1+\eta}{\eta}\right)^2(\xi^2+\eta^2) - ds\sqrt{\xi^2+\eta^2}\right) \qquad (5.1)$$

$$W_{it} = \frac{1}{2}\omega A_{ss}f_{ys}n_s s(\xi+\eta) \qquad (5.2)$$

$$W_{ir} = \frac{1}{2}\omega r l s^2 \left(\frac{\xi}{\eta}\right)^2 (1+\eta)^2 \tag{5.3}$$

where W_{ic} is the internal work from the concrete, W_{it} is the internal work from the transverse reinforcement, W_{ir} is the internal work from the reaction stress, A_{ss} is the cross sectional area of the stirrups, f_{ys} is the yield strength of the stirrups, and n_s is the number of stirrups over the length of anchorage. η is a free parameter, by which the internal work can be optimized. The other geometrical quantities are shown in figure 5.3.

The total internal work from the surroundings is found by adding the three contributions in (5.1)–(5.3).

$$W_{is} = W_{ic} + W_{it} + W_{ir} \tag{5.4}$$

Doing this and using (4.5), the dimensionless total internal work from the surroundings can be written

$$C = \frac{s}{\pi d}\left[\frac{(1+\eta)^2}{\eta^2\sqrt{\xi^2+\eta^2}}\left(\rho(\xi^2+\eta^2) + \xi^2\frac{r}{f_c}\right) - 2\frac{d}{s}\rho + \frac{d}{s}\psi\frac{\xi+\eta}{\sqrt{\xi^2+\eta^2}}\right] \tag{5.5}$$

where the stirrup reinforcement degree is defined as

$$\psi = \frac{A_{ss}f_{ys}n_s}{dl f_c} \tag{5.6}$$

The optimal value for η can be found by differentiating (5.5) with respect to η. It turns out that η can be determined from

$$\frac{r}{f_c}\xi^2(1+\eta)(\eta^3+3\eta^2+2\xi^2) = \rho(\xi^2+\eta^2)(1+\eta)(\eta^3-\eta^2-2\xi^2) + \psi\frac{d}{s}\xi\eta^3(\xi-\eta) \tag{5.7}$$

Unfortunately it is not generally possible to find an explicit expression for η, but η can be found using an iterative routine on (5.7). If the relationship between, for instance, C and $\frac{r}{f_c}$ needs to be found, this can be done in a simple way. A value for η is assumed and inserted into (5.7), by which $\frac{r}{f_c}$ can be found. Inserting the corresponding values of η and $\frac{r}{f_c}$ into (5.5), a value for C is found and one point in the relation between C and $\frac{r}{f_c}$ is determined. This procedure continues until the complete relationship is established. Examples appear in figures 5.4 and 5.5, where curves for different values of the geometrical parameters $\frac{s}{d}$ and ξ are shown for the

Figure 5.4: *The relationship between $\frac{C}{\rho}$ and $\frac{r}{\rho f_c}$ for rotation mechanism no. 1, for different values of $\frac{s}{d}$.*

stirrup reinforcement degree, ψ equal to zero. The expressions (5.5) and (5.7) are divided by the effectiveness factor for tension ρ, so that the curves will be independent of the material properties. In figure 5.6 curves for different values of $\frac{\psi}{\rho}$ are shown.

As can be seen in figure 5.6, the contribution from the stirrups is almost constant for different values of $\frac{r}{\rho f_c}$.

In practice $\frac{r}{\rho f_c}$ is normally less than 10; therefore only a small part of the curves shown in the figures will be used.

To find the load carrying capacity τ of the anchorage for specific values of the geometry, the stirrups and the support reaction stress the dimensionless internal work C is determined first. The value for C is inserted into the expressions for the local failure, expressions (4.9) and (4.17) or (4.18), producing the lowest value for τ.

The mechanism shown in figure 5.3, named rotation mechanism no. 1, reflects reasonably well the anchorage failure at a beam support in a corner bar. The solution found from this mechanism is an upper bound solution,

Figure 5.5: *The relationship between $\frac{C}{\rho}$ and $\frac{r}{\rho f_c}$ for rotation mechanism no. 1, for different values of ξ.*
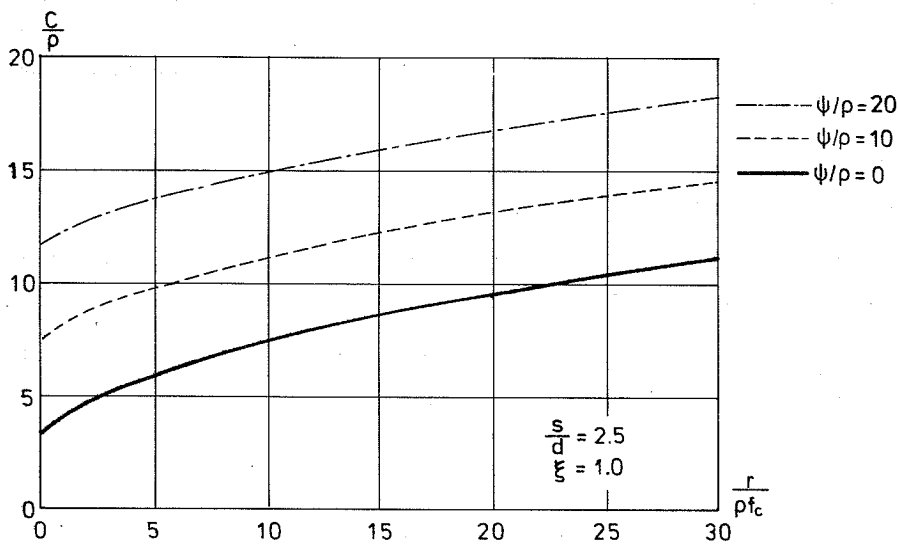
Figure 5.6: *The relationship between $\frac{C}{\rho}$ and $\frac{r}{\rho f_c}$ for rotation mechanism no. 1, for different values of $\frac{\psi}{\rho}$.*
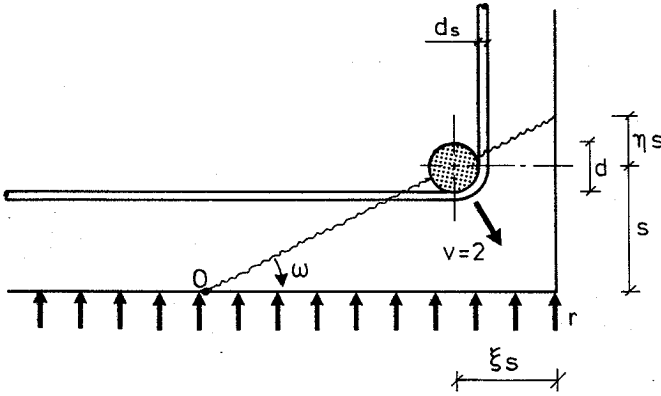
Figure 5.7: *Rotation mechanism no. 2; geometry and yield line pattern.*

and it is probably not equal to the corresponding lower bound solution. The rotation point is fixed to the vertical concrete edge, but an improved solution can be found by placing the rotation point inside the section. A compression zone will then appear in the horizontal section, from the rotation point to the vertical concrete edge. Moreover, the yield line from the bar to the bottom horizontal edge does not necessarily have to be a straight line, a curved yield line can also be used. Extending the solution to cover this kind of failure mechanism, will make the expressions more complicated. In chapter 6 this mechanism is treated in the case of anchorage at supports of more than one layer of reinforcement.

Rotation mechanism no. 2 is identical with rotation mechanism no. 1, except that the rotation point is placed at the bottom horizontal edge of the concrete section, instead of at the vertical edge, see figure 5.7. In the case of anchorage at a support, this mechanism is only decisive when the suppport stress is small or the geometry of the section is unusual.

Using the symbols in figure 5.7, the following expressions for the internal work are obtained

$$W_{ic} = \omega \rho f_c l \left(\frac{1}{2} s^2 \left(\frac{1+\eta}{\eta} \right)^2 (\xi^2 + \eta^2) - ds \frac{\sqrt{\xi^2 + \eta^2}}{\eta} \right) \tag{5.8}$$

$$W_{it} = \frac{1}{2} \omega A_{ss} f_{ys} n_s s \frac{\xi + \eta}{\eta} \tag{5.9}$$

$$W_{ir} = \frac{1}{2}\omega r l s^2 \left(\frac{\xi(1+\eta)}{\eta}\right)^2 \tag{5.10}$$

where $\omega = \frac{v\eta}{s\sqrt{\xi^2+\eta^2}}$.

Using (5.4) and (4.5), the dimensionless total internal work can be written

$$C = \frac{s}{\pi d}\left[\frac{(1+\eta)^2}{\eta\sqrt{\xi^2+\eta^2}}\left(\rho(\xi^2+\eta^2)+\xi^2\frac{r}{f_c}\right) - 2\frac{d}{s}\rho + \frac{d}{s}\psi\frac{\xi+\eta}{\sqrt{\xi^2+\eta^2}}\right] \tag{5.11}$$

where the only difference from (5.5), valid for rotation mechanism no. 1, is that η in the first item in the denominator, is not squared.

By differentiating (5.11) with respect to η, it is found that the optimal value can be determined from

$$\frac{r}{f_c}\xi^2(1+\eta)(2\eta^2-\xi^2\eta+\xi^2) = \rho(\xi^2+\eta^2)(1+\eta)(2\eta^3+\xi^2\eta-\xi^2) + \psi\frac{d}{s}\xi\eta^2(\xi-\eta) \tag{5.12}$$

It is not possible in this case to isolate η ; therefore an explicit expression for C can not be found. However, the same procedure as explained in connection with rotation mechanism no. 1, can be used.

$\frac{C}{\rho}$ is shown as a function of $\frac{r}{\rho f_c}$ in figures 5.8 and 5.9

Comparing figure 5.5 with figure 5.9, it can be seen that rotation mechanism no. 2 is decisive for small values of $\frac{r}{\rho f_c}$ in the case of $\xi = 0.5$. In the other cases shown in figures 5.8 and 5.9 rotation mechanism no. 2 is not decisive compared to rotation mechanism no. 1.

5.1.2 Translation mechanisms

The first translation mechanism dealt with, is shown in figure 5.10 and will be called *translation mechanism no. 1*. It is assumed that the concrete corner moves outward at the constant velocity of $v = 2$. The failure mechanism consists of two yield lines following straight lines, going from the concrete surfaces to the center of the bar.

The contributions to the internal work can be written

$$\begin{aligned}
W_{ic} = \frac{1}{2}vlf_c \Bigg[&(\lambda - \mu\sin(\theta+\kappa_1))\left(\frac{\xi s}{\cos\kappa_1} - \frac{1}{2}d\right) \\
&+(\lambda - \mu\cos(\theta-\kappa_2))\left(\frac{s}{\cos\kappa_2} - \frac{1}{2}d\right)\Bigg]
\end{aligned} \tag{5.13}$$
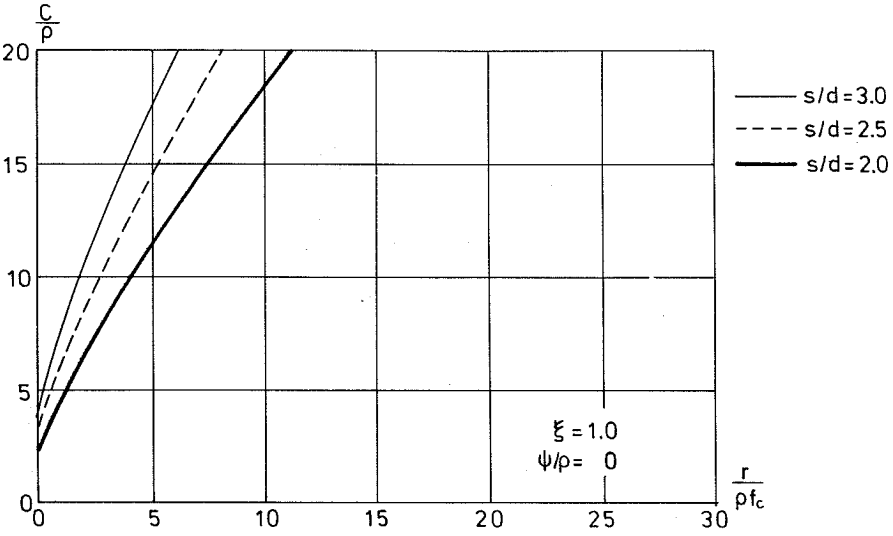
Figure 5.8: *The relationship between $\frac{C}{\rho}$ and $\frac{r}{\rho f_c}$ for rotation mechanism no. 2, for different values of $\frac{s}{d}$.*
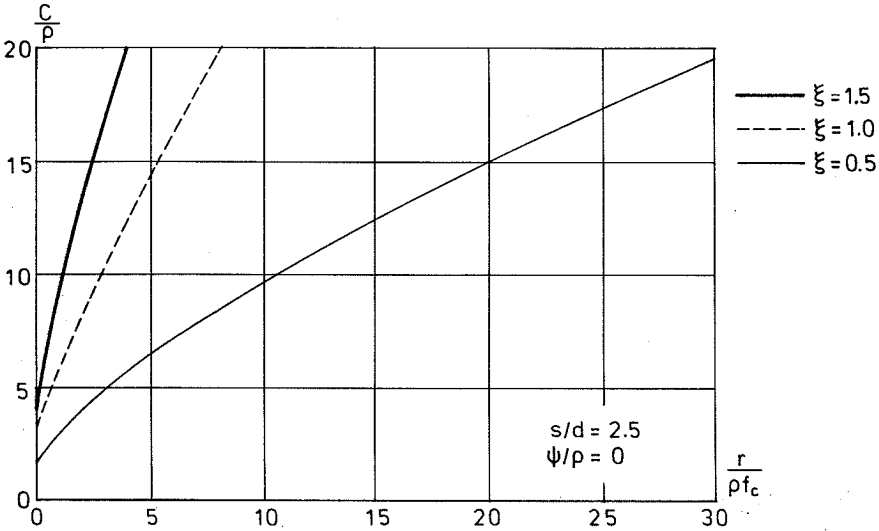
Figure 5.9: *The relationship between $\frac{C}{\rho}$ and $\frac{r}{\rho f_c}$ for rotation mechanism no. 2, for different values of ξ.*
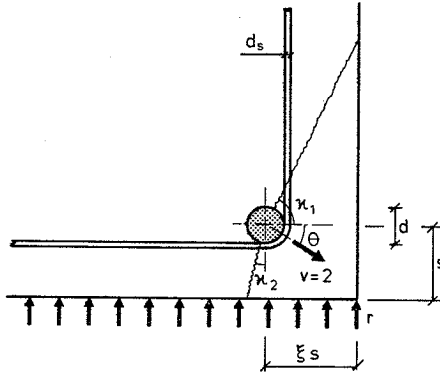
Figure 5.10: *Translation mechanism no. 1; geometry and yield line pattern.*

$$W_{it} = \frac{1}{2} v A_{ss} f_{ys} n_s (\sin\theta + \cos\theta) \tag{5.14}$$

$$W_{ir} = v r l s \sin\theta (\xi + \tan\kappa_2) \tag{5.15}$$

The total dimensionless internal work is then found to be

$$
\begin{aligned}
C = \frac{s}{\pi d} & \left[(\lambda - \mu\sin(\theta + \kappa_1)) \left(\frac{\xi}{\cos\kappa_1} - \frac{1}{2}\frac{d}{s} \right) \right. \\
& + (\lambda - \mu\cos(\theta - \kappa_2)) \left(\frac{1}{\cos\kappa_2} - \frac{1}{2}\frac{d}{s} \right) \\
& + 2\frac{r}{f_c}\sin\theta(\xi + \tan\kappa_2) \\
& \left. + \frac{d}{s}\psi(\sin\theta + \cos\theta) \right]
\end{aligned}
\tag{5.16}
$$

where $\theta + \kappa_1 \in [\varphi; \frac{\pi}{2}]$ and $\kappa_2 + \frac{\pi}{2} - \theta \in [\varphi; \frac{\pi}{2}]$.

It is not possible in general to minimize the expression analytically. However, the number of variables can be reduced by assuming that the failure must look like the axisymmetrical failure as much as possible. This can be done by demanding that the direction of the velocity divides the angle between the two yield lines into two equal angles. This can be written as

$$\kappa_2 = 2\theta + \kappa_1 - \frac{\pi}{2} \tag{5.17}$$

Using (5.16) and (5.17) only two unknown parameters are to be decided, which can be done numerically. It can be shown that the optimal value for C appears when $\kappa_2 = 0$, for all values of $\frac{r}{\rho f_c}$, except for small values of $\frac{r}{\rho f_c}$
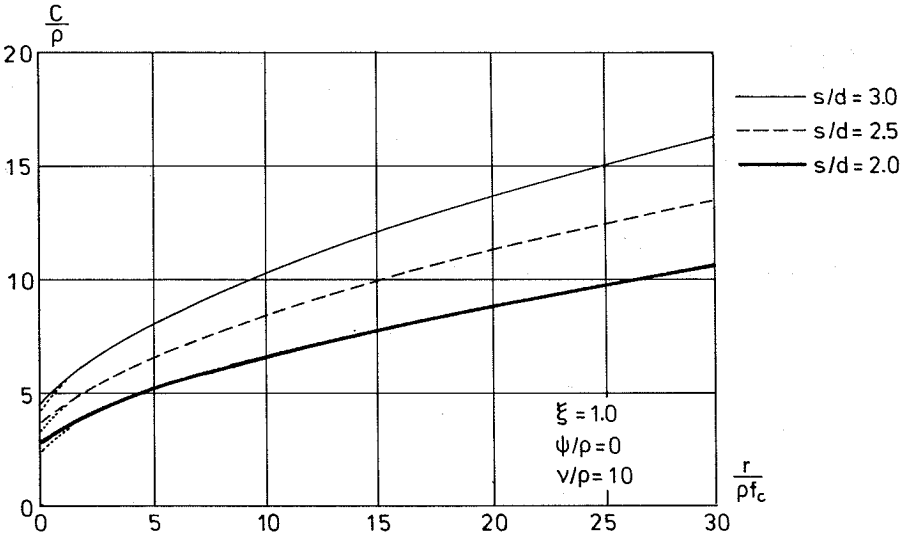
Figure 5.11: *The relationship between $\frac{C}{\rho}$ and $\frac{r}{\rho f_c}$ for translation mechanism no. 1, for different values of $\frac{s}{d}$. The dotted line indicates the relation, when κ_2 is not necessarily equal to zero.*

$(\frac{r}{\rho f_c} < 1)$. Inserting $\kappa_2 = 0$ and (5.17) into (5.16) yields

$$C = \frac{s}{\pi d} \left[(\lambda - \mu \cos \theta) \left(\frac{\xi}{\sin(2\theta)} + 1 - \frac{d}{s} \right) \right.$$
$$\left. + 2\frac{r}{f_c} \xi \sin \theta + \frac{d}{s} \psi (\sin \theta + \cos \theta) \right] \tag{5.18}$$

where $\theta \in [0; \frac{\pi}{2} - \varphi]$.

It is not possible to minimize this expression analytically with respect to θ. The same procedure as with the rotation mechanisms can be used. The expression is differentiated and equalized to zero. The expression obtained in doing this is used to determine values of, for instance, $\frac{r}{\rho f_c}$ for different values of θ. The corresponding values are inserted into (5.18), and the relationship between $\frac{C}{\rho}$ and $\frac{r}{\rho f_c}$ is then determined. In figures 5.11 and 5.12 examples are shown

As can be seen in the figures, the difference between the values obtained, when κ_2 is not necessarily equal to zero, indicated by a dotted line, and the values for $\kappa_2 = 0$ are not large and only limited to a small interval close to
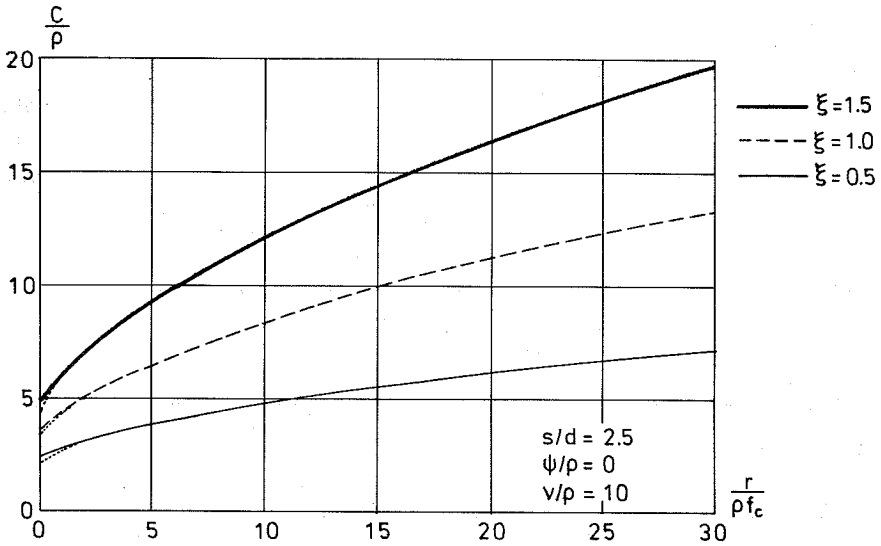
Figure 5.12: *The relationship between $\frac{C}{\rho}$ and $\frac{r}{\rho f_c}$ for translation mechanism no. 1, for different values of ξ. The dotted line indicates the relation, when κ_2 is not necessarily equal to zero.*

$\frac{r}{\rho f_c} = 0$. Consequently, for normal geometries, like the examples shown in the figures, it is possible with reasonable accuracy, to use expression (5.18) instead of (5.16) and (5.17).

If the failure pattern is changed in such a way, that the yield lines touch the bar at the top and bottom points of the periphery, see figure 5.13, it is possible to minimize with respect to two of the three parameters.

The total dimensionless internal work for translation mechanism no. 2 can be found to be

$$C = \frac{s}{\pi d} \left[(\lambda - \mu \sin(\theta + \kappa_1)) \frac{\xi}{\cos \kappa_1} \right.$$
$$+ (\lambda - \mu \cos(\theta - \kappa_2)) \frac{\chi}{\cos \kappa_2}$$
$$\left. + 2 \frac{r}{f_c} \sin \theta (\xi + \chi \tan \kappa_2) + \frac{d}{s} \psi (\sin \theta + \cos \theta) \right] \qquad (5.19)$$

where $\chi = 1 - \frac{1}{2} \frac{d}{s}$ is introduced. The angles must satisfy $\theta + \kappa_1 \in [\varphi; \frac{\pi}{2}]$ and $\kappa_1 + \frac{\pi}{2} - \theta \in [\varphi; \frac{\pi}{2}]$. Differentiation of (5.19) with respect to κ_1, κ_2, and θ,
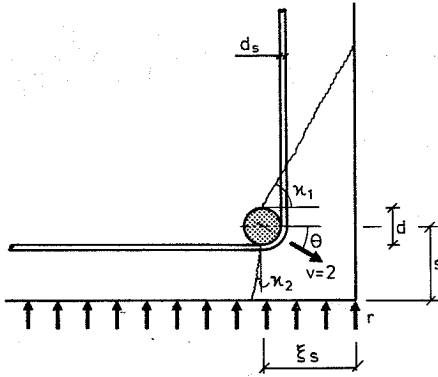
Figure 5.13: *Translation mechanism no. 2, geometry and yield line pattern.*

yields the following expressions, respectively

$$\sin \kappa_1 = \frac{\mu}{\lambda} \cos \theta \qquad (5.20)$$

$$\sin \kappa_2 = \sin \theta \, \frac{\mu - 2\frac{r}{f_c}}{\lambda} \qquad (5.21)$$

$$\tan \theta = \frac{(1 - \frac{2}{\mu} \frac{r}{f_c})(\xi + \chi \tan \kappa_2) + \frac{d}{s} \frac{\psi}{\mu}}{\xi \tan \kappa_1 + \chi - \frac{d}{s} \frac{\psi}{\mu}} \qquad (5.22)$$

Unfortunately it is not possible to solve these three equations. Inserting (5.20) and (5.21) into (5.19), results in an expression for C with only one parameter

$$C = \frac{s}{\pi d} \left[\xi(\sqrt{\lambda^2 - \mu^2 \cos^2 \theta} - (\mu - 2\frac{r}{f_c}) \sin \theta) \right.$$
$$+ \chi \left(\sqrt{\lambda^2 - (\mu - 2\frac{r}{f_c})^2 \sin^2 \theta} - \mu \cos \theta \right)$$
$$\left. + \frac{d}{s} \psi (\sin \theta + \cos \theta) \right] \qquad (5.23)$$

It is relatively easy, using this expression to produce relations between C and one of the quantities on the right hand side of the equal sign. The method described in connection with the rotation mechanisms can be used, where

$$0 = \xi \left[\frac{\mu^2 \tan \theta}{\sqrt{\lambda^2(1 + \tan^2 \theta) - \mu^2}} - (\mu - 2\frac{r}{f_c}) \right]$$

$$+\chi \tan \theta \left[\mu - \frac{(\mu - 2\frac{r}{f_c})^2}{\sqrt{\lambda^2(1 + \tan^2 \theta) - (\mu - 2\frac{r}{f_c})^2 \tan^2 \theta}}\right]$$

$$+\frac{d}{s}\psi(1 - \tan \theta) \tag{5.24}$$

must be fulfilled to obtain optimal values. (5.24) is the coefficient of the differential of (5.23).

The yield line going from the bar to the bottom surface must be controlled, so that it does not exceed the intersection between the horizontal and the vertical edge of the section. If this is the case, wedge mechanism no. 3, treated in the next section, will be decisive. In normal cases this situation will appear only for large values of the dimensionless reaction stress $\frac{r}{f_c}$. Of course it must also be checked that the upper yield line does not exceed the height of the section, but this will normally only be the case if the height is minimal.

Using $\kappa_2 = 0$, (5.17), and (5.19), it can be shown that the values obtained, are a little larger in comparison than the values from translation mechanism no. 1. This is because the yield lines are longer in mechanism no. 2, other things being equal. In practice the difference between the two mechanisms is without significance.

Translation mechanism no. 1 can be simplified in another way than that expressed in (5.17). Assuming the angle between the direction of the displacement and the yield lines to be $\frac{\pi}{2}$, a mechanism as shown in figure 5.14 appears. This mechanism will be called *translation mechanism no. 3*.

Using the expression for translation mechanism no. 1, the expression for C in this case can be found to be

$$C = \frac{s}{\pi d}\left[2\rho\left(\frac{\xi}{\sin \theta} + \frac{1}{\cos \theta} - \frac{d}{s}\right) + 2\frac{r}{f_c}\sin \theta(\xi + \tan \theta) + \frac{d}{s}\psi(\sin \theta + \cos \theta)\right] \tag{5.25}$$

Not even in this case is it possible to minimize the expression analytically. Of course the same procedure as with the other mechanisms can be used to develop relations between C and one of the contained quantities.
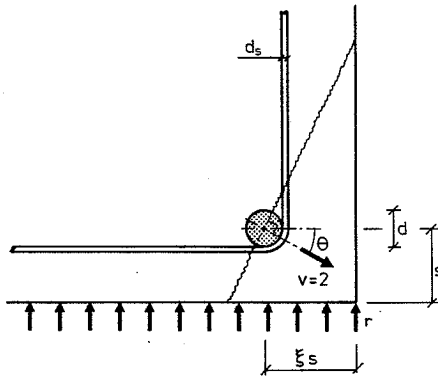
Figure 5.14: *Translation mechanism no. 3, geometry and yield line pattern*

In figures 5.15 and 5.16, $\frac{C}{\rho}$ is shown as a function of $\frac{r}{\rho f_c}$ for different values of $\frac{s}{d}$ and ξ, respectively.

Comparing figures 5.15 and 5.16 with figures 5.11 and 5.12, respectively, it can be seen that translation mechanism no. 1 produces values for $\frac{C}{\rho}$ less than the values obtained from translation mechanism no. 3, which is also to be expected.

The translation mechanism in the case of anchorage at supports of more than one layer of reinforcement is treated in chapter 6.

5.1.3   Wedge mechanisms

The previously discused mechanisms, the rotation and the translation mechanisms, are typical corner mechanisms. If the bar is placed at a distance from a corner or placed in a special position near the corner (compared with the total dimensions of the section), it is very likely that another kind of mechanism will be decisive. The wedge mechanisms must be considered here.

Wedge mechanism no. 1, shown in figure 5.17 will be treated first. The yield line pattern consists of two yield lines following a straight line, going from the center of the bar to the bottom surface of the section. When failure occurs, the wedge is displaced vertically at a velocity of $v = 2$.
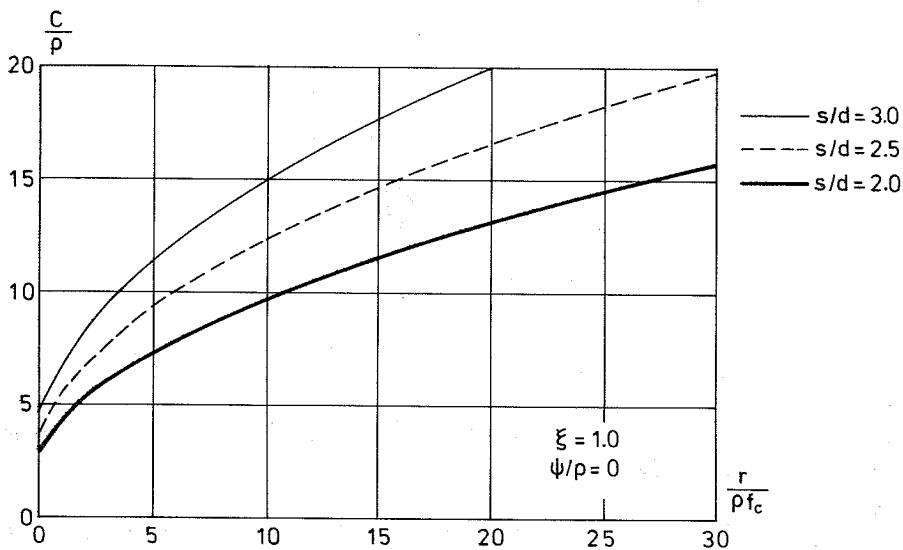
Figure 5.15: *The relationship between $\frac{C}{\rho}$ and $\frac{r}{\rho f_c}$ for translation mechanism no. 3, for different values of $\frac{s}{d}$.*
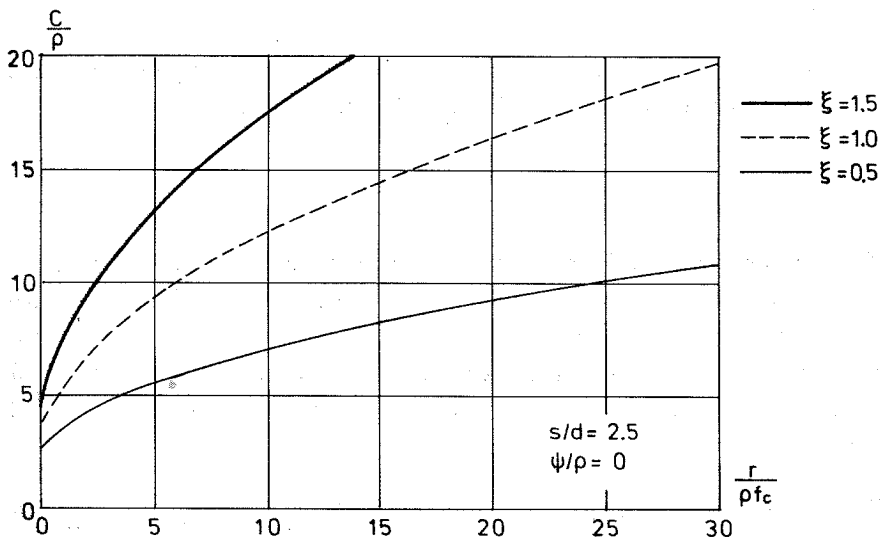
Figure 5.16: *The relationship between $\frac{C}{\rho}$ and $\frac{r}{\rho f_c}$ for translation mechanism no. 3, for different values of ξ.*
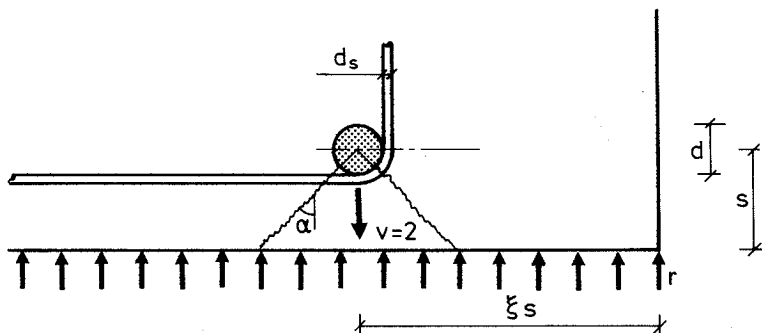
Figure 5.17: *Wedge mechanism no. 1; geometry and yield line pattern.*

If the rules, which have been used above, taking the transverse reinforcement into account, are to be used here, the active area will change with the angle α. If α is equal to zero, the contribution is zero, because it is assumed that the reinforcement can carry longitudinal stresses only. If $\alpha = \frac{\pi}{2}$ the total reinforcement area will be active. The actual value will lie between these two limits, and the active area of the transverse reinforcement will be $A_{ss} \sin \alpha$. This reduction will be taken into account, but as can be seen, the maximum reduction will be 60%, corresponding to $\alpha = \varphi$.

The contributions to the internal work are

$$W_{ic} = vlf_c(\lambda - \mu \sin \alpha)\left(\frac{s}{\cos \alpha} - \frac{1}{2}d\right) \tag{5.26}$$

$$W_{it} = \frac{1}{2}vA_{ss}f_{ys}n_s \sin \alpha \tag{5.27}$$

$$W_{ir} = 2vlrs \tan \alpha \tag{5.28}$$

The total dimensionless internal work is then found to be

$$C = 2\frac{s}{\pi d}\left[(\lambda - \mu \sin \alpha)\left(\frac{1}{\cos \alpha} - \frac{d}{2s}\right) + 2\frac{r}{f_c}\tan \alpha + \frac{d}{2s}\psi \sin \alpha\right] \tag{5.29}$$

Inserting $\alpha = \varphi$ into (5.29), the expression for C becomes

$$C = 2\frac{s}{\pi d}\left[\nu\left(\frac{2}{\sqrt{k}} - \frac{1}{k+1}\frac{d}{s}\right) + \frac{r}{f_c}\frac{k-1}{\sqrt{k}} + \frac{d}{2s}\psi\frac{k-1}{k+1}\right] \tag{5.30}$$

This expression is valid when $\left(\frac{\partial C}{\partial \alpha}\right)_{\alpha=\varphi}$ is larger than or equal to zero, which can be written

$$\frac{r}{f_c} \geq \frac{1}{(k+1)^2}\left[(k+1)(\nu - 2k\rho) + 2\frac{d}{s}k\sqrt{k}\left(\rho - \frac{\nu - \psi}{k+1}\right)\right] \tag{5.31}$$
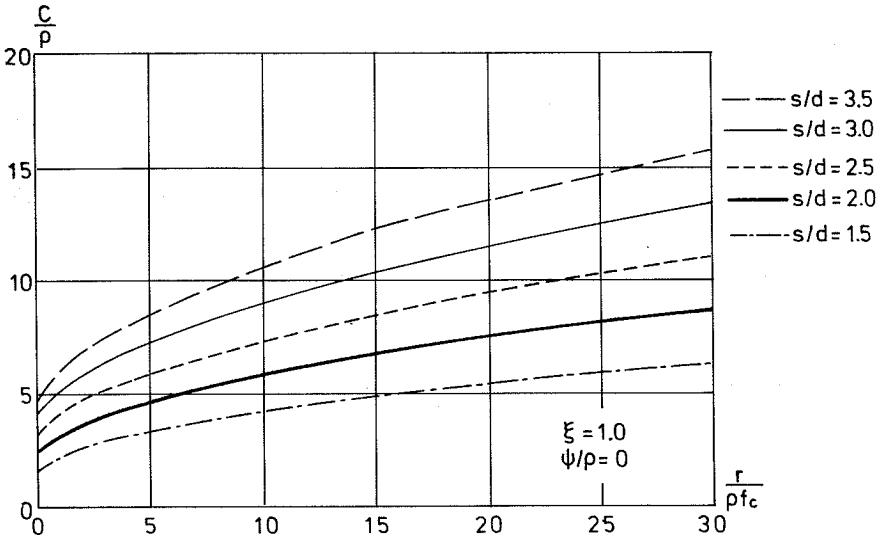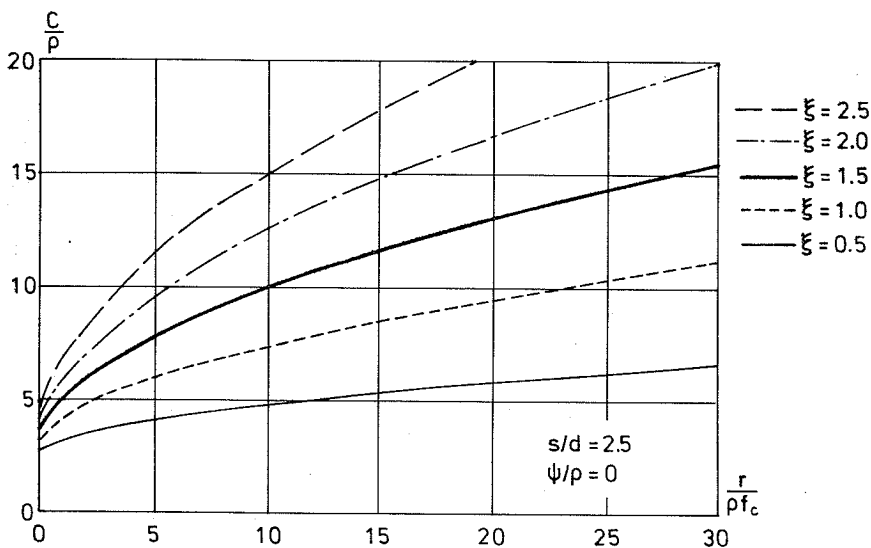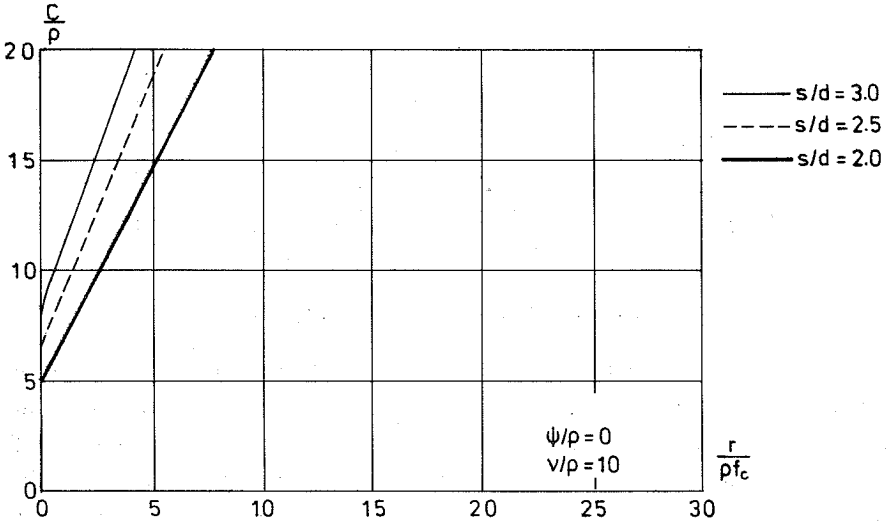
Figure 5.18: *The relationship between $\frac{C}{\rho}$ and $\frac{r}{\rho f_c}$ for wedge mechanism no. 1, for different values of $\frac{s}{d}$.*

It is not analytically possible to minimize (5.29) for α larger than φ, but this can of course be done numerically.

In figure 5.18, $\frac{C}{\rho}$ is shown as a function of $\frac{r}{\rho f_c}$, for different values of $\frac{s}{d}$. As can be seen from (5.29), the mechanism is independent of the value of ξ. The yield line nearest the corner of the section must not exceed the intersection point between the vertical and the horizontal edge of the section; therefore the curves are not valid for small values of ξ.

There is a problem with wedge mechanism no. 1. It is assumed that the bar in the failure situation moves at a velocity of $v = 1$ away from the concrete section and that a part of the concrete cover moves a distance $v = 1$ away from the bar (and at a velocity of $v = 2$ away from the concrete section). This means that the space near the bar, produced by the concrete moving away from the section, must have a dimension which is at least equal to the diameter of the bar. As can be seen in figure 5.17, this condition is not fulfilled. The mechanism is therefore changed to the one shown in figure 5.19 called *Wedge mechanism no. 2.*
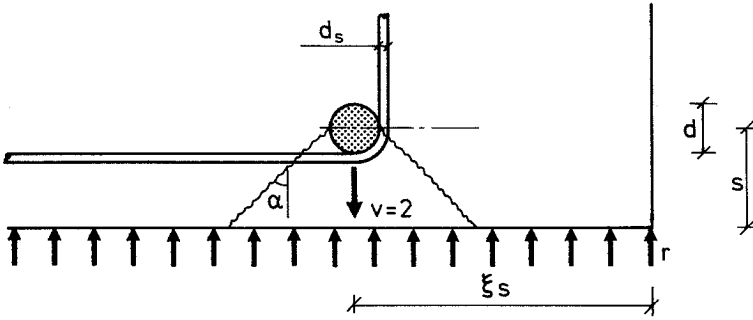
Figure 5.19: *Wedge mechanism no. 2; geometry and yield line pattern.*

Wedge mechanism no. 2 looks like no. 1, but the yield lines touch the bar at the intersection point between the periphery of the bar and a horizontal line though the center of the bar. The load found from mechanism no. 2 will always be larger than the load from mechanism no. 1, because the yield lines, other things being equal, are longer. However, mechanism no. 1 is not geometrically possible and can, strictly speaking, not be used. The mechanism appearing in practice is probably a combination of the two mechanisms.

The problem with the contribution from the stirrups is not as pronounced in wedge mechanism no. 2 as it is in no. 1. The active area is almost identical with the total area for the possible values of α [1]. The reduction of the contribution from the stirrups is negligible and will not be considered in this mechanism.

The following expression for the total dimensionless internal work can be obtained

$$C = 2\frac{s}{\pi d}\left[\frac{\lambda - \mu\sin\alpha}{\cos\alpha} + 2\frac{r}{f_c}\left(\tan\alpha + \frac{d}{2s}\right) + \frac{d}{2s}\psi\right] \qquad (5.32)$$

Minimizing this expression with respect to α returns

$$C = 2\frac{s}{\pi d}\left[2\sqrt{(\rho + \frac{r}{f_c})(\nu - k\rho - \frac{r}{f_c})} + \frac{d}{s}\frac{r}{f_c} + \frac{d}{2s}\psi\right] \quad \text{for} \quad \frac{r}{f_c} < \frac{1}{k+1}(\nu - 2k\rho) \qquad (5.33)$$

$$C = 2\frac{s}{\pi d}\left[\frac{\nu}{\sqrt{k}} + \frac{r}{f_c}\left(\frac{k-1}{\sqrt{k}} + \frac{d}{s}\right) + \frac{d}{2s}\psi\right] \quad \text{for} \quad \frac{r}{f_c} \geq \frac{1}{k+1}(\nu - 2k\rho) \qquad (5.34)$$

---

[1] α will be between φ and $\frac{\pi}{2}$
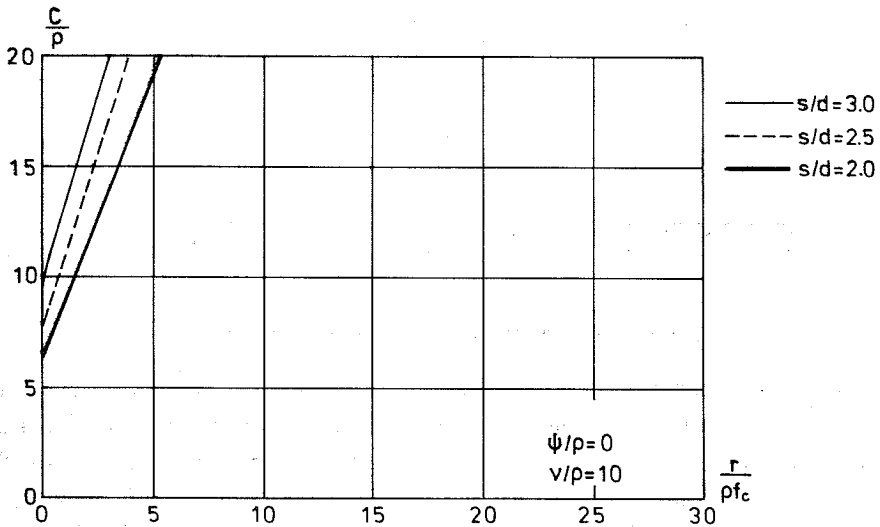
Figure 5.20: *The relationship between $\frac{C}{\rho}$ and $\frac{r}{\rho f_c}$ for wedge mechanism no. 2, for different values of $\frac{s}{d}$.*

where α is determined by

$$\sin \alpha = \frac{\mu - 2\frac{r}{f_c}}{\lambda} \qquad (5.35)$$

(5.33) corresponds to $\alpha > \varphi$ and (5.34) corresponds to $\alpha = \varphi$.

The relationship between $\frac{C}{\rho}$ and $\frac{r}{\rho f_c}$ for wedge mechanism no. 2 is in princi-
ple the same as for wedge mechanism no. 1, but the values for $\frac{C}{\rho}$ are larger.
In figure 5.20 examples are shown.

For a certain value of the horizontal distance from the bar to the vertical
surface of the section ξ, the right yield line in figures 5.17 and 5.19 will
change to a horizontal line, going from the bar to the vertical surface of
the section. This mechanism appears in the translation mechanisms with
three free parameters in section 5.1.2. For smaller values of ξs the "normal"
translation mechanism appeares. This situation is outlined in figure 5.21.

Mechanism **I** in figure 5.21 is the wedge mechanism and mechanisms **II**–
IV are the translation mechanism with the limitations $\theta \in [0; \frac{\pi}{2}]$. The last
mechanism, named **V**, has not been treated yet. If ξ is small, this mecha-
nism can be decisive. The mechanism is similar to the wedges mechanisms
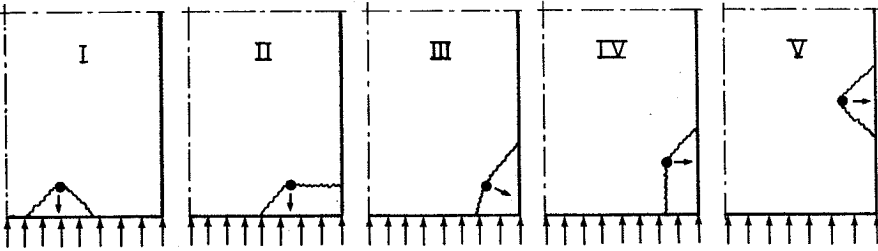
Figure 5.21: *Different mechanisms for different geometrical properties of the section*
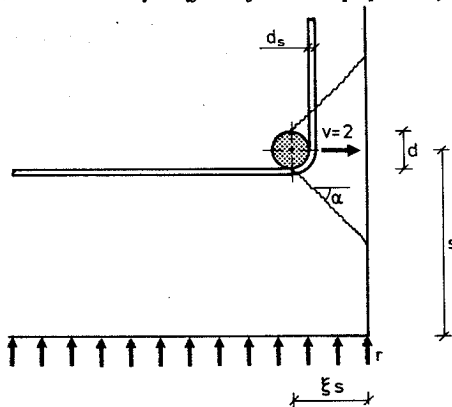
Figure 5.22: *Wedge mechanism no. 3; geometry and yield line pattern.*

treated above, but the direction of the displacement is horizontal instead of vertical. The mechanism is shown in a larger scale in figure 5.22.

The mechanism will be named *wedge mechanism no. 3*. The yield line pattern is assumed to be similar to the yield line pattern in mechanism no. 2. The solution can then be obtained from the expressions for mechanism no. 2, (5.33) − (5.35), making $\frac{r}{f_c} = 0$ and changing s to ξs.

$$C = \frac{1}{\pi}\left[4\frac{\xi s}{d}\sqrt{\rho(\nu - k\rho)} + \psi\right] \text{ for } \rho < \frac{\nu}{2k} \qquad (5.36)$$

$$C = \frac{1}{\pi}\left[2\frac{\xi s}{d}\frac{\nu}{\sqrt{k}} + \psi\right] \text{ for } \rho \geq \frac{\nu}{2k} \qquad (5.37)$$

In the case where $\frac{s}{d} = 2.5$, $\xi = 0.5$, $\frac{\nu}{\rho} = 10$, and $\psi = 0$, the value for $\frac{C}{\rho}$, obtained from (5.37), is 3.90, corresponding to $\alpha \simeq 45$ degrees. For $\xi = 1.0$, (5.37) can not be used because the geometry limits the lower yield line.
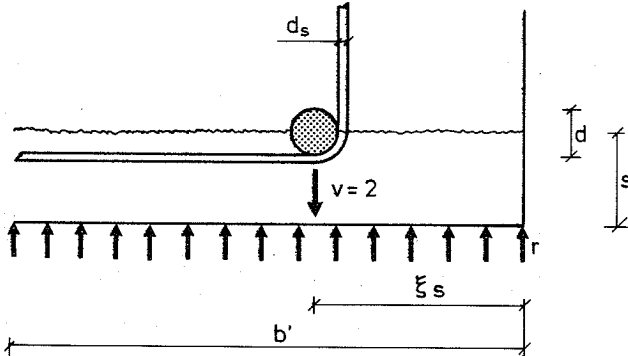
Figure 5.23: *Plate mechanism, geometry and yield line pattern.*

Using (5.32) with $\frac{r}{f_c}$, s changed to ξs, and $\alpha \simeq 38.7$ degrees, corresponding to $\tan \alpha = 0.8$, yields $\frac{C}{\rho} \simeq 7.90$.

It must be observed that wedge mechanism no. 1 corresponds to translation mechanism no. 1 and wedge mechanism no. 2 corresponds to translation mechanism no. 2.

5.1.4 Plate mechanism

The plate mechanism is unusual, because it cannot take place for a single bar only; all the bars in the section have to participate in the failure mechanism. However, if the section has one bar only, the plate mechanism can of course take place for this bar. To obtain an expression, which can be compared with the other mechanisms, a hypothetical case is treated first, see figure 5.23.

The yield line pattern in the *plate mechanism* consists of a horizontal yield line through the center of the bar. The bottom concrete cover is at failure displaced by $v = 2$ in a vertical direction, opposite to the reaction stress r.

The following expressions are obtained for the different internal works

$$W_{ic} = vld\rho f_c(b' - d) \tag{5.38}$$

$$W_{it} = \frac{1}{2}vA_{ss}f_{ys}n_s \tag{5.39}$$

$$W_{ir} = vlb'r \tag{5.40}$$
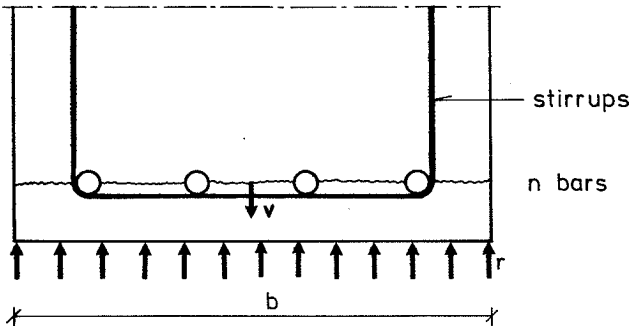
Figure 5.24: *Bottom of a beam section having n bars and normal stirrups.*

By means of (5.38) – (5.40), the total dimensionless internal work can be found

$$C = \frac{2}{\pi}\left[\rho\left(\frac{b'}{d} - 1\right) + \frac{r}{f_c}\frac{b'}{d} + \frac{1}{2}\psi\right] \tag{5.41}$$

Expression (5.41) can be generalized to be valid for a beam having the width b, n bars and normal stirrups, see figure 5.24.

In this case the expression for the total dimensionless internal work can be given by

$$C = \frac{2}{\pi n}\left[\rho\left(\frac{b}{d} - n\right) + \frac{r}{f_c}\frac{b}{d} + \psi\right] \tag{5.42}$$

(5.42) is shown in figures 5.25 and 5.26 for different values of the parameters.

5.2 Comparison of the Mechanisms

The different mechanisms in section 5.1 are compared here. The corner mechanisms, (the rotation and the translation mechanisms), will be compared. The transition between the wedge mechanism and the translation mechanism will be discussed and the load obtained from the two mechanisms will be compared. Finally, the plate mechanism will be compared to the rotation mechanism.

The limits for the different mechanisms are not discussed in the previous. To be correct, the variable parameters cannot be chosen freely in all the mechanisms, independent of the geometrical properties. But as will be seen in the following discussion on the translation/wedge mechanism, the problem is not generally an actual one, when all the mechanisms are considered.
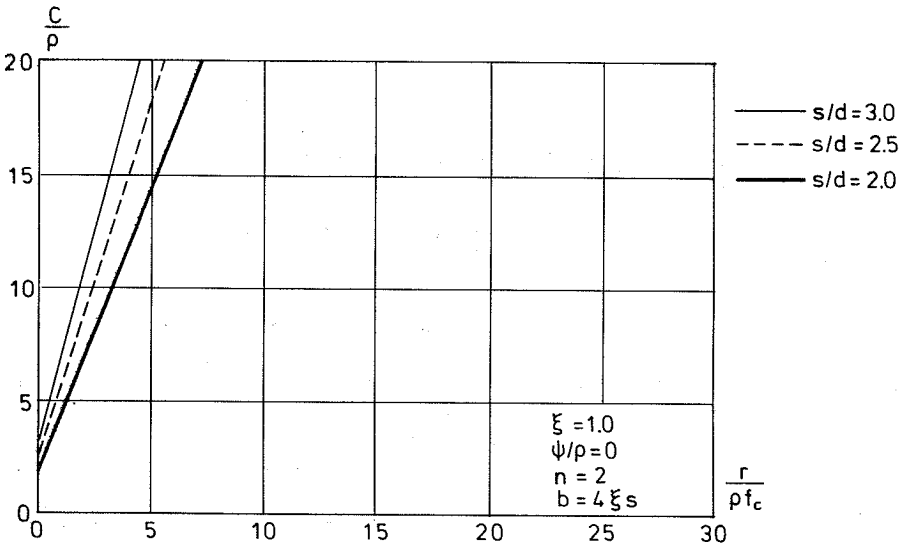
Figure 5.25: $\frac{C}{\rho}$ from (5.42) as a function of $\frac{r}{\rho f_c}$ for different values of $\frac{s}{d}$, in the case $b = 4\xi s$ and $n = 2$.
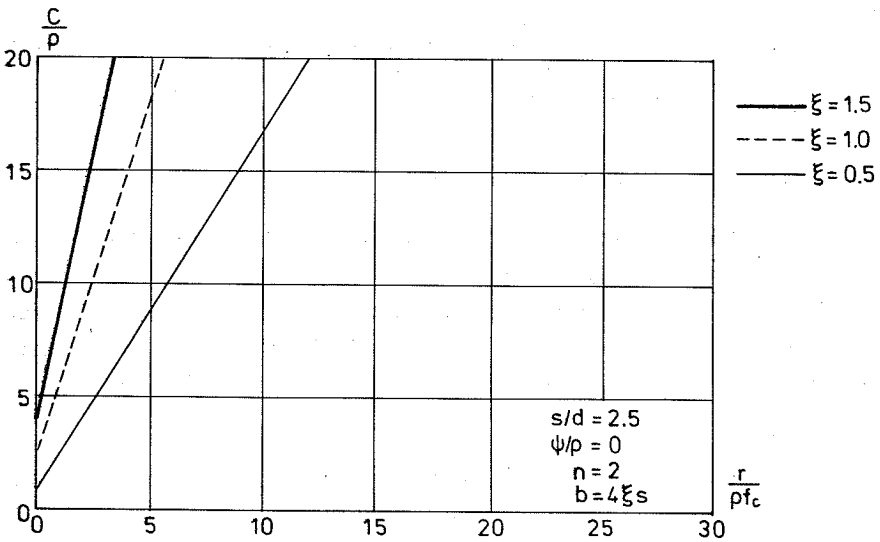
Figure 5.26: $\frac{C}{\rho}$ from (5.42) as a function of $\frac{r}{\rho f_c}$ for different values of ξ, in the case $b = 4\xi s$ and $n = 2$.
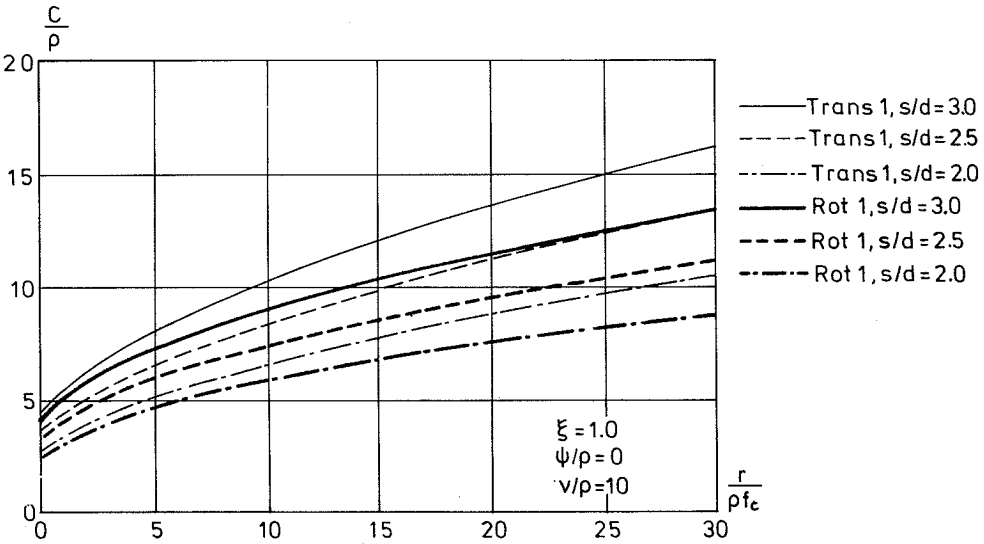
Figure 5.27: $\frac{C}{\rho}$ as a function of $\frac{r}{\rho f_c}$ for rotation mechanism no. 1 and translation mechanism no. 1, for different values of $\frac{s}{d}$.

When one mechanism is not geometrically possible anymore, another will automatically take over, because the load obtained from the new one will be lower. In the case of the rotation and translation mechanisms, the intersection point between the vertical surface of the section and the upper yield line, going from the bar to the vertical surface of the section, must be inside the section. If the height of the section is minimal and the limit point is exceeded, the mechanisms will change in such a way, that the upper yield line will go from the reinforcing bar, vertically up to the top of the section. In the case of beams it will not normally be necessary to check this limit, but in the case of a corner bar in a slab, it is very likely that the failure mechanism will be one with a vertical yield line going through the center of the bar. Expressions for these limit mechanisms are expounded in chapter 6.

In figure 5.27, $\frac{C}{\rho}$ is shown as a function of $\frac{r}{\rho f_c}$ for rotation mechanism no. 1, and translation mechanism no. 1 for different values of $\frac{s}{d}$.

In the cases illustrated the rotation mechanism yields values for $\frac{C}{\rho}$ less than

the values obtained from the translation mechanism. For $\frac{r}{\rho f_c} = 0$ the values are almost identical. In general the rotation mechanism is the better of the two, but in some cases the translation mechanism yields the lower values, for instance, for $\frac{s}{d} = 2.5$, $\xi = 0.5$, $\psi = 0$, $\frac{\nu}{\rho} = 10$, and small values of $\frac{r}{\rho f_c}$. However, the difference between them is in this case limited.

As indicated in figure 5.21, the wedge and the translation mechanisms are basically the same kind of mechanism. When one mechanism is not valid anymore, the other will take over. It must be noticed that the mechanisms in figure 5.21, **II** and **IV**, cannot appear when (5.17) is used, because the angles between the yield lines and the displacement direction cannot be equal in this case. Assuming that mechanism **IV** can appear, the expression for C can be written

$$C = \frac{1}{\pi}\left[2\frac{\xi s}{d}\sqrt{\rho(\nu - k\rho)} + 2\frac{s}{d}\rho\left(1 - \frac{1}{2}\frac{d}{s}\right) + \psi\right] \quad \text{for} \quad \rho < \frac{\nu}{2k} \quad (5.43)$$

$$C = \frac{1}{\pi}\left[\frac{\xi s}{d}\frac{\nu}{\sqrt{k}} + 2\frac{s}{d}\rho\left(1 - \frac{1}{2}\frac{d}{s}\right) + \psi\right] \quad \text{for} \quad \rho \geq \frac{\nu}{2k} \quad (5.44)$$

The expressions can be compared with the expressions for wedge mechanism no. 3.

Assuming $\frac{\rho}{\nu} < \frac{1}{2k}$ expressions (5.37) and (5.43) are valid and it is seen that wedge mechanism no. 3 will be less than the special translation mechanism represented by (5.43) and (5.44) when

$$\xi\sqrt{\frac{\nu}{\rho} - k} \leq 1 - \frac{d}{2s} \quad (5.45)$$

For $\xi s = k_1 d$, where k_1 is a constant, (5.45) can be rewritten into

$$\frac{s}{d} \geq \frac{1}{2}\left(1 + 2k_1\sqrt{\frac{\nu}{\rho} - k}\right) \quad (5.46)$$

For the case where $k_1 = 2.5$, $k = 4$, and $\frac{\nu}{\rho} = 10$ (5.46) yields $\frac{s}{d} \simeq 6.6$. This indicates that wedge mechanism no. 3 will be decisive only in cases where the geometry is special. Furthermore, if the ratio between the tensile and compression strengths of the concrete is less than the used value, the value for $\frac{s}{d}$ will be larger and the wedge mechanism will be decisive in fewer cases.

In the same manner the mechanisms in figure 5.21, **I** and **II**, can be compared. The difference from the analysis above, is that the reaction has an
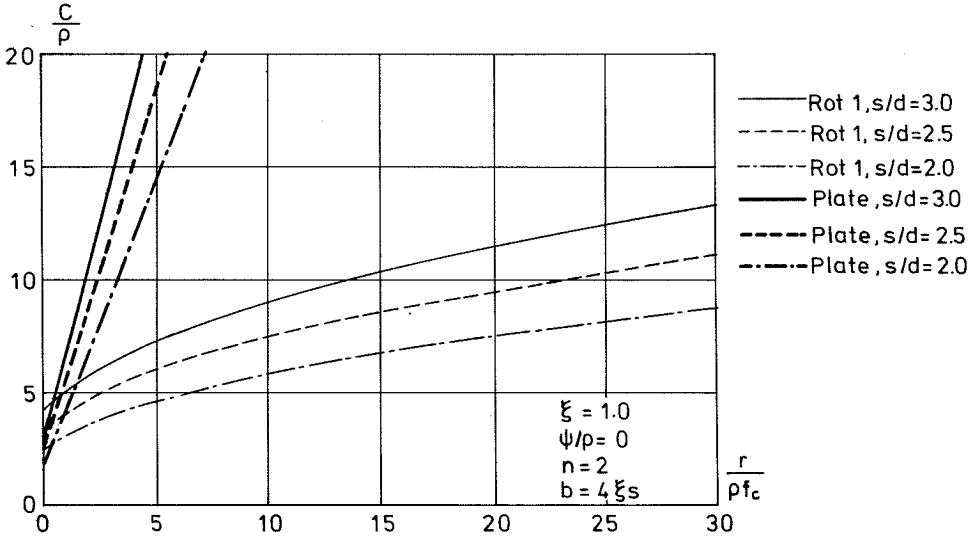
Figure 5.28: $\frac{C}{\rho}$ as a function of $\frac{r}{\rho f_c}$ for rotation mechanism no. 1 and the plate mechanism, for different values of $\frac{s}{d}$.

influence in this case, i.e. it is not only the tensile strength which governs the problem (when the geometry is not considered). Assuming $\alpha = \varphi$ it can be shown that the equation corresponding to (5.45) in this case becomes

$$\xi \geq \frac{\frac{\nu}{\rho} + (k-1)\frac{r}{\rho f_c}}{2\sqrt{k}\left(1 + \frac{r}{\rho f_c}\right)} + \frac{1}{2}\frac{d}{s} \qquad (5.47)$$

where wedge mechanism no. 2 is used.

Inserting $k = 4$, $\frac{\nu}{\rho} = 10$, $\frac{r}{\rho f_c} = 10$, and $\frac{s}{d} = 2.5$ into (5.47) gives $\xi \geq 1.1$. Hence the wedge mechanism in this case can be decisive in some situations. However, translation mechanism III in figure 5.21 should probably be used instead of II. But the main conclusion, that the wedge mechanism can be decisive in some cases, will not change.

Figure 5.28 shows $\frac{C}{\rho}$ as a function of $\frac{r}{\rho f_c}$ for different values of $\frac{s}{d}$, for rotation mechanism no. 1 and the plate mechanism.

As can be seen from the figure, the plate mechanism yields values of $\frac{C}{\rho}$ less than the values obtained from the rotation mechanism, when $\frac{r}{\rho f_c}$ is small as

in the cases shown. However, in practice, the plate mechanism will not in general be decisive in the case of anchorage at supports.

Comparing figures 5.8 and 5.9 with figures 5.25 and 5.26, valid for rotation mechanism no. 2 and the plate mechanism it can be seen that for small values of $\frac{\tau}{\rho f_c}$ these two mechanisms are almost identical in the cases shown.

All things considered, it seems as if rotation mechanism no. 1 describes the conditions at a beam support better than the other mechanisms. In some cases the rotation mechanism does not result in the lowest load, but in general it is the best one when only a single mechanism is used.

5.3   Complete failure Mechanisms

The failure mechanisms in section 5.1 are valid for a single bar only, apart from the generalized plate mechanism. An anchorage failure in a section has to include all active bars in the actual section. Hence the mechanism must be combined in such a way, that the total load carrying capacity is minimized.

Considering a beam having $n = 3$ bars, the complete failure mechanism could, for instance, consist of rotation mechanisms for the two corner bars and a wedge mechanism for the bar in the middle. The total force is found by determining $\frac{\tau}{f_c}$ for the 3 bars, taking into account possible different local failures for the bars, adding them, and then determining the total force which can be carried. Another way of carrying out the calculations, is to determine the value of the total dimensionless internal work C for the different bars. These values are added and divided by the number of bars n, which produces a mean value for C. This value for C is now used in the expressions for the local failure and $\frac{\tau}{f_c}$ is found. The force in one bar can now be determined and the total force can be calculated by multiplying this value with the number of bars n. Carrying out the calculations in this way is not theoretically correct, because the different bars might have different local failures, and because the expressions for the local failures do not have a linear relationship between $\frac{\tau}{f_c}$ and C, except for the expression for failure shape 2a. In practice the difference between the load carrying

capacity calculated correctly and that calculated by the simplified method, is normally without any significance. Furthermore the simplified method is easier to use, because the best combination of mechanisms in the section can be found only by considering the value of C. Henceforth the simplified method is used, unless otherwise stated.

As mentioned in section 5.1.4 the plate mechanism is special because it constitutes a complete mechanism in itself. Expression (5.42) for C in a beam having n bars can of course be compared with the expressions for C found from the best combination of the other mechanisms.

5.4 Discussion

In the preceding the cross section considered is mainly a beam section. In the case of slabs, the expressions developed can be used without any changes. The corner mechanism is not as important for slabs because the corner bars form only a small part of the total number of bars. Hence it is mainly the wedge and plate mechanisms which are used. The complete failure mechanisms are produced in the same way as for beams. This indicates that slabs in principle do not create any problems, as compared with beams.

The solutions for the failure in the surroundings, set up in section 5.1, are based on the upper bound theorem. In the majority of the mechanisms it is doubtful whether the solutions are accurate. Lower bound solutions could of course be carried out, but the expressions would probably be very complicated. Figure 5.29 illustrates what the rotation mechanism would be like, if it were to correspond to a likely stress field.

As can be imagined, the solutions for both the modified rotation mechanism and the corresponding lower bound solution are too complicated to use in practical calculations. Lower bound solutions for the failure in the surroundings are not treated in more detail here. The modified rotation mechanism and a modified translation mechanism are treated in chapter 6 in the case of anchorage at a support of more than one layer of reinforcement.
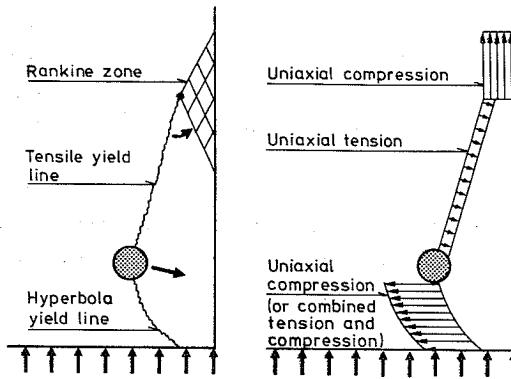
Figure 5.29: *Modified rotation mechanism and the corresponding stresses.*

The expressions set up previously all correspond to a failure in the concrete with yield lines going from the bar to the surface of the concrete section. If the reinforcing bar is placed at a distance from the concrete edges, parallel to the longitudinal direction of the bar, these kinds of failure will probably not occur. As mentioned in section 4.4, an anchorage failure in this case will certainly be a failure which can be considered to be a local failure[2], i.e. the failure pattern only involves the concrete and possible surrounding reinforcement immidiately around the bar. This case will not be treated here, but it must be observed that this type of failure constitutes an upper limit for the anchorage strength.

The kind of structural element assumed previously is an idealization of the ones appearing in practice. Often the beam or slab will continue for a certain length beyond the support. Using the expressions set up and not taking into account this length results in a safe value for the strength. However, the construction without any length beyond the support considered, appears in reality; therefore the best thing to begin with, is to develop the theory without taking into account the length beyond the support.

It is assumed that the support stress is evenly distributed at failure. This assumption requires that the support plate is not rigid. However, the dis-

---

[2]This must not be confused with the Local Failure treated in chapter 4.
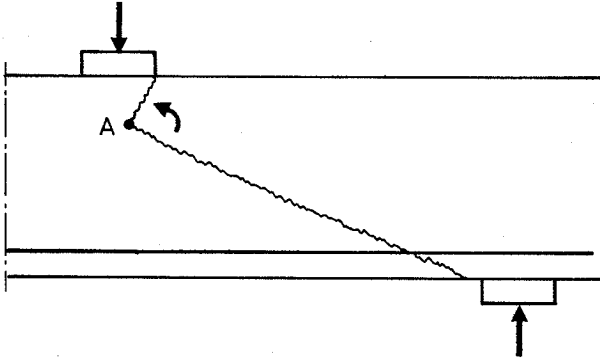
Figure 5.30: *Combined shear-bending failure at a beam end.*

placements in an anchorage at failure are small compared to the deformations for the whole structure up to failure. Hence the support stress can be assumed to be evenly distributed even if the support plate is rigid.

Hitherto it has just been accepted that an anchorage failure can take place in the way described. But in fact, in a real structure, is it possible for the bar to move forward[3] in the failure situation, as assumed in the calculations of the local failure around a bar ?. If the beam in figure 5.1 is considered and the only failure which appears in the structure is the anchorage failure, it is not possible for the bar to move forward. Hence the anchorage failure cannot take place in the way described here without involving other parts of the structure. Because of this, other kinds of failure must develop parallel to the anchorage failure. The other failure types can, for instance, be a combined shear-bending failure, as shown in figure 5.30, where the displacement consists of a rotation about a point A, under the load plate.

The beam in figure 5.30 with the illustrated failure pattern, can fail in at least two ways. The reinforcement yields or the connection between the reinforcement and the concrete over the support disappears. In the first possibility the beam fails in principle, in a normal shear or bending failure. The second possibility is identical with, what has previously been called an anchorage failure.

The reinforcement can only move forward and the anchorage failure develops if displacements like the one in figure 5.30 take place. Therefore,

---

[3]Increment in the displacement in the direction of the force in the bar.

the anchorage failure must take place as a failure "inside" other kinds of failure. This results in difficulty in distinguising the anchorage failure from other kinds of failure. However, theoretically it is possible to separate the anchorage failure from the other kinds of failure.

With the kind of superior failure as indicated in figure 5.30, dowel action will probably appear in the bars. The dowel action is possibly of little importance, but it cannot be denied that it will have an influence in some situations. The dowel action will undoubtedly influence the failure pattern when the structure is unloaded - a horizontal crack through the bars which was not visible when the load was active can appeare.

It must be concluded that it is acceptable to assume the displacements in the anchorage failure to be independent of the other displacements appearing in the structure. Therefore the expressions developed in the preceding are applicable for structures in practice.

Chapter 6

Anchorage at Supports of More Layers of Reinforcement

In this chapter anchorage of more than one layer of reinforcement at a beam support is treated. Failure mechanisms for bars placed over one another in a corner are considered.

Expressions for C, the total dimensionless internal work, will be set up. Contributions from concrete, stirrups, and support reaction will be taken into account. In the case of anchorage at supports of one layer of reinforcement, it was assumed that the surrounding reinforcement, the stirrups, followed the main reinforcement in the movements at failure, i.e. the displacement was taken to be $\frac{1}{2}v$, where v is the displacement of the concrete cover moving away from the concrete section at failure. In this case this assumption seems to be reasonable, at all events in the case of the rotation, the translation, and the wedge mechanisms, where the stirrups are placed close to the bar and the yield lines go from the bar to the nearest concrete edge. In the case of anchorage in more than one layer, the situation can be as shown on the left in figure 6.1, where a yield line pattern is indicated.

At failure the concrete cover is displaced away from the concrete section by the velocity v. Assuming the stirrups to follow the main reinforcement the velocity is $\frac{1}{2}v$ for these contributions. But as seen in figure 6.1 this can not be possible immediately, because that part of the stirrups, located in the concrete cover moving away from the section, will accompany the concrete. This problem can be solved in at least two ways. The dowel action in the stirrups is taken into account in the calculations. However, this seems to be
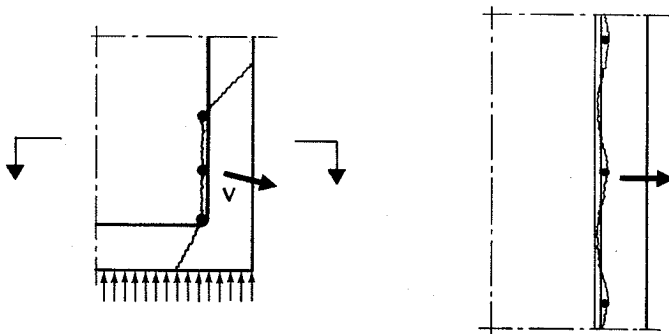
Figure 6.1: *Anchorage in more than one layer at a support.*

too detailed a model in comparison to the way in which the expressions
for the axisymmetrical local failure are used. Another possibility is to as-
sume that the yield lines go around the stirrups as indicated in figure 6.1
on the right. This type of failure will yield almost the same load as the
original failure pattern, when the distance between the stirrups is not too
small. In the light of this, it is assumed, that the stirrups follow the main
reinforcement at failure, even if this is not entirely theoretically correct.

6.1   Failure mechanisms

The mechanisms considered here contain in general more variable parame-
ters than the corresponding mechanisms in chapter 5. This results in more
freedom but also in more complicated expressions. Mechanisms correspond-
ing to the rotation and the translation mechanisms are treated.

6.1.1   Rotation mechanism

The expressions for the local failure can be used immediately in a failure
mechanism involving one or more than one bar, if all bars moves equally.
The total dimensionless internal work, C, is found as C for the entire mecha-
nism divided by the number of bars, see for instance section 5.1.4. However,
if all the bars are not displaced in the same way, it can in some cases be
shown, that the expressions for the local failure can be used. C then has to
be calculated taking into consideration the special conditions.
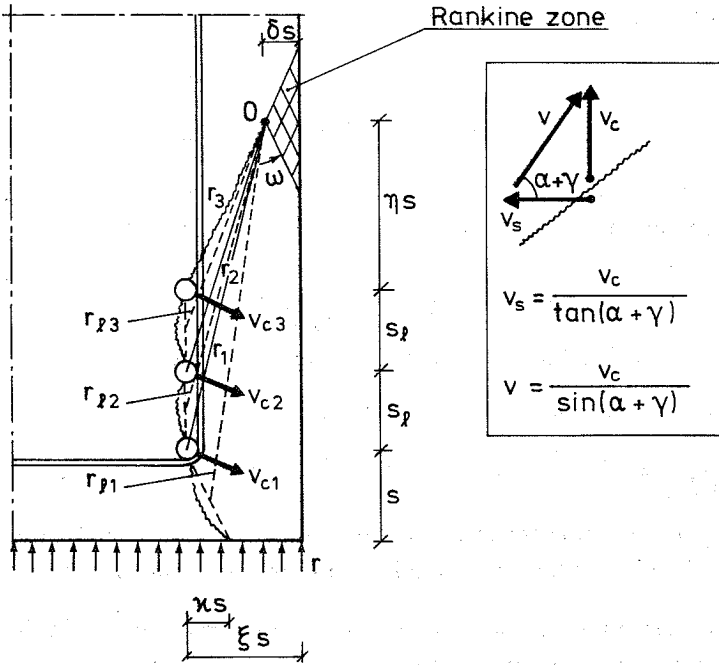
Figure 6.2: *Rotation mechanism for one or more than one layer of reinforcement; geometri and yield line pattern.*

In the case of the rotation mechanism for more than one layer of reinforcement, the direction and size of the displacements for the different bars are not equal. In figure 6.2 an example with three bars is shown.

The displacements results from a rotation ω, about a point O, placed the vertical distance ηs from the top bar and the horizontal distance δs from the vertical surface of the concrete section. The distance between the bars and the point of rotation is denoted by r_i, and the displacement for the different bars is denoted v_{ci}, where i is equal to 1, 2, or 3 for the first, the second, and the third layer, respectively. v_{ci} is equal to the displacement of the concrete in the calculations for the local failure in chapter 4. The remaining quantities shown in figure 6.2 will be introduced later.

The total external work can be written as

$$\frac{W_e}{\pi d l f_c} = \frac{\tau_1}{f_c}v_{s1} + \frac{\tau_2}{f_c}v_{s2} + \frac{\tau_3}{f_c}v_{s3} \qquad (6.1)$$

assuming that the diameter d is equal for all the bars.

Furthermore, assuming the force in all bars to be equal and the angles α and γ in the local failure to be equal for the different bars, (6.1) can be found to be

$$\frac{W_e}{\pi d l f_c} = \frac{\tau}{f_c}\frac{v_{c1}}{\tan(\alpha + \gamma)}\left(1 + \frac{r_2}{r_1} + \frac{r_3}{r_1}\right) \qquad (6.2)$$

where the relationship on the right in figure 6.2 have been used.

The total internal work can be written as

$$\frac{W_i}{\pi d l f_c} = (D_1 v_1 + C_1 v_{c1}) + (D_2 v_2 + C_2 v_{c2}) + (D_3 v_3 + C_3 v_{c3}) \qquad (6.3)$$

where D_i is the total dissipation in the concrete from the local failure around bar No. i and C_i is the corresponding internal work from the surroundings.

Using the assumptions mentioned above and the relationship in figure 6.2, the expressions for the internal work can be written into

$$\frac{W_i}{\pi d l f_c} = D_1\frac{v_{c1}}{\sin(\alpha + \gamma)}\left(1 + \frac{r_2}{r_1} + \frac{r_3}{r_1}\right) + \left(C_1 + C_2\frac{r_2}{r_1} + C_3\frac{r_3}{r_1}\right) \qquad (6.4)$$

Using the upper bound theorem on (6.2) and (6.4) yields

$$\frac{\tau}{f_c} = \frac{D}{\cos(\alpha + \gamma)} + \frac{C_1 + C_2\frac{r_2}{r_1} + C_3\frac{r_3}{r_1}}{1 + \frac{r_2}{r_1} + \frac{r_3}{r_1}}\tan(\alpha + \gamma) \qquad (6.5)$$

which is equal to the expression in chapter 4 if

$$C = \frac{C_1 + C_2\frac{r_2}{r_1} + C_3\frac{r_3}{r_1}}{1 + \frac{r_2}{r_1} + \frac{r_3}{r_1}} \qquad (6.6)$$

D is the total dissipation in the concrete from the local failure around one bar. The total dimensionless internal work C_T can be introduced as

$$C_T = \frac{C_1 r_1 + C_2 r_2 + C_3 r_3}{r_i} \qquad (6.7)$$

where r_i corresponds to the bar having a velocity v_{ci} of 2. The denominator in (6.6) is changed to $\frac{(r_1 + r_2 + r_3)}{r_i}$ in this case.

In the case of n_l layers of reinforcement, the dimensionless internal work can be calculated as

$$C = \frac{C_T}{\frac{r_1+r_2+.....r_{nl}}{r_i}} \tag{6.8}$$

where v_{ci} is equal to 2 for bar number i. C_T is calculated as if there were only one bar. The expression for C can be inserted directly into the expressions for the local failure from chapter 4.

This solution is probably an upper bound solution, because the geometrical quantities α and γ and the shear stress are assumed to be equal for the different bars. However, the method is simple and the expressions for the local failure can be used without any changes.

In the following calculations it is assumed that there are n_l layers of reinforcement, where n_l is a positive integer, that the distance between the different layers is equal to s_ℓ, and that all the bars have the same geometrical properties. The yield line pattern is assumed to consist of a compression zone, the Rankine zone in figure 6.2, a tensile zone similar to the tensile zone for the rotation mechanism in section 5.1.1, and curved yield lines below the bars. Assuming the curved yield lines to be hyperbolas, the dissipation in them can be determined in a simple way, as described in Jensen [81.3] and Exner [83.1]. The quantities η, κ, and δ are variable parameters.

Assuming the velocity at the bottom bar to be equal to 2, the angle of rotation can be given as

$$\omega = \frac{2}{s\sqrt{(\xi - \delta)^2 + \left(\eta + (n_l - 1)\frac{s_l}{s}\right)^2}} \tag{6.9}$$

The dimensionless internal work can be found by using the principles above

$$
\begin{aligned}
C = \frac{\frac{1}{2}\omega s}{\sum_{i=1}^{n_l} \frac{r_i}{r_1}} \frac{s}{\pi d} \Bigg[& \nu\delta^2 + \rho\left(\sqrt{(\xi - \delta)^2 + \eta^2} - \frac{1}{2}\frac{d}{s}\right)^2 \\
& + (\lambda - \mu \sin\alpha_{l1})\frac{r_{l1}}{s}\left(\sqrt{\kappa^2 + 1} - \frac{1}{2}\frac{d}{s}\right) \\
& + \left(\frac{s_l}{s} - \frac{d}{s}\right)\sum_{i=2}^{n_l}(\lambda - \mu \sin\alpha_{li})\frac{r_{li}}{s} \\
& + \frac{d}{s}\psi\left(\xi - \delta + \eta + \frac{s_l}{s}(n_l - 1)\right)
\end{aligned}
$$

$$+\frac{r}{f_c}(\xi - \delta - \kappa)^2\Bigg] \tag{6.10}$$

where

$$r_i = s\sqrt{(\xi - \delta)^2 + \left(\eta + \frac{s_l}{s}(n_l - i)\right)^2} \quad , \quad i \in \{1, 2, ...n_l\} \tag{6.11}$$

$$r_{li} = \sqrt{x_{li}^2 + y_{li}^2} \quad , \quad i \in \{1, 2, ...n_l\} \tag{6.12}$$

$$\sin \alpha_{l1} = \frac{y_{l1} - x_{l1}\kappa}{|r_{l1}|\sqrt{\kappa^2 + 1}} \tag{6.13}$$

$$\sin \alpha_{li} = \frac{y_{li}}{|r_{li}|} \quad , \quad i \in \{2, 3, ...n_l\} \tag{6.14}$$

x_{li} and y_{li} can be determined from

$$x_{l1} = s\left(\xi - \delta + \frac{1}{2}\kappa\left(1 + \frac{\frac{d}{2s}}{\sqrt{\kappa^2 + 1}}\right)\right) \tag{6.15}$$

$$y_{l1} = s\left(\eta + \frac{s_l}{s}(n_l - 1) + \frac{1}{2}\left(1 + \frac{\frac{d}{2s}}{\sqrt{\kappa^2 + 1}}\right)\right) \tag{6.16}$$

$$x_{li} = s(\xi - \delta) \quad , \quad i \in \{2, 3, ...n_l\} \tag{6.17}$$

$$y_{li} = s\left(\eta + \frac{s_l}{s}\left(n_l - i + \frac{1}{2}\right)\right) \quad , \quad i \in \{2, 3....n_l\} \tag{6.18}$$

As can be seen, the expressions are complicated and it is difficult to carry out the calculations analytically. However, it is possible to minimize with respect to the three variable parameters η, κ, and δ using a numerical method. The variable parameters are limited to $\eta \in \left[0; \frac{h}{s} - 1 - (n_l - 1)\frac{s_l}{s}\right]$, $\kappa \in [-\infty; \xi]$, and $\delta \in [0; \xi]$.

If the height of the section, h, is minimal compared with the other dimensions, another failure pattern than that shown in figure 6.2 will appear; for instance the one shown in figure 6.3

The expression for the dimensionless internal work can in this case be written

$$C = \frac{s}{\sum_{i=1}^{n_l} r_i} \frac{s}{\pi d} \left[\rho\left(\left(\frac{h}{s}\right)^2 - 2\frac{d}{s}\sum_{i=1}^{n_l} r_i\right) + \frac{d}{s}\psi\left(\frac{h}{s} - 1 + \frac{s_t}{s}\right) - \frac{r}{f_c}\xi^2\right] \tag{6.19}$$

where

$$r_i = s\left(\frac{h}{s} - 1 - \frac{s_l}{s}(i - 1)\right) \tag{6.20}$$
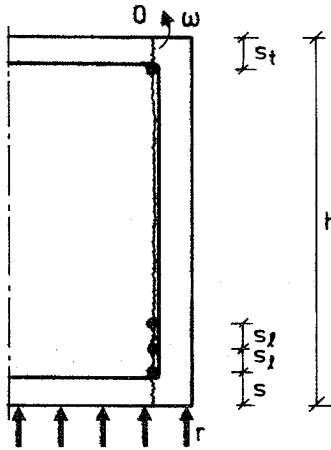
Figure 6.3: *Limit for rotation mechanism, geometri and yield line pattern.*

and s_t is the vertical distance from the top of the beam to the center of the top bar.

In a diagram showing C as a function of $\frac{r}{f_c}$, (6.19) will decrease for increasing $\frac{r}{f_c}$ following a straight line. The normal rotation mechanism (6.10) will, all other things being equal, increase for increasing $\frac{r}{f_c}$. (6.19) will therefore in some cases be decisive for large $\frac{r}{f_c}$ values. In figure 6.4 the expressions (6.10) and (6.19) are shown in a $(\frac{r}{\rho f_c}, \frac{C}{\rho})$ diagram for different values of n_l, the number of reinforcement layers.

As can be seen from figure 6.4, expression (6.19), the limit for (6.10), is decisive only for large values of $\frac{r}{\rho f_c}$, for n_l equal to 3 for the cases shown.

In addition to this, the difference between (6.10) and (6.19) is negligible in the interval where (6.19) is less than (6.10). The situation will of course change for other values of the parameters, but the case shown in figure 6.4 will in general still be valid. The mechanism illustrated in figure 6.3 will be less than the one in figure 6.2 only in unusual cases. It must be observed that the load carrying capacity decreases for increasing n_l, i.e. it might be unsafe to use the expressions for one layer of reinforcement in the case of more than one layer of reinforcement.

The mechanism in figure 6.2, hereafter called the complex rotation mecha-
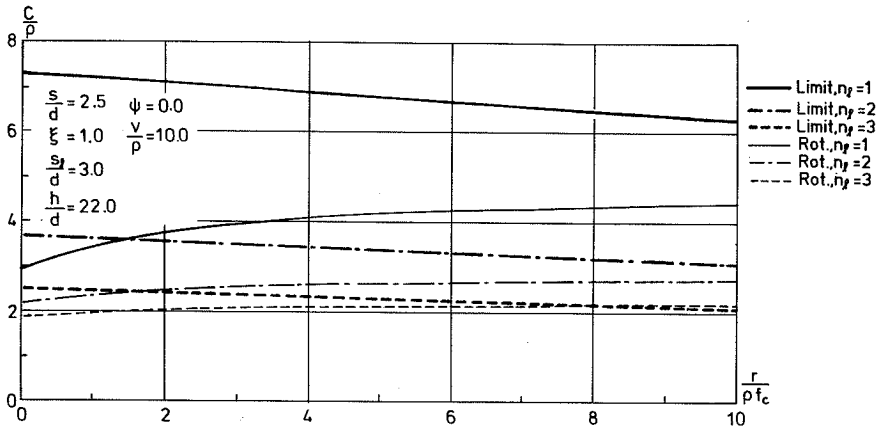
Figure 6.4: $\frac{C}{\rho}$ *as a function of* $\frac{\tau}{\rho f_c}$ *for expression (6.10), denoted* rot., *and (6.19), denoted* limit, *for different values of the number of reinforcement layers* n_l.

nism, can be compared with the mechanism in figure 5.3, named rotation mechanism No. 1, in the case of one layer of reinforcement, i.e. $n_l = 1$. In figure 6.5 two examples are shown.

The well known fact that upper bound calculations reproduce the load carrying capacity with reasonable accuracy, even if the assumed failure mechanism is far from the correct one, seems also to be the fact in the case dealt with here. Of course the complex rotation mechanism is probably not the exact one, but as mentioned in section 5.4, the correct solution (corresponding to displacements by rotation) must be similar to the complex rotation mechanism. Even though the complex rotation mechanism is not the correct mechanism, it must be noticed that the difference in the value of $\frac{C}{\rho}$ for the two mechanisms in figure 6.5 is small, while there is some difference in the yield line patterns obtained. Because it is possible to use a simple mechanism and still obtain acceptable results, it has been attempted to simplify the expressions for the complex rotation mechanism in two ways. The two new mechanisms are outlined in figure 6.6.

The mechanism to the left in figure 6.6 will be known as *the vertical line rotation mechanism,* because κ is assumed to be equal to zero. The other
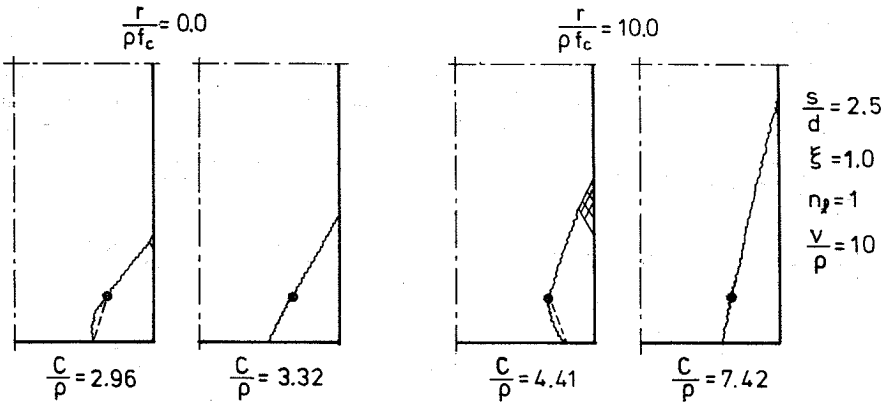
Figure 6.5: *Optimal yield line patterns and dimensionless internal work $\frac{C}{\rho}$ for $\frac{r}{\rho f_c}$ equal to 0 and 10, respectively, for the complex rotation mechanism and rotation mechanism No 1.*
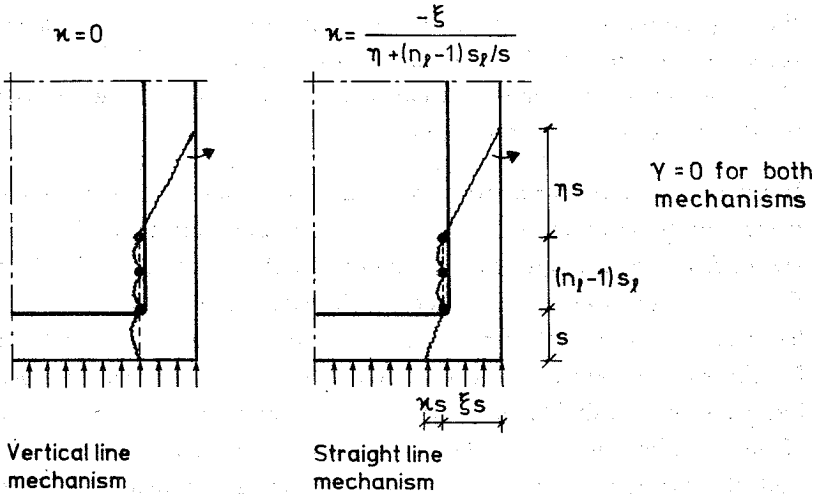
Figure 6.6: *Simplified rotation mechanisms.*
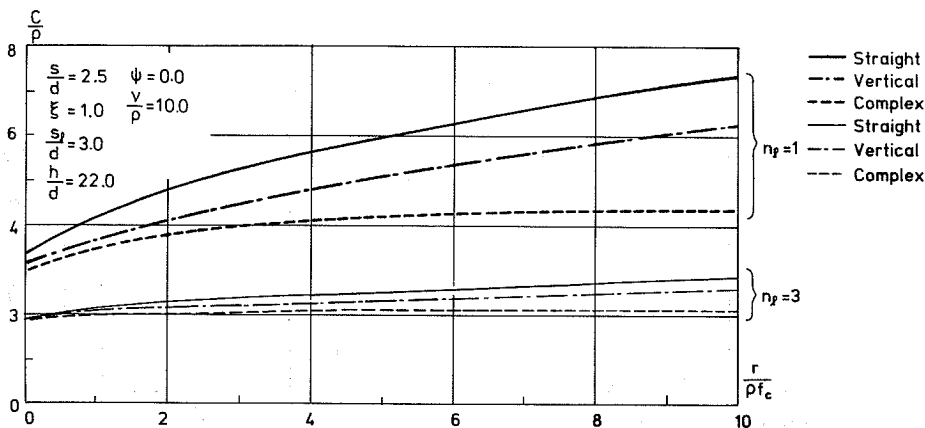
Figure 6.7: $\frac{C}{\rho}$ as a function of $\frac{r}{\rho f_c}$ for the mechanism in figures 6.2 and 6.6, for different values of n_l.

mechanism will be known as *the straight line rotation mechanism*, because the yield line from the lowest bar to the bottom edge of the concrete section is assumed to be a straight line. κ is in this case determined in such a way that a pure tensile yield line will occur. In both mechanisms δ is equal to zero, i.e. the compression zone is removed. In figure 6.7, $\frac{C}{\rho}$ as a function of $\frac{r}{\rho f_c}$ for the two simplified mechanisms is shown, together with expression (6.10) for the original mechanism.

In figure 6.7 curves for n_l equal to 1 and 3 are shown. As can be seen, the values for $\frac{C}{\rho}$ obtained from the vertical line mechanism are less than the values from the straight line mechanism in the cases shown in the figure. For other values of the parameters, the straight line mechanism can be less than the vertical line mechanism. It must be noticed that the curves for the same n_l are fundamentally equal for the three mechanisms. This indicates the possibility of using one of the simplified mechanisms instead of the complex one, even if the load is a little larger. It must be mentioned that the expression for C for the straight line mechanism is more simple than for the vertical line mechanism, especially when n_l is equal to 1.

The type of rotation mechanism used here is not the only possible one but it is a very likely one. In figure 6.8 probable mechanisms and combinations of mechanisms are illustrated.
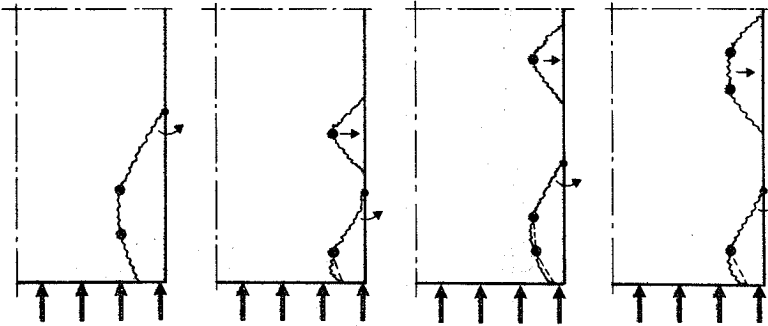
Figure 6.8: *Rotation mechanisms and combinations of mechanisms.*

The mechanism shown to the left in figure 6.8 is identical to the rotation mechanism, except that the yield lines under the bars are assumed to follow straight lines. The expressions for C are in this case more complicated than the expressions for the mechanism treated in this section, and the values obtained are almost equal, when the same number of variable parameters are used.

This yield line pattern and the other yield line patterns in figure 6.8 will not be discussed in detail here. The wedge mechanisms are dealt with in section 5.1.3; therefore there is no difficulty in carrying out the calculations for the combined mechanisms. However, the combined mechanisms will only be decisive in unusual cases, so it is not necessary to check sections with normal geometri for this mechanism.

Sections with normal geometri will probably fail either due to the rotation mechanism treated in this section, or due to the translation mechanism treated in the next section.

6.1.2   Translation mechanisms

The translation mechanism for anchorage in more than one layer is in principle not more difficult to treat than the translation mechanism for one layer of reinforcement. All the bars are assumed to move in the same direction and with the same displacement. The yield line pattern used in the calculations is outlined in figure 6.9.
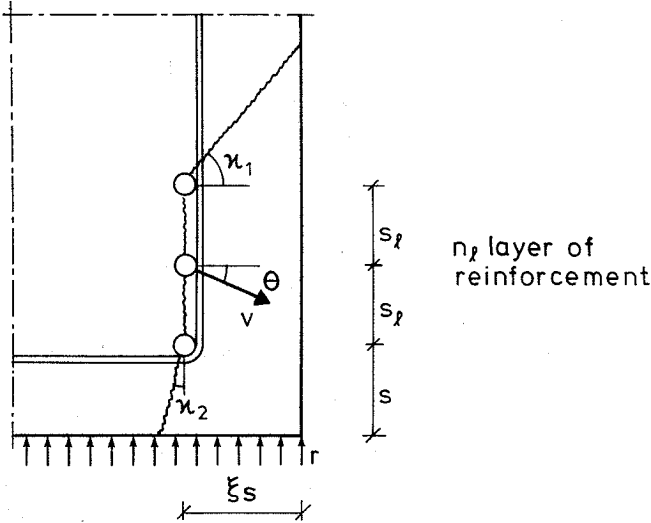
Figure 6.9: *Translation mechanism for one or more than one layer of reinforcement; geometri and yield line pattern.*

The expression for C per bar can, in the case shown in figure 6.9, be found to be

$$
\begin{aligned}
C = \frac{1}{n_l}\frac{s}{\pi d} \quad & \left[(\lambda - \mu \sin(\theta + \kappa_1)) \left(\frac{\xi}{\cos \kappa_1} - \frac{d}{2s} \right) \right. \\
& + (\lambda - \mu \cos(\theta - \kappa_2)) \left(\frac{1}{\cos \kappa_2} - \frac{d}{2s} \right) \\
& + (\lambda - \mu \cos \theta) \left(\frac{s_1}{s} - \frac{d}{s} \right)(n_l - 1) \\
& + \frac{d}{s}\psi(\sin \theta + \cos \theta) \\
& + \left. \frac{r}{f_c} \sin \theta (\xi + \tan \kappa_2) \right]
\end{aligned}
\tag{6.21}
$$

where $\theta + \kappa_1 \in [\varphi; \frac{\pi}{2}]$, $\kappa_2 + \frac{\pi}{2} - \theta \in [\varphi; \frac{\pi}{2}]$, $\kappa_1 \in [0; \frac{\pi}{2}[$, $\kappa_2 \in] - \frac{\pi}{2}, \frac{\pi}{2}[$, and $\theta \in [-\frac{\pi}{2}, \frac{\pi}{2}]$ for $n_l = 1$ and $\theta \in [-(\frac{\pi}{2} - \varphi); \frac{\pi}{2} - \varphi]$ for $n_l > 1$.

Comparing (6.21) with the corresponding expression (5.16) it can be seen that they are equal, apart from the factor $\frac{1}{n_l}$ in front of the expression and the term which includes s_l and n_l. Therefore, the calculations are almost identical with the calculations carried out in section 5.1.2. As with those calculations, it is also not possible here to minimize analytically the
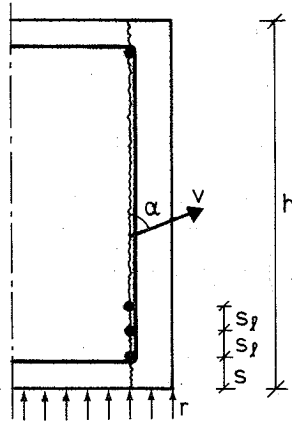
Figure 6.10: *Limit for translation mechanism, geometri and yield line pattern.*

expression with respect to the variable parameters θ, κ_1, and κ_2.

In section 5.1.2 the angle θ is limited to be between 0 and $\frac{\pi}{2} - \varphi$. Doing this the contribution from the reaction stress r will always be greater than or equal to zero. In this section these bounds will not be imposed, i.e. C can decrease for increasing $\frac{r}{f_c}$. A negative contribution from the reaction indicates that the concrete corner can break off without involving the anchorage. The load carrying capacity can in this case be found to be $\frac{r}{\nu f_c} = 1$. The value of the effectiveness factor ν is probably not the same in the case of this corner failure and of the normal anchorage failure, but it shows that the reaction stress in some situations does not increase the load, but limit it.

Allowing θ to be negative, compression stresses can appear in the stirrups. If compression stresses are accepted in the stirrups $\sin\theta$ must be changed to $|\sin\theta|$ in the term, including ψ in (6.21), but if they are not, $\sin\theta$ must be changed to 0 for $\theta < 0$ in the same term.

As with the rotation mechanism in the previous section, an upper limit for the load carrying capacity will appear when the yield lines go from the bottom to the top of the section. In figure 6.10 an example is shown.

C can in this case be written

$$C = \frac{1}{n_l}\frac{s}{\pi d}\left[\Omega(\lambda - \mu\sin\alpha) + 2\frac{d}{s}\psi\sin\alpha - 2\frac{r}{f_c}\cos\alpha\right] \tag{6.22}$$

where $\Omega = \frac{h}{s} - \frac{d}{s}n_l$ and $\alpha \in [\varphi; \pi - \varphi]$.

Minimizing (6.22) with respect to α yields

$$C = \frac{1}{n_l}\frac{s}{\pi d}\left[\Omega\lambda - \sqrt{\left(2\frac{r}{f_c}\right)^2 + \left(\Omega\mu - 2\frac{d}{s}\psi\right)^2}\right] \quad \text{for} \quad \frac{r}{f_c} \le \frac{1}{2}\tan\varphi\left(\Omega\mu - 2\frac{d}{s}\psi\right) \tag{6.23}$$

$$C = \frac{1}{n_l}\frac{s}{\pi d}\frac{2}{k+1}\left[\Omega\nu + (k-1)\frac{d}{s}\psi - 2\sqrt{k}\frac{r}{f_c}\right] \quad \text{for} \quad \frac{r}{f_c} > \frac{1}{2}\tan\varphi\left(\Omega\mu - 2\frac{d}{s}\psi\right) \tag{6.24}$$

(6.23) and (6.24) corresponds to

$$\sin\alpha = \frac{\Omega\mu - 2\frac{d}{s}\psi}{\sqrt{\left(2\frac{r}{f_c}\right)^2 + \left(\Omega\mu - 2\frac{d}{s}\psi\right)^2}} \tag{6.25}$$

$$\sin\alpha = \sin\varphi \tag{6.26}$$

respectively.

In figure 6.11 the translation mechanism, expression (6.21), and the limit for the translation mechanism, expressions (6.23) and (6.24), are shown in a $(\frac{r}{\rho f_c}, \frac{C}{\rho})$ diagram.

Consider figure 6.11 it can be seen that the limit mechanism in the cases shown is not decisive compared to the original translation mechanism. For $n_l = 1$ the values of $\frac{C}{\rho}$ are greater than 8.0; therefore no curve is shown in the figure. Generally, the limit mechanism will be decisive in unusual cases only.

Comparing the curves from expression (6.21) it is seen that for $\frac{r}{\rho f_c} > 7.3$ the values of $\frac{C}{\rho}$ for $n_l = 1$ are less than for n_l equal to 2 and 3. This shows that the failure involving only the bottom bar will be decisive for large values of $\frac{r}{\rho f_c}$.

The maximum of the curves from (6.21) in figure 6.11 is characterized by $\theta = 0$ and, for suitably small values of $\frac{\ell}{\nu}$, $\kappa_2 = 0$, i.e. the maximum point is
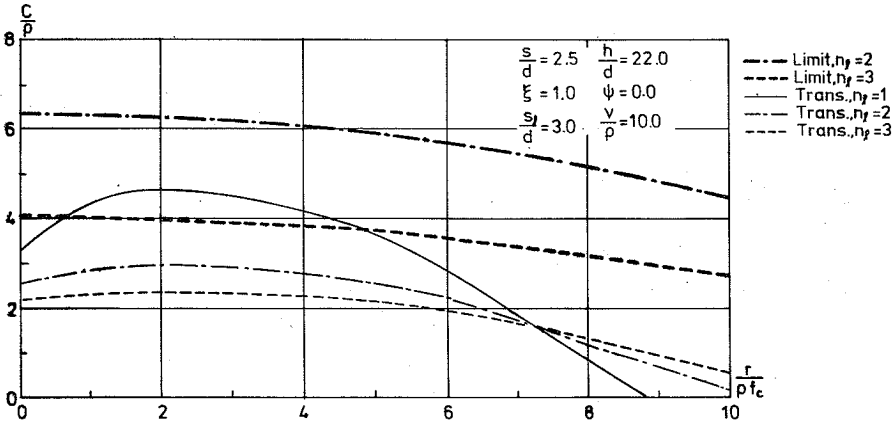
Figure 6.11: $\frac{C}{\rho}$ as a function of $\frac{r}{\rho f_c}$ for the translation mechanisms, expressions (6.21), and the limit for the translation mechanism, expression (6.23) and (6.24), for different values of n_l.

a function of κ_1 only. The descending part is characterized by $\theta + \kappa_1 = \varphi$ and on the lowest part $\kappa_2 + \frac{\pi}{2} - \theta = \varphi$. Inserting these two relations into (6.21), produces an expression for C with only one parameter.

$$
\begin{aligned}
C = \frac{1}{n_l}\frac{s}{\pi d} \Big[\ & (\lambda - \mu \sin\varphi)\left(\frac{\xi}{\cos(\varphi-\theta)} + \frac{1}{\sin(\varphi-\theta)} - \frac{d}{s}\right) \\
& + (\lambda - \mu\cos\theta)\left(\frac{s_l}{s} - \frac{d}{s}\right)(n_l - 1) \\
& + \frac{d}{s}\psi(\sin\theta + \cos\theta) \\
& + 2\frac{r}{f_c}\sin\theta(\xi + \cot(\varphi - \theta)) \qquad \Big]
\end{aligned}
\tag{6.27}
$$

However, it is not possible, even in this case, to minimize the expression with respect to θ.

Expression (6.27) is shown together with (6.21) in figure 6.12. As can be seen in the figure, the correspondence between the two sets of curves is satisfactory for large values of $\frac{r}{\rho f_c}$. In the next section it will be demonstrated that this is approximately the interval in which the translation mechanism is decisive compared to the rotation mechanism.

6.2   Comparison of Mechanisms

$\frac{C}{\rho}$ as a function of $\frac{r}{\rho f_c}$ for the rotation and translation mechanisms is shown in figure 6.13.
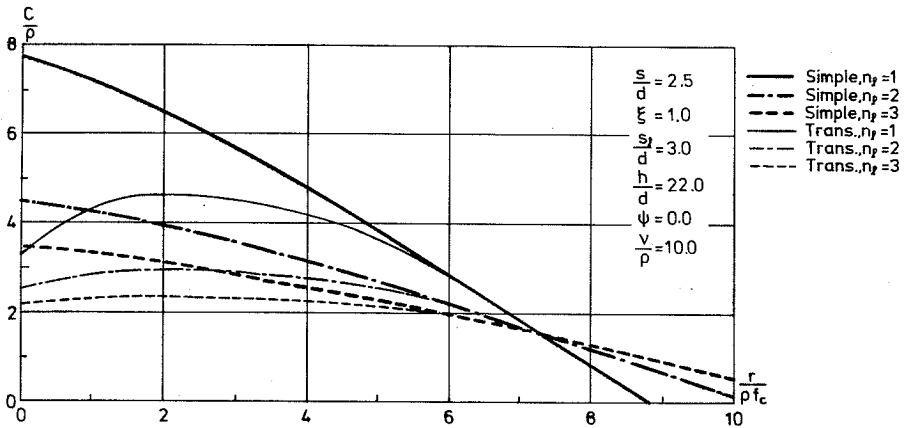
Figure 6.12: $\frac{c}{\rho}$ as a function of $\frac{r}{\rho f_c}$ for expression (6.21) (trans) and (6.27) (simple) for different values of n_l.

In the figure the rotation mechanism is decisive for $\frac{r}{\rho f_c}$ less than approximately 0.45, changing with the value of n_l. For larger values of $\frac{r}{\rho f_c}$ the translation mechanism is decisive. In chapter 5, where the rotation and translation mechanisms have been treated in the case of one layer of reinforcement, the rotation mechanism was in general decisive. This difference in conclusion appears because the translation mechanism in this chapter has more variable parameters and the interval allowed is greater than in chapter 5.

As can be observed by comparing figure 6.12 with 6.13 the simplified translation mechanism is a reasonable approximation of the translation mechanism for the interval in which the translation mechanism is decisive in comparison to the rotation mechanism.

6.3   Discussion

The expressions for the failure mechanisms for anchorage of more than one layer of reinforcement at a beam support are a little complicated. Hence the expressions have been attempted to be simplified, but the simplified expressions are nor quite simple. The simplified expressions seem to correspond to the original expressions with satisfactory accuracy.
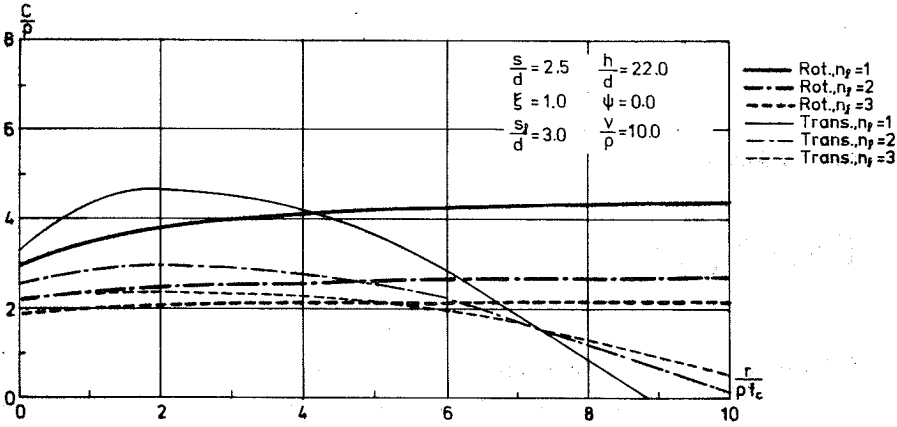
Figure 6.13: $\frac{C}{\rho}$ as a function of $\frac{r}{\rho f_c}$ for the rotation mechanism, expression (6.10), and the translation mechanism expression, (6.21), for different values of n_l.

Previously expressions for C have been developed. The strength of the anchorage can be found by inserting the optimal value for C into the expressions for the local failure set up in chapter 4.

As discussed in section 5.4, an anchorage failure at a beam support is possible only if another type of failure is in progress. This is also the case when anchorage at a beam support of more than one layer of reinforcement is under discussion. An anchorage failure cannot appear separately.

The curves for C as a function of $\frac{r}{\rho f_c}$ in the preceding sections show that the strength decreases for increasing number of reinforcement layers n_l for the used parameters, which was also expected. The strength of an anchorage with more than one layer of reinforcement can not be greater than the strength of one where the bars are placed in a single layer. This shows that the failure mechanisms treated in chapter 5 can be decisive, even if there is more than one layer of reinforcement at the support. The combined mechanisms illustrated in figure 6.8, can also in some cases be decisive.

Chapter 7

Lap Splices

Failure mechanisms for lap splices in the case of one layer of reinforcement will be treated below. The distance between the two bars in a splice is assumed to be zero. However, tests indicate that the strength of a lap splice is not sensitive as to whether the distance is zero or larger than zero. Hence the expressions are also applicable when the distance is not zero (within certain limits).

In the expressions for the total dimensionless internal work, C, contributions from the concrete and surrounding reinforcement are taken into account. The surrounding reinforcement is assumed to consist of normal stirrups. It is assumed that the stirrups follow the main reinforcements in the displacements at failure. This is probably not always correct, as mentioned in chapter 6, but a minor change in the failure mechanisms makes the assumption more acceptable. The contribution from the surrounding concrete is separated into two parts: A contribution from the failure in the concrete along the lap length, similar to that used in chapters 5 and 6, and a contribution from the end failure. The failure surface will in some way or another pass the concrete surface. This will in general lead to an additional contribution to the internal work; hereafter named *the end failure contribution*. The effectiveness factor for tension, ρ, in the end failure is symbolised by ρ_e in the expressions. Doing this makes it possible to distinguish between the different contributions.

The two bars in a lap splice are assumed to move with the same displacement (in opposite directions). It is also assumed that the local failure occuring around the two bars is similar. Therefore the external work and the internal
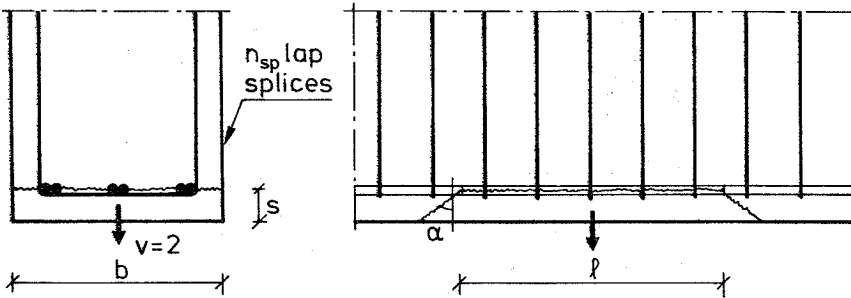
Figure 7.1: *The plate mechanism; geometry and yield line pattern.*

work from the local failure are equal for the two bars. Hence C is determined as the total internal work in the failure surface divided by 2. However, in some cases of a corner splice, it is assumed that only the bar nearest the corner moves at failure, see section 7.1.3.

7.1 Failure Mechanisms

The failure mechanisms are divided into three basic types, *the plate mechanisms, the wedge-plate mechanisms, and the corner mechanisms.* Generally every type contains more than one mechanism. Expressions for the total dimensionless internal work C, are expounded. The principle in the calculations is similar to that used in chapters 5 and 6.

It is assumed that the splices are located at the bottom of the beam section considered and that the bars in the lap splices are placed alongside one another in a horizontal plane.

7.1.1 Plate mechanism

A beam section with n_m *main bars* is considered. It is assumed that all the bars in the section are spliced, i.e. $n_m = 2n_{sp}$, where n_{sp} is the *number of lap splices.* The mechanism dealt with, is illustrated in figure 7.1.

The end failure surface is assumed to be a plane going from the bars to the bottom edge of the concrete, as illustrated in figure 7.1, to the right. The
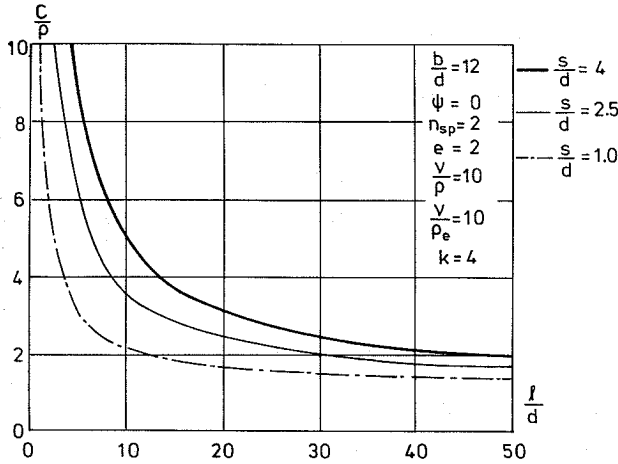
Figure 7.2: $\frac{C}{\rho}$ as a function of $\frac{\ell}{d}$ from (7.1).

total dimensionless internal work in this case becomes

$$C = \frac{1}{2\pi n_{sp}}\left[2\rho\left(\frac{b}{d} - 2n_{sp}\right) + 2\psi + e\frac{b}{d}\frac{s}{d}\frac{d}{\ell}E_e\right] \tag{7.1}$$

where e is the number of end failure contributions, $e \in \{0,1,2\}^1$, and

$$E_e = \frac{\lambda_e - \mu_e\sin\alpha}{\cos\alpha} \tag{7.2}$$

The material parameters λ_e and μ_e are defined as λ and μ, expression (2.8) and (2.9), except that ρ in this expression is changed to ρ_e. Minimizing (7.2) with respect to α, the following appears

$$E_e = \begin{cases} 2\sqrt{\rho_e(\nu - k\rho_e)} & \text{for } \frac{\rho_e}{\nu} < \frac{1}{2k} \sim \sin\alpha = \frac{\mu_e}{\lambda_e} \\ \frac{\nu}{\sqrt{k}} & \text{for } \frac{\rho_e}{\nu} \geq \frac{1}{2k} \sim \sin\alpha = \sin\varphi \end{cases} \tag{7.3}$$

As mentioned in chapter 5, the plate mechanism is special compared to the other mechanisms because it in general does not have to be combined with other mechanisms; it constitutes a complete mechanism in itself.

The well known relationship between the load and the lap length appears in expression (7.1), see figure 7.2.

From (7.1) it can also be seen that C increases for increasing values of the stirrup reinforcement degree ψ. This also corresponds to what is observed in tests.

---

[1]For lap splices e is normally equal to 2.
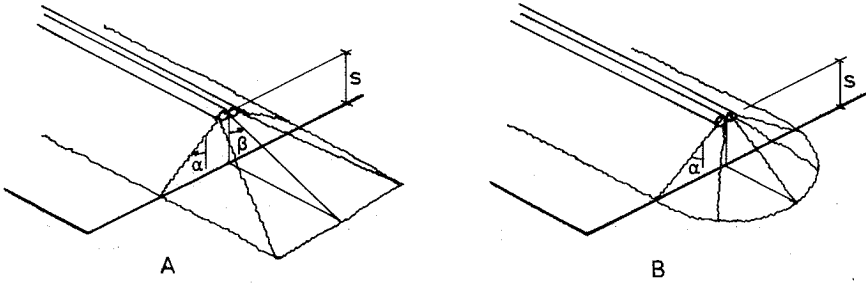
Figure 7.3: *End failure patterns for the wedge-plate mechanism in the case of one lap splice.*

It must be noticed that the expressions for the plate mechanisms and the mechanisms dealt with below are also valid for lap splices in slabs. The expressions can be used directly.

7.1.2   Wedge-plate mechanisms

The wedge-plate mechanism is a combination of the plate mechanism from the preceeding section and wedge mechanism no. 2 from chapter 5. The mechanism includes the wedge mechanism for one lap splice corresponding to the wedge mechanism in chapter 5, but is otherwise valid for an unspecified number of splices.

At all events two types of end failure patterns can be considered in this case; a failure mechanism with plane surfaces and one consisting partly of a cone and a plane can be used. The mechanisms are illustrated in figure 7.3 in the case of **one** lap splice. In reality one of the bars will continue beyond the end failure surface, but for clarity both bars are considered to end at the end failure surface.

The plane mechanism, denoted A in the figure, has two variable parameters, α and β, and the cone mechanism, denoted B, has one variable parameter, α. α is used in both mechanisms because it is in fact the same geometrical angle, but of course the optimal value for α can in the two cases be different. It must be noticed that the angle α is influenced by the mechanism along the lap length, whereas β in the plane mechanism is independent of this in principle.

The end failure mechanisms have been compared in the case of $\alpha = \beta = \varphi$.
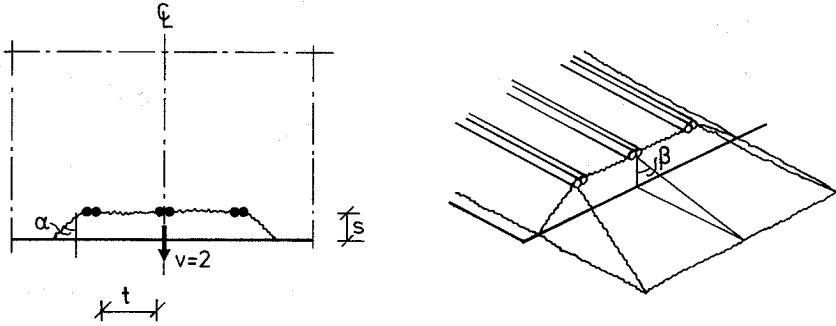
Figure 7.4: *Wedge-plate mechanism; geometry and yield line pattern.*

In this case it was found that for $\frac{s}{d}$ less than approximately 2.5, the plane mechanism gives less values than the cone mechanism (difference approximately 80% for $\frac{s}{d} = 0.5$ and 30% for $\frac{s}{d} = 1$) and for larger values the situation is just the opposite (maximum difference approximately 20% for $\frac{s}{d} = \infty$).

The cone mechanism has been used by Petersen & Panek [87.7] in the case of anchorage at supports in slabs.

In the calculations below the plane end failure mechanism is used. The failure pattern is shown in figure 7.4, where the end failure surface is illustrated to the right.

Using the symbols in the figure, the following expression for the total dimensionless internal work can be obtained

$$C = \frac{1}{2n_{sp}} \frac{s}{\pi d} \left[2\frac{\lambda - \mu \sin \alpha}{\cos \alpha} + 2\rho(n_{sp} - 1)\frac{t}{s} + 2\frac{d}{s}\psi \right.$$
$$\left. + e\frac{s}{d}\frac{d}{\ell} \left(\frac{\lambda_e - \mu_e \sin \alpha}{\cos \alpha} \tan \beta + \frac{\lambda_e - \mu_e \sin \beta}{\cos \beta}(\Gamma + \tan \alpha) \right) \right] \quad (7.4)$$

where

$$\Gamma = 2n_{sp}\frac{d}{s} + (n_{sp} - 1)\frac{t}{s} \quad (7.5)$$

Differentiating (7.4) with respect to α and β and equalizing the obtained expressions to zero yields

$$\sin \alpha = \frac{2(\mu \cos \beta + e\frac{s}{\ell}\mu_e \sin \beta) - e\frac{s}{\ell}\lambda_e}{2\lambda \cos \beta + e\frac{s}{\ell}\lambda_e \sin \beta} \quad (7.6)$$
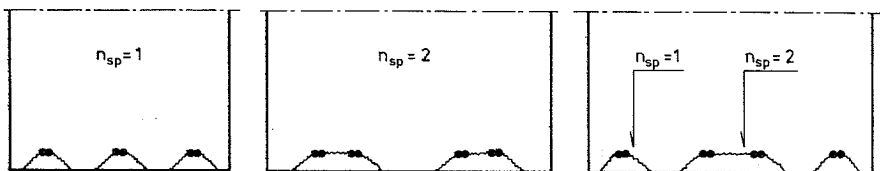
Figure 7.5: *Examples of mechanisms where the expressions for the wedge-plate mechanism can be used.*

$$\sin \beta = \frac{\mu_e(\Gamma \cos \alpha + 2 \sin \alpha) - \lambda_e}{\lambda_e(\Gamma \cos \alpha + \sin \alpha)} \quad (7.7)$$

where $\alpha \geq \varphi$ and $\beta \geq \varphi$ must be satisfied. Unfortunately it is not possible to solve these two equations with respect to the angles α and β. However, a simple procedure can be used. The optimal value for α is determined from (7.6) for e equal to zero (see section 5.1.3). This value is then inserted into (7.7). Using this method, the determined values of α and β are not the optimal ones, but, as in the majority of upper bound calculations, the minimum is rather flat so the mistake using this method is limited. It is observed that (7.7) is satisfied using this simple method.

Considering (7.4), it is noticed that C decreases for increasing $\frac{\ell}{d}$ and increases for increasing ψ in the same way as the plate mechanism.

The wedge-plate mechanism can be used to treat various mechanisms similar to the mechanism shown in figure 7.4. Examples of this are illustrated in figure 7.5.

The expressions for the wedge-plate mechanism are used with the number of splices n_{sp} equal to what is shown in the figure. Other combinations than shown, can of course be used. The mechanism to the right in figure 7.5 can be decisive when the splices in the corners are not placed close to the vertical edges. If they are located close to the edges, the wedge mechanism will probably not be decisive; the corner splices will fail in another way. The next section deals with failure mechanisms in corner splices.

7.1.3 Corner mechanisms

As previously mentioned, the corner mechanisms differ from the other mechanisms for splices in the way the bars are assumed to move at failure. In the
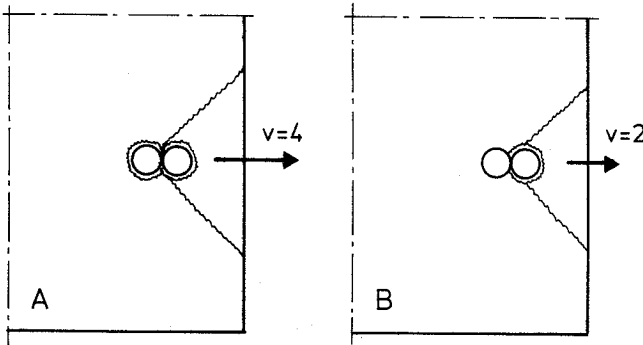
Figure 7.6: *Wedge mechanism for a corner splice.* **A** *illustrates that both bars in the splice move at failure and* **B** *that only the bar nearest the edge moves.*

other mechanisms both bars are assumed to move at failure and contribute to the external work, while in a corner splice only the bar nearest the edge is assumed to move. Two examples of mechanisms are shown in figure 7.6.

A mechanism similar to wedge mechanism no. 3 in section 5.1.3 is used. Mechanism **A** in the figure illustrates that both bars move at failure. The concrete corner, the wedge, moves away from the concrete section at the velocity of $v = 4$. In mechanism **B** only the bar nearest the edge moves and the velocity of the concrete wedge is therefore $v = 2$. In mechanism **A** the internal work must be divided by 2 to find the internal work for one bar. The velocity in mechanism **A** is double that in **B**, but the work in **A** is divided by 2, which means that there is no difference here in reality. However, there is a difference which appears in the length of the yield lines, when the yield line patterns are assumed to be as illustrated in figure 7.6. All things considered, the difference between the mechanism, will not be significant for practical purposes. In the calculations above, it is assumed that only the bar nearest the edge moves at failure, if the direction of the displacement is not vertical.

The corner mechanisms and the corresponding expressions for the total dimensionless internal work are shown in figure 7.7.

The end failure patterns for the *side-wedge* and the *bottom-wedge* mechanisms are in principle equal to the end failure for the wedge-plate mechanism dealt with in the previous section. The *rotation no. 1* and the *no. 2* mech-

$C =$
Side-wedge $\xi\frac{s}{\pi d}\left[2\frac{\lambda-\mu\sin\alpha}{\cos\alpha} + \frac{1}{\xi}\frac{d}{s}\psi + e\xi\frac{s}{d}\frac{d}{l}\left(\frac{\lambda_e-\mu_e\sin\alpha}{\cos\alpha}\tan\beta + \frac{\lambda_e-\mu_e\sin\beta}{\cos\beta}\left(\frac{d}{s}+\tan\alpha\right)\right)\right]$
Bottom-wedge $\frac{1}{2}\frac{s}{\pi d}\left[\frac{\lambda-\mu\sin\alpha}{\cos\alpha} + 2\rho\left(\xi-\frac{d}{2s}\right) + \frac{d}{s}\psi + \frac{1}{2}e\frac{s}{d}\frac{d}{l}\left(\frac{\lambda_e-\mu_e\sin\alpha}{\cos\alpha}\tan\beta + \frac{\lambda_e-\mu_e\sin\beta}{\cos\beta}\left(2\xi+3\frac{d}{s}+\tan\alpha\right)\right)\right]$
Rotation no. 1 $\frac{s}{\pi d}\left[\rho\left(\left(\frac{1+\eta}{\eta}\right)^2\sqrt{\xi^2+\eta^2}-2\frac{d}{s}\right) + \frac{d}{s}\psi\frac{\xi+\eta}{\sqrt{\xi^2+\eta^2}} + 0.36e\frac{s}{d}\frac{d}{l}\frac{\xi(1+\eta)^3}{\eta\sqrt{\xi^2+\eta^2}}\sqrt{\lambda_e^2-\mu_e^2}\right]$
Rotation no. 2 $\frac{s}{\pi d}\left[\rho\left(\frac{(1+\eta)^2}{\eta}\sqrt{\xi^2+\eta^2}-2\frac{d}{s}\right) + \frac{d}{s}\psi\frac{\xi+\eta}{\sqrt{\xi^2+\eta^2}} + 0.36e\frac{s}{d}\frac{d}{l}\frac{\xi^2(1+\eta)^3}{\eta\sqrt{\xi^2+\eta^2}}\sqrt{\lambda_e^2-\mu_e^2}\right]$
Translation $\frac{s}{\pi d}\left[2\rho\left(\frac{\xi}{\sin\theta}+\frac{1}{\cos\theta}-\frac{d}{s}\right) + \frac{d}{s}\psi(\sin\theta+\cos\theta) + \frac{1}{2}e\frac{s}{d}\frac{d}{l}\tan\theta(1+\xi\cot\theta)^2\sqrt{\lambda_e^2-\mu_e^2}\right]$
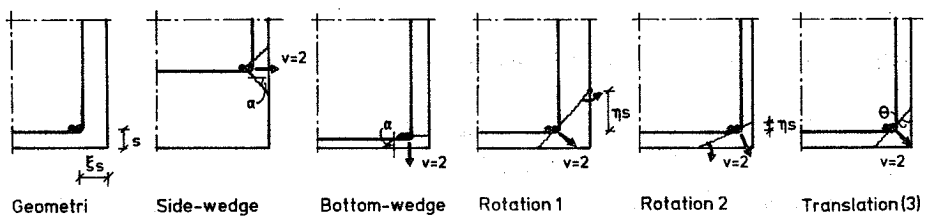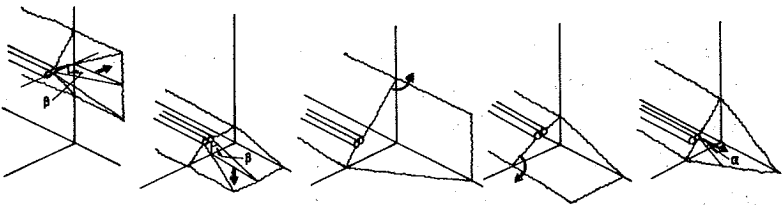
Figure 7.7: *Corner mechanisms and expressions for the total dimensionless internal work C.*

anisms are identical to the mechanisms in section 5.1.1, and the *translation* mechanism is identical to translation mechanism no. 3 in section 5.1.2. The end failure is included here, which not is the case in the mechanisms in section 5.1.

The end failure pattern for the translation mechanism is a plane with the constant angle α between the displacement direction and the plane. The end failure for the rotation mechanisms are not as simple. Variational principles using the Euler-Lagrange differential equation have been implemented to find a solution. Because the theoretically correct solution is complicated, it has been simplified and can be presented as shown in figure 7.7. The calculations can be seen in Andreasen [84.3].

A mechanism similar to the side-wedge mechanism, but with a vertical yield line, going from the bar nearest the edge to the bottom edge of the concrete section, instead of the lowest inclined yield line, has also to be considered, if it is to be correct. However, the difference between this mechanism and the rotation and translation mechanisms will be negligible. Hence this mechanism is not included here.

As can be seen in figure 7.7, the solution for one mechanism is generally complicated. The best of the 5 mechanisms, the one giving the lowest value for C in an actual case, has to be found. This mechanism can then be combined with the wedge- plate mechanism. This demonstrates the difficulty in carrying out this calculation.

7.2   Comparison of the Mechanisms

Because the expressions for the internal work for the various mechanisms for lap splices are complicated, some guidelines for selecting the best mechanism are given here. The guidelines need be considered only as an instruction and an aid to excluding some of the mechanisms in an actual case.

In figure 7.8 a horizontal and an inclined yield line without end failures are compared.
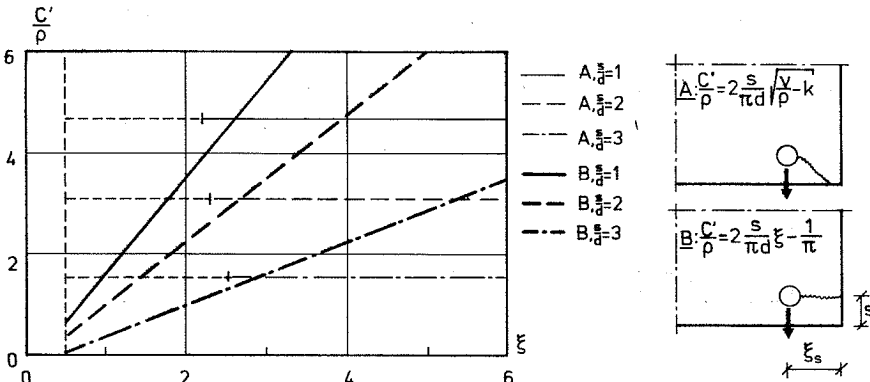
Figure 7.8: *The internal work as a function of ξ for a horizontal and an inclined yield line.*

For the cases shown, the mechanism with the horizontal yield line is decisive for ξ approximately less than 2.7. For $\frac{s}{d} = \infty$ the limit for ξ is $\sqrt{6}$ and for $\frac{s}{d}$ equal to $1/2$, the value is $1 + \sqrt{6}$. For values of $\frac{s}{d}$ occuring in practice the limit for ξ will therefore not change much.

This shows that the horizontal cover must be more than approximately three times the vertical cover before the wedge mechanism is decisive compared to the plate mechanism. Therefore the horizontal distance between two lap splices must be more than 6 times larger than the vertical cover to result in a decisive wedge mechanism. Incidentally the analysis carried out here is similar to the one in section 5.2, in the case of anchorage at supports of one layer of reinforcement.

The corner mechanisms can be decisive if the width of the section is large and the corner bars are located near the vertical edge. The side-wedge mechanism[2] can be decisive if the vertical cover is large and the bottom-wedge mechanism can be decisive if it is small. Rotation mechanism no. 1 will be less than rotation mechanism no. 2 for $\xi > 1$. For ξ approximately equal to 1, the translation mechanism[3] can be decisive, compared to the rotation mechanisms.

Expressions for when the various mechanisms are decisive, can be developed,

---

[2] In section 5.1.3 this mechanism is named wedge mechanism no. 3

[3] In section 5.1.2 this mechanism is named translation mechanism no. 3
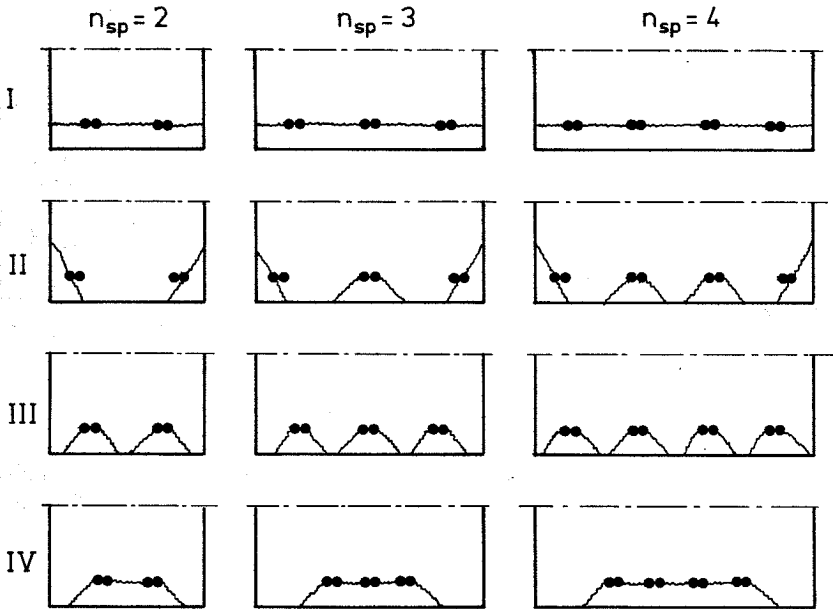
Figure 7.9: *Complete failure mechanisms from the mechanisms in section 7.1.*

but they are very complicated. Such expressions will obscure the situation rather than clarify it. Using one's common sense will be more helpful.

7.3   Complete Failure Mechanisms

A section with n_{sp} lap splices (n_m main bars, $n_m = 2n_{sp}$) is considered. The failure mechanisms from section 7.1 must be combined to obtain a complete failure mechanism involving all splices in the section. As mentioned in section 7.1.1, the plate mechanism is a complete failure mechanism in itself.

Many different combinations of the mechanisms have to be considered. In figure 7.9 some examples are shown. The corner mechanisms in row number II can be one of the 5 types of mechanisms dealt with in section 7.1.3. The mechanisms in row numbers III and IV are a few of the possible combinations resulting from the wedge-plate mechanism. Of course other combinations than those illustrated, have to be considered too.
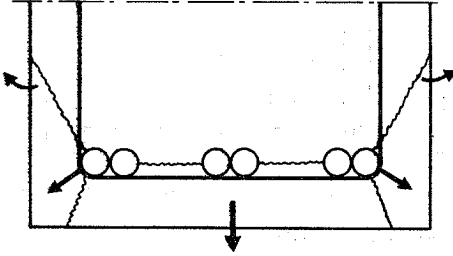
Figure 7.10: *Special mechanism.*

7.4 Discussion

Many failure mechanisms have to be considered in the case of lap splices. Furthermore, the expressions for determining the load carrying capacity for the various mechanisms are complicated. To practical calculations the expressions must be simplified. This is done in chapter 10, where the theoretical load carrying capacity is compared to the load obtained in tests.

The expressions are developed in preparation for tension lapped splices, but in principle they can also be used to splices in compression. However the effectiveness factors will probably not be the same in the case of compression as in tension.

Other mechanisms than those dealt with in the previous can be decisive in some cases, for instance the mechanism illustrated in figure 7.10.

The yield lines below the bars near the corners are fixed in such a way that they will be tensile yield lines. This mechanism can in some cases produce values for C lower than the values from the plate mechanism. The only problem with this type of mechanism is that the expression for C is even more complicated than for the mechanisms treated in the preceeding. This special mechanism and similar mechanisms will not be discussed in more detail here, but the possibility of finding mechanisms producing lower values for C than the mechanisms in section 7.1, must be noted.

The expressions for lap splices are expounded assuming normal stirrups. If other kinds of surrounding reinforcements are used in an actual case, this can be taken into account by changing the contribution from the stirrups

$$2\psi \qquad\qquad 2\psi \rightarrow 4\psi \qquad\qquad 2\psi \rightarrow 6\psi \qquad 2\psi \rightarrow 2\psi + 6\psi'\sin\beta$$
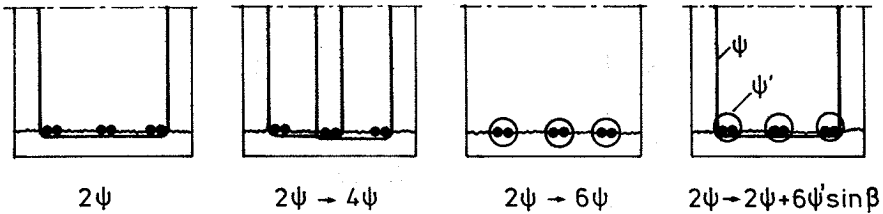
Figure 7.11: *Contribution from surrounding reinforcement in the case of the plate mechanism.*

in the expressions. Figure 7.11 shows how this can be done in a few cases. The plate mechanism is assumed to be decisive.

To the left the usual case is illustrated. Assuming the contribution from the stirrups to be 2ψ in this case, it is shown how this contribution must be changed in the other cases illustrated. The way it is shown in the figure it is just a matter of *how many times surrounding reinforcement crosses the horizontal yield line* for how many contributions should be taken into account. If the angle between the longitudinal direction of the surrounding reinforcing bar and the yield line, β, is different from $\frac{\pi}{2}$, a reduction factor of the value $\sin\beta$ must be introduced[4]. Especially in the case of spirals, shown in the two cross sections to the right in figure 7.11, the reduction can be considerable.

In principle the expressions for the internal work cover only the case where the lap splices are located in the bottom of the section and the two bars in a splice are placed adjacent to each other in a horizontal plane (see figure 7.12.A). This is the most common case which appears in structures in practice. However, they may be located elsewhere. For instance the splices can be located in the top of the section instead, see figure 7.12.B. In this case the expressions developed, can be used without changes.

Another possibility is that the bars in a splice are placed over one another, as shown in figure 7.12.C. The expressions can not be used directly but the principles used to expound them can be used advantageously in this case. Figure 7.12.D illustrates a special case which can occur in high beams. The

---

[4]This is similar to the discussion in section 5.1.3
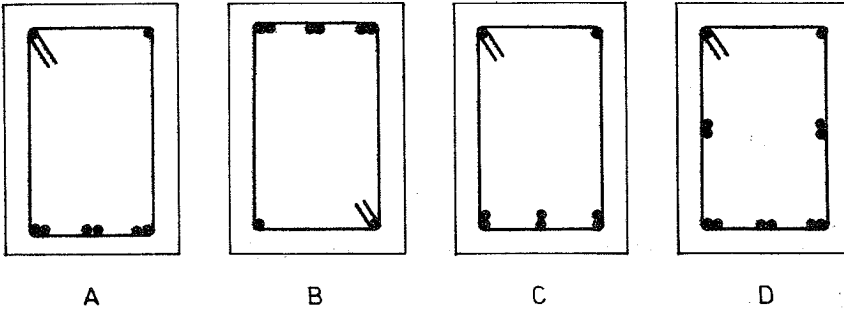
Figure 7.12: *Various locations of the lap splices.*

expressions can be used directly to treat this problem. The splices in the middle part of the section will probably fail in a wedge mechanism.

Although not all possible locations of lap splices are covered by the developed expressions, it is not difficult to deal with other problems. In the cases where the expressions can not be used directly, the principles from the calculations can be utilized. Therefore it is relatively easy to treat almost all types of lap splices.

The expressions set up in the previous are valid for lap splices in both beams and slabs. In the case of slabs, the plate and the wedge-plate mechanisms will probably normally be decisive. The corner mechanisms will only be applicaple if the width of the slab is small.

Chapter 8

Test Results for Anchorage at Supports

Several tests for anchorage at supports are reported in the literature but only a few of them can be used directly. In some of the tests the force in the reinforcement immediately in front of the support is not measured or the support length is not specified. Amongst others, this is the case in Hillerborg [57.1], Matthey & Watstein [61.2], Morita & Fujii [82.5], Nilsson [70.2], and Larsson [70.3]. In other tests in the literature, the anchorage above the support, or on a part of it, is prevented by special arrangements (see e.g. Bodén [85.7], Champerlin [56.1], Dastidar [69.5], Kemp & Wilhelm [79.7], Kemp [86.6], Larsson [57.2], and Roberts [69.6]).

The force in the reinforcement immediately in front of the support and the anchorage length are important parameters, which have to be known. It can be difficult to measure the force when testing on normal beams and it is not certain which anchorage length must be used. Using special test specimens, which particularly consider these problems, it is not difficult to find the value of these quantities. The problem when using specimens which are different from structures in practice, is to appraise if the behaviour is equal for both the idealized specimen and the structure in practice. The anchorage failure at supports in a normal structure can not take place without involving other parts of the structure, as discussed in section 5.4. As mentioned there, the anchorage failure can be considered to be a local failure, appearing as a result of the global failure under development and that the anchorage failure can be separated from this global "failure". This indicates that a test specimen can be idealized, but it must reflect the

fact that the anchorage failure can not appear in a normal beam without involving other parts than the anchorage.

Two test series, described in Jensen [82.1], [82.2] and Rathkjen [72.1], are useful. The tests are carried out on idealized specimens fulfilling the requirements mentioned above. Rotation mechanism no. 1 described in section 5.1 is used as the failure mechanism. Generally, using rotation mechanism no. 1 is best, and the expressions for the load carrying capacity are more simple than those for the translation mechanisms. However, the rotation mechanism no. 1 is not as good as the rotation mechanism in section 6.1, as shown in figure 6.7 ($n_\ell = 1$), but it is more simple. The difference between the more complex rotation mechanism and rotation mechanism no. 1 is methodical. Therefore it is possible to use the simple rotation mechanism without loss of accuracy. The load carrying capacity is a function of the effectiveness factors which have to be determined from tests. It means that in using the simple mechanism, the value for the effectiveness factors is less than if the complex mechanism had been used.

The effectiveness factors found from an upper bound solution can be used in a lower bound solution, and can be used in another upper bound solution, if this solution is theoretically better. The opposite is not allowed. However, it is best and most correct to use corresponding solutions and effectiveness factors.

As mentioned in section 2.2, the effectiveness factors are, in almost all known cases, determined from tests. Therefore they are empirical factors, but they are factors which can be given a physical meaning; they can be related to the behaviour of the concrete. Making use of a lower or an upper bound solution for a problem, the influence from the various parameters appears automatically, including the influence from the effectiveness factors, i.e. this kind of solution is stronger than a fully empirical one. Using such a solution with effectiveness factors found from tests, will result in the correct variation with the parameters and can with reflection be used in intervals not covered by tests.

The effectiveness factors can be found from tests by requiring correspondence between tests and theory for every test. Doing this, there will be

the same number of values for the effectiveness factors as the number of tests. The best relationships between the effectiveness factors and the concrete strength, and maybe other parameters, can then be found. Using these relationships for the effectiveness factors in determining the theoretical strength, the theory can now be compared to the test results.

The theory is compared to the tests by determining the ratio between the load obtained in the tests and the corresponding theoretical strength, *test/theory*, for every test. The mean value, the standard deviation, and the coefficient of variation for all the values for the ratio can then be determined.

The test values can be assumed to be normal distributed and the theoretical strengths can be considered to be certain values. Hence the ratio test/theory is also normal distributed and the simple mean and standard deviation calculations can be used. However, using the ratio test/theory, the unsafe values (theory>test) are weighted less than the safe values , which is not reasonable. Nevertheless, the ratio is calculated in this way but one should take note if there are too many, very small, unsafe values. In the majority of cases, the ratio is close to 1 and the difference in weight for a safe and an unsafe value is almost equal. It can be seen on the determined scatter, if this is not the case.

The final expressions for the load carrying capacity must be applicable for calculations in practice. Consequently the expressions for the rotation mechanism are attempted simplified.

8.1   Test Results

Test results from two test programs, Jensen [82.1],[82.2] and Rathkjen [72.1], are used in the comparison between the developed theory and tests. Both test programs include test specimens with and without surrounding reinforcement. The majority of the tests had 2 main bars, but tests with 1 and 3 bars are also included. Figures 8.1 and 8.2 show the specimen and the main principle in the testing of the specimen for Jensen's and Rathkjen's tests, respectively. For a more thorough description of the test procedure, the reader is referred to the original reports.
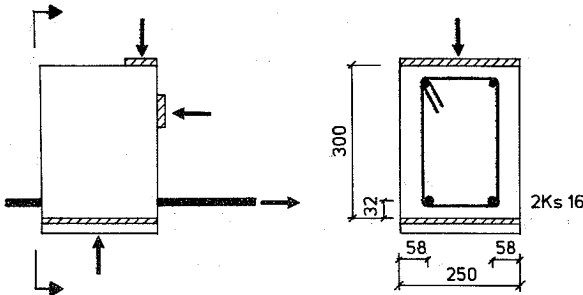
Anchorage length:
l =130 mm in serie 130–133,13H,
                          13V,13M,13S
l =190 mm in serie 190–192,19H,
                          19V,19M
l =260 mm in serie 261–262
Reinforcement:
Ks 900 (Swedish kamsteel),
d =16 mm,D =0.069,F =0.57

Measurements in mm.

Figure 8.1: *Test specimen used by Jensen [82.1] and [82.2]. The tests are from series 130-133, 190-192, 261-262, 13H, 13V, 19H, 19V, 13M, 13S, and 19M.*
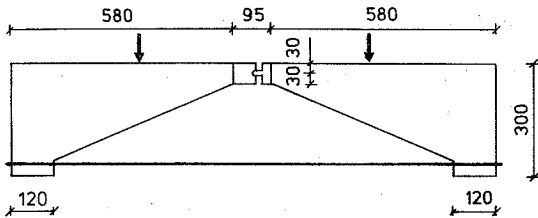
Anchorage length:
l =120 mm in all tests

Reinforcement:
Ks 560 (Danish kam steel)
d =10 or 14 mm,D =0.062,F =0.59
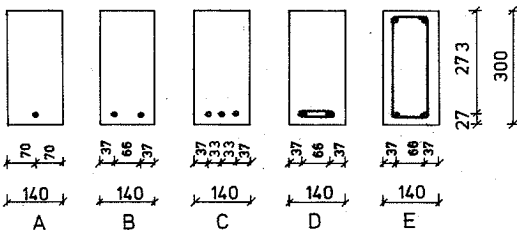
Measurements in mm

Figure 8.2: *Test specimen used by Rathkjen [72.1]. Test numbers 13-39, 52-54, 57, 80-83, 90-97, 107-109, and 110-125 are used.*

The values for the rib parameters D (4.6) and F (4.12) for the main reinforcement used in the tests, are noted in the figures. It was not possible to find values for the parameters u and a, see figure 4.1, but the values of $u+a$ have been given. Therefore F is not completely accurate but the deviation from the correct value is estimated to be without great significance.

The test results in the references, which are said to fail in an anchorage failure, are included in the analysis. Some specimens fail in another way, for instance by yielding of the main reinforcement or sliding failure in the plane over the reinforcement, and some are said to contain not satisfactorily compressed concrete; these tests are not included. Furthermore, some of Rathkjens tests are omitted because the force in the reinforcement was not measured during the test.

In Rathkjen [72.1] the yield strength of the surrounding reinforcement is not reported on. Information was obtained from Rathkjen concerning this.

The data for the tests are given in tables in appendix A. The values of the ratio test/theory are also included; this is described below.

Rotation mechanism no. 1 from section 5.1 is, as mentioned, used as the failure mechanism in all the specimens.

Experimentally the effectiveness factor for tension, ρ, was supposed to be equal to zero. For tests both with and without surrounding reinforcement, the calculations show that the agreement between test and theory was not satisfactory. The scatter on the ratio test/theory was too large, and there was a systematic deviation. The effectiveness factor for compression, ν, was assumed to be a constant, divided by the square root of the uniaxial cylindrical compression strength for the concrete. The value for the constant was found to be approximately 7–9, when the compressive strength is measured in MPa. Comparing the value for the constant to what is previously found in the literature, see the survey in chapter 2, it can be seen that it is too large. This indicates that the tensile strength for the concrete must be taken into account, as it is done in the expressions.

Functions for the ratio between the effectiveness factors $\frac{\rho}{\nu}$ in accordance with the two models, (2.18) and (2.19), set up in section 2.2, were therefore
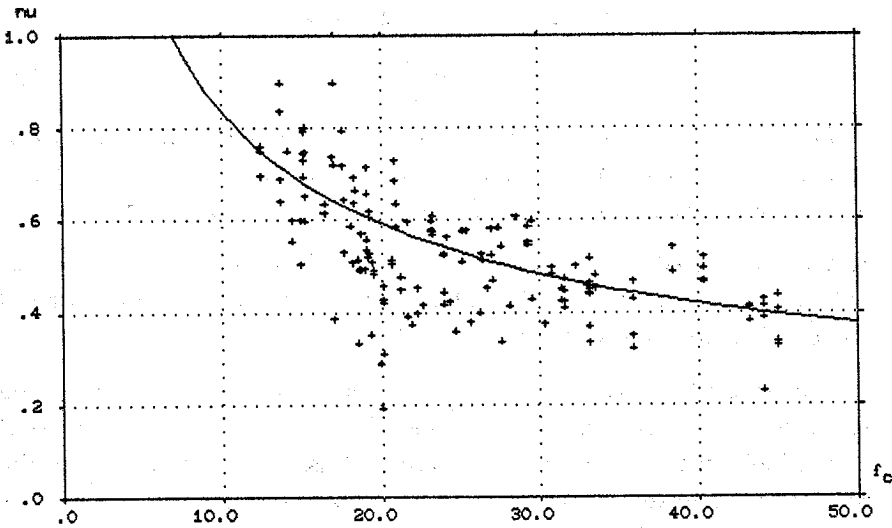
Figure 8.3: *The effectiveness factor, ν, as a function of the uniaxial compression strength for the concrete, f_c, for the tests without stirrups.*

used. To complete the investigation other functions, such as $\sqrt{f_c}/c_1$, $f_c^{\frac{1}{8}}/c_2$, and $c_3/f_c^{\frac{1}{4}}$, where c_1, c_2, and c_3 are constants, for $\frac{\rho}{\nu}$, were also tried. It turned out that the constant model, expression (2.19), is the best. However, the difference between the various models is not large, so if another model than the constant model is preferred, it will probably be possible to use it. In accordance with the analysis here and that in section 2.2 the constant model is used in the following discussion. It was found that

$$\frac{\rho}{\nu} = 0.10 \tag{8.1}$$

agreed reasonably well with the test results. (8.1) is used in the test treatment below. The value of ν can be found by demanding that the test value and the theoretical strength correspond for every test. In figure 8.3 the determined values of ν are shown as a function of the uniaxial compression strength for the concrete f_c.

Assuming the relationship between ν and f_c to be of the type $\nu = k_1/\sqrt{f_c}$, where k_1 is a constant, the best value for k_1 can be determined (the scatter

is minimal). Doing this the following is obtained

$$\nu = \frac{2.65}{\sqrt{f_c}} \qquad (8.2)$$

(8.2) is shown in the figure. The relationship (8.2) between ν and f_c corresponds to what is found in many other cases, where concrete structures are treated by using the theory of plasticity, see the review in section 2.2.

It must be noticed that the obtained values for the effectiveness factor ν are within the normal and expected interval. This indicates that the obtained value of $\frac{\ell}{\nu}$ is not totally inaccurate.

The dimensionless shear stress $\frac{\tau}{f_c}$ as a function of the dimensionless reaction stress $\frac{r}{f_c}$ is shown in figure 8.4 for some of Jensen's tests. The theoretical curves indicated in the figure are determined using the expressions for the rotation mechanism, (5.5) and (5.7), the expressions for the effectiveness factors, (8.1) and (8.2), and the actual expression for the local failure.

As can be seen, the theoretical strength describes reasonably well the influence on $\frac{\tau}{f_c}$ from $\frac{r}{f_c}$ compared with the tests. Also the influence from the concrete strength appears to be satisfactorily described.

The theoretical load carrying capacity is compared to the test results. The same expressions as were used to determine the theoretical curves in figure 8.4 are used here. The main value and the standard deviation on the ratio test/theory for the 140 tests without stirrups, are found to be 1.001 and 0.118, respectively. Figure 8.5 shows the dimensionless theoretical strength (theory) as a function of the dimensionless test strength (test).

The correspondence between test and theory is satisfactory, as can be seen in the figure. Only a few test results $\left(\left(\frac{\tau}{f_c}\right)_{test} \geq 0.8\right)$ deviate significantly from the theoretical strengths. These are tests with relatively low concrete compression strength and large values for the dimensionless reaction stress. However, the theoretical strengths are lower than the test strengths; therefore the theory is on the safe side in these cases. The obtained values of the ratio test/theory are given in appendix A.

In Jensen's tests the anchorage length ℓ, are 130, 190, or 260 mm. These tests can be used to check if τ is independent of ℓ, which theoretically is the
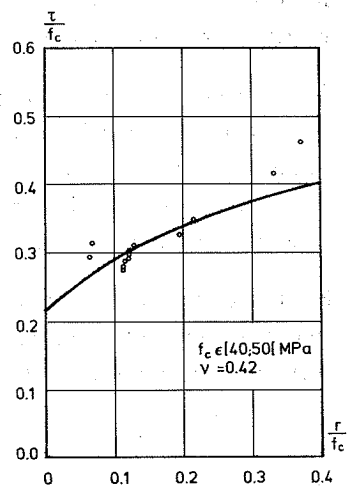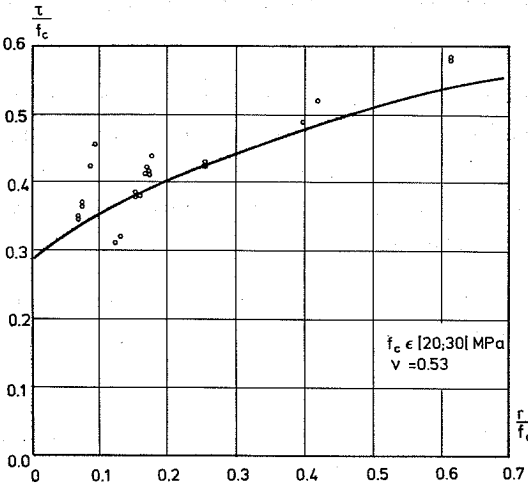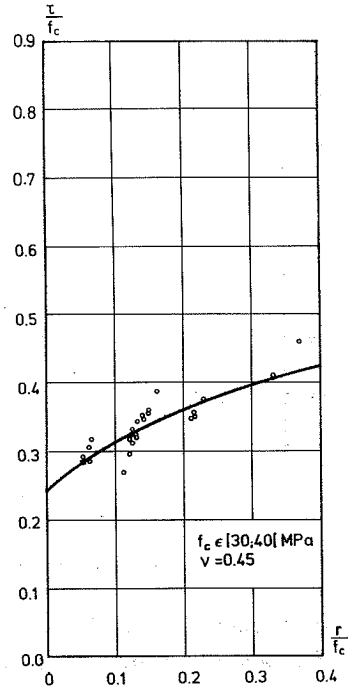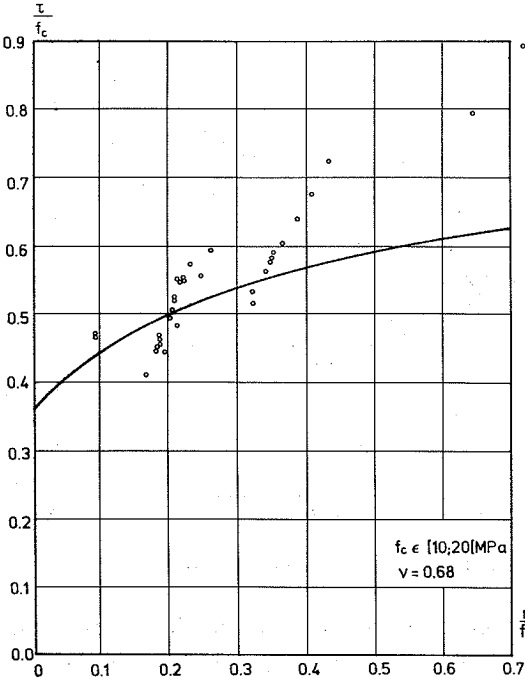
Figure 8.4: *The dimensionless shear stress $\frac{\tau}{f_c}$ as a function of the dimensionless reaction stress $\frac{r}{f_c}$ for some of Jensen's tests.*
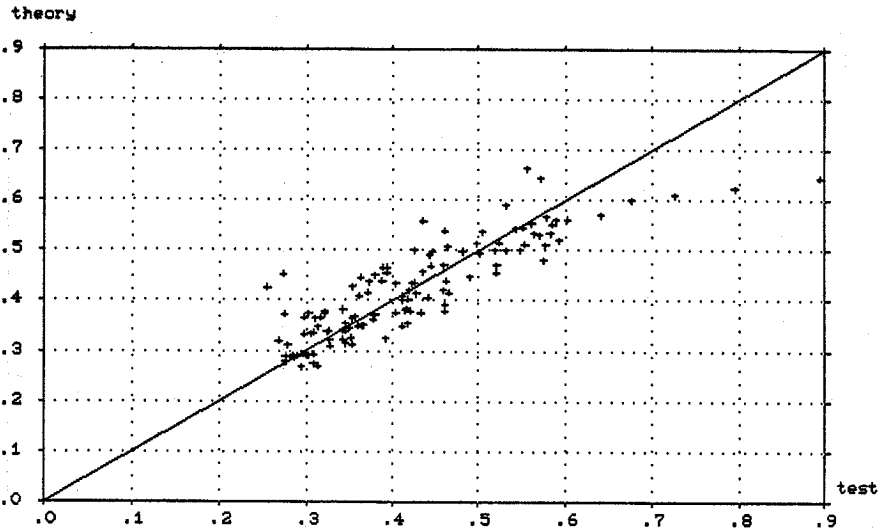
Figure 8.5: *Theory versus test results $(\frac{\tau}{f_c})$ for the 140 tests without stirrups.*

case when the end failure contribution is not included in the expressions. The analysis shows an influence, where the strength decreases slightly for increasing anchorage length, but this is not significant in this case. Particularly for calculations in practice, it will be without importance.

In the case of real beams (not idealized test specimens like Jensen's or Rathkjen's), there will be an end failure contribution to the load carrying capacity. As mentioned in chapter 5, this contribution is normally insignificant, but for very small anchorage lengths the influence can be considerable. This problem is further discussed in the next section.

For the tests with surrounding reinforcement it turns out that ν has to be changed. The following function has been found to result in satisfactory correspondence between test and theory

$$\nu = \frac{3.05}{\sqrt{f_c}} \tag{8.3}$$

Using this expression to determine the theoretical strength, the mean value and the standard deviation on the ratio test/theory for the 44 tests with stirrups was found to be 1.007 and 0.092, respectively. In appendix A
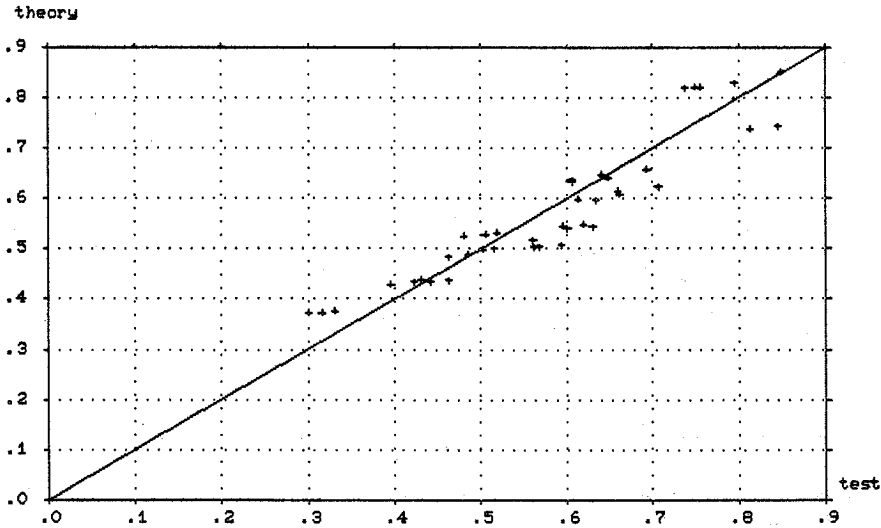
theory

Figure 8.6: *Theory versus test results* $(\frac{\tau}{f_c})$ *for the 44 tests with surrounding reinforcement.*

the ratio test/theory for all the tests is given: Figure 8.6 is similar to figure 8.5 and shows the dimensionless theoretical strength as a function of the dimensionless test strength.

In cases other than anchorage, it is also found that the amount of reinforcement increases the effectiveness factor ν, so the increase found here was expected. However, it would have been more natural if the two functions, (8.2) and (8.3), were continuous. It is possible to develop such a function but the results in using this will probably not be better than when using (8.2) and (8.3).

Because the theoretical expressions for rotation mechanism no. 1 are too complicated for practical use, they are simplified. This can be done by using a Taylor series for the total dimensionless internal work, C, as a function of the relative horizontal distance from the concrete edge to the center of the bar ξ about $\xi = \xi_0$. Doing this and using $\xi_0 = 1.2$ and the variable dimensionless parameter η equal to 2.5 or 4.4, the expression for the internal work can be written as

$$C = \frac{1}{\pi} \left[\rho \left(\tfrac{s}{d}(4.42 + 0.85\xi) - 2 \right) \right.$$
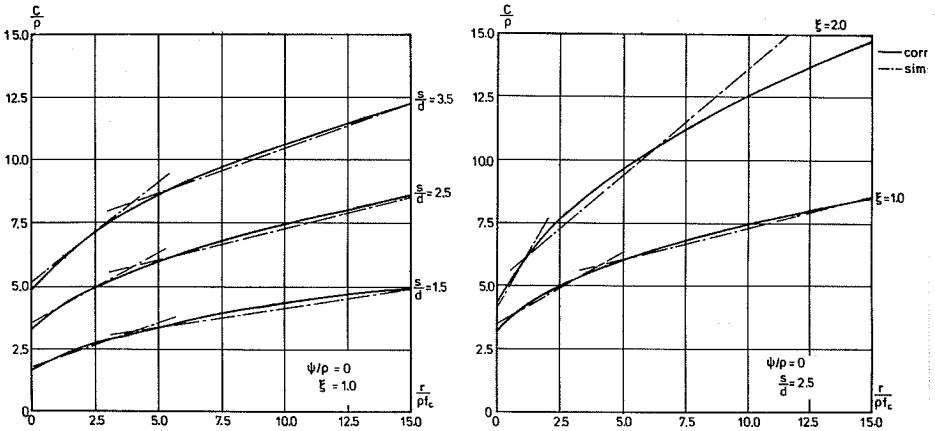
Figure 8.7: $\frac{C}{\rho}$ as a function of $\frac{r}{\rho f_c}$ for rotation mechanism no. 1, (5.5) and (5.7), and the simplified rotation mechanism, (8.4) and (8.5).

$$
\begin{aligned}
&\phantom{C = \frac{1}{\pi}\Big[}+\psi(1.15+0.15\xi)\\
&\phantom{C = \frac{1}{\pi}\Big[}+\tfrac{r}{f_c}\tfrac{s}{d}(1.54\xi-0.83)\Big] \quad \text{for} \quad \frac{r}{f_c}<\left(\frac{r}{f_c}\right)_\ell \qquad (8.4)\\
C = \frac{1}{\pi}&\ \Big[\rho\left(\tfrac{s}{d}(6.39+0.40\xi)-2\right)\\
&+\psi(1.05+0.15\xi)\\
&+\tfrac{r}{f_c}\tfrac{s}{d}(0.77\xi-0.44)\Big] \quad \text{for} \quad \frac{r}{f_c}\geq\left(\frac{r}{f_c}\right)_\ell \qquad (8.5)
\end{aligned}
$$

where

$$
\left(\frac{r}{f_c}\right)_\ell = \frac{\rho\tfrac{s}{d}(1.98-0.45\xi)-0.10\psi}{\tfrac{s}{d}(0.77\xi-0.38)} \qquad (8.6)
$$

The simplified expressions are in figures 8.7 and 8.8 compared to the theoretically correct expression. As can be seen, the correspondence is generally satisfactory. The simplified expressions vary with regard to the parameters in the same way as the theoretical ones do.

For the stirrup reinforcement ratio other than zero, the situation is identical with what is illustrated in figures 8.7 and 8.8; the agreement between the simplified and the correct rotation mechanism is reasonable.

Using (8.4) and (8.5) in the comparison with the test results, the mean value
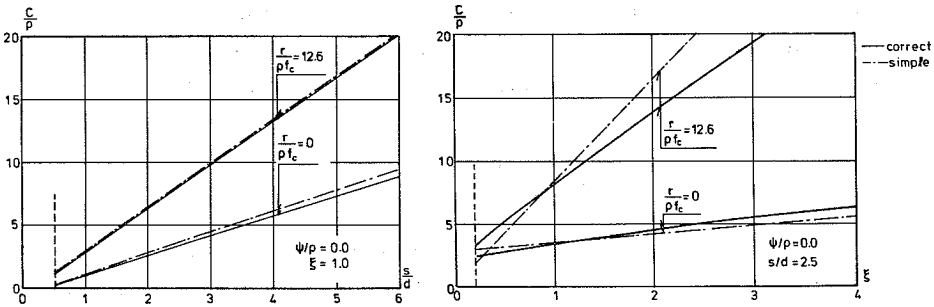
Figure 8.8: $\frac{C}{\rho}$ as a function of $\frac{s}{d}$ and ξ, respectively, for rotation mechanism no. 1, (5.5) and (5.7), and the simplified rotation mechanism, (8.4) and (8.5).

was 1.011 and the standard deviation was 0.114 on the ratio test/theory for the 140 tests without surrounding reinforcement. For the 44 tests with surrounding reinforcement, the mean value was 1.017 and the standard deviation was 0.089. These values are almost identical to the values obtained when using the theoretically correct expressions for C. The results from the analyses are given in appendix A. The simplified expressions seem to give results with satisfactory accuracy in the interval for the parameters appearing in practice. Moreover, the expressions are not more complicated, so that they can be used for calculations in practice.

8.2 Discussion

The effectiveness factors ν and ρ are supposed to be equal in the local failure and in the failure mechanism appearing perpendicular to the longitudinal direction of the bar. This is not entirely correct, but the analysis and the final (simplified) expressions would be even more complicated than is the case now. It is also questionable if the results would, after all, be better; the scatter on the ratio test/theory from the analysis carried out is satisfactory and is probably difficult to reduce.

As mentioned in the previous section, the rib parameter F (4.12) is not determined entirely accurately, while D (4.6) is satisfactory. This is because

data about the width of ribs in the direction of the bar axis, u, was not reported in the references, only the distance from the middle of one rib to the middle of the next could be found. This problem is considered to be of less importance because the values of the effectiveness factors are calibrated from this. If F nevertheless is determined using expression (4.12), it will not cause an unsafe situation because the value of F will be less than that used here, other things being equal.

The tests used in the preceeding section were carried out on specimens simulating end supports in beams. Other tests which illustrates the influence from a compression stress, perpendicular to the concrete surfaces on the anchorage strength, are also carried out (e.g. Untrauer & Henry [65.3]). These tests show the same as those for end supports in beam; the strength of the anchorage increases for increasing compression stress on the concrete surfaces, and the effectiveness factors decrease for increasing concrete strength.

Anchorage tests on beams are carried out by Andreasen [84.3] and Petersen & Panek [87.7]. In both test series two or three bars were anchored at a support, starting at the end of the beam. In Petersen & Panek's tests the concrete section was wide, because the tests were to simulate the conditions in a slab, and the anchorage length divided by the diameter of the bars varied between 2.3 and 9.2. In Andreasen's tests the width was within the normal range for beams and the ratio $\frac{\ell}{d}$ was 5 or 10. Comparing these test results with the results from the tests included here it can be seen that the strength, τ, is larger, especially for the specimen with a very short anchorage length. The reason for this can be the end failure contribution, which can be decisive in beams. However, an inclined crack from the load to the support plate normally appear in beams, see figure 8.9, which will change the end failure (see also section 5.4 where the problem is discussed).

In reality the anchorage length will not be ℓ but $\ell' = \ell_e + \ell$ in this case. For very short anchorage lengths, the relative increase will be larger than for long anchorage lengths. The test by Petersen & Panek shows this very clearly.

As mentioned in chapter 5, it will be very difficult to take the end failure,
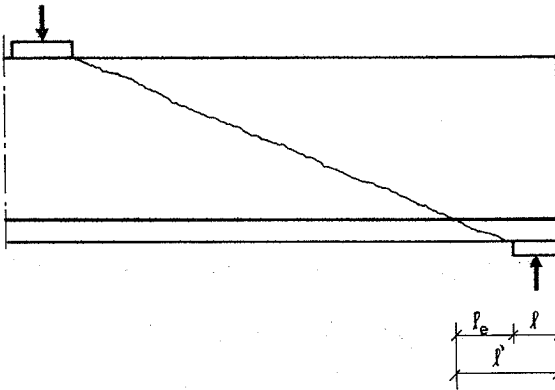
Figure 8.9: *Inclined crack in a beam.*

with regard to the inclined crack, into consideration. The expressions for the load carrying capacity will probably be very complicated.

All things considered, Andreasen's [84.3] and Petersen & Panek's [87.7] tests show that the expressions expounded here without consideration of the end failure, are safe in the case of monolithic beams.

The local failure is often determined by failure shape 2a, expression (4.17) when kam steel is used in the case of anchorage at supports. In this case the dimensionless shear stress $\frac{\tau}{f_c}$ is a linear function of the dimensionless internal work C. Inserting the simplified expressions for the rotation mechanism, (8.4) or (8.5), into the expressions for failure shape 2a will result in a linear relationship between $\frac{\tau}{f_c}$ and $\frac{r}{f_c}$. Comparing this with the expressions (3.12) and (3.13) set up by Nielsen [74.1], it can be seen that the relations are fundamentally equal. The only difference is the factors which are multiplied by the quantities $\frac{1}{\sqrt{f_c}}$ and $\frac{r}{f_c}$. In the case of the simplified expressions for the rotation mechanism, the factors depend on the geometrical properties, which is not the case in (3.12) and (3.13). However, the order of magnitude of the factors in the two sets of formulas is the same. In preliminary calculations Nielsen's expression can therefore be used.

Chapter 9

Test Results for Anchorage of Two and Three Layers at Supports

In the literature no tests of anchorage at supports with more than one layer of reinforcement were found. A few tests, reported in Andreasen [88.1], were therefore carried out to illustrate the problem. This pilot test series can only be considered as preliminary.

The theoretical curves in chapter 6 show that the strength for one bar decreases for increasing numbers of layers of reinforcement, n_ℓ, other things being equal. The conditions depend of course, on the geometrical properties as discussed in chapter 6. Andreasen's [88.1] tests indicate the same; the strength decreases for increasing n_ℓ. Hence it is essential to know what to do in practice.

Because of the limited amount of tests the analysis carried out here can only give a hint about the conditions with several layer of reinforcement. More tests with varying material and geometrical data must be used in a final analysis.

The theoretical expressions for the strength of an anchorage with more than one layer of reinforcement are a little complicated. In chapter 6 it is shown how the expressions can be simplified. However, the simplified expressions are certainly still too complicated for practical use. Further simplification, for instance, analogous to what was done in the case of one layer of reinforcement in the previous chapter, must be carried out.
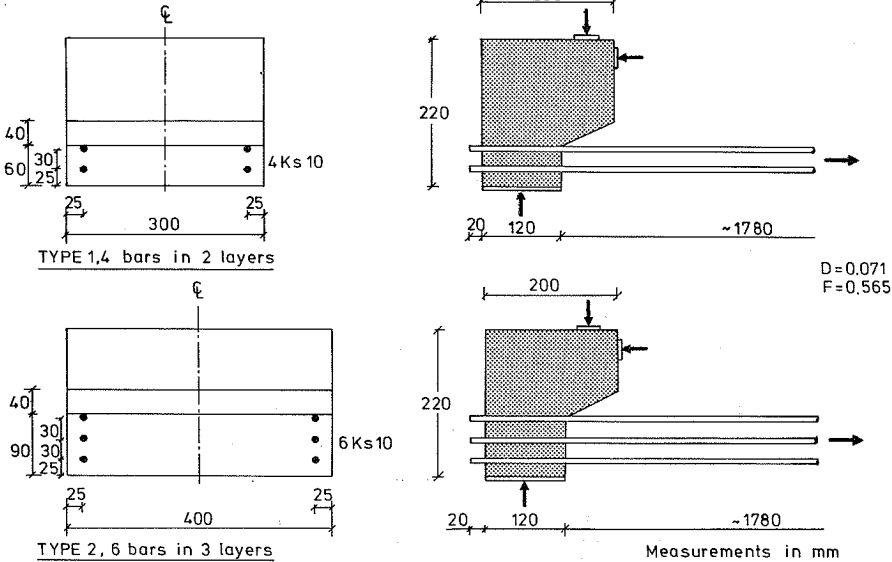
Figure 9.1: *Main principle in the test set up and geometry of the two types of specimens in Andreasen [88.1].*

9.1 Test Results

In Andreasen [88.1] the total number of tests carried out is 8; 4 tests with a 4 bar specimen and 4 tests with a 6 bar specimen, see figure 9.1. The other test data and the results are given in appendix B.

Unfortunately it is not certain that the tests with 6 bars in 3 layers failed in the anchorage. An analysis carried out in [88.1] indicates a kind of a bending failure. However, in one of the tests a local weakness in one of the corners resulted in failure for a low load. Nevertheless, the tests with the type 2 specimens are included here to complete the study.

The rib parameters D and F are shown in figure 9.1. As in chapter 8, the value for F is determined by assuming the width of the ribs, u, to be zero. This makes it possible to compare the theoretical strengths and the obtained values for the effectiveness factors with what is found in the previous chapter.

The tests with anchorage in two and three layers of reinforcement can be compared to the tests with anchorage in one layer. In figure 9.2 some
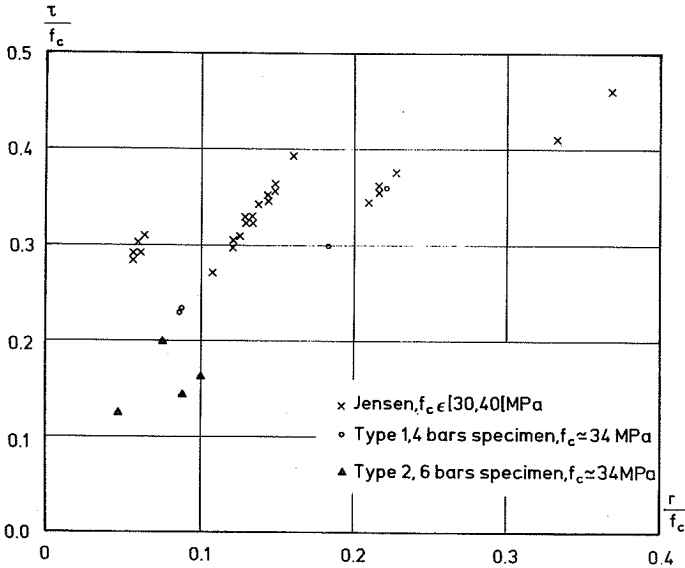
Figure 9.2: $\frac{\tau}{f_c}$ as a function of $\frac{r}{f_c}$ for some of Jensen's [82.1] and [82.2] test results and the results from the specimen in figure 9.1.

of Jensen's [82.1] and [82.2] test results used in the previous chapter, see figure 8.1, are shown together with the results from Andreasen [88.1].

The results can not be compared directly because the geometrical properties are not equal in the two test programs. However, it can be used as a rough guide. It can be seen that the test results correspond reasonably with the theoretical results from chapter 6; the strength decreases with increasing reinforcement layers, all other things being equal.

Figures 9.3 and 9.4 show the test results for 2 and 3 layers of reinforcement, together with curves for the rotation and translation mechanisms from chapter 6. Curves for various values of the effectiveness factor ν are shown.

In the tests the concrete compression strength f_c was approximately 34 MPa. Using (8.2) valid for one layer of reinforcement, the order of magnitude for the effectiveness factor ν is found to be 0.45. The figures show that the values for ν in the case of two layers of reinforcement are larger and in the case of three layers, the values are generally less than this value. It was

tau/f_c
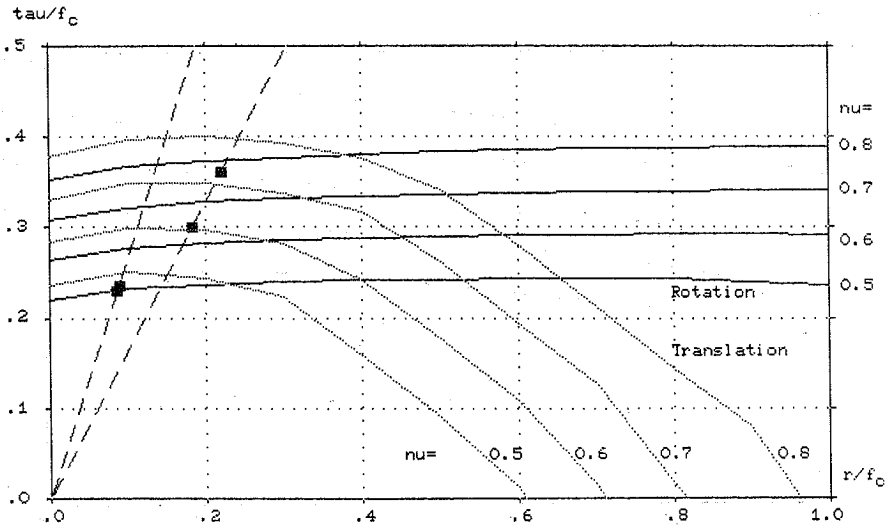
Figure 9.3: *Test results and theoretical curves for 2 layers of reinforcement. The limit mechanisms are included.*

tau/f_c
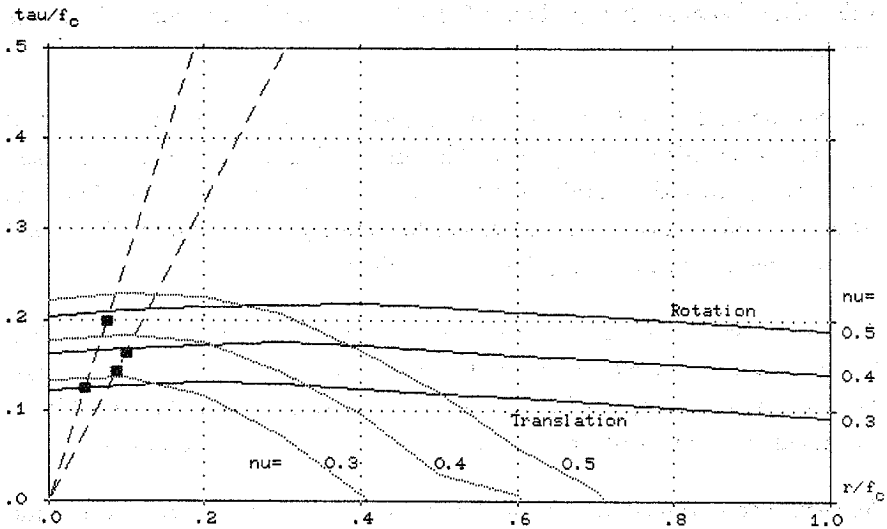
Figure 9.4: *Test results and theoretical curves for 3 layers of reinforcement. The limit mechanisms are included.*
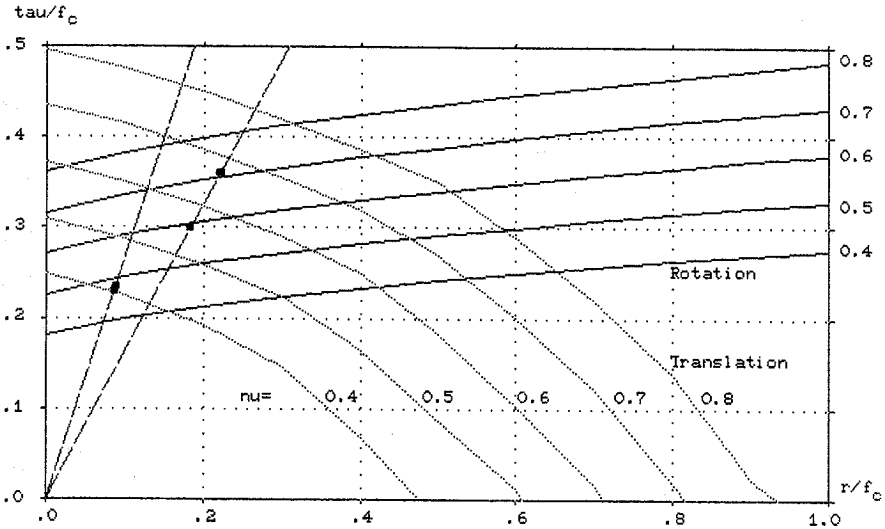
Figure 9.5: *Test results and simplified theoretical curves for 2 layers of reinforcement.*

expected that the ν value for the three layer specimens would be less than this value, because they probably failed before the full anchorage load was applied.

Expression (8.2) was developed, using a mechanism similar to the simplified rotation mechanism in chapter 6. This mechanism must therefore be used when comparing the obtained values for ν in the case of more than one layer of reinforcement with the values for one layer. In figures 9.5 and 9.6 the test results and the simplified mechanisms are shown.

As can be seen, the values for ν are lowered. In two of the tests with 2 layers of reinforcement, the value for ν is very close to 0.45. In the other two, the values are approximately 0.6 and 0.7, respectively. For the 3 layer specimens only one test has $\nu \simeq 0.45$, the others have lower values.

As seen, the obtained values for the effectiveness factor ν are in the same interval as with one layer of reinforcement. However, the scatter is large and there are too few tests to carry out a complete analysis. More tests have to be performed before a simple calculation method can be developed.
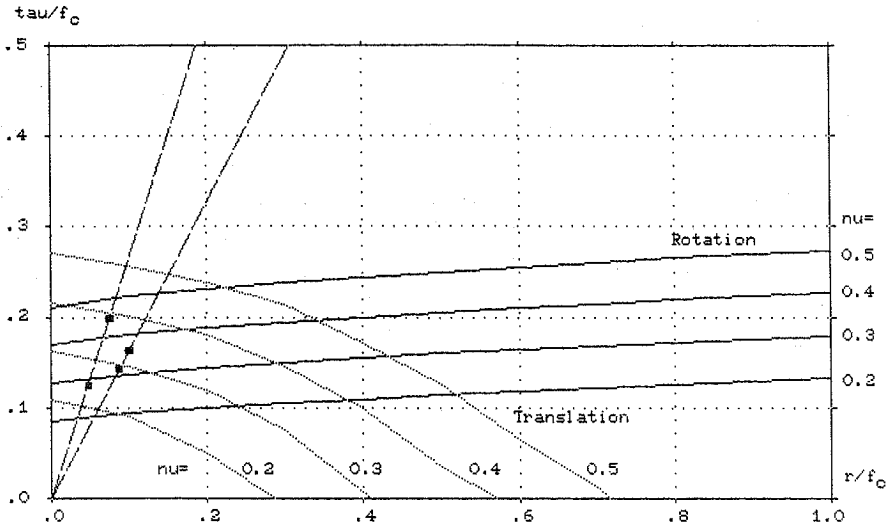
Figure 9.6: *Test results and simplified theoretical curves for 3 layers of reinforcement.*

9.2   Discussion

The analysis carried out in the preceeding section is not thorough; there are too few test results. However, the calculations illustrate the tendency for anchorage in more than one layer and they show that the expounded expressions in section 6.1 are probably applicable in this case. The test results show that the strength per bar decreases with increasing numbers of reinforcement layers. The geometrical properties of course have an influence on the failure mechanism and the load carrying capacity.

More tests have to be carried out before a complete analysis can be performed. Tests with 2, 3, and maybe 4 layers, and reinforcement placed not only near the corners, should both be included. Also tests with one layer should be included, because they can be used as reference and be compared to the test results used in chapter 8. In the light of the tests, simplified expressions as in the case of one layer of reinforcement can certainly be developed.

In reality the force in the bars in different layers are not necessarily equel as assumed in the theoretical expression and in the tests carried out. The effect

from varying forces in the different layers must of course also be examined.

In the case of more than one layer of reinforcement, the theoretical strength, τ, according to the rotation mechanism, does not increase much for increasing reaction stress, r. This indicates that the strength according to this mechanism can be determined simply by ignoring the reaction stress. The decending part for larger r is described well by the simplified translation mechanism. The relationship between the strength τ and the reaction stress r is then composed of a constant and a descending line, and the strength would then be relatively simple to determine.

Chapter 10

Test Results for Lap Splices

In contradistinction to anchorage at supports, many test series have been carried out on lap splices. Splices in reinforcement have interested designers for as long as reinforced concrete has been used, because the reinforcement is often not long enough. Many different splice methods have been proposed but the most frequently used, is probably the method where the bars are placed alongside one another over a specified length, the lap length. This type of splice is called a lap splice.

The load carrying capacity of an anchorage is not reached when the first crack appears. Normally the load can be increased beyond this point, see e.g. Tepfers [73.1].

Tests show that close to failure, the shear stress along the anchorage length can be taken to be a constant, see for instance Tepfers [73.1], Ferguson & Briceno [69.1], Thompson et al. [79.4], and Olsen [88.2],[88.3]. This is also mentioned in chapter 3, where different theories to determine the anchorage strength, mainly for lap splices, are expounded.

The geometry of the beams treated in the following is illustrated in figure 10.1.

The distance between the two bars in a lap splice is assumed to be zero. However tests with bars not placed alongside one another are also included in the analysis.

The rib parameters D (4.6) and F (4.12) are determined assuming $a + u$ to be the distance from mid rib to the middle of the next rib, and u to be
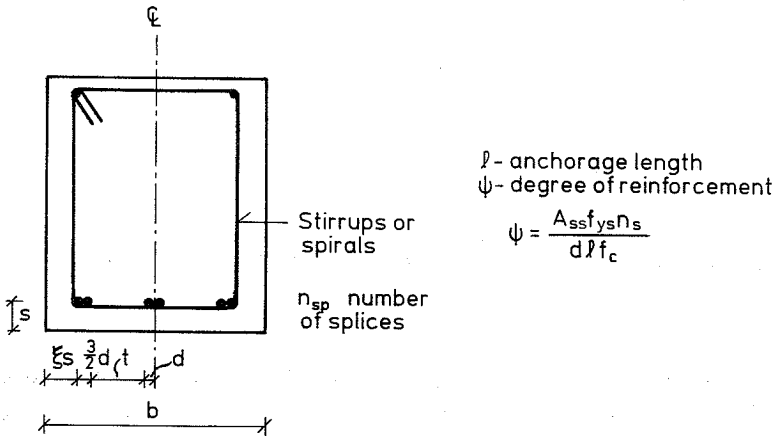
Figure 10.1: *Main geometry for tests on lap splices.*

equal to zero. D is correct while F is a little too large. The error in doing this is probably without practical significance, because the value of the effectiveness factors take into account the way in which the rib parameters are determined.

In some cases it is not possible, from the informaton in the references, to obtain all the parameters to determine D and F. The actual national standard specifications are then used. This is of course not correct, but it yields values which are probably less than the values which appeared in reality.

The test results from the literature are compared to the theory using the load ratio test/theory as a measure of the correspondence between them. Doing this the safe values are weighted more than the unsafe values, but as mentioned in the introduction in chapter 8, the danger of this is not large. Nevertheless the results from the analysis must be examined critically and carefully.

In the literature many surveys of the results of lap splice tests are given. Here some general observations from Tepfers [73.1] will be presented. It is observed that the concrete acts more plastic for small concrete strengths than for large ones. The load carrying capacity increases for increasing concrete covers. The increase is largest for the vertical cover. The dimensions

of the ribs on the reinforcing bars are observed to influence the strength; the rougher the stronger. The horizontal distance between the two bars in a lap splice does not influence the load carrying capacity much; the strength is more sensitive to which type of failure pattern appears. Surrounding reinforcement, like stirrups and spirals, increases the strength and makes the failure more plastic. With surrounding reinforcement the specimen failed gradually in contrast to the specimen without surrounding reinforcement which failed almost without warning.

Surrounding reinforcement can be taken into account in at least two ways; assuming the reinforcement to obtain the same strain as the concrete or assuming the surrounding reinforcement to yield. In the literature both effects are observed in tests. However, the problem with test observations is that they are influenced strongly by the measurement technique; the question is if the measurement instruments are located in the correct points and the measurement scans are taken at the moment of failure. Here it is assumed that the surrounding reinforcement yields in the sections intersected by yield lines in the concrete.

10.1 Test Results

As mentioned above, a large number of tests on lap splices is reported in the literature and many of the tests can be used in an analysis. The most extensive test series is probably the one by Tepfers [73.1] and many of his tests are included in the calculations. In addition to this, tests from Bergholdt [74.2], Chinn et al. [55.1], Orr [76.1], Reynolds & Beeby [82.3], Zekany et al. [81.1], Ferguson & Breen [65.1], Chamberlin [58.1], Ferguson & Krishnaswamy [71.1], Ferguson & Briceno [69.1], and Thompson et al. [79.4] are used. All test data are given in appendix C.

In the expressions for the load carrying capacity of lap splices in chapter 7, the effectiveness factor for tension in the end failure surface is denoted by ρ_e. Then it is possible to distinquish between the tensile stress in the yield lines along the lap length and the end failure, when comparing the theoretical expressions with test results. The failure along the lap length develops with increasing load, while the end contribution probably only acts at the last

moment. Hence the strains along the lap length are larger than in the end failure. This means the effectiveness factor will be less along the lap than in the end. Comparing with test results, shows that using

$$\frac{\rho}{\nu} = 0.002 \tag{10.1}$$

$$\frac{\rho_e}{\nu} = 0.10 \tag{10.2}$$

yields a satisfactory agreement. The effectiveness factor for tension in the local failure is taken to be equal to ρ in the failure along the lap length.

It has also been attempted to use $\rho = \rho_e$ and ν as a function of $\frac{\ell}{d}$ and f_c, where ℓ is the lap length, d is the diameter of the bars, and f_c is the uniaxial concrete compression strength. The results from this analysis and the one mentioned above are almost identical. Nevertheless (10.1) and (10.2) are used because the final expressions are more simple, than when using $\rho = \rho_e$ and $\nu = f(\frac{\ell}{d}, f_c)$.

Lap splices in normal and wide sections are included in the analysis. In addition to this tests on sections with spacing between the spliced bars, splices with varying moment, staggered splices, and sections with two layers of splices are also included. It turns out that the expressions can also be used in these cases. These special tests are discussed in more detail after the results of the analysis on the "normal" tests are presented.

Various analyses are carried out. The first analysis presented, is the most complicated, because all the mechanisms from chapter 7 are used. In every test the best complete failure mechanism is determined by combining the various failure mechanisms for lap splices, see for instance figure 7.9. The theoretical load carrying capacity is then compared to the load obtained in the tests. Because of the complexity of the expressions, the calculations must be carried out numerically. The result of the analysis for every test is given in appendix C and the main results are presented in table 10.1 in column **A**. The other analysis shown in the table will be presented below.

The effectiveness factors are determined using (10.1), (10.2), and

$$\nu = \frac{2.9}{\sqrt{f_c}} \tag{10.3}$$

Analysis	A	B	C	D	E	F
Mean value	1.041	1.036	1.004	1.017	0.993	1.020
Standard deviation	0.215	0.209	0.198	0.184	0.200	0.198
Coefficient of variation	0.206	0.202	0.197	0.181	0.201	0.194
Number of tests	334	334	334	310	357	333

A : All mechanisms; correct determination of the variable parameters.

B : All mechanisms; simple determination of the variable parameters.

C : Plate mechanism.

D : Plate mechanism; limits for the geometrical parameters introduced.

E : Plate mechanism; tests with spirals included.

F : Simplified plate mechanism and local failure 2; test with spirals
included, limits for the geometrical parameters introduced.

Table 10.1: *Main results (test/theory) from the various analyses carried out on the lap splice tests in appendix C.*

As can be seen, the coefficient of variation for the ratio test/theory is approximately 0.2. This is a rather large value compared to what is normally obtained[1]. However in the case of the punching shear strength of slabs, treated in Hess et al [78.3], the same is found. There the scatter in the individual test series was much smaller, and a considerable part of the scatter is therefore appraised to stem from the various ways used to measure the compressive strength of the concrete. It is also the case here; in the individual series the scatter is in the normal range. The scatter in all the tests is probably caused by the different ways used to measure the compressive strength and by the fact that it has not been possible to find the correct values of the rib parameters D and F in all tests.

Because the theoretically correct expressions for the failure mechanisms in chapter 7 are complicated, they have been attempted to be simplified. The wedge-plate mechanism in section 7.1.2 is complicated because the two equations, (7.6) and (7.7), can not in general be solved analytically. In the numerical calculations it is observed that the angle β is normally close to

---

[1]Normally the coefficient of variation is between 0.1 and 0.15 for tests on concrete structures

φ, the angle of friction for the concrete. Assuming $\beta = \varphi$ and using $e = 2$, (10.1), and (10.2), expression (7.6) can be written

$$\sin \alpha = \frac{39.76 - 5\frac{s}{\ell}}{39.6 + 21\frac{s}{\ell}} \tag{10.4}$$

where $\alpha \in [\varphi; \pi/2]$.

The two corner mechanisms, the side-wedge and the bottom wedge mechanisms, treated in section 7.1.3, are similar to the wedge-plate mechanism. (10.4) can therefore also be used in this mechanism, if $\frac{s}{\ell}$ is changed to $\xi\frac{s}{\ell}$ in the case of the side-wedge mechanism.

For the two rotation mechanisms, rotation no. 1 and rotation no. 2 in section 7.1.3, the variable dimensionless parameter η is taken to be constant. For rotation no. 1, $\eta = 0.90$, and for rotation no. 2, $\eta = 0.45$, are used. These values are determined on the basis of the tests where the rotation mechanisms were decisive. Using a constant value of η is similar to the simplifications in the case of anchorage at a support with one layer of reinforcement, chapter 8.

The translation mechanism, which is the least corner mechanism, is simplified by assuming that only the end contribution is active. Doing this, the variable angle θ can be found from

$$\tan \theta = \xi \tag{10.5}$$

Using these simplifications, the results shown in table 10.1 column **B** are obtained. As is seen, the result is almost identical to the previous result using the theoretically correct expressions. The deviation from the theoretically correct analysis of the ratio test/theory is in general less than 0.01. The theoretical value is larger than that obtained in the theoretically correct analysis because the values used for the parameters are not the optimal ones.

It is noticed that the expression for the plate mechanism is not simplified; it is simple enough without further simplifications.

Because the plate mechanism is simple and because it is decisive in most of the tests, this mechanism has been attempted to be used alone. The result

of this analysis is given in table 10.1, column **C**. As can be seen, the result is even better than the result from the analysis using all the mechanisms, columns **A** and **B**. However, the theoretical strength in the tests with

$$\xi \frac{s}{d} < 0.8 \tag{10.6}$$

deviates somewhat from the previous analysis. Therefore the following limits are introduced

$$\xi \frac{s}{d} \geq 0.8 \tag{10.7}$$

$$\frac{s}{d} \geq 0.8 \tag{10.8}$$

$$\frac{\ell}{d} \geq 7.0 \tag{10.9}$$

(10.7) is a result of (10.6) and is a measure for the horizontal cover for the bars near the corners. $\frac{s}{d}$ is a measure for the vertical cover and (10.8) is included for "symmetry" reasons around the bisector in the corners. (10.9) is introduced as a limit for calculations in practice.

Excluding the tests not fulfilled (10.7) – (10.9), and still using the plate mechanism, the result shown in column **D** is obtained. The standard deviation and the coefficient of variation are seen to be reduced, compared to **C**.

In the analysis shown above, tests without surrounding reinforcement and tests with normal stirrups are included. In column **E** the result of an analysis using the plate mechanism, including the tests with spirals around the splices, is shown. No limits on the geometrical parameters are used. The mean value is a little less than that obtained in **C**, because the theoretical strength in the tests with spirals done by Tepfers [73.1], is too large compared to the test results. In the tests with spirals from the other references the results are satisfactory. The reason why Tepfers's tests do not agree, is not found, but in general spirals yield special conditions, not appearing when using normal stirrups, see figure 10.2.

If the spiral is located excentrically compared to the lap splice ($f \neq 0$), the force in the reinforcement must be multiplied by $\cos \beta_1$, see the figure to the left. In the longitudinal direction of the main reinforcement there
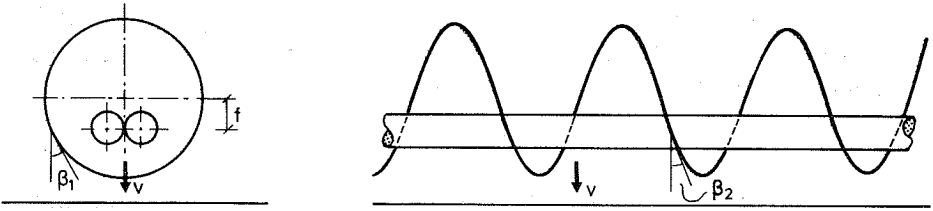
Figure 10.2: *Spirals around lap splices.*

can also be an angle between the vertical (direction of the displacement of the concrete cover) and the longitudinal direction of the spirals; therefore a reduction of $\cos \beta_2$ must be included, see figure 10.2 to the right.

As is seen, the contribution from the spirals is very sensitive to the position of the spirals in relation to the lap splices. The total yield force in spirals must therefore only be included if it is quite sure that the spiral are located concentrically ($f = 0$) and there is no angle between vertical and the spirals in the longitudinal direction of the main bars ($\beta_2 = 0$). This must of course also be the case after the casting of the structure.

The last column **F** in table 10.1 represents the result of the final analysis. Because local failure 2 in chapter 4 is divided into two expressions, it is not always easy to decide which of the expressions for failure shape 1 and 2 should be used in an actual case. Hence the two expressions, (4.17) and (4.18), for local failure 2 are rewritten into one expression, given by

$$\frac{\tau}{f_c} = \frac{F\nu}{40}\left[1 + \sqrt{1 + 2400\frac{C}{F\nu}}\right] \qquad (10.10)$$

For $\frac{C}{F\nu}$ less than 1.2, the difference between the correct expressions and this expression is less than approximately 3%. For $\frac{C}{F\nu} \leq 2.0$, the difference is less than 14%, expression (10.10) being less than the correct expression. In figure 10.3, $\frac{\tau}{F\nu f_c}$ is shown as a function of $\frac{C}{F\nu}$ for failure shape 1 and the simplified failure shape 2 for various values of $\frac{F}{D}$.

As can be seen in the figure, failure shape 2 will always be decisive for $\frac{F}{D}$ less than approximately 8. For $\frac{F}{D}$ larger than 8, both failure shape 1 and 2 can be decisive. The point of distinction is not exactly $\frac{F}{D} = 8$, but the
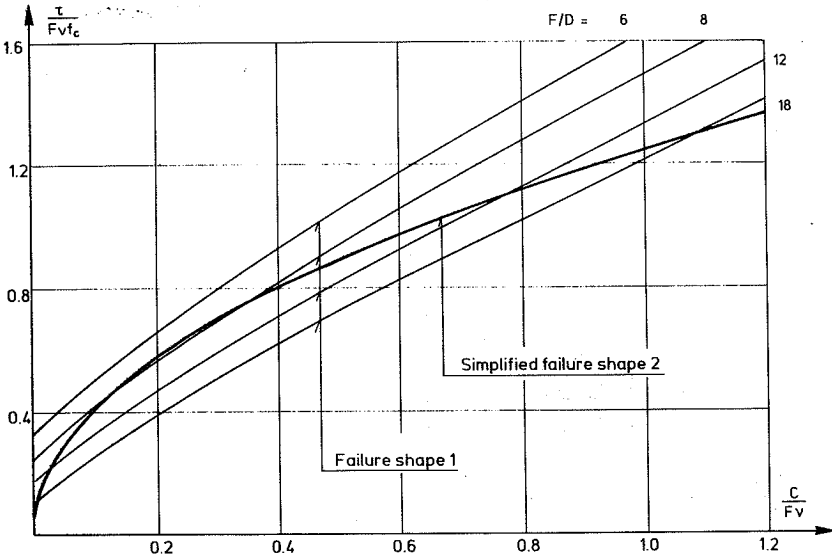
Figure 10.3: $\frac{\tau}{F\nu f_c}$ as a function of $\frac{C}{F\nu}$ for failure shape 1, (4.9) and the simplified failure shape 2, (10.10), for various values of $\frac{F}{D}$.

difference between failure shape 1 and 2 is small for $\frac{F}{D}$ approximately equal to 8 for certain values of $\frac{C}{F\nu}$ [2].

The expression for the plate mechanism is simple compared to the other mechanisms. However, it can be simplified to some extent. Because the effectiveness factor for tension ρ is assumed to be small, (10.1), the contribution from ρ in the expression for the plate mechanism (7.1) can, with sufficient accuracy be assumed to be zero. The factor eE_e in the end contribution is approximately equal to 1 when using (10.2) and (7.3). Consequently the expression for the plate mechanism can be written as

$$C = \frac{1}{2\pi n_{sp}} \left[\nu \frac{bs}{d\ell} + n_{ss}\psi \right] \qquad (10.11)$$

where n_{ss} is the number of stirrups or spiral sections crossed by the horizontal yield line, see for instance figure 7.11.

In column $\mathbf{F}$, table 10.1, the result of the analysis using (10.10) and (10.11) is shown. The tests with spirals are included and the limits (10.7) - (10.9)

[2]The value of $\frac{F}{D}$ where failure shape 1 and the correct failure shape 2 only have one common point is approximately 7.1.
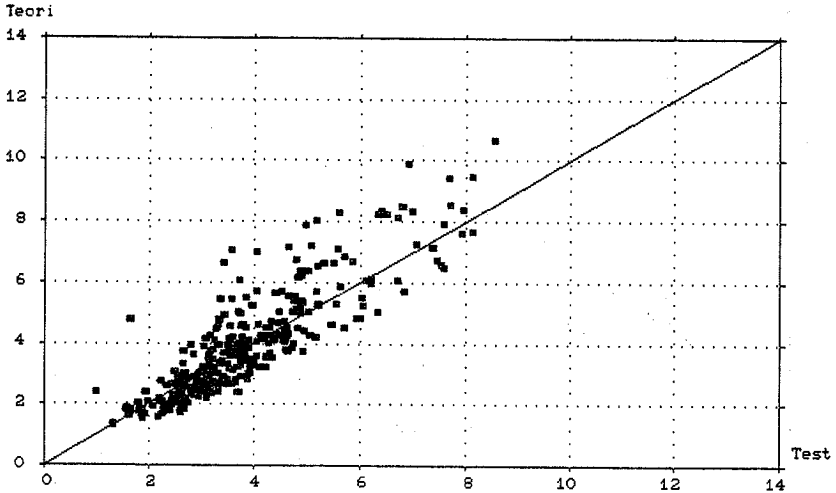
Figure 10.4: *Theoretical load carrying capacity as a function of test results for the 333 tests included in the analysis in table 10.1, column* **F**.

are used. The result is satisfactory compared to the other analyses. In figure 10.4 the theoretical load carrying capacity is shown as a function of the test results for the 333 tests included in the analysis in column **F**.

In general the scatter is large in the analysis presented above, compared to what is normally obtained. However, in many other problems the tensile strength does not influence as much as is the case in lap splices. In addition to this, many test series are included which often influence the scatter, because the concrete strength is not measured by the same procedure each time. Furthermore, the used values for the rib parameters D and F are certainly not the correct ones in all tests. In some cases it was not possible to obtain the actuel values appearing in the tests, wherefore the actual national standard specifications for deformed reinforcement were used in these cases.

In figures 10.5 – 10.9 some of the test results are shown as functions of various parameters. A theoretical curve, based on the simplified expressions for the plate mechanism (10.11), is also illustrated. Local failure 2 is determined using (10.10). The theoretical curve is determined using the
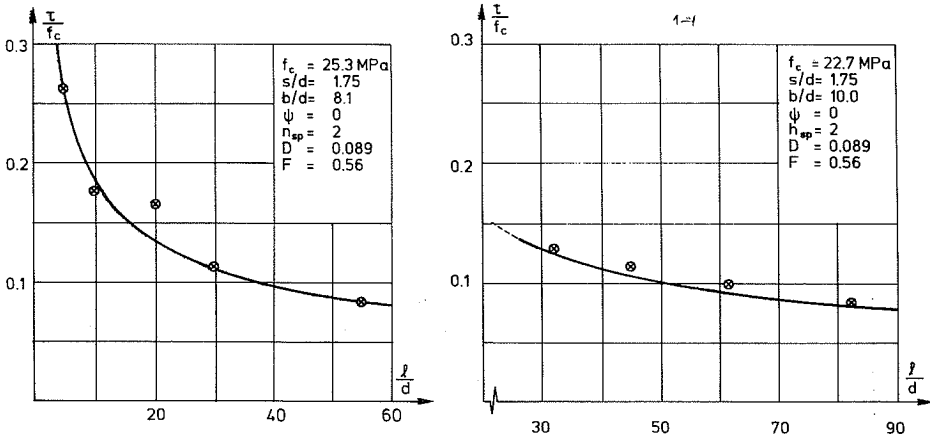
Figure 10.5: $\frac{\tau}{f_c}$ as a function of $\frac{\ell}{d}$ for Tepfers's test series 657 no. 1-4 (right) and 37-40 (left).

values for the parameters shown in the figures. Figures 10.5 and 10.6 show the dimensionless strength $\frac{\tau}{f_c}$ as a function of the dimensionless anchorage length $\frac{\ell}{d}$. $\frac{\tau}{f_c}$ is shown as a function of the covers $\frac{s}{d}$ and ξ in figure 10.7, and as a function of the uniaxial compressive strength for the concrete f_c in figure 10.8. Figure 10.9 shows $\frac{\tau}{f_c}$ as a function of ψ, the degree of surrounding reinforcement.

As can be seen from the figures, the correspondence between the tests and the theoretical load carrying capacity is in general satisfactory.

It is observed that the curve in figure 10.8 is described very accurately by the simple equation

$$\frac{\tau}{f_c} = \frac{0.6}{\sqrt{f_c}} \tag{10.12}$$

The difference between the values of $\frac{\tau}{f_c}$ from (10.12) and the correct expression is less than 0.002 for $f_c \in [5; 100] MPa$. In fact if the correct expression for failure shape 2a were used for the local failure and the plate mechanism for the failure in the surroundings it can be shown that the strength $\frac{\tau}{f_c}$ is equal to $\frac{k_1}{\sqrt{f_c}}$, where k_1 is a constant.

(10.12) is similar to expression (3.18) obtained from the Danish Code of Practice, DS 411. The constant value in the numerator is approximately
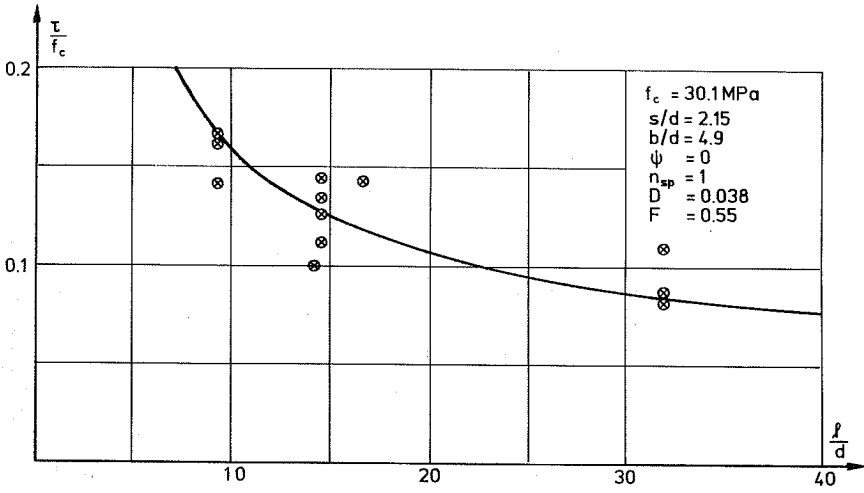
Figure 10.6: $\frac{\tau}{f_c}$ as a function of $\frac{\ell}{d}$ for Chinn et al.'s tests D7,9,10,14,20,22,25,26,33,34,35,39.
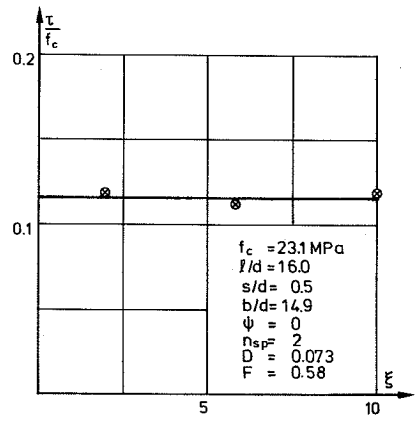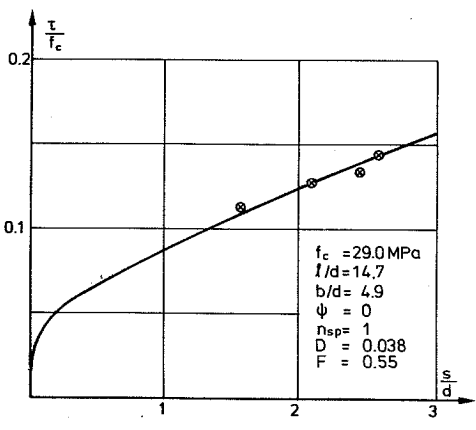
Figure 10.7: $\frac{\tau}{f_c}$ as a function of $\frac{s}{d}$ and ξ, respectively. Tests no. D7,9,14,39 from Chinn et al. (left) and Series 732 no. 120-122 from Tepfers (right).
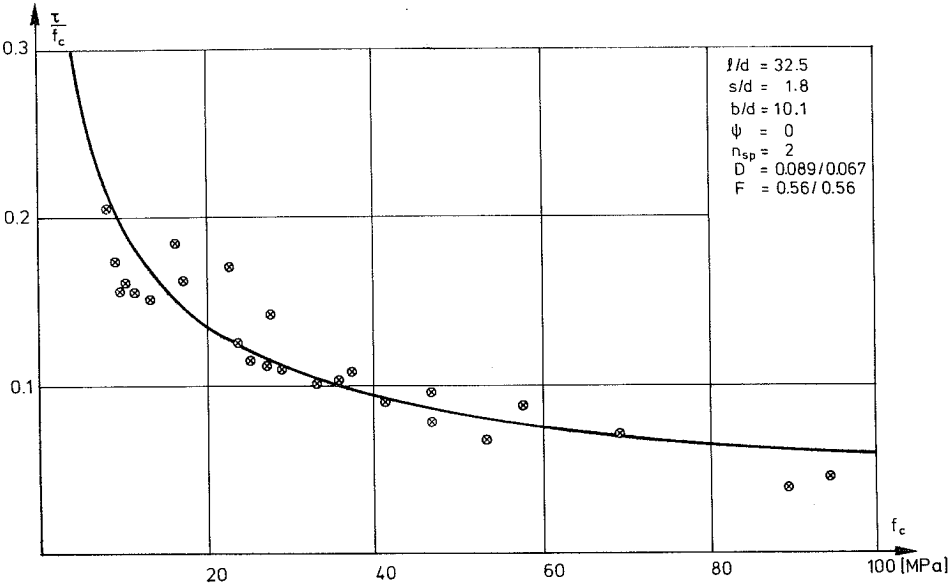
Figure 10.8: $\frac{\tau}{f_c}$ as a function of f_c for tests series 732 no. 1-17, 35-37, 51-55 from Tepfers.
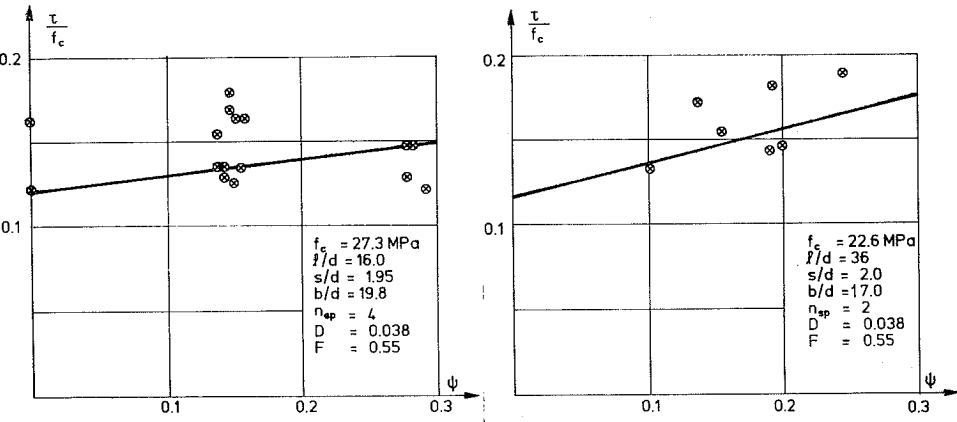
Figure 10.9: $\frac{\tau}{f_c}$ as a function of ψ for tests no. 1-16 from Zekany et al. (left) and 8F30b-8F36g, 11R36a from Ferguson & Breen (right).

0.75 instead of 0.6 in (10.12). This means that the load obtained from DS 411 is unsafe in this case. However, the tests in figure 10.8 are without surrounding reinforcement, which is required according to the code. Nevertheless, the figure indicates that the method, in DS 411 can produce unsafe values for the load in some cases.

Tests with special lap splice arrangements are also reported in the litterature, for instance tests with spacing between the bars in a lap splice, splices in varying moment regions, staggered splices, splices in two layers, and splices subjected to impact loadings. Some of these tests are included in the previous analyses.

In Champerlin [58.1], the spacing between the bars in a lap splice varies. In the tests characterized by a number and an a, the distance is 0 mm, and those by b and c the distance is approximately 12.7 mm and 25.4 mm, respectively. These tests are included in the analysis and in appendix C the results can be seen. It is observed that the difference in the load carrying capacity is almost independent of the spacing. The same is concluded by Tepfers [73.1].

The tests by Ferguson & Krishnaswamy [71.1], Ferguson & Briceno [69.1], and Zekany et al. [81.1] in Appendix C are on lap splices placed in varying moment regions. The stress in the bars at the maximum moment over the lap length is used in the calculations. As can be seen in appendix C, the load obtained in the tests is generally a little larger than the theoretical loads.

Some of the tests by Ferguson & Briceno [69.1] and Thompson et al. [79.4] had staggering splices, or not all bars in the section were spliced, see figure 10.10.

It turns out that the developed expressions can also be used in this case. The width is determined with respect to how many bars are spliced in the section, see b_{eff} in the figure. The number of spliced bars n_{sp} is equal to the actual number of spliced bars. Surrounding reinforcement is only included if it "goes around" the spliced bars, e.g. in the example to the left
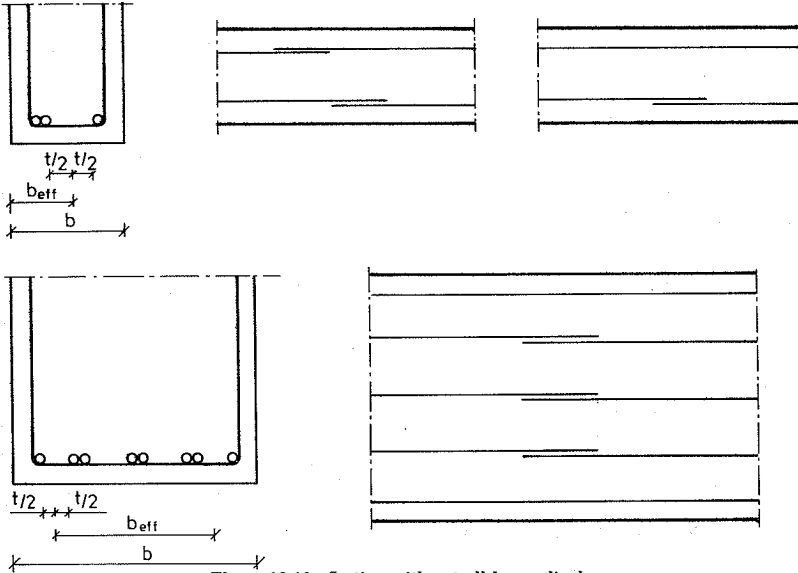
Figure 10.10: *Section with not all bars spliced.*

in figure 10.10 n_{ss} is equal to 1. This rule generally results in conservative values for the theoretical load carrying capacity in the tests used.

The width and the number of bars in the test specimens used by Thompson et al. [79.4] were great compared to the other tests. The ratio between the width and the diameter $\frac{b}{d}$ was between 22 and 36, and the number of splices was 4, 5, or 6. The strain in all the bars was measured along the lap length. These measurements show that the strain distribution across the section is approximately constant and along the lap the distribution is approximately linear. The force in the corner splices is almost equal to the force in the internal bars; the difference being less than 15%. In the calculations in appendix C, the mean value for all the splices in the section is used. The strain in the stirrups was also measured and the results show that at failure the yield stress was reached at the corner splices. In some of the tests the corner bars were not spliced; those tests are discussed above. In the reference it is concluded that in wide beams or in slabs the corner bars do not have much influence. The expressions developed here are a little conservative in the case of wide sections.

Tepfers [73.1] carried out tests with splices in more than one layer. One of them, with 8 splices in two layers (732:167), failed in the anchorage. Assuming the 8 splices to carry the same load and using the simple expressions set up in this section, the result is reasonable, see appendix C. The geometrical parameters are determined, assuming there were only 4 splices in one layer.

Tests with leca concrete are also included by Tepfers [73.1], tests 732:167-172. The result using the simple expressions is satisfactory, see appendix C.

Lap splice tests with high strength concrete have been carried out by Olsen [88.2] and [88.3]. The uniaxial concrete compression strength, f_c, was in the range 20 to 100 MPa. The preliminary results indicate that the method expounded here corresponds satisfatory with the test results for concrete compression strengths up to approximately 60 MPa. For the concrete strength f_c in the range 75–100 MPa it seems like the expressions developed here is unsafe (10–15%). There is refered to Olsen [88.2] and [88.3] for a more detailed description.

The method set up here to determine the strength of lap splices is not used in tests subjected to impact loading. However, Tepfers [73.1] and Orangun et al. [75.1], [77.3] mention that the expressions for the statically loaded splices can also be used in the case of impact load, perhaps with small changes.

10.2   Discussion

The deviation in the ratio test/theory is large in the case treated in the preceding section. As mentioned, this can be due to the way the rib parameters D and F are determined in the cases where information could not be found in the references. In addition to this many test series are included in the analysis. This normally increases the scatter because the concrete strength is probably measured, using different methods. Other than this, special tests are included, for instance many tests with varying moment over the anchorage length. However, seen in the light of the complexity of the problem, the results are satisfactory.

The limits for the geometrical parameters introduced in (10.7) − (10.9) are without practical significance. Factors other than the load carrying capacity, e.g. durability, will result in larger cover on the main reinforcement than predicted by (10.7) and (10.8). (10.9) should not necessarily be followed but special note must be taken of very small values of $\frac{\ell}{d}$, because the contribution including $\frac{\ell}{d}$ goes to infinity for $\frac{\ell}{d} \to 0$. The strength for $\frac{\ell}{d}$ less than 7, can, for instance, be assumed to be equal to the value for $\frac{\ell}{d} = 7$.

In concrete structures, when using the theory of plasticity, the value of the effectiveness factor for compression ν often increases when the amount of transverse reinforcement increases[3]. However, this is not the case here; the effectiveness factor is the same with and without surrounding reinforcement. This can be caused by dowel action in the surrounding reinforcement which therefore reduces the strength. In the case of spirals, the influence is very sensitive to the location in relation to the bars in the lap splice, as illustrated in figure 10.2, which may be the case in some of the tests included in the analysis. Another possibility is that the influence from the surrounding reinforcement in the expressions for the various failure mechanisms is too great. This could be the reason here because the expressions are developed from upper bound calculations.

In lap splices vertical cracks often appear at the end of the anchorage length for a lower load than the failure load. Despite these cracks it can be observed on photos of failed specimen that the end failure can develop, see for instance Tepfers [73.1]. Assuming the plate mechanism to be decisive the concrete cover will move vertical at failure, which means that the displacement is parallel to the cracks. The cover along the anchorage length will then by shear in the tensile cracks bring the end failure in action.

Tests with impact loading are not included in the analysis. As mentioned in the previous section, Tepfers [73.1] and Orangun et al. [75.1] conclude that the expressions for the static case can also be used in this case. However, this subject needs further investigation before applying the theory to practice.

---

[3]Distributed reinforcement going through the yield line.
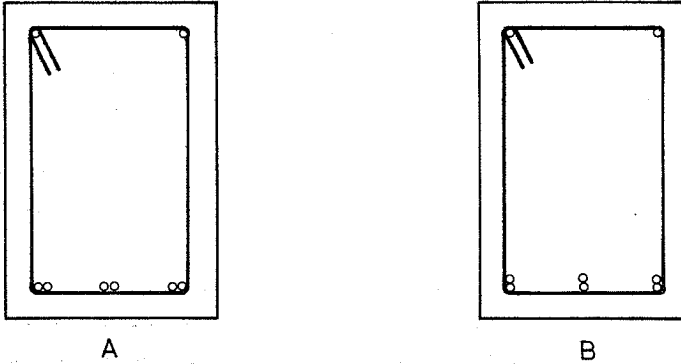
Figure 10.11: *Horizontal and vertical lap splices.*

As mentioned in connection with figure 10.8, the strength $\frac{\tau}{f_c}$ can be described as $\frac{k_1}{\sqrt{f_c}}$ in special cases, where k_1 is a constant, see (10.12). This is similar to the way the strength can be presented in the Danish Code of Practice for Concrete Structures, DS 411. However, in DS 411, k_1 is independent of the geometrical properties appearing in the actual case. The expressions in DS 411 can therefore in some situations be unsafe.

In the tests included in the analyses, the spliced bars are mainly located adjacent to one another in a horizontal plane, as illustrated in figure 10.11.A.

This is the normal way of placing lap splices. However, the location illustrated in figure 10.11.B is also possible. The expressions developed do not cover this case directly, but with some changes they can be used. Using the simplified expression for the plate mechanism set up in the previous section, will certainly yield safe values for the load carrying capacity in this case. This is related to the discussion in section 7.1.3, especially figure 7.6. The simple expression can therefore also be used in this and related cases as a safe estimation of the load carrying capacity.

Chapter 11

Design Recommendations

The expressions and methods developed previously and applicable to calculations in practice, are summarized here. In some cases more simplifications are introduced, compared to what is given in the preceding chapters.

The expressions have been compared to test results. The range for the included parameters in the tests is reported in connection with the expressions. If the case in question deviate from the area covered by tests, the expressions must be used with caution. However, if this is the case, the best is to use the theoretically correct expressions and include more mechanisms.

In some cases it is not possible to use the expressions for the mechanisms treated previously directly, or it is not certain which of the mechanisms should be used. This is demonstrated in a few special examples at the end of this chapter.

11.1   Local failure

The local failure is the failure immediately around the deformed reinforcing bar. The local failure is treated only assuming that the surroundings can deliever a certain resistance. This failure is dealt with in detail in chapter 4.

It appears that two, in principle, different types of failure may occur, named *failure shape 1* and *failure shape 2*. Failure shape 1 is given by one expression while failure shape 2 is composed of two expressions. The expressions for failure shape 2 have been simplified to only one expression here.

The decisive failure shape is determined by the surroundings and the geometry of the deformations on the reinforcement. The two dimensionless
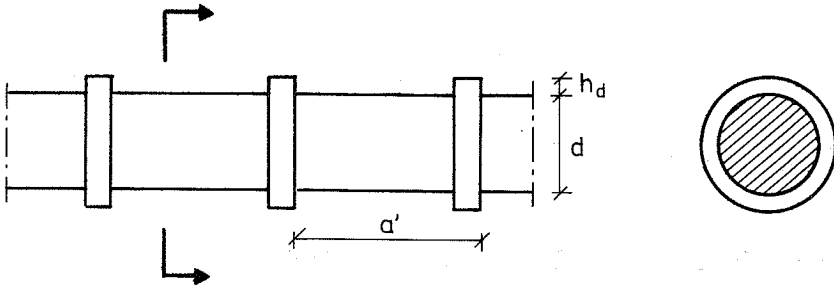
Figure 11.1: *Geometry of a deformed reinforcing bar.*

rib parameters D and F are of importance here. They can be given by

$$D = \frac{(d + h_d)h_d}{2da'} \tag{11.1}$$

$$F = \frac{1}{2} + \frac{h_d}{d} \tag{11.2}$$

where the symbols are explained in figure 11.1.

The expressions for the local failure can be written

$$\frac{\tau}{f_c} = \text{min of} \begin{cases} \frac{D\nu}{4}\left[3\left(1 + \frac{C}{D\nu}\right) + 5\sqrt{1 + 2\frac{C}{D\nu}}\right] \\ \frac{F\nu}{40}\left[1 + \sqrt{1 + 2400\frac{C}{F\nu}}\right] \end{cases} \tag{11.3}$$

where the upper expression in (11.3) is valid for failure shape 1 and the lower is valid for failure shape 2. τ is the average shear stress along the reinforcing bar, $\tau = \frac{T}{\pi d\ell}$, where T is the tensile force in a single bar and ℓ the anchorage length, f_c is the uniaxial cylindrical compression strength for the concrete, ν is the effectiveness factor, and C is the dimensionless internal work from the surroundings, $C = \frac{W_i}{\pi d\ell f_c}$, where W_i is the internal work from the surroundings.

As written in (11.3) the expression giving the smaller value of $\frac{\tau}{f_c}$ is used in the case in question. The expressions are illustrated in figure 11.2.

For $\frac{F}{D}$ less than 8, the expression for failure shape 2, the lower in (11.3), can be used with sufficient accuracy for all values of C. For $\frac{F}{D}$ larger than 8, the smaller of the expression in (11.3) must be used.

Expressions for the dimensionless internal work from the surroundings, C, for anchorage at supports with one layer of reinforcement and for lap splices,
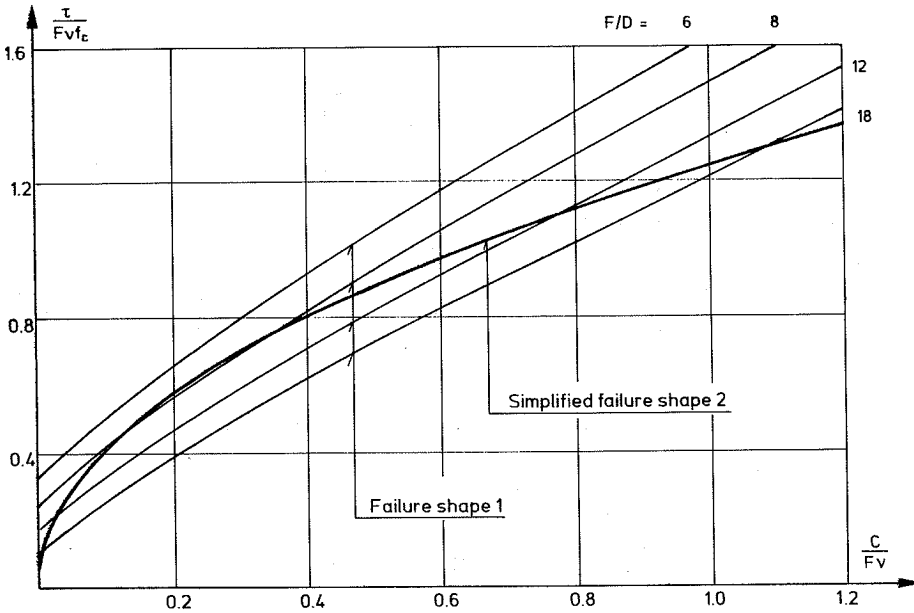
Figure 11.2: *The load carrying capacity as a function of the work from the surroundings.*

are given in the following two sections. The value of C is determined by the given expressions and this value is inserted into the expressions for the local failure, (11.3).

11.2 Anchorage at Supports

In the preceding section, the simple expressions expounded in chapter 8 for anchorage with one layer of reinforcement at supports are given. The expressions are developed on the basis of theoretical considerations, see chapter 5, and test results, see chapter 8.

The expressions are based on the mechanism named *rotation mechanism no. 1* in chapter 5. The expressions for the dimensionless internal work are given by

$$C = \frac{1}{\pi} \left[0.1\nu \left(\frac{s}{d}(4.42 + 0.85\xi) - 2 \right) \right.$$
$$\left. + \psi(1.15 + 0.15\xi) \right.$$
$$\left. + \frac{\tau}{f_c}\frac{s}{d}(1.54\xi - 0.83) \right] \qquad \text{for} \quad \frac{\tau}{f_c} < \left(\frac{\tau}{f_c} \right)_\ell \qquad (11.4)$$

Reaction stress:

$r = \dfrac{R}{b l}$

Stirrup reinforcement degree:

$\psi = \dfrac{\frac{\pi}{4} d_s^2 \, f_{ys} \, n_s}{d \, l \, f_c}$

where

d$_s$ diameter of stirrups
f$_{ys}$ yield stress of stirrups
n$_s$ number of stirrups over
  the anchorage length
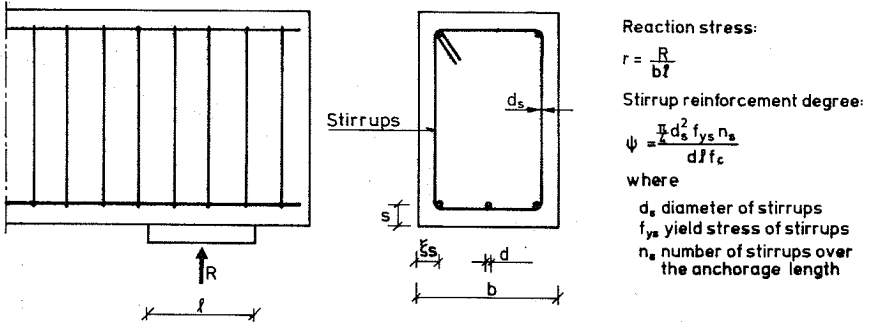
Figure 11.3: *Geometrical parameters for anchorage at supports.*

$$C = \frac{1}{\pi} \left[0.1\nu \left(\frac{s}{d}(6.39 + 0.40\xi) - 2 \right) \right.$$
$$+ \psi(1.05 + 0.15\xi)$$
$$\left. + \frac{r}{f_c} \frac{s}{d}(0.77\xi - 0.44) \right] \qquad \text{for} \quad \frac{r}{f_c} \geq \left(\frac{r}{f_c} \right)_\ell \tag{11.5}$$

where

$$\left(\frac{r}{f_c} \right)_\ell = \frac{0.1\nu \frac{s}{d}(1.98 - 0.45\xi) - 0.10\psi}{\frac{s}{d}(0.77\xi - 0.38)} \tag{11.6}$$

and

$$\nu = \begin{cases} \frac{2.65}{\sqrt{f_c}} & \text{without stirrups} \\ \frac{3.05}{\sqrt{f_c}} & \text{with stirrups} \end{cases} \tag{11.7}$$

f_c is inserted into (11.7) in MPa. The geometrical parameters are illustrated in figure 11.3.

The expressions have been compared to 140 tests without stirrups and 44 tests with stirrups. The mean and standard deviations from these analyses were 1.011 ± 0.114 and 1.017 ± 0.085, respectively.

The tests used to confirm the expressions, covered the following range of the parameters:

$\frac{s}{d} \in [1.92; 2.70]$, $\xi \frac{s}{d} \in [2.64; 5.00]$, $\xi \in [1.37; 2.59]$

$\frac{b}{d} \in [10.0; 15.6]$, $\frac{\ell}{d} \in [8.1; 16.3]$, $\psi \in [0; 0.809]$

$f_c \in [9.9; 45.0] MPa$, $r \in [0.9; 15.0] MPa$, $\tau \in [4.7; 18.6] MPa$

$\frac{r}{f_c} \in [0.040; 0.720]$, $\frac{\tau}{f_c} \in [0.255; 0.895]$, $D \in [0.062; 0.069]$

$F \in [0.57; 0.59]$.

One of the two expressions, (11.4) or (11.5), resulting in the lower value for C, in an actual case should be used. The best value for C then is inserted into the expressions for the local failure, expressions (11.3), and the lower value for $\frac{\tau}{f_c}$ can be determined.

Expressions (11.4) and (11.5) are Taylor Series of a more complicated expression. In some cases the simple expressions can not be used. This situation appears when one of the expressions after ν and $\frac{\tau}{f_c}$ inside the normal brackets in (11.4) and (11.5), becomes negative. The theoretically correct expression for *rotation mechanism no. 1* from chapter 5 must then be used.

In the case of anchorage at supports with one layer of reinforcement, the rotation mechanism is decisive in many cases. However, if the geometry is special or deviates much from the range covered by tests, another mechanism may be decisive. In this case the mechanisms treated in chapter 5 can be used.

11.3 Lap Splices

The expression for lap splices shown here is founded in the theoretical expressions in chapter 7. The theoretical expressions are compared to test results in chapter 10 and on the basis of this a simple method to determine the strength of lap splices is found.

The expression is based on the mechanism named *plate mechanism* in chapter 7. The expression for the dimensionless internal work can be given by

$$C = \frac{1}{2\pi n_{sp}} \left[\nu \frac{bs}{d\ell} + n_{ss}\psi \right] \tag{11.8}$$

where

$$\nu = \frac{2.9}{\sqrt{f_c}} \quad , \quad f_c \text{ in MPa} \tag{11.9}$$

ν must not be determined to be larger than 1.

The geometrical parameters $b, s, d,$ and ℓ are shown in figure 11.4. n_{sp} is the number of lap splices in the section, n_{ss} is the number of stirrups and spirals intersected by the straight line through the lapped bars, see figure 11.5, and
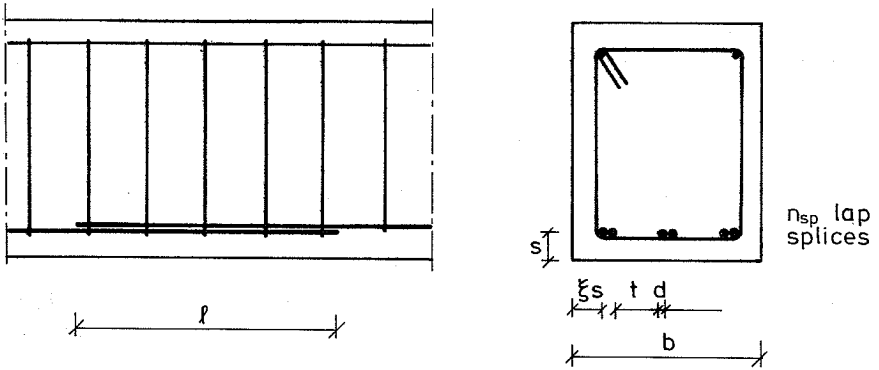
Figure 11.4: *Geometrical parameters for lap splices.*
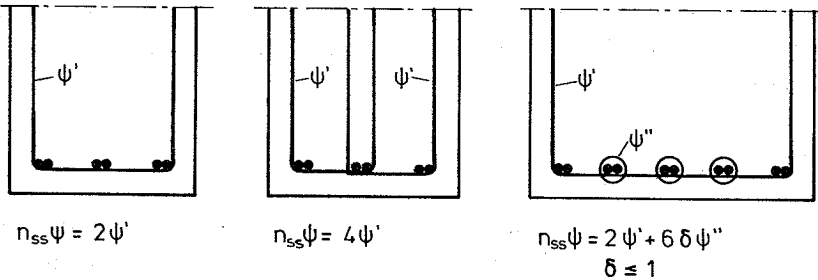
Figure 11.5: *Number of contributions from the surrounding reinforcement.*

ψ is the reinforcement degree of the surrounding reinforcement. ψ is defined as $\psi = \frac{\frac{\pi}{4}d_s^2 f_{ys} n_s}{d\ell f_c}$, where d_s is the diameter of the surrounding reinforcement, f_{ys} is the yield strength of the surrounding reinforcement, and n_s is the number of stirrups or spirals over the anchorage length.

(11.8) has been compared to test results. In the final analysis 333 tests were included, both with and without surrounding reinforcement. The mean and standard deviation from this analysis were 1.020 and 0.198, respectively.

The tests used, cover the following range of the parameters:

$$\frac{s}{d} \in [0.81; 6.50] \quad , \quad \xi\frac{s}{d} \in [1.09; 8.42] \quad , \quad \xi \in [0.34; 7.76]$$
$$\frac{t}{d} \in [0.37; 17.67] \quad , \quad \frac{b}{d} \in [4.8; 44.0] \quad , \quad \frac{\ell}{d} \in [8.3; 82.5]$$
$$\psi \in [0.0; 1.978] \quad , \quad f_c \in [6.00; 94.0] MPa \quad , \quad \tau \in [1.0; 8.5] MPa$$
$$\frac{\tau}{f_c} \in [0.038; 0.533] \quad , \quad D \in [0.030; 0.089] \quad , \quad F \in [0.54; 0.61]$$
$$n_{sp} \in [1; 6] \quad , \quad n_{ss} \in [0; 12]$$

If the given range for the parameters is exceeded, the mechanisms from chapter 7 must be used. The simple determination of the variable parameters in the various mechanisms given in chapter 10 can be used. The calculations are easily carried out and the best complete failure mechanism for the section is determined.

In the comparison of (11.8) with tests, some special tests have been included, for instance tests with spacing between the bars in a lap splice, splices in varying moment regions, staggered splices, and splices in two layers. These tests and the results from the calculations are described in more detail in chapter 10, to which there is referred.

In the case of sections where not all bars are spliced (in the same plane), (11.8) can also be used. The width is determined with respect to the number of spliced bars, as half the distance to bars not spliced is included in the width. n_{sp} is equal to the actual number of spliced bars and n_{ss} is equal to the number of surrounding reinforcing bars placed adjacent and perpendicular to the line through the centres of the lapped bars. A more detailed description is given in connection with figure 10.10.

If the surrounding reinforcement consists of spirals, the total yield force can not be expected to contribute to the internal work. If the spiral is not located concentrically compared to the lap splice, a reduction must be introduced, because the spiral is not perpendicular to the line through the centres of the lapped bars. In addition to this, a reduction must be made in the longitudinal direction. This is why the factor δ, less than or equal to one, is included in the expression to the right in figure 11.5. These reductions are explained in more detail in connection with figure 10.2.
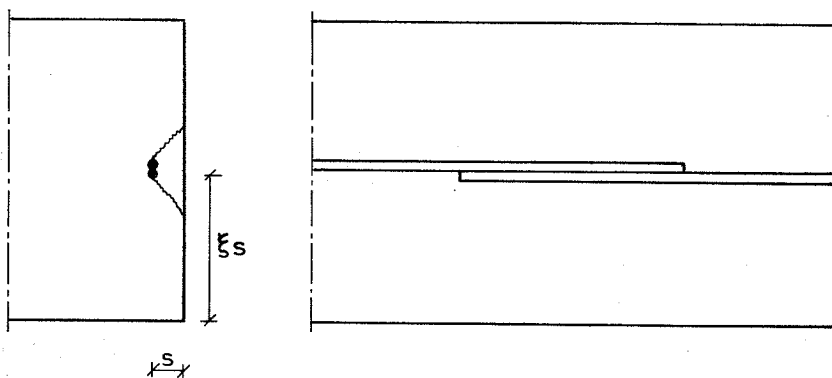
Figure 11.6: *One lap splice in a wide section.*

The load carrying capacity is obtained by inserting the determined value of the dimensionless internal work C into the expressions for the local failure, (11.3). The smaller value obtained from these expressions is used.

11.4 Special Examples

A few special examples where the previous expressions can not be used directly, are illustrated here. The principles for the way in which the calculations can be carried out, are shown.

The first example is shown in figure 11.6.

This is a lap splice placed in a wide section compared to the diameter of the lapped bars. Because $\xi\frac{s}{d}$ is large, the simple expression based on the plate mechanism in section 11.3 can not be used. In this case the wedge-plate mechanism will probably be decisive, expression (7.4). The number of lap splices n_{sp} is here equal to 1 and the number of end contributions e is equal to 2. Furthermore, it can be assumed that β is equal to φ, the angle of friction for the concrete, wherefore α can be determined from (7.6) or (10.4). The load carrying capacity is found by inserting the obtained value for C into (11.3).

Consider figure 11.7, showing two reinforcing bars anchored by means of a U-stirrup.
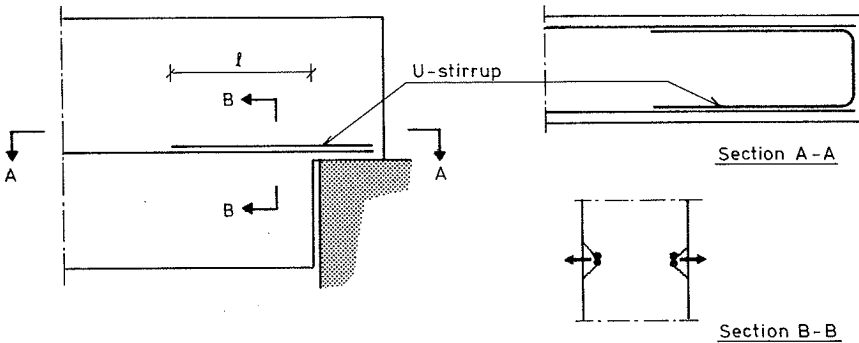
Figure 11.7: *Anchorage by means of a U-stirrup.*
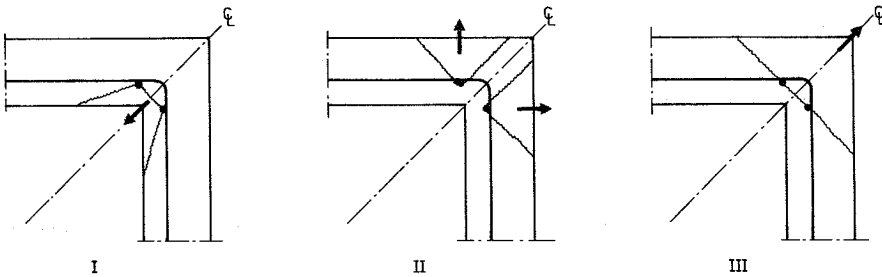
Figure 11.8: *Anchorage of bars located close to the connection between two sections.*

The problem is finding the anchorage length ℓ shown in the figure. Because there is only an active force in the main bars, it is not a lap splice problem. The expressions for anchorage at supports must be used. The bars are only close to one concrete edge, wherefore the expressions for the wedge mechanism in section 5.1.3 are used. Denoting the distance from the concrete edge to the centre of the reinforcement by s, see section B-B in figure 11.7, expression (5.33) or (5.34) for $\frac{r}{f_c} = 0$ can, for instance, be used to determine C. The load carrying capacity can be found from (11.3).

In figure 11.8 two bars are located close to the intersection of two sections.

The expressions given in section 11.2 for anchorage at supports, based on the rotation mechanism, will probably not be decisive in this case. Other
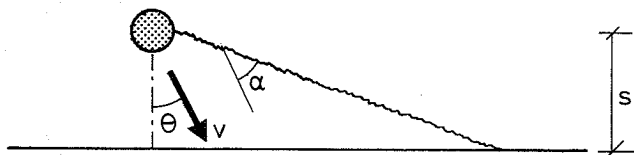
Figure 11.9: *Skew yield line from bar to concrete edge.*

mechanisms, as indicated in the figure, have to be considered. The mechanism shown in figure 11.8.I can not be treated directly by the expressions set up in chapter 5, while the expression for the wedge mechanism can be used for II. The mechanism III in the figure is not covered by the expressions but because it is a tensile yield line, it is not difficult to carry out the calculations for this mechanism. Mechanism I is more complicated and is dealt with in more detail here, for showing how cases not covered by the expressions developed in this report, can be treated.

The yield line between the two bars is a tensile yield line and causes no problems, while the two skew yield lines from the bars to the concrete edges must be treated separately. In figure 11.9 a "failure mechanism" illustrating the skew yield line is shown.

The yield line pattern does not contribute a correct failure mechanism, but it is useful for the calculations. The concrete cover below the yield line is assumed to move with the velocity v, inclined the fixed angle θ to the line perpendicular to the edge, see the figure. For θ equal to zero, the mechanism is in principle identical to the wedge mechanism. The internal work in the yield line W_i' can be written as

$$\frac{W_i'}{\frac{1}{2}vs\ell f_c} = \frac{\lambda - \mu \sin\alpha}{\cos(\alpha + \theta)} \tag{11.10}$$

Differentiating this expression with respect to α and equalizing the coefficient of differential to zero, yields

$$\sin\alpha = \frac{\mu}{\lambda}\cos^2\theta - \sin\theta\sqrt{1 - \left(\frac{\mu}{\lambda}\cos\theta\right)^2} \tag{11.11}$$

where $\sin \alpha \geq \sin \varphi$ must be fulfilled.

The optimal value for the internal work can then be obtained to

$$\frac{W_i'}{2vs\ell f_c} = \begin{cases} \mu \sin \theta + \sqrt{\lambda^2 - \mu^2 \cos^2 \theta} & \text{for } \cos \theta \geq \frac{\lambda \cos \varphi}{\sqrt{\lambda^2 + \mu^2 - 2\mu\lambda \sin \varphi}} \\ \frac{2\nu}{2\sqrt{k}\cos \theta - (k-1)\sin \theta} & \text{for } \cos \theta < \frac{\lambda \cos \varphi}{\sqrt{\lambda^2 + \mu^2 - 2\mu\lambda \sin \varphi}} \end{cases}$$

$$(11.12)$$

For the case in figure 11.8.I the angle θ is equal to $\frac{\pi}{4}$. For $\frac{\ell}{\nu}$ equal to 0.1, means that the second expression in (11.12) must be used, corresponding to $\alpha = \varphi$. The dimensionless internal work C for the mechanism is then found by adding the contribution from (11.12) to the contribution from half the tensile yield line. It is observed that the velocity v is equal to 2 and that C is equal to $\frac{W_i}{\pi d\ell f_c}$, where W_i is the total internal work in the mechanism corresponding to one bar. The smallest value for C in the three mechanisms in figure 11.8 is inserted into the expressions for the local failure.

As can be seen from the previous, it is in principle not difficult to carry out calculations not directly covered by the simple cases dealt with in sections 11.2 and 11.3. Of course, if the case in question is not covered by one of the cases treated in the preceding chapters, theoretical calculations must be carried out. However, these calculations are normally not complicated. The majority of cases appearing in practice will be covered by the expressions expounded here; therefore it is not often that theoretical calculations must be carried out.

Chapter 12

Summarized Comments

Anchorage of deformed reinforcing bars are treated previously. The theory of plasticity is used as a basis for the theoretical calculations carried out. Since concrete is not a rigid plastic material, modification factors are introduced. These factors are known as effectiveness factors and they are applied to the uniaxial concrete compression and tensile strengths. Only in a few cases is it possible to determine the value of the effectiveness factors analytically. Usually they must be found by comparing the developed theory with test results. Hence they are empirical factors.

The results obtained for concrete structures, not including the tensile strength of the concrete in the theoretical expressions, are often satisfactory. However, in the case of anchorage, tensile stresses in the concrete must be taken into account and this produces a problem. In plastic calculations only the load carrying capacity is determined accurately, but the value of the two effectiveness factors must be determined for every test when comparing the theory with test results. This means that there are two unknown parameters but only one equation. Is a lot of test results available, a two-dimensional regression analysis can be carried out, but this is not done here. Instead the value of the effectiveness factor for tension is attempted to be determined by some simple tests. It is found that the ratio between the effectiveness factor for tension and compression can be assumed to be constant with satisfactory accuracy.

When using the effectiveness factor for concrete in compression, it is often explained by the falling branch in the stress-strain relationship in uniaxial compression. The area under the modified stress-strain curve and the

real curve is said to be equal. This calculation has meaning only if the relationship between the stress and the strain is unambiguous, i.e. the relationship is independent of, for instance, the dimensions of the test specimen. However, tests have shown that this is not the case; the falling branch changes when the dimensions are changed, while the rising parts are almost identical. The tests show that if the relationship instead is described as a stress-displacement curve, the falling branch is independent of the dimensions. These observations are identical to what is observed in the case of uniaxial tension in concrete. In this case it is explained by the localisation of the cracks in the concrete. When the cracks are not distributed over the length of the specimen, it is not correct to determine the strain as the total displacement divided by the length of the specimen. It seems therefore as concrete acts equally in both tension and compression; the deformations are concentrated mainly in bands. Even though it is not correct, the effectiveness factors are used. In the theory of plasticity the localisation of the cracks is included indirectly when using yield lines. The advantage in using the plasticity theory is that relatively simple solutions can be obtained. However, the limitations of the solutions must be kept in mind.

Many anchorage tests show that close to failure, the strain distribution in the reinforcement along the anchorage length is approximately linear, increasing from the unloaded end to the maximum in the loaded end. This means, other things being equal, that the shear stress along the surface of the bar can be determined to be evenly distributed over the anchorage length. However, the stresses in the concrete decrease for increasing strains after the maximum stress has been reached. In the case of anchorage, this will also be the case and it is included in the expressions for the local failure around the bar. The shear stress is carried by compression and tension in the concrete, and these stresses are limited so as not to exceed the plastic strength for the concrete.

The anchorage failure is divided into three separate parts: The local failure occurring immediately around and along the reinforcing bar, the failure in the surroundings involving one bar, and the complete failure in the section including all bars.

The local failure is treated by upper and lower bound calculations. Corresponding values for the load carrying capacity are obtained. Hence the solutions are theoretically correct.

The failure in the surroundings in an axisymmetrical specimen is also treated by upper and lower bound calculations. Agreement between the solutions is obtained in a part of the relevant interval. The result indicates that upper bound calculations can be carried out by assuming that the surrounding concrete is displaced axisymmetrically away from the reinforcement by a constant velocity. Doing this, upper bound calculation, are in principle simple to carry out.

In practice the surroundings are seldom axisymmetrical with respect to the reinforcement, but the expressions for the local failure are used, even if this is not the case. The expressions for the local failure are, amongst others, functions of the dimensionless internal work from the surroundings, when using upper bound calculations. The other included parameters are in principle known quantities. The only problem left after the local failure has been solved, is therefore to determine the value of the dimensionless internal work from the surroundings. This can be done, as mentioned, by using a constant displacement field. Every type of problem has to be considered separately because different failure mechanisms are probably decisive.

Failure mechanisms for anchorage at supports with both one layer and more than one layer of reinforcement and for lap splices are considered. The load obtained from these mechanisms is compared to test results and on the basis of this, simple expressions are developed. However, the simplified expressions are definitely safe to use only in the range of the parameters covered by tests. In other cases the more complicated expressions must be used.

In the case of lap splices, many test results from various test series are included in the development of the simple expressions. In the case of anchorage at supports with one layer of reinforcement, there are test results from only two test series. As a means of controlling the developed expressions, it would therefore be desirable if there were tests from other series and if there were test results from specimens similar to constructions in

practice. In this case, the force in the reinforcement immediately in front of the support should be measured. In addition to this, it would be interesting to have more tests done on anchorage with more than one layer at a support. There could, for instance, be tests with 6 bars in 2 layers, 12 bars in 3 layers etc.

In the expressions for the local failure immediately around the bar, two dimensionless rib parameters D and F are included. The value of these parameters decides which of the two types of local failure will occur. The optimal situation with respect to the dimensions of the deformations on the reinforcement will appear, when the two local failure types yield approximately the same load carrying capacity. This occurs for $\frac{F}{D} \simeq 8$. The ratio $\frac{F}{D}$ is approximately equal to the ratio between the distance between the ribs, a, and the height of the ribs, h_d, which gives that $a \simeq 8h_d$ results in optimal dimensions of the deformations on the reinforcement, other things being equal.

Using the theory of plasticity for a problem, the load carrying capacity is obtained. Comparing the developed expressions with test results, the determined mean and standard deviations on, for instance, the ratio between the test load and the theoretical load will tell something about the uncertainty in using the expressions. However, if the correct estimation of the uncertainty should be found, a statistical analysis must be carried out. The load and the material properties must be described as stochastic quantities. Such calculations are not carried out here, but they could be interesting. One problem with calculations taking into account the variation of load and strength, is that they can normally not be carried out analytically, and consequently the calculations must be carried out by means of EDP. When EDP is necessary, this can be utilized to give a more correct description of the behaviour of the concrete than that given by the effectiveness factors, e.g. a fracture mechanics approach could be used. It would then be possible to use the correct stress-strain and stress-displacement relations. The calculations would be extensive because both fracture mechanics and stochastic calculations are each copious.

In the types of anchorage problems dealt with in this report, the reinforcing
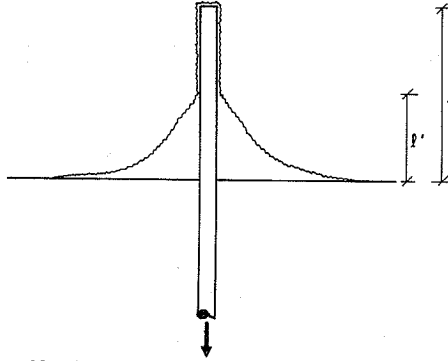
Figure 12.1: *Anchorage of bar far from concrete edges, parallel to the longitudinal direction of the bar.*

bars are located close to at least one concrete edge, parallel to the longitudinal direction of the bar. In upper bound calculations the yield lines therefore go from the bar to the concrete edges. However, if the bar is located far from concrete edges, upper bound calculations will lead to very high values of the load carrying capacity. This may be true but there must be an upper limit for the load which can be carried. For a specified distance to the edge, the bar is pulled out at failure, involving only the concrete close to the bar. The failure will probably be one similar to the punching shear failure. If the anchorage length, ℓ, is great, the punching cone will probably not extend to the end of the bar, but only a distance ℓ', see figure 12.1.

It is not immediately possible to determine the value of ℓ'; calculations have to be carried out. However, this pull- out problem is very interesting and it ought to be solved. In addition to this, other types of anchorage arrangements similar to this, should be investigated.

The pull-out problem shown in figure 12.1 demonstrates that anchorage of deformed reinforcing bars is mainly governed by the compression strength of the concrete. In the case shown, the punching shear failure is a compression failure and at the farther end of the bar, the resistance from the surroundings is large, wherefore the local failure will be a compression type failure.

In the majority of the tests included in the comparison with the theory, the concrete cover is within the normal range. However, in a few tests in the case of lap splices the cover was small, and the tests show that the anchorage

strength is considerable for anchorages with small or no concrete covers. This information can be used, for example, in the case of fire damaged structures. More tests have to be carried out before design rules can be developed.

The expounded expressions for anchorage at supports and lap splices have been compared to test results appearing from specimens loaded by static load. Test results from dynamically loaded specimens are not included. Other investigations show that the principle in the expressions based on static tests, does not change in the case of a pulsating load. However, it is necessary to compare the theory with test results before applying it to such cases.

In the case of lap splices, only tests with tension in the spliced bars are included. For compression in the bars, the theoretical expressions can be used, but the value of the effectiveness factors must probably be changed. This has to be investigated.

In summarising, it must be said that it seems likely that the theory of plasticity can be used in the case of anchorage. The developed theoretical expressions are compared to test results and the empirical modification factors, the effectiveness factors, are determined. The value of the factors obtained, is within the normal range compared to other analyses.

It is not correct to use the theory of plasticity on concrete structures, but nevertheless it is very useful. By the use of the theory of plasticity it is possible to avoid gross blunders, because the theoretical considerations automatically show prospective upper limits and the like. Theoretical solutions must always be compared to test results and must be examined critically.

In the future, in the case of concrete structures, the calculations based on the theory of plasticity will probably be replaced by other methods, where the concrete is described more accurately. These calculations must undoubtedly be carried out numerically by means of a computer. Nevertheless, the solutions from the plastic calculations and other simple methods will still be indispensable as a control for the results from the numerical calculations.

Bibliography

[1833]   Lamé, Clapeyron: *Mémoire sur l'équilibre intérieur des corpssolides homogènes.* Mém. divers savans, Vol. 4, 1833.

[28.1]   Richart, F.E., A. Brandtzaeg, R.L. Brown: *A Study of the Failure of Concrete under Combined Compressive Stresses.* University of Illinois, Eng. Expt. Stat., Bulletin No. 185, pp. 1-102.

[38.1]   Gvozdev, A.A.:*Opredelenie valichiny razrushayushchei nagruzki dlya staticheski neopredelimykh sistem, preterpevayushchikh plasticheskie deformatsii.* Svornik trudov konferentsii po plasticheskim deformatsiyan, Moscow-Leningrad, Akademia Nauk SSSR, 1938, pp. 19-30. (English translation: The determination of the value of the collapse load for statically indeterminate systems undergoing plastic deformation. International Journal of Mechanical Sciences, Vol. 1, 1960, pp. 322-333).

[39.1]   Menzel, C.A.: *Some Factors Influencing Results of Pull-out Bond Tests.* ACI Journal, Proceedings Vol. 35, June 1939, p. 517.

[46.1]   Clark, A.P.: *Comparative Bond Efficiency of Deformed Concrete Reinforcing Bars.* ACI Journal, Proceedings Vol. 4, No. 4, Dec. 1946, pp. 381-400.

[49.1]   Balmer, G.G.: *Shearing Strength of Concrete Under High Triaxial Stress.* U.S. Bareau of Reclamation, Structural Research Laboratory, Report SF-23, pp. 26.

[52.1]   Prager, W.: *The general Theory of Limit Design.* Proceedings of the 8th International Congress of Theory of Applied Mechanich, Istanbul, 1952, Vol. II, pp. 65-72.

[52.2]   Drucker, D.C., W. Prager, H.J. Greenberg: *Extended limit design theorems for continuous media.* Quarterly of Applied Mathematics, Vol. 9, 1952, pp. 381-389.

[52.3]   Drucker, D.C., W. Prager: *Soil mechanics and plastic analysis of limit design.* Quarterly of Applied Mathematics, Vol. 10, 1952, pp. 157-165.

[55.1]   Chinn, J., Ferguson, P.M., Thompson, J.N.: *Lapped Splices in Reinforced Concrete Beams.* ACI Journal, Proceedings Vol. 52, no. 15, Oct. 1955, pp. 201-213.

[56.1]   Champerlin, S.J.: *Spacing of Reinforcement in Beams.* ACI Journal, Proceedings, Vol. 53, No. 6, July 1956, pp. 113-134.

[57.1]   Hillerborg, H.: *Anchorage Failure in Reinforced Concrete Beams without Shear Reinforcement.* RILEM Symposium on Bond and Crack Formation in Reinforced Concrete, Stockholm, 1957, pp. 215- 222.

[57.2]   Larsson, H.: *On the Anchorage of High Quality Corrugated Reinforcing Bars Kam 60 and Kam 90 in Concrete Beams.* RILEM Symposium on Bond and Crack Formation in Reinforced Concrete, Stockholm, 1957, pp. 233-252.

[58.1]   Chamberlin, S.J.: *Spacing of Spliced Bars in Beams.* ACI Journal, Proceedings Vol. 54, no. 38, Feb. 1958, pp. 689-697.

[59.1]   Prager, W.: *An Introduction to Plasticity.* Addison-Wesley Publishing Company. Reading 1959. 148 pp.

[61.1]   Rehm, G.: *Ueber die Grundlagen des Verbundes zwischen Stahl und Beton.* Deutscher Ausschuss für Stahlbeton, Berlin, Heft 138, 1961.

[61.2]   Mathey, R.G., D. Watstein: *Investigation of Bond in Beam and Pull-Out Specimens with High-Yield-Strength Deformed Bars.* ACI Journal, Proceedings, Vol. 57, No. 9, March 1961, pp. 1071-1090.

[63.1]   Rusch, H., H. Hilsdorf: *Verformungseigenschaften von Beton unter zeutrischen Zugspannungen.* (Deformation Characteristics of Con-

crete under Biaxial Tension). Voruntersuchungen, MPA Bauwesen, Bericht No. 44, Munich, May 1963.

[63.2]   Alami, Z.Y., P.M. Ferguson: *Accuracy of Models Used in Research on Reinforced Concrete.* ACI Journal, Proceedings Vol. 60, November 1963, pp. 1643-1663.

[63.3]   Hanson, J.A.: *Strength of Structural Lightweight Concrete Under Combined Stress.* Journal of PCA Research Development Laboratory, 5, No. 1, pp. 39-46.

[65.1]   Ferguson, P.M., J.E. Breen: *Lapped Splices for High Strength Reinforcing Bars.* ACI Journal, Proceedings Vol. 62, No. 63, Sept. 1965, pp. 1063-1078.

[65.2]   Sandbye, P.: *A Plastic Theory for Plain Concrete.* Bygningsstatiske Meddelelser, Dansk Selskab for Bygningsstatik, Copenhagen, 1965, pp. 41-62.

[65.3]   Untrauer, R.E., R.L. Henry: *Influence of Normal Pressure on Bond Strength.* ACI Journal, Proceedings, Vol. 62, No. 36, May 1965, pp. 577-589.

[66.1]   Lutz, L.A.: *The Mechanics of Bond and Slip of Deformed Reinforcing Bars in Concrete.* Department of Structural Engineering, School of Civil Engineering, Cornell University, Report no. 324, August 1966.

[66.2]   Hughes, B.P., G.P. Chapman: *The complete Stress-Strain Curve for Concrete in Direct Tension.* Bulletin RILEM, No. 3, March 1966, pp. 95-97.

[67.1]   Lutz, L.A., Gergely, P.: *Mechanics of Bond and Slip of Deformed Bars in Concrete.* ACI Journal, Proceedings Vol. 64, no. 11, Nov. 1967, pp. 711-721.

[68.1]   Prager, W., P.G. Hodge: *Theory of Perfectly Plastic Solids.* Dover Publications, New York, 1968, 264 pp.

[68.2]   Evans, R.H., M.S. Maratha: *Microcracking and Stress-Strain Curves for Concrete in Tension.* Materiaux et Construction, No. 1, January-February 1968, pp. 61-64.

[69.1]   Ferguson, P.M., E.A. Briceno: *Tensile Lap Splices, Part I: Retaining Wall type, Varying Moment Zone.* Center for Highway Research, The University of Texas at Austin, Research Report 113-2, July 1969.

[69.2]   Nielsen, M.P.: *Om forskydningsarmering i jernbetonbjælker, Diskussion (About Shear-reinforcement in Reinforced Concrete Beams, Discussion).* Bygningsstatiske Meddelelser, Vol. 40, No. 1, 1969, pp. 60-63.

[69.3]   Chen, W.F., D.C. Drucker: *Bearing Capacity of Concrete Blocks or Rock.* Journal of the Engineering Mechanics, Proceedings ASCE, Vol. 95, No. EM4, August 1969, pp. 955-978.

[69.4]   Nielsen, M.P.: *Om Jernbetonskivers Styrke.* Copenhagen 1969, pp. 254. (Englisk Edition: On the Strength of Reinforced Concrete Discs. Acta Polytechnica Scandinavia, Ci 70, Copenhagen 1971, pp. 261).

[69.5]   Dastidav, N.R.G.: *The Bursting Effect and Bond Development length of Deformed Bars.* University of London, Ph.D. Thesis, 1969, pp. 226.

[69.6]   Roberts, N.P.: *Limit State Theory of Anchorage Bond in Reinforced Concrete.* University of London, Ph.D. Thesis, 1969, pp. 202.

[70.1]   Lutz, L.A.: *Analysis of Stresses in Concrete Near a Reinforcing Bar Due to Bond and Transverse Cracking.* ACI Journal, Proceedings, Vol. 67, no. 45, Oct. 1970, pp. 778-787.

[70.2]   Nilsson, I.H.E.: *Upplaysproblem vid Betonbjalklag (Support problems in Concrete Beams).* Chalmers Tekniska Högskola, Institutionen för Konstruktionsteknik, Betongbyggnad, Rapport 70:3, Göteborg, maj 1970.

[70.3]   Larsson, H.: *Forankringsproblem vid Balkupplag (Anchorage prob-
          lems at Beam Supports)*. Chalmers Tekniska Högskola, Institutio-
          nen för Konstruktionsteknik, Betongbyggnad, Rapport 70:2, Göte-
          borg, Juni 1970.

[71.1]   Ferguson, P.M., C.N. Krishnaswarny: *Tensile Lap Splices, Part
          2: Design Recommendations for Retaining Wall Splices and Large
          Bar Splices*. Center for Highway Research, The University of Texas
          at Austin, Research Report No. 113-3, April 1971.

[71.2]   Newman, K., J.B. Newman: *Failure Theories and Design Cri-
          teria for Plain Concrete*. The Proceedings of the Southampton
          1969 Civil Engineering Materials Conference, Structure, Solid Me-
          chanics and Engineering Design, Part 2, Editor: M. Teeni, Wiky-
          Interscience, London, 1971, pp. 963-995.

[71.3]   Goto, Y.: *Cracks Formed in Concrete Around Deformed Tension
          Bars*. ACI Journal, Proceedings, Vol. 68, no. 26, April 1971, pp.
          244-251.

[72.1]   Rathkjen, A. *Forankringsstyrker af Armeringsjern ved Bjælkeun-
          derstøtninger. (The Bond Strength of Reinforcing Bars at Beam
          Supports)*. Civil Engineering Academy of Denmark, Ren og An-
          vendt Mekanik, Aalborg, Report 7203, 1972.

[72.2]   Gravesen, S. H. Krenchel: *Betons tryk-, træk-, spalte- og
          bøjningstrækstyrke. Foreløbige resultater i ABK-sag 1/62 (The
          Compression-, the Tensile-, the Splitting- and the Bending- ten-
          sile strength of Concrete*. Interum Solution Report from ABK- case
          1/62). Department of Structural Engineering, Technical University
          of Denmark, Januar 1972.

[72.3]   Izbicki, R.J.: *General Yield Condition, 1. Plane Deformation*. Bul-
          letin de l'Academie Polonaise des Sciences, Serie des Sciences Tech-
          niques, Vol. XX, No. 7-8, 1972.

[73.1]   Tepfers, R.: *A Theory of Bond Applied to Overlapped Ten-
          sile Reinforcement Splices for Deformed Bars*. Chalmers Tekniska

Högskola, Division of Concrete Structures, Göteborg, Publ. 73.2, 1973.

[74.1]   Nielsen, M.P.: *Beton 1. del 1, Materialer (Concrete 1, part 1, Materials)*. Civil Engineering Academy of Denmark, Aalborg, 1974.

[74.2]   Bergholdt, M.: *Forankringsforsøg med 10 mm kamstål (Anchorage test with 10 mm Kam Steel)*. Civil Engineering Academy of Denmark, Ren og Anvendt Mekanik, Lyngby, Report 74:46, Maj 1974.

[74.3]   Bræstrup, M.W.: *Plastic Analysis of Shear in Reinforced Concrete*. Magazine of Concrete Research, Vol. 26, no. 89, December 1974, pp. 221-228.

[74.4]   Hobbs, D.W., C.D. Pomeroy: *Nomograms for the Failure of Plain Concrete Subjected to Short-term Multiaxial Stresses*. Contribution to D.J. Hannant. The Structural Engineer, London, Vol. 52, No. 5, May 1974, pp. 151-165.

[75.1]   Orangun, C.O., J.O. Jirsa, J.E. Breen: *The Strength of Anchor Bars: A Reevaluation of Test Data on Development Length and Splices*. Center for Highway Research, The University of Texas at Austin, Research Report 154-3F, January 1975.

[75.2]   Jensen, B.C.: *Lines of Discontinuity for Displacements in the Theory of Plasticity and Reinforced Concrete*. Magazine of Concrete Research, Vol. 27, No. 92, September 1975, pp. 143-150.

[75.3]   Nielsen, M.P., M.W. Bræstrup: *Plastic Shear Strength of Reinforced Concrete Beams*. Bygningsstatiske Meddelelser, Vol. 46, No. 3, 1975, pp. 61-99.

[76.1]   Orr, D.M.F. *Lap Splicing of Deformed Reinforcing Bars*. ACI Journal, Proceedings, Vol. 73, no. 53, Nov. 1976, pp. 622-627.

[76.2]   Jensen, B.C.: *Nogle Plasticitetsteoretiske beregninger af beton og jernbeton*. Technical University of Denmark, Institute of Building Design, Lyngby, Report No. 111, 1976, 115 pp. (English edition: Some Applications of Plastic Analysis to Plain and Reinforced Concrete. Report No. 123, 1977, 119 pp.)

[76.3] Hillerborg, A., M. Modeer, P.E. Petersson: *Analysis of Crack Formation and Crack Growth in Concrete by Means of Fracture Mechanics and Finite Elements.* Cement and Concrete Research, Vol. 6, 1976, pp. 773-782.

[76.4] Bræstrup, M.W., M.P. Nielsen, B.C. Jensen, F. Bach: *Axisymmetric Punching of Plain and Reinforced Concrete.* Department of Structural Engineering, Technical University of Denmark, Serie R, No. 75, 1976, pp. 33.

[77.1] Ottosen, N.S.: *A Failure Criterion for Concrete.* Journal of Engineering Mechanic Division, No. EM4, August 1977.

[77.2] Bach, F., M.P. Nielsen, M.W. Bræstrup: *Forskydningsforsøg med jernbetonbjælker (Shear tests on Reinforced Concrete Beams).* Department of Structural Engineering, Technical University of Denmark, Serie I, No. 49, 1977, pp. 19.

[77.3] Orangun, C.O., J.O. Jirsa, J.E. Breen: *A Reevaluation of Test Data on Development Length and Splices.* ACI Journal Proceedings, Vol. 74, No. 11, March 77, pp. 114-122.

[78.1] Chen, W.F.: *Constitutive Equations for Concrete.* IABSE Colloquium, Copenhagen, 1979, Session I. Plasticity in Reinforced Concrete, Introductory Report, Vol. 28, October 1978, pp. 11-34.

[78.2] Hillerborg, A.: *A Model for Fracture Analysis.* Division on Building Materials, Lund Institute of Technology, Report IVBM- 3005, 1978.

[78.3] Hess, U., B.C. Jensen, M.W. Bræstrup, M.P. Nielsen, F. Bach: *Gennemlokning af Jernbetonplader (Punching Shear of Reinforced Concrete Slabs).* Department of Structural Engineering, Technical University of Denmark, Serie R, No. 90, 1978, pp. 63.

[78.4] Nielsen, M.P., M.W. Bræstrup, B.C. Jensen, F. Bach:*Concrete Plasticity.* Danish Society for Structural Science and Engineering, Special Publication, October 1978, pp. 129.

[78.5] Wang, P.T., S.P. Shah, A.E. Naaman: *Stress-Strain Curves of Normal and Lightweight Concrete in Compression.* ACE Journal, Proceedings, Vol. 75, No. 11, November 1978, pp. 603-611.

[79.1] Losberg, A., Olson, P.-Å.: *Bond failure of Deformed Reinforcing Bars based on the longitudinal Splitting Effect of the Bars.* ACI Journal, Proceedings, Vol. 76, no. 1, Jan. 1979, pp. 5-18.

[79.2] Eligehausen, Von R.: *Übergreifungsstöße zugbeanspruchter Rippenstäbe mit geraden Stabenden.* Deutscher Ausschuss für Stahlbeton, Berlin, Heft 301, 1979.

[79.3] Soretz, S., Hölzenbein, H.: *Influence of Rib Dimensions of Reinforcing Bars on Bond and Bendability.* ACI Journal, Proceedings Vol. 76, no. 6, Jan 1979, pp. 111-125.

[79.4] Thompson, M.A., J.O. Jirsa, J.E. Breen, D.F. Meinheit: *Behavior of Multiple Lap Splices in Wide Sections.* ACI Journal, Proceedings Vol. 76, no. 12, Feb. 1976, pp. 227-248.

[79.5] Exner, H.: *On the effectiveness factor in Plastic Analysis of Concrete.* IABSE Colloquium, Plasticity in Reinforced Concrete, Copenhagen, Vol. 29, 1979, pp. 35-42.

[79.6] Roikjær, M., C. Pedersen, M.W. Bræstrup, M.P. Nielsen, F. Bach: *Bestemmelse af ikke-forskydningsarmerede bjælkers forskydningsbæreevne (Shear Capacity of Beams Without Shear Reinforcement).* Department of Structural Engineering, Technical University of Denmark, Serie I, No. 62, 1979, pp. 44.

[79.7] Kemp, E.L., W.J. Wilhelm: *Investigations of the Parameters Influencing Bond Cracking.* ACI Journal, Proceedings, Vol. 76, No. 3, Jan. 1979, pp. 47-71.

[80.1] Bach, F., M.P. Nielsen, M.W. Bræstrup: *Shear Tests on Reinforced Concrete T-Beams.* Department of Structural Engineering Technical University of Denmark, Serie R, No. 120, 1980, pp. 86.

[81.1] Zekany, A.J., Neumann, S., Jirsa, J.O., Breen, J.E.: *The Influence of Shear on Lapped Splices in Reinforced Concrete.* Center

of Transportation Research, Bureau of Engineering Research, The University of Texas at Austin, Research Report 242- 2, July 1981.

[81.2]   Petersson, P.-E.: *Crack Growth and Development of Fracture Zones in Plain Concrete and Similar Materials.* Division of Building Materials, Lund Institute of Technology, Report TVBM- 1006, Lund, Sweden, 1981, pp. 174.

[81.3]   Jensen, J.F.: *Plasticitetsteoretiske Løsninger for Skiver og Bjælker af Jernbeton (Plastic Solutions for Disks and Beams of Reinforced Concrete).* Department of Structural Engineering, Technical University of Denmark, Lyngby, Serie R, no. 141, Ph.D. Thesis, 1981, pp. 153.

[82.1]   Jensen, J.H.: *Forkammede Armeringsstængers Forankring specielt ved Vederlag (Anchorage of Deformed Reinforcing Bars at Supports).* Part 1, Department of Structural Engineering, Technical University of Denmark, Lyngby, Serie R, no. 156, 1982.

[82.2]   Jensen, J.H.: *Forkammede Armeringsstængers Forankring specielt ved Vederlag (Anchorage of Deformed Reinforcing Bars at Supports).* Part 2, Appendix A-F. Department of Structural Engineering, Technical University of Denmark, Lyngby, Serie R, no. 157, 1982.

[82.3]   Reynolds, G.C., Beeby, A.W.: *Bond Strength of Deformed Bars.* Applied Science Publishers Ltd., Ripple Road, Barking, Essex, England, 1982, pp. 434-445.

[82.4]   Tepfers, R.: *Lapped Tensile Reinforced Splices.* Journal of the Structural Division, Proceedings of the American Society of Civil Engineers, ASCE, Vol. 108, No. ST1, January 1982, pp. 283- 301.

[82.5]   Morita, S., S. Fujii: *Bond Capacity of Deformed Bars due to Splitting of surrounding Concrete.* Bond in Concrete. Applied Science Publichers Ltd., Ripple Road, Barking, Essex, Editor P. Partos, England, 1982, pp. 331-341.

[83.1]   Exner, H.: *Plasticitetsteori for Coulomb materialer (Theory of Plasticity for Coulombs materials).* Department of Structural En-

gineering, Technical University of Denmark, Lyngby, Serie R., No. 175, Ph.D. Thesis, 1983, pp. 258.

[83.2]   Exner, H.: *Betonbjælkers Bøjningsbæreevne (The Bending Capacity of Concrete Beams)*. Department of Structural Engineering, Technical University of Denmark, Lyngby, Serie R, no. 176, 1983.

[83.3]   Nielsen, M.P., B. Feddersen: *Effektivitetsfaktoren ved Bøjning af Jernbetonbjælker (The Effectiveness Factor of Reinforced Concrete Beams in Bending)*. Department of Structural Engineering, Technical University of Denmark, Serie R, No. 173, 1983, pp. 35.

[83.4]   Feddersen, B., M.P. Nielsen: *Effektivitetsfaktoren ved Vridning af Jernbetonbjælker (The Effectiveness Factor of Reinforced Concrete Beams in Pure Torsion)*. Department of Structural Engineering, Technical University of Denmark, Serie R, No. 174, 1983, pp. 40.

[84.1]   Nielsen, M.P.: *Limit Analysis and Concrete Plasticity*. Prentice-Hall, Inc., Englewood, Cliffs, New Jersey, 1984.

[84.2]   Hess. U.: *Plasticitetsteoretisk Analyse af forankring og Stød af Forkammet Armering i Beton (An analysis of Anchorage and Splices of Deformed Reinforcing Bars in Concrete according to the Theory of Plasticity)*. Department of Structural Engineering, Technical University of Denmark, Lyngby, Serie R, No. 184, Ph.D. thesis, 1984.

[84.3]   Andreasen, B.S.: *Ribbeståls Forankringsstyrke i Beton efter Plasticitetsteorien (The Bond Strength of Deformed Reinforcing Bars according to the Theory of Plasticity)*. Civil Engineering Academy of Denmark, SKM, Lyngby, Batchelor Thesis, Jan. 1984.

[84.4]   Feddersen, B., M.P. Nielsen: *Plastic Analysis of Reinforced Concrete Beams in Pure Bending or Pure Torsion*. Bygningsstatiske Meddelelser, Danish Society of Structural Science and Engineering, Vol. 55, No. 2, 1984, pp. 37-61.

[84.5]   DS411: *Dansk Ingeniørforenings Norm for Betonkonstruktioner (Dansk Ingeniørforenings Code of Practice for the Structural Use*

of Concrete, DS411). An English edition is available. 3. udgave, Marts 1984, pp. 98.

[85.1]   Nagatomo, K., Kaku, T.: *Experimental and Analytical Study on Bond Characteristics of Reinforcing Bars with only a Single Transverse Rib.* Transactions of the Japan Concrete Institute, Vol. 7, 1985, pp. 333-340.

[85.2]   Gopalaratnam, V.S., S.P. Shah: *Softening Response of Plain Concrete in Direct Tension.* ACI Journal, no. 82-27, Maj-June 1985, pp. 310-323.

[85.3]   Torrent, R.J., J.J. Brooks: *Application of the Highly Stressed Volume Approach to Correlated Results from different Tensile Tests of Concrete.* Magazine of Concrete Research, Vol. 37, no. 132, Sept. 1985, pp. 175-184.

[85.4]   Andreasen, B.S.: *Trykmembranvirkning i betonplader (Compression Membrane Action in Concrete Slabs).* Department of Structural Engineering, Technical University of Denmark, Master Thesis, Lyngby, July 1985, pp. 211.

[85.5]   Gustafsson, P.J.: *Fracture Mechanics Studies of Non-Yielding Materials Like Concrete, Modelling of Tensile Fracture and Applied Strength Analyses.* Division of Building Materials, Lund Institute of Technology, Report TVBM-1007, Sweden 1985.

[85.6]   Olsson, P.-Å.: *A Fracture Mechanics and Experimental Approach on Anchorage Splitting.* Nordic Concrete Research, 1985, pp. 136-158.

[85.7]   Bodén, A.: *Armeringsvidenhæftning i Fiberbeton (Bond in Fibre Reinforced Concrete).* Institution för Brobyggnad, Kungliga Tekniska Högskolan, Stockholm, Meddelanda 2/85, pp. 158.

[85.8]   Tsubaku, T., T. Hashimoto, S. Ikeda, S. Yamanobe: *Bond Analysis of a Concrete Member using the Boundary Element Method.* Trans. of the Japan Concrete Inst., Vol. 7, 1985, pp. 361-368.

[86.1]   Mier, J.G.M. van: *Fracture of Concrete under Complex Stress.* HERON, vol. 31, no. 3, 1986, pp. 90.

[86.2]   Mier, J.G.M. van: *Multiaxial Strain-Softening of Concrete, Part I: Fracture*. Materiaux et Constructions, Vol. 19, no. 111, 1986, pp. 179-190.

[86.3]   Andreasen, B.S., M.P. Nielsen: *Dome Effect in Reinforced Concrete Slabs*. Department of Structural Engineering, Technical University of Denmark, Serie R, No. 212, 1986, pp. 49.

[86.4]   Olson, P.-Å.: *A Fracture Mechanics and Experimental Approach on Anchorage Splitting*. Bond and Anchorage of Reinforcement in Concrete, Nordic Seminar, 23. October 1985, Chalmers University of Technology, Division of Concrete Structures, Publication 86:1, 1986, pp. 99-106.

[86.5]   Furuuchi, H., Y. Kakuta: *Nonlinear Behavior in Dowel Action of Reinforcing Bars*. Trans. of the Japan Concrete Inst., Vol. 8, 1986, pp. 289-294.

[86.6]   Kemp, E.L.: *Bond in Reinforced Concrete: Behavior and Design Criteria*. ACI Journal, Vol. 83, No. 7, Jan.-Feb. 1986, pp. 50-57.

[86.7]   Andreasen, B.S.: *The Bond Strength of Deformed Reinforcing Bars*. Chalmers University of Technology, Division of Concrete Structures, Publication 86:1, 1986, pp. 44-58.

[86.8]   Andreasen, B.S., M.P. Nielsen: *The Bond Strength of Reinforcing Bars at Supports*. Proceedings from Symposium in Fundamental Theory of Reinforced and Prestressed Concrete, Nanjing Institute of Technology, Nanjing, China, 1986, pp. 387- 397.

[87.1]   Kærn, J., C.: *Numerisk Brudstadieberegning for Stift, Plastiske Materialer (Numerical Collapse load calculation for Rigid Plastic Materials)*. Department of Structural Engineering, Technical University of Denmark, Lyngby, Serie R, no. 181, Ph.D. thesis, 1987.

[87.2]   Boswell, L.F., Z. Chen: *A General Failure Criterion for Plain Concrete*. Int. J. Solids Structures, Vol. 23, No. 5, 1987, pp. 621-630.

[87.3]   Cedolin, L., S.D. Yoli, I. Iori: *Tensile Behaviour of Concrete.* Jour-
         nal of Engineering Mechanics, Vol. 113, No. 3, March 1987, pp.
         431-449.

[87.4]   Wang, C.-Z., Z.-h. Guo, X.-q. Zhang: *Experimental Investigation
         of Biaxial and Triaxial Compressive Concrete Strength.* ACI Ma-
         terials Journal, Vol. 84, No. M11, March-April 1987, pp. 92-100.

[87.5]   Ditlevsen, O.: *The Structural System Reliability Problem.* Quali-
         tative Considerations. ICASP5, Vancouver, May, 1987.

[87.6]   Soroushian, P., K. Obaseki, M. Rojas, H.S. Najm: *Behavior of
         Bars in Dowel Action against Concrete Cover.* ACI Structural
         Journal, No. 84-S18, March-April 1987. pp. 170-176.

[87.7]   Petersen, M.G., N.E. Panek: *Forankring ved Pladeverderlag (An-
         chorage at Supports in Slabs).* Civil Engineering Academy of Den-
         mark, SKM, Lyngby, Batchelor Thesis, June 1987.

[88.1]   Andreasen, B.S.: *Anchorage Tests with   Ribbed Reinforcing
         Bars in more than one Layer at a Beam Support.* Department of
         Structural Engineering, Technical University of Denmark, Lyngby,
         Serie R, no. 239, Part of a Ph.D. Thesis, 1988.

[88.2]   Olsen N.H.: *Implementation of High Strength Concrete in Build-
         ing Structures* . Department of Structural Engineering, Technical
         University of Denmark, Lyngby, Serie R, In preparation , Part of
         a Ph.D. Thesis, 1988.

[88.3]   Olsen N.H.: *Anchorage Tests with Deformed Reinforcing Bars in
         High Strength Concrete* . Department of Structural Engineering,
         Technical University of Denmark, Lyngby, Serie R, In preparation,
         Part of a Ph.D. Thesis, 1988.

[88.4]   Andreasen, B.S., M.P. Nielsen: *Membrane Action in Slabs.* Bygn-
         ingsstatiske Meddelelser, Danish Society of Structural Science and
         Engineering, In preparation, 1988.

[88.5]   Andreasen, B.S., M.P. Nielsen: *Membrane Action in One-way
         Slabs.* Bygningsstatiske Meddelelser, Danish Society of Structural
         Science and Engineering, In preparation, 1988.

[88.6]   Nielsen, M.P., B.S. Andreasen,G. Chen: *Dome Effect in Reinforced Concrete Slabs.* New Zealand, 1988.

[88.7]   Chen, G.: *Plastic Analysis of Shear in Beams, Deep Beams and Corbels.* Department of Structural Engineering, Technical University of Denmark, Lyngby, Serie R, no.237, Ph.D. Thesis, 1988.

Appendix A

Anchorage at Supports

The test results of anchorage of one layer of reinforcement at supports are given here. The tests are treated in chapter 8 and the test specimen and the main principle in the test set-ups are illustrated in figure 8.1 and 8.2.

The tests are presented in table A.1 and A.2, where the first table shows tests without stirrups and the second table shows tests with stirrups. In the tables the following data are given: The reference, the test number, the values of the geometrical parameters ξ and $\frac{s}{d}$, the uniaxial concrete compression strength f_c in MPa, the stirrup reinforcement degree ψ, the dimensionless reaction stress $\frac{r}{f_c}$, the dimensionless shear strength $\frac{\tau}{f_c}$ and two columns with the ratios between the load obtained in the tests and the corresponding theoretical load carrying capacity.

The theoretical load in the two last columns is determined from different expressions. In the column denoted by *correct* theoretical correct expressions ((5.5) and (5.7)) have been used and in the column denoted by *simple* simplified expressions ((8.4) and (8.5)) have been used. The effectiveness factors are determined from (8.1), (8.2), and (8.3).

In the analysis 184 tests are included, of which 140 are without stirrups and 44 are with stirrups. The values for the mean and standard deviation on the ratio test/theory are given in the two tables. For all the 184 tests the analysis using the correct expression result in a mean value of 1.062 and a standard deviation of 0.112. The respective values in the simple analysis are 1.012 and 0.108.

Reference	no.	ξ	$\frac{s}{d}$	f_c	ψ	$\frac{\tau}{f_c}$	$\frac{\tau}{f_c}$	$\frac{test}{theory}$ correct	$\frac{test}{theory}$ simple
Jensen [82.1] & [82.2]	25301	1.81	2.00	23.1	0.000	0.074	0.366	1.043	1.042
	2502	1.81	2.00	23.1	0.000	0.073	0.364	1.039	1.037
	3501	1.81	2.00	29.3	0.000	0.069	0.345	1.099	1.100
	3502	1.81	2.00	29.3	0.000	0.069	0.345	1.099	1.100
	4501	1.81	2.00	38.4	0.000	0.062	0.308	1.119	1.122
	4502	1.81	2.00	40.4	0.000	0.063	0.313	1.159	1.164
	4503	1.81	2.00	40.4	0.000	0.059	0.294	1.099	1.101
	15311	1.81	2.00	12.4	0.000	0.221	0.550	1.008	1.030
	1512	1.81	2.00	12.4	0.000	0.221	0.550	1.008	1.030
	2011	1.81	2.00	26.9	0.000	0.153	0.380	1.022	1.045
	2012	1.81	2.00	26.9	0.000	0.153	0.380	1.022	1.045
	2211	1.81	2.00	23.2	0.000	0.166	0.412	1.027	1.050
	2212	1.81	2.00	23.2	0.000	0.177	0.441	1.086	1.110
	2511	1.81	2.00	17.5	0.000	0.231	0.575	1.198	1.225
	2512	1.81	2.00	17.5	0.000	0.210	0.521	1.107	1.132
	3011	1.81	2.00	30.8	0.000	0.145	0.360	1.033	1.056
	3012	1.81	2.00	30.8	0.000	0.145	0.360	1.033	1.056
	3511	1.81	2.00	31.4	0.000	0.131	0.326	0.961	0.982
	3512	1.81	2.00	31.4	0.000	0.131	0.326	0.961	0.982
	4011	1.81	2.00	43.2	0.000	0.119	0.296	1.011	1.034
	4012	1.81	2.00	43.2	0.000	0.120	0.299	1.020	1.043
	4013	1.81	2.00	31.6	0.000	0.119	0.297	0.894	0.912
	4014	1.81	2.00	31.6	0.000	0.130	0.324	0.959	0.980
	4511	1.81	2.00	44.1	0.000	0.121	0.300	1.030	1.054
	4512	1.81	2.00	44.1	0.000	0.114	0.282	0.980	1.001
	4513	1.81	2.00	38.4	0.000	0.158	0.392	1.206	1.233
	15321	1.81	2.00	13.7	0.000	0.437	0.725	1.188	1.189
	1522	1.81	2.00	13.7	0.000	0.407	0.675	1.125	1.132
	2521	1.81	2.00	19.0	0.000	0.348	0.577	1.131	1.137
	2522	1.81	2.00	19.0	0.000	0.321	0.532	1.063	1.074
	3521	1.81	2.00	23.9	0.000	0.255	0.423	0.974	0.989
	3522	1.81	2.00	23.9	0.000	0.257	0.426	0.979	0.994
	4521	1.81	2.00	33.2	0.000	0.215	0.357	0.970	0.986
	4522	1.81	2.00	33.2	0.000	0.215	0.356	0.967	0.983

Table A.1

Reference	no.	ξ	$\frac{s}{d}$	f_c	ψ	$\frac{\tau}{f_c}$	$\frac{\tau}{f_c}$	$\frac{test}{theory}$ correct	$\frac{test}{theory}$ simple
Jensen [82.1] & [82.2]	25331	1.81	2.00	17.0	0.000	0.720	0.895	1.388	1.287
	2532	1.81	2.00	17.0	0.000	0.639	0.795	1.276	1.207
	2533	1.81	2.00	23.1	0.000	0.612	0.585	1.061	0.985
	2534	1.81	2.00	23.1	0.000	0.612	0.585	1.061	0.985
	3531	1.81	2.00	29.3	0.000	0.418	0.520	1.142	1.104
	3532	1.81	2.00	29.3	0.000	0.394	0.490	1.094	1.065
	4531	1.81	2.00	33.2	0.000	0.369	0.459	1.091	1.063
	4532	1.81	2.00	33.2	0.000	0.331	0.411	1.005	0.992
	4533	1.81	2.00	40.4	0.000	0.371	0.461	1.176	1.131
	4534	1.81	2.00	40.4	0.000	0.334	0.415	1.089	1.061
	15901	1.81	2.00	16.9	0.000	0.094	0.466	1.122	1.125
	1502	1.81	2.00	16.9	0.000	0.094	0.466	1.122	1.125
	2501	1.81	2.00	20.8	0.000	0.087	0.433	1.152	1.157
	2502	1.81	2.00	20.8	0.000	0.093	0.461	1.215	1.223
	3501	1.81	2.00	33.5	0.000	0.061	0.303	1.040	1.039
	3502	1.81	2.00	33.5	0.000	0.057	0.286	0.991	0.987
	4501	1.81	2.00	33.2	0.000	0.057	0.284	0.981	0.976
	4502	1.81	2.00	33.2	0.000	0.058	0.289	0.996	0.992
	15911	1.81	2.00	12.4	0.000	0.218	0.543	0.998	1.020
	1512	1.81	2.00	12.4	0.000	0.203	0.504	0.939	0.959
	2011	1.81	2.00	26.9	0.000	0.169	0.421	1.110	1.135
	2012	1.81	2.00	26.9	0.000	0.153	0.380	1.022	1.045
	2211	1.81	2.00	23.2	0.000	0.168	0.417	1.037	1.061
	2212	1.81	2.00	23.2	0.000	0.168	0.417	1.037	1.061
	2511	1.81	2.00	17.5	0.000	0.209	0.520	1.106	1.131
	2512	1.81	2.00	17.5	0.000	0.209	0.520	1.106	1.131
	3011	1.81	2.00	30.8	0.000	0.141	0.351	1.012	1.035
	3012	1.81	2.00	30.8	0.000	0.141	0.351	1.012	1.035
	3511	1.81	2.00	31.4	0.000	0.131	0.326	0.961	0.982
	3512	1.81	2.00	31.4	0.000	0.124	0.308	0.918	0.937
	4011	1.81	2.00	43.2	0.000	0.111	0.276	0.956	0.977
	4012	1.81	2.00	43.2	0.000	0.111	0.276	0.956	0.977
	4013	1.81	2.00	31.6	0.000	0.137	0.342	1.002	1.025
	4014	1.81	2.00	31.6	0.000	0.123	0.306	0.915	0.935
	4512	1.81	2.00	44.1	0.000	0.124	0.309	1.056	1.080
	15921	1.81	2.00	15.1	0.000	0.363	0.602	1.070	1.081
	1521	1.81	2.00	15.1	0.000	0.386	0.640	1.121	1.128
	3521	1.81	2.00	35.9	0.000	0.209	0.346	0.975	0.990
	3522	1.81	2.00	35.9	0.000	0.228	0.378	1.044	1.056
	4521	1.81	2.00	45.0	0.000	0.212	0.352	1.078	1.088
	4522	1.81	2.00	45.0	0.000	0.197	0.327	1.019	1.033

Table A.1

Reference	no.	ξ	$\frac{s}{d}$	f_c	ψ	$\frac{r}{f_c}$	$\frac{\tau}{f_c}$	$\frac{\text{test}}{\text{theory correct}}$	$\frac{\text{test}}{\text{theory simple}}$
Jensen [82.1] & [82.2]	15611	1.81	2.00	13.7	0.000	0.186	0.464	0.915	0.934
	1512	1.81	2.00	13.7	0.000	0.200	0.498	0.968	0.990
	2511	1.81	2.00	19.0	0.000	0.163	0.404	0.932	0.952
	3511	1.81	2.00	23.9	0.000	0.122	0.303	0.810	0.824
	3512	1.81	2.00	23.9	0.000	0.129	0.321	0.849	0.866
	4511	1.81	2.00	33.2	0.000	0.108	0.268	0.838	0.854
	15621	1.81	2.00	15.1	0.000	0.355	0.589	1.053	1.064
	1522	1.81	2.00	15.1	0.000	0.338	0.561	1.014	1.028
	2521	1.81	2.00	17.0	0.000	0.351	0.582	1.091	1.100
	20131	1.81	2.00	15.2	0.000	0.259	0.592	1.139	1.163
	20132	1.81	2.00	15.2	0.000	0.242	0.553	1.079	1.103
	20231	1.81	2.00	16.4	0.000	0.185	0.460	0.976	0.998
	20232	1.81	2.00	16.4	0.000	0.185	0.460	0.976	0.998
	20191	1.81	2.00	15.2	0.000	0.210	0.481	0.966	0.988
	20192	1.81	2.00	15.2	0.000	0.194	0.443	0.904	0.924
	20291	1.81	2.00	16.4	0.000	0.179	0.445	0.951	0.971
	20292	1.81	2.00	16.4	0.000	0.179	0.445	0.951	0.971
Rathkjen [72.1]	13	2.59	1.93	26.4	0.000	0.128	0.419	0.997	1.062
	14	2.59	1.93	25.1	0.000	0.063	0.404	1.076	1.134
	15	2.59	1.93	25.3	0.000	0.074	0.416	1.082	1.147
	16	2.59	1.93	24.1	0.000	0.099	0.428	1.035	1.103
	17	2.59	1.93	28.1	0.000	0.081	0.321	0.858	0.912
	18	2.59	1.93	29.5	0.000	0.060	0.313	0.899	0.949
	19	2.59	1.93	20.1	0.000	0.108	0.274	0.606	0.645
	20	2.59	1.93	22.2	0.000	0.203	0.425	0.850	0.894
	21	2.59	1.93	18.6	0.000	0.107	0.389	0.835	0.889
	22	1.37	1.93	32.3	0.000	0.163	0.328	1.061	1.059
	23	1.37	1.93	33.1	0.000	0.085	0.276	0.995	0.969
	24	1.37	1.93	14.1	0.000	0.166	0.463	1.054	1.038
	25	1.37	1.93	19.0	0.000	0.151	0.343	0.899	0.887
	26	1.37	1.93	19.4	0.000	0.121	0.317	0.865	0.846
	27	1.37	1.93	19.1	0.000	0.236	0.361	0.881	0.882
	28	1.37	1.93	18.5	0.000	0.098	0.311	0.854	0.826
	29	1.37	1.93	18.0	0.000	0.368	0.435	0.951	0.953
	30	1.37	1.93	27.4	0.000	0.113	0.354	1.132	1.112
	31	1.37	1.93	26.7	0.000	0.099	0.279	0.898	0.877
	32	1.37	1.93	27.6	0.000	0.140	0.343	1.065	1.056
	33	1.37	1.93	26.3	0.000	0.173	0.346	1.017	1.014
	34	1.37	1.93	28.5	0.000	0.260	0.418	1.178	1.181
	35	1.37	1.93	29.5	0.000	0.256	0.411	1.178	1.181

Table A.1

Reference	no.	ξ	$\frac{s}{d}$	f_c	ψ	$\frac{\tau}{f_c}$	$\frac{\tau}{f_c}$	$\frac{test}{theory}$ correct	$\frac{test}{theory}$ simple
Rathkjen [72.1]	36	2.59	1.93	18.1	0.000	0.200	0.461	0.857	0.906
	37	2.59	1.93	19.2	0.000	0.155	0.446	0.899	0.957
	38	2.59	1.93	19.2	0.000	0.183	0.524	1.017	1.078
	39	2.59	1.93	18.9	0.000	0.111	0.394	0.845	0.900
	52	2.59	1.93	21.6	0.000	0.195	0.518	1.036	1.092
	53	2.59	1.93	22.2	0.000	0.040	0.275	0.739	0.765
	54	2.59	1.93	24.3	0.000	0.048	0.298	0.814	0.850
	57	2.59	1.93	25.1	0.000	0.051	0.353	0.970	1.015
	107	2.59	1.93	18.5	0.000	0.062	0.255	0.598	0.627
	110	1.37	2.70	14.4	0.000	0.457	0.556	0.839	0.838
	111	1.37	2.70	14.4	0.000	0.400	0.572	0.890	0.892
	112	1.37	2.70	14.9	0.000	0.288	0.531	0.899	0.901
	113	1.37	2.70	14.9	0.000	0.215	0.436	0.782	0.778
	114	1.37	2.70	21.2	0.000	0.137	0.363	0.814	0.801
	115	1.37	2.70	21.2	0.000	0.121	0.373	0.854	0.835
	116	1.37	2.70	18.2	0.000	0.341	0.578	1.021	1.024
	117	1.37	2.70	18.2	0.000	0.186	0.548	1.095	1.087
	118	1.37	2.70	20.6	0.000	0.116	0.388	0.883	0.861
	119	1.37	2.70	20.6	0.000	0.077	0.371	0.894	0.852
	120	1.37	2.70	20.9	0.000	0.324	0.570	1.075	1.077
	121	1.37	2.70	17.6	0.000	0.158	0.501	1.015	1.001
	122	1.37	2.70	17.6	0.000	0.094	0.393	0.862	0.827
	123	1.37	2.70	18.3	0.000	0.260	0.564	1.058	1.061
	124	1.37	2.70	19.5	0.000	0.117	0.380	0.844	0.822
	125	1.37	2.70	19.5	0.000	0.079	0.353	0.828	0.789
Mean Value								1.001	1.011
Standard Deviation								0.118	0.114

Table A.1: *Anchorage tests without stirrups.*

Reference	no.	ξ	$\frac{s}{d}$	f_c	ψ	$\frac{\tau}{f_c}$	$\frac{\tau}{f_c}$	$\frac{\text{test}}{\text{theory}}$ correct	$\frac{\text{test}}{\text{theory}}$ simple
Jensen [82.1] & [82.2]	11031	1.81	2.00	9.9	0.398	0.341	0.849	0.997	1.013
	11032	1.81	2.00	9.9	0.398	0.341	0.849	0.997	1.013
	11531	1.81	2.00	17.9	0.220	0.265	0.660	1.074	1.092
	11532	1.81	2.00	17.9	0.220	0.284	0.707	1.136	1.153
	12533	1.81	2.00	15.8	0.249	0.257	0.640	0.988	1.005
	12534	1.81	2.00	15.8	0.249	0.279	0.694	1.056	1.073
	13531	1.81	2.00	31.4	0.125	0.173	0.430	0.978	0.997
	13532	1.81	2.00	31.4	0.125	0.173	0.430	0.978	0.997
	14531	1.81	2.00	39.4	0.100	0.121	0.301	0.807	0.822
	14532	1.81	2.00	39.4	0.100	0.121	0.301	0.807	0.822
	21531	1.81	2.00	16.9	0.809	0.299	0.755	0.920	0.924
	21531	1.81	2.00	16.9	0.809	0.301	0.749	0.912	0.915
	22531	1.81	2.00	20.8	0.657	0.327	0.814	1.102	1.100
	22532	1.81	2.00	20.8	0.657	0.340	0.845	1.137	1.133
	23531	1.81	2.00	33.5	0.408	0.193	0.480	0.915	0.924
	23532	1.81	2.00	33.5	0.408	0.203	0.505	0.956	0.964
	24531	1.81	2.00	38.4	0.356	0.195	0.485	0.994	1.002
	24532	1.81	2.00	38.4	0.356	0.186	0.463	0.956	0.965
	11091	1.81	2.00	9.9	0.354	0.320	0.795	0.959	0.976
	11092	1.81	2.00	9.9	0.354	0.297	0.738	0.902	0.917
	11591	1.81	2.00	17.9	0.196	0.132	0.630	1.160	1.173
	11592	1.81	2.00	17.9	0.196	0.266	0.662	1.089	1.108
	12591	1.81	2.00	32.0	0.109	0.178	0.442	1.019	1.039
	12592	1.81	2.00	32.0	0.109	0.186	0.462	1.056	1.076
	12593	1.81	2.00	15.8	0.222	0.244	0.606	0.956	0.973
	12594	1.81	2.00	15.8	0.222	0.244	0.606	0.956	0.973
	13591	1.81	2.00	31.4	0.111	0.170	0.423	0.975	0.994
	13592	1.81	2.00	31.4	0.111	0.159	0.396	0.924	0.942
	14591	1.81	2.00	39.3	0.089	0.133	0.331	0.881	0.898
	14592	1.81	2.00	39.3	0.089	0.127	0.316	0.848	0.864

Table A.2

Reference	no.	ξ	$\frac{s}{d}$	f_c	ψ	$\frac{r}{f_c}$	$\frac{\tau}{f_c}$	$\frac{test}{theory}$ correct	$\frac{test}{theory}$ simple
Rathkjen [72.1]	90	1.37	1.93	20.5	0.137	0.267	0.502	1.008	1.010
	91	1.37	1.93	20.5	0.137	0.284	0.562	1.117	1.120
	92	1.37	1.93	21.0	0.267	0.296	0.601	1.111	1.114
	93	1.37	1.93	21.0	0.267	0.263	0.519	0.977	0.979
	94	1.37	1.93	20.0	0.421	0.300	0.634	1.062	1.064
	95	1.37	1.93	20.0	0.421	0.306	0.613	1.024	1.025
	96	1.37	1.93	20.0	0.561	0.313	0.649	1.010	1.012
	97	1.37	1.93	20.0	0.561	0.290	0.606	0.952	0.954
	80	1.37	1.93	20.9	0.285	0.300	0.619	1.129	1.132
	81	1.37	1.93	20.9	0.285	0.290	0.595	1.091	1.093
	82	1.37	1.93	20.0	0.116	0.306	0.594	1.170	1.173
	83	1.37	1.93	20.0	0.116	0.291	0.568	1.128	1.131
	108	1.37	1.93	17.1	0.045	0.252	0.516	1.030	1.028
	109	1.37	1.93	17.1	0.090	0.262	0.561	1.083	1.083
Mean Value								1.007	1.017
Standard Deviation								0.092	0.089

Table A.2: *Anchorage tests with stirrups.*

Appendix B

Anchorage in Two and Three Layers at Supports

The results from tests with anchorage at supports of two and three layer of reinforcement used in chapter 9 are given in table B.1. The tests are described in details in Andreasen [88.1]. To determinate $\frac{r}{f_c}$ and $\frac{\tau}{f_c}$ the mean value of the concrete strength f_c is used.

Test No.	No. of bars	Width b [mm]	f_c [MPa]	$\frac{r}{f_c}$	$\frac{\tau}{f_c}$
1-1.1	4	300	34.4	0.089	0.236
1-1.2	4	300	35.2	0.086	0.229
1-2.1	6	400	33.7	0.075	0.199
1-2.2	6	400	34.4	0.047	0.125
2-1.1	4	300	32.2	0.183	0.299
2-1.2	4	300	33.7	0.221	0.361
2-2.1	6	400	35.6	0.087	0.142
2-2.2	6	400	33.0	0.100	0.163

Mean concrete strength $f_c = 34.1 MPa$.

Table B.1: *Test results from anchorage at supports of two and three layer of reinforcement.*

Appendix C

Lap Splices

Test results for lap splices are shown here. The tests are used in chapter 10 to investigate the usefulness of the theoretical expressions developed in chapter 7.

In table C.1 the test data and results are shown for the 357 tests. In the table the following informations are given: The test number, the rib parameters for the reinforcement D and F, the number of lap splices n_{sp}, the geometrical properties, the uniaxial concrete compression strength f_c in MPa, the stirrup reinforcement degree ψ, and the dimensionless shear strength obtained in the tests $\frac{\tau}{f_c}$. The rib parameters D and F are defined in expression (4.6) and (4.12). The geometrical parameters $\frac{t}{d}$, ξ, $\frac{s}{d}$, $\frac{b}{d}$ and $\frac{\ell}{d}$ are illustrated in figure 10.1.

In table C.2 results from various analysis are presented. The results are given as the ratio between the load obtained in the tests and the corresponding theoretical load carrying capacity. The analysis are separated into

A : All mechanisms; correct determination of the variable parameters.

B : All mechanisms; simpel determination of the variable parameters.

C : Plate mechanism.

D : Plate mechanism; limits for the geometrical parameters introduced.

E : Plate mechanism; tests with spirals included.

F : Simplified plate mechanism and local failure 2; test with spirals included, limits for the geometrical parameters introduced.

The theoretical load is determined using the effectiveness factors given in expression (10.1), (10.2), and (10.3). For a more detailed description of the various analysis there are referred to chapter 10. The theoretical expressions used in the analysis are given in chapter 7.

Serie	no.	D	F	n_{sp}	$\frac{t}{d}$	ξ	$\frac{s}{d}$	$\frac{b}{d}$	$\frac{l}{d}$	f_c	ψ	$\frac{\tau}{f_c}$
Tepfers [73.1]												
732	1	0.089	0.56	2	2.13	1.48	1.69	10.1	32.5	17.2	0.000	0.163
	2	0.089	0.56	2	2.13	1.25	2.00	10.1	32.5	23.4	0.000	0.129
	3	0.089	0.56	2	2.13	1.54	1.63	10.1	32.5	35.7	0.000	0.106
	4	0.089	0.56	2	2.06	1.38	1.81	10.1	32.5	46.4	0.000	0.098
	5	0.089	0.56	2	2.50	1.55	1.50	10.1	32.5	57.4	0.000	0.090
	6	0.089	0.56	2	2.00	1.64	1.56	10.1	32.5	64.3	0.000	0.072
	7	0.089	0.56	2	2.56	1.16	1.94	10.1	32.5	9.2	0.000	0.173
	8	0.089	0.56	2	2.44	1.42	1.63	10.1	32.5	9.9	0.000	0.157
	9	0.089	0.56	2	2.31	1.22	1.94	10.1	32.5	21.6	0.000	0.174
	10	0.089	0.56	2	2.81	1.13	1.88	10.1	32.5	27.7	0.000	0.142
	11	0.089	0.56	2	1.94	1.41	1.81	10.1	32.5	16.0	0.000	0.187
	12	0.089	0.56	2	2.00	1.38	1.81	10.1	32.5	7.8	0.000	0.208
	13	0.055	0.56	2	1.63	1.27	2.13	10.0	32.5	10.0	0.000	0.165
	14	0.055	0.56	2	1.69	1.27	2.13	10.1	32.5	13.2	0.000	0.151
	15	0.055	0.56	2	1.63	1.42	1.94	10.1	32.5	28.6	0.000	0.110
	16	0.055	0.56	2	1.56	1.33	2.13	10.2	32.5	33.0	0.000	0.102
	17	0.055	0.56	2	2.44	1.31	1.81	10.2	32.5	46.7	0.000	0.079
732	35	0.089	0.56	2	2.19	1.48	1.69	10.2	32.5	37.4	0.000	0.113
	36	0.089	0.56	2	2.38	1.40	1.69	10.1	32.5	94.0	0.000	0.047
	37	0.089	0.56	2	1.69	1.73	1.63	10.3	32.5	88.6	0.000	0.038
	38	0.032	0.55	2	11.75	1.30	2.13	20.3	40.0	26.5	0.000	0.138
	39	0.073	0.59	2	12.00	1.10	2.50	20.5	40.0	24.2	0.000	0.205
	40	0.041	0.56	2	7.70	1.17	2.30	16.1	32.0	22.5	0.000	0.174
	41	0.073	0.58	2	7.60	1.55	2.00	16.8	32.0	23.5	0.000	0.202
	42	0.046	0.57	2	3.79	0.78	2.40	10.5	27.4	34.5	0.000	0.126
	43	0.078	0.57	2	2.26	1.02	2.55	10.5	27.4	22.7	0.000	0.140
	44	0.089	0.56	2	2.13	0.62	4.06	10.1	32.5	22.2	0.000	0.159
	45	0.089	0.56	2	2.25	0.69	3.56	10.1	32.5	19.6	0.000	0.187
	46	0.089	0.56	2	1.88	10.00	0.56	16.1	32.5	27.4	0.000	0.109
	47	0.089	0.56	2	1.75	3.50	1.63	16.1	32.5	18.1	0.000	0.150
	48	0.089	0.56	2	2.00	4.36	1.56	18.6	32.5	20.4	0.000	0.166
	49	0.089	0.56	2	1.50	4.89	0.56	10.0	32.5	16.9	0.000	0.173
732	50	0.089	0.56	2	2.00	0.13	5.13	6.4	32.5	19.1	0.000	0.128
	51	0.067	0.56	2	2.19	1.48	1.69	10.2	32.5	26.3	0.000	0.114
	52	0.067	0.56	2	2.19	1.44	1.69	10.1	32.5	25.1	0.000	0.116

Table C.1

Serie	no.	D	F	n_{sp}	$\frac{t}{d}$	ξ	$\frac{s}{d}$	$\frac{b}{d}$	$\frac{l}{d}$	f_c	ψ	$\frac{\tau}{f_c}$
Tepfers [73.1]												
732	53	0.067	0.56	2	2.44	1.35	1.75	10.2	32.5	11.4	0.000	0.159
	54	0.067	0.56	2	2.31	1.60	1.56	10.3	32.5	40.3	0.000	0.088
	55	0.067	0.56	2	2.13	1.58	1.63	10.3	32.5	52.9	0.000	0.068
	56	0.067	0.56	2	8.30	1.17	2.30	16.7	32.0	14.9	0.000	0.218
	57	0.067	0.56	2	8.60	1.20	2.00	16.4	32.0	16.8	0.000	0.210
	58	0.089	0.56	2	1.81	1.00	0.50	5.8	32.5	15.8	0.000	0.048
	59	0.078	0.57	2	0.53	1.39	1.76	8.4	37.9	16.0	0.000	0.112
	60	0.078	0.57	2	0.63	1.28	1.87	8.4	16.8	16.0	0.000	0.156
	61	0.046	0.57	2	0.37	1.67	1.50	8.4	37.9	16.3	0.000	0.100
	62	0.046	0.57	2	0.37	1.56	1.61	8.4	16.8	17.9	0.000	0.109
	63	0.087	0.57	2	5.17	1.20	2.08	13.2	18.3	17.0	0.000	0.219
	64	0.087	0.57	2	5.42	1.26	1.92	13.3	26.7	12.6	0.000	0.256
	65	0.087	0.57	2	5.00	1.46	1.83	13.3	35.0	16.9	0.000	0.159
	66	0.087	0.57	2	5.08	1.19	2.17	13.3	43.3	16.9	0.000	0.158
	67	0.060	0.58	2	5.50	1.33	1.75	13.2	18.3	19.5	0.000	0.161
	68	0.060	0.58	2	6.00	1.25	1.67	13.2	26.7	19.5	0.000	0.132
	69	0.060	0.58	2	5.67	1.35	1.67	13.2	35.0	18.5	0.000	0.153
	70	0.060	0.58	2	4.58	1.89	1.50	13.3	43.3	18.5	0.000	0.133
	71	0.089	0.56	2	2.56	2.58	1.94	15.6	32.5	21.1	0.000	0.149
	72	0.089	0.56	2	2.19	3.38	2.00	18.7	32.5	23.1	0.000	0.166
	73	0.089	0.56	2	2.00	4.09	2.06	21.9	32.5	23.8	0.000	0.139
	74	0.089	0.56	2	2.56	0.47	4.63	9.9	32.5	22.8	0.000	0.144
	75	0.089	0.56	2	2.31	0.41	5.69	9.9	32.5	22.8	0.000	0.151
	76	0.089	0.56	2	2.38	0.34	6.50	9.9	32.5	6.3	0.000	0.157
	77	0.089	0.56	2	2.44	0.35	6.44	9.9	32.5	14.4	0.000	0.215
732	100	0.073	0.59	2	12.38	0.94	2.00	19.1	6.3	16.7	0.000	0.361
	101	0.073	0.59	2	11.13	1.46	1.63	18.9	13.1	16.7	0.000	0.224
	102	0.073	0.59	2	11.63	1.50	1.50	19.1	18.8	16.7	0.000	0.201
	103	0.073	0.59	2	10.00	1.64	1.75	18.8	25.0	16.7	0.000	0.205
	104	0.032	0.55	2	11.25	1.12	2.13	19.0	6.3	16.7	0.000	0.309
	105	0.032	0.55	2	11.63	1.28	1.75	19.1	12.5	16.7	0.000	0.231
	106	0.032	0.55	2	11.50	1.18	1.75	19.0	18.8	16.7	0.000	0.178
	107	0.032	0.55	2	11.25	1.19	2.00	19.0	25.0	16.7	0.000	0.175
	108	0.045	0.55	2	16.67	1.15	2.17	24.7	8.3	13.8	0.000	0.533
	109	0.045	0.55	2	17.17	1.17	2.00	24.8	16.7	13.8	0.000	0.337

Table C.1

Serie	no.	D	F	n_{sp}	$\frac{t}{d}$	ξ	$\frac{s}{d}$	$\frac{b}{d}$	$\frac{l}{d}$	f_c	ψ	$\frac{\tau}{f_c}$
Tepfers [73.1]												
732	110	0.045	0.55	2	16.33	1.31	2.17	25.0	25.0	13.8	0.000	0.274
	111	0.045	0.55	2	17.67	1.10	1.67	24.3	33.3	13.8	0.000	0.196
	112	0.041	0.56	2	8.50	0.90	2.00	15.1	5.0	13.8	0.000	0.311
	113	0.041	0.56	2	8.50	1.00	1.80	15.1	10.0	13.8	0.000	0.203
	114	0.041	0.56	2	8.50	1.20	1.50	15.1	15.0	13.8	0.000	0.162
	115	0.041	0.56	2	8.30	1.05	1.80	15.1	20.0	13.8	0.000	0.170
	116	0.073	0.58	2	8.10	1.18	1.70	15.1	5.0	15.0	0.000	0.327
	117	0.073	0.58	2	7.70	1.47	1.50	15.1	10.0	15.0	0.000	0.222
	118	0.073	0.58	2	8.00	1.34	1.50	15.0	15.0	15.0	0.000	0.178
	119	0.073	0.58	2	9.10	0.83	1.80	15.1	19.0	15.0	0.000	0.191
	120	0.073	0.58	2	10.80	1.00	0.50	14.8	16.0	23.1	0.000	0.119
	121	0.073	0.58	2	7.10	4.80	0.50	14.9	16.0	23.1	0.000	0.111
	122	0.073	0.58	2	3.00	9.00	0.50	15.0	16.0	23.1	0.000	0.120
	123	0.073	0.58	2	10.90	0.21	2.40	14.9	16.0	23.1	0.000	0.141
	124	0.073	0.58	2	7.10	1.13	2.20	15.1	16.0	23.1	0.000	0.167
	125	0.073	0.58	2	3.40	2.20	2.00	15.2	16.0	23.1	0.000	0.211
732	126	0.073	0.58	2	11.00	0.16	3.10	15.0	16.0	23.1	0.000	0.176
	127	0.073	0.58	2	7.10	0.83	3.00	15.1	16.0	23.1	0.000	0.217
	128	0.073	0.58	2	2.70	1.21	3.70	14.7	16.0	21.1	0.000	0.163
	129	0.041	0.56	2	10.90	1.00	0.50	14.9	16.0	21.1	0.000	0.096
	130	0.041	0.56	2	6.60	5.60	0.50	15.2	16.0	21.1	0.000	0.115
	131	0.041	0.56	2	2.80	6.29	0.70	14.6	16.0	21.1	0.000	0.133
	132	0.041	0.56	2	10.90	0.33	1.80	15.1	15.5	21.1	0.000	0.103
	133	0.041	0.56	2	7.70	1.38	1.60	15.1	15.5	21.1	0.000	0.151
	134	0.041	0.56	2	3.00	2.55	1.80	15.2	15.3	21.1	0.000	0.168
	135	0.041	0.56	2	10.50	0.23	3.40	15.1	16.0	21.1	0.000	0.156
	136	0.041	0.56	2	7.00	0.81	3.20	15.2	16.0	26.2	0.000	0.215
	137	0.041	0.56	2	3.10	1.37	3.30	15.1	15.0	26.2	0.000	0.187
	138	0.073	0.58	2	6.60	1.32	1.90	14.6	16.0	17.2	0.000	0.257
	139	0.073	0.58	2	6.60	1.32	1.90	15.2	16.0	17.2	0.000	0.267
	140	0.041	0.56	2	6.80	1.35	2.00	15.2	14.7	17.2	0.000	0.250
	141	0.041	0.56	2	6.90	1.44	1.80	15.1	15.0	17.2	0.000	0.225
	142	0.073	0.58	2	6.80	1.35	2.00	15.2	15.8	30.7	0.000	0.199
	143	0.073	0.58	2	6.90	1.30	2.00	15.1	15.5	30.7	0.000	0.202
	144	0.041	0.56	2	7.10	1.15	2.00	14.7	14.8	30.7	0.000	0.195

Table C.1

Serie	no.	D	F	n_{sp}	$\frac{i}{d}$	ξ	$\frac{s}{d}$	$\frac{b}{d}$	$\frac{l}{d}$	f_c	ψ	$\frac{\tau}{f_c}$
Tepfers [73.1]												
732	145	0.041	0.56	2	6.80	1.25	2.00	14.8	14.8	30.7	0.000	0.193
	146	0.073	0.58	2	6.90	1.20	2.00	14.7	15.6	44.6	0.000	0.158
	147	0.073	0.58	2	7.10	1.30	2.00	15.3	14.5	44.6	0.000	0.182
	148	0.041	0.56	2	7.00	1.30	2.00	15.2	15.7	44.6	0.000	0.153
	149	0.041	0.56	2	6.90	1.35	2.00	15.3	14.5	44.6	0.000	0.150
	151	0.073	0.58	2	6.80	1.30	2.00	15.0	15.0	50.5	0.000	0.150
	152	0.041	0.56	2	7.00	1.19	2.10	15.0	14.4	50.5	0.000	0.149
	153	0.041	0.56	2	6.70	1.30	2.00	14.9	14.0	50.5	0.000	0.150
	154	0.073	0.58	2	6.90	1.20	2.00	14.7	15.2	57.6	0.000	0.121
	155	0.073	0.58	2	7.20	1.25	2.00	15.2	15.6	57.6	0.000	0.138
	158	0.073	0.58	2	7.00	1.30	2.00	15.2	15.2	71.9	0.000	0.113
	159	0.073	0.58	2	6.70	1.39	1.80	14.7	16.2	71.9	0.000	0.107
	160	0.041	0.56	2	6.70	1.25	2.00	14.9	14.3	71.9	0.000	0.110
732-L	167	0.089	0.56	2	2.19	1.42	1.75	10.2	32.5	25.6	0.000	0.125
	168	0.055	0.56	2	2.00	1.52	1.69	10.1	32.5	25.6	0.000	0.136
	169	0.089	0.56	2	1.88	1.59	1.69	10.3	32.5	18.0	0.000	0.146
	170	0.055	0.56	2	2.68	1.39	1.75	10.3	32.5	18.0	0.000	0.159
	171	0.089	0.56	2	2.50	1.35	1.75	10.3	32.5	16.2	0.000	0.162
	172	0.055	0.56	2	2.13	1.41	1.81	10.3	32.5	16.2	0.000	0.167
732-8	176	0.073	0.58	4	6.17	0.91	2.30	30.1	60.0	18.1	0.000	0.135
747	1	0.050	0.57	2	4.00	1.77	1.98	14.0	20.8	25.4	0.000	0.127
	2	0.050	0.57	2	4.00	1.67	2.10	14.0	28.8	25.8	0.000	0.136
	3	0.050	0.57	2	4.00	1.67	2.10	14.0	36.8	22.5	0.000	0.121
	4	0.073	0.56	2	3.72	1.83	1.98	14.0	20.8	20.6	0.000	0.173
	5	0.073	0.56	2	3.68	1.48	2.46	13.9	36.8	26.8	0.000	0.142
	6	0.073	0.56	2	4.00	1.78	1.94	13.9	52.8	30.8	0.000	0.101
	7	0.081	0.61	2	2.97	1.16	2.09	10.8	16.3	24.6	0.000	0.136
	8	0.081	0.61	2	2.81	1.50	1.69	10.9	28.8	20.1	0.000	0.132
	12	0.073	0.56	2	4.40	1.51	2.18	14.0	20.8	28.0	0.751	0.305
	13	0.081	0.61	2	2.69	1.50	1.75	10.9	16.3	28.3	0.209	0.197
	14	0.081	0.61	2	3.00	1.41	1.75	10.9	16.3	27.1	0.388	0.236
	15	0.081	0.61	2	3.00	1.41	1.75	10.9	16.3	27.7	0.592	0.249
	16	0.060	0.56	2	3.72	1.76	2.10	14.1	20.8	37.8	0.000	0.105
	17	0.060	0.56	2	4.08	1.62	2.14	14.0	28.8	39.1	0.000	0.091
	18	0.060	0.56	2	3.68	1.51	2.46	14.1	36.8	42.2	0.000	0.089

<div align="center">Table C.1</div>

Serie	no.	D	F	n_{sp}	$\frac{t}{d}$	ξ	$\frac{s}{d}$	$\frac{b}{d}$	$\frac{l}{d}$	f_c	ψ	$\frac{\tau}{f_c}$
Tepfers [73.1]												
123S	1	0.089	0.56	2	1.00	1.46	2.06	10.0	15.0	23.0	0.000	0.201
	2	0.089	0.56	2	1.00	1.46	2.06	10.0	25.0	30.5	0.000	0.140
	3	0.089	0.56	2	1.00	1.46	2.06	10.0	35.0	30.7	0.000	0.111
	4	0.089	0.56	2	1.00	1.46	2.06	10.0	45.0	29.4	0.000	0.100
	7	0.089	0.56	2	1.00	1.46	2.06	10.0	60.0	31.1	0.000	0.082
	8	0.089	0.56	2	1.00	1.46	2.06	10.0	15.0	27.1	0.418	0.210
	9	0.089	0.56	2	1.00	1.46	2.06	10.0	25.0	30.0	0.226	0.159
	10	0.089	0.56	2	1.00	1.46	2.06	10.0	35.0	29.7	0.163	0.146
	13	0.089	0.56	2	1.00	1.46	2.06	10.0	35.0	30.2	0.481	0.176
	14	0.089	0.56	2	1.00	1.46	2.06	10.0	45.0	28.0	0.403	0.145
	19	0.089	0.56	2	1.00	1.46	2.06	10.0	45.0	27.5	0.479	0.130
657	1	0.089	0.56	2	2.25	1.35	1.75	10.0	32.5	22.8	0.000	0.128
	2	0.089	0.56	2	2.25	1.35	1.75	10.0	45.0	22.8	0.000	0.113
	3	0.089	0.56	2	2.25	1.35	1.75	10.0	63.8	22.5	0.000	0.098
	4	0.089	0.56	2	2.25	1.35	1.75	10.0	82.5	22.5	0.000	0.082
	5	0.089	0.56	2	2.25	1.35	1.75	10.0	20.0	21.3	0.519	0.213
	6	0.089	0.56	2	2.19	1.35	1.75	9.9	32.5	21.3	0.320	0.181
	7	0.089	0.56	2	2.25	1.35	1.75	10.0	45.0	22.4	0.219	0.164
	8	0.089	0.56	2	2.19	1.35	1.75	9.9	63.8	22.4	0.155	0.141
	9	0.089	0.56	2	2.25	1.35	1.75	10.0	32.5	24.3	0.105	0.143
	10	0.089	0.56	2	2.25	1.35	1.75	10.0	32.5	24.3	0.497	0.213
	11	0.089	0.56	2	2.25	1.35	1.75	10.0	32.5	23.0	0.296	0.165
	12	0.089	0.56	2	2.19	1.35	1.75	9.9	32.5	23.0	0.493	0.221
	13	0.089	0.56	2	1.94	0.85	2.94	9.9	45.0	22.6	0.000	0.133
	14	0.089	0.56	2	2.88	1.84	1.13	10.0	45.0	22.6	0.000	0.106
	15	0.089	0.56	2	3.06	1.31	2.63	12.9	45.0	23.3	0.000	0.145
	16	0.089	0.56	2	4.63	1.33	3.06	15.8	45.0	23.3	0.000	0.151
	22	0.087	0.57	2	5.17	0.62	2.17	10.8	5.0	21.8	0.000	0.322
	23	0.087	0.57	2	5.17	0.62	2.17	10.8	10.0	24.9	0.000	0.249
	24	0.087	0.57	2	5.17	0.62	2.17	10.8	20.0	28.6	0.000	0.191
	25	0.087	0.57	2	5.17	0.62	2.17	10.8	30.0	22.6	0.000	0.177
	25A	0.087	0.57	2	5.17	0.62	2.17	10.8	55.0	29.3	0.000	0.098
	37	0.089	0.56	2	2.88	0.64	1.75	8.1	5.0	24.0	0.000	0.262
	38	0.089	0.56	2	2.88	0.64	1.75	8.1	10.0	25.0	0.000	0.178
	39	0.089	0.56	2	2.88	0.64	1.75	8.1	20.0	23.8	0.000	0.167
	40	0.089	0.56	2	2.88	0.64	1.75	8.1	30.0	27.5	0.000	0.114
	40A	0.089	0.56	2	2.88	0.64	1.75	8.1	55.0	26.4	0.000	0.084

Table C.1

Serie	no.	D	F	n_{sp}	$\frac{t}{d}$	ξ	$\frac{s}{d}$	$\frac{b}{d}$	$\frac{l}{d}$	f_c	ψ	$\frac{\tau}{f_c}$
Tepfers [73.1]												
715,56	4	0.089	0.56	2	2.31	1.35	1.75	10.1	20.0	28.4	0.416	0.236
	6	0.089	0.56	2	2.31	1.35	1.75	10.1	20.0	10.7	1.102	0.348
	7	0.089	0.56	2	2.31	1.35	1.75	10.1	20.0	45.6	0.256	0.168
	9	0.089	0.56	2	2.31	1.35	1.75	10.1	32.5	26.9	0.274	0.181
	10	0.089	0.56	2	2.31	1.35	1.75	10.1	32.5	29.1	0.406	0.171
715,56	52	0.089	0.56	2	3.13	3.69	0.81	12.1	32.5	27.7	0.000	0.133
	53	0.089	0.56	2	3.38	2.09	1.44	12.4	32.5	28.7	0.000	0.147
	54	0.089	0.56	2	3.44	1.11	2.69	12.4	32.5	28.0	0.000	0.151
	55	0.089	0.56	2	3.50	0.83	3.63	12.5	32.5	36.1	0.000	0.129
	61	0.055	0.56	2	2.44	1.35	1.75	10.2	20.0	35.9	0.329	0.189
	64	0.087	0.57	2	4.33	1.76	1.75	13.5	18.3	17.9	0.879	0.313
	65	0.087	0.57	2	4.52	1.31	2.42	13.3	26.7	16.3	0.967	0.317
	71	0.067	0.56	2	1.81	1.53	1.75	10.2	13.8	6.0	1.978	0.275
	72	0.067	0.56	2	1.88	1.53	1.75	10.3	20.0	17.5	0.675	0.205
	73	0.067	0.56	2	2.06	1.52	1.69	10.2	26.3	18.9	0.625	0.215
Berholdt [74.2]												
	9	0.064	0.56	2	4.00	1.00	2.50	12.0	28.3	28.1	0.000	0.163
	12	0.064	0.56	2	4.00	1.00	2.50	12.0	28.3	22.3	0.108	0.188
	13	0.064	0.56	2	4.00	1.00	2.50	12.0	23.3	21.0	0.277	0.176
	14	0.064	0.56	2	4.00	1.00	2.50	12.0	23.3	18.1	0.161	0.243
	15	0.064	0.56	2	4.00	1.00	2.50	12.0	23.3	25.6	0.000	0.181
Chinn et al [55.1]												
	D1	0.038	0.55	2	1.00	1.67	1.50	9.0	14.7	26.8	0.000	0.145
	D2	0.038	0.55	2	3.00	1.00	1.50	9.0	13.7	33.2	0.000	0.113
	D3	0.038	0.55	2	4.00	1.00	2.50	12.0	14.7	30.0	0.000	0.144
	D4	0.038	0.55	2	4.00	1.00	2.50	12.0	21.3	30.8	0.000	0.122
	D5	0.038	0.55	1	0.00	1.27	2.50	7.3	14.7	28.8	0.000	0.181
	D6	0.038	0.55	2	1.67	1.23	2.05	9.7	14.7	29.9	0.000	0.128
	D7	0.038	0.55	1	0.00	0.87	2.19	4.8	14.7	30.7	0.000	0.127
	D8	0.038	0.55	2	1.67	1.01	2.47	9.7	14.7	31.5	0.000	0.132
	D9	0.038	0.55	1	0.00	0.79	2.42	4.8	14.7	30.2	0.000	0.134
	D10	0.038	0.55	1	0.00	0.78	2.47	4.8	9.3	29.4	0.000	0.162
	D12	0.038	0.55	1	0.00	0.75	2.66	5.0	21.3	31.2	0.000	0.116
	D13	0.038	0.55	1	0.00	1.80	2.42	9.8	14.7	33.2	0.000	0.176
	D14	0.038	0.55	1	0.00	1.22	1.61	4.9	14.7	33.2	0.000	0.113
	D15	0.038	0.55	1	0.00	3.26	1.33	9.7	14.7	29.6	0.000	0.171

Table C.1

Serie	no.	D	F	n_{sp}	$\frac{i}{d}$	ξ	$\frac{s}{d}$	$\frac{b}{d}$	$\frac{l}{d}$	f_c	ψ	$\frac{\tau}{f_c}$
Chinn et al [55.1]												
	D17	0.038	0.55	1	0.00	1.25	1.57	4.9	21.3	24.7	0.000	0.127
	D19	0.038	0.55	1	0.00	1.58	2.77	9.8	21.3	29.2	0.000	0.169
	D20	0.038	0.55	1	0.00	0.84	2.39	5.0	9.3	29.2	0.000	0.168
	D21	0.038	0.55	1	0.00	1.78	2.46	9.8	14.7	30.9	0.000	0.168
	D22	0.038	0.55	1	0.00	1.25	1.58	4.9	9.3	30.9	0.000	0.141
	D23	0.038	0.55	1	0.00	1.25	1.54	4.8	21.3	30.9	0.000	0.102
	D24	0.038	0.55	1	0.00	2.74	1.58	9.7	21.3	30.7	0.000	0.116
	D25	0.038	0.55	1	0.00	0.75	2.54	4.8	32.0	35.2	0.000	0.088
	D26	0.038	0.55	1	0.00	1.31	1.50	4.9	32.0	35.2	0.000	0.084
	D29	0.038	0.55	1	0.00	0.84	2.35	4.9	14.7	51.6	0.000	0.101
	D30	0.038	0.55	1	0.00	0.76	2.58	4.9	21.3	51.6	0.000	0.082
	D31	0.030	0.54	1	0.00	1.27	2.71	9.8	14.7	32.4	0.000	0.230
	D32	0.038	0.55	1	0.00	1.77	2.46	9.7	14.7	32.4	0.000	0.170
	D33	0.038	0.55	1	0.00	1.21	1.63	5.0	14.4	33.3	0.000	0.097
	D34	0.038	0.55	1	0.00	0.77	2.49	4.8	16.7	26.2	0.000	0.142
	D35	0.038	0.55	1	0.00	0.78	2.43	4.8	32.0	26.2	0.000	0.110
	D36	0.030	0.54	1	0.00	2.22	1.99	9.8	14.7	30.4	0.000	0.199
	D38	0.038	0.55	1	0.00	1.02	2.53	6.2	14.7	21.8	0.000	0.149
	D39	0.038	0.55	1	0.00	0.76	2.58	4.9	14.7	21.8	0.000	0.145
	D40	0.038	0.55	1	0.00	2.95	1.50	9.8	21.3	36.4	0.000	0.120
Orr [76.1]												
	2	0.037	0.55	2	4.00	1.00	2.50	12.0	30.0	18.3	0.000	0.182
	3	0.037	0.55	2	4.00	1.00	2.50	12.0	22.5	18.3	0.000	0.192
	4	0.037	0.55	2	4.00	1.00	2.50	12.0	15.0	18.3	0.000	0.201
Reynols & Beeby [82.3]												
E	1	0.040	0.55	2	6.63	0.74	1.94	12.5	8.8	40.0	0.000	0.120
	2	0.040	0.55	2	6.38	0.86	1.81	12.5	15.0	40.0	0.000	0.102
	5	0.040	0.55	1	0.00	3.28	1.75	12.5	18.1	40.0	0.000	0.121
Zekany et al [81.1]												
	1T	0.038	0.55	4	2.97	1.00	1.95	19.8	16.0	25.5	0.290	0.120
	2B	0.038	0.55	4	2.97	1.00	1.95	19.8	16.0	25.9	0.286	0.147
	3T	0.038	0.55	4	2.97	1.00	1.95	19.8	16.0	26.0	0.284	0.127
	4B	0.038	0.55	4	2.97	1.00	1.95	19.8	16.0	26.0	0.284	0.147
	5B	0.038	0.55	4	2.97	1.00	1.95	19.8	16.0	28.4	0.153	0.162
	6T	0.038	0.55	4	2.97	1.00	1.95	19.8	16.0	28.6	0.152	0.131
	7T	0.038	0.55	4	2.97	1.00	1.95	19.8	16.0	26.4	0.000	0.122
	8B	0.038	0.55	4	2.97	1.00	1.95	19.8	16.0	26.4	0.000	0.156

Table C.1

Serie	no.	D	F	n_{sp}	$\frac{t}{d}$	ξ	$\frac{s}{d}$	$\frac{b}{d}$	$\frac{l}{d}$	f_c	ψ	$\frac{\tau}{f_c}$
Zekany et al [81.1]												
	9B	0.038	0.55	4	2.97	1.00	1.95	19.8	16.0	29.0	0.150	0.163
	10T	0.038	0.55	4	2.97	1.00	1.95	19.8	16.0	29.0	0.150	0.125
	11T	0.038	0.55	4	2.97	1.00	1.95	19.8	16.0	26.5	0.137	0.134
	12B	0.038	0.55	4	2.97	1.00	1.95	19.8	16.0	26.5	0.137	0.153
	13T	0.038	0.55	4	2.97	1.00	1.95	19.8	16.0	27.8	0.148	0.177
	14B	0.038	0.55	4	2.97	1.00	1.95	19.8	16.0	27.8	0.148	0.167
	15B	0.038	0.55	4	2.97	1.00	1.95	19.8	16.0	28.4	0.144	0.129
	16T	0.038	0.55	4	2.97	1.00	1.95	19.8	16.0	28.4	0.144	0.132
	17T	0.038	0.55	4	2.97	1.00	1.95	19.8	16.0	37.4	0.109	0.085
	18B	0.038	0.55	4	2.97	1.00	1.95	19.8	16.0	37.4	0.109	0.121
	19B	0.038	0.55	4	2.97	1.00	1.95	19.8	16.0	34.8	0.118	0.132
	20T	0.038	0.55	4	2.97	1.00	1.95	19.8	16.0	34.8	0.118	0.112
	21T	0.037	0.55	5	2.67	1.00	2.28	24.2	14.2	39.0	0.000	0.124
	22B	0.037	0.55	5	2.67	1.00	2.28	24.2	14.2	39.0	0.000	0.146
	23B	0.037	0.55	5	2.67	1.00	2.28	24.2	14.2	39.3	0.179	0.161
	24T	0.037	0.55	5	2.67	1.00	2.28	24.2	14.2	39.3	0.179	0.114
Ferguson & Breen [65.1]												
8R	18a	0.037	0.55	2	6.50	1.67	2.25	17.0	18.0	23.9	0.000	0.173
	24a	0.037	0.55	2	6.50	1.73	2.17	17.0	24.0	24.3	0.000	0.174
	30a	0.037	0.55	2	6.50	1.84	2.03	17.0	30.0	20.9	0.000	0.145
8F	36a	0.037	0.55	2	6.50	1.97	1.91	17.0	36.0	32.1	0.000	0.104
	36b	0.037	0.55	2	6.50	1.98	1.90	17.0	36.0	26.0	0.000	0.113
	39a	0.037	0.55	2	6.50	1.84	2.03	17.0	39.0	25.2	0.000	0.131
	42a	0.037	0.55	2	6.50	1.88	2.00	17.0	42.0	18.3	0.000	0.147
	42b	0.037	0.55	2	6.50	1.92	1.95	17.0	42.0	26.4	0.000	0.117
8R	42a	0.037	0.55	2	6.50	1.82	2.06	17.0	42.0	22.8	0.000	0.127
	48a	0.037	0.55	2	6.50	1.90	1.98	17.0	48.0	21.0	0.000	0.124
	64a	0.037	0.55	2	6.50	1.85	2.02	17.0	64.0	24.5	0.000	0.099
	80a	0.037	0.55	2	6.50	1.88	2.00	17.0	80.0	25.8	0.000	0.081
8F	36k	0.037	0.55	2	2.84	2.96	1.88	17.0	36.0	23.9	0.000	0.106
11R	24a	0.038	0.55	2	6.51	2.23	1.68	17.0	23.4	25.6	0.000	0.145
	30a	0.038	0.55	2	6.51	2.63	1.43	17.0	29.3	27.8	0.000	0.121
	36a	0.038	0.55	2	6.51	2.40	1.56	17.0	35.1	31.5	0.000	0.097
	36b	0.038	0.55	2	6.51	2.43	1.54	17.0	35.1	23.1	0.000	0.122
	42a	0.038	0.55	2	6.51	2.43	1.55	17.0	41.0	24.3	0.000	0.106
	48a	0.038	0.55	2	6.51	2.38	1.59	17.0	46.8	21.7	0.000	0.122
	48b	0.038	0.55	2	6.51	2.32	1.62	17.0	46.8	23.0	0.000	0.113

Table C.1

Serie	no.	D	F	n_{sp}	$\frac{t}{d}$	ξ	$\frac{s}{d}$	$\frac{b}{d}$	$\frac{l}{d}$	f_c	ψ	$\frac{\tau}{f_c}$
Ferguson & Breen [65.1]												
11R	48a	0.038	0.55	2	6.51	2.40	1.56	17.0	46.8	38.8	0.000	0.077
	48b	0.038	0.55	2	6.51	1.91	1.96	17.0	46.8	21.4	0.000	0.118
11F	60a	0.038	0.55	2	6.51	2.30	1.63	17.0	58.5	18.0	0.000	0.127
	60b	0.038	0.55	2	6.51	2.40	1.56	17.0	58.5	28.2	0.000	0.080
11R	60a	0.038	0.55	2	6.51	2.51	1.50	17.0	58.5	18.5	0.000	0.122
	60b	0.038	0.55	2	6.51	2.15	1.74	17.0	58.5	23.9	0.000	0.105
8F	30b	0.037	0.55	2	6.50	1.88	2.00	17.0	30.0	18.0	0.193	0.181
	36c	0.037	0.55	2	6.50	1.91	1.97	17.0	36.0	18.9	0.153	0.154
	36d	0.037	0.55	2	6.50	1.84	2.03	17.0	36.0	24.7	0.200	0.146
	36e	0.037	0.55	2	6.50	1.91	1.97	17.0	36.0	28.8	0.101	0.132
	36f	0.037	0.55	2	6.50	1.88	2.00	17.0	36.0	26.1	0.189	0.143
	36g	0.037	0.55	2	6.50	1.84	2.03	17.0	36.0	21.2	0.137	0.170
	36h	0.037	0.55	2	6.50	1.79	2.09	17.0	36.0	13.2	0.510	0.201
	36j	0.037	0.55	2	6.50	1.88	2.00	17.0	36.0	12.5	0.536	0.242
11R	36a	0.037	0.55	2	6.73	1.97	1.97	17.5	36.0	20.8	0.243	0.189
Chamberlin [58.1]												
1	a	0.030	0.54	2	4.00	1.00	2.50	12.0	6.0	30.2	0.000	0.179
	b	0.030	0.54	2	4.00	1.00	2.50	12.0	6.0	30.2	0.000	0.179
3	a	0.030	0.54	2	4.00	1.00	2.50	12.0	12.0	30.7	0.000	0.154
	b	0.030	0.54	2	4.00	1.00	2.50	12.0	12.0	30.7	0.000	0.155
	c	0.030	0.54	2	4.00	1.00	2.50	12.0	12.0	30.7	0.000	0.157
2	a	0.030	0.54	1	0.00	2.20	2.50	12.0	6.0	30.5	0.000	0.324
	b	0.030	0.54	1	0.00	2.20	2.50	12.0	6.0	30.5	0.000	0.339
4	a	0.030	0.54	1	0.00	2.20	2.50	12.0	12.0	30.1	0.000	0.210
	b	0.030	0.54	1	0.00	2.20	2.50	12.0	12.0	30.1	0.000	0.216
	c	0.030	0.54	1	0.00	2.20	2.50	12.0	12.0	30.1	0.000	0.214
Ferguson & Krishnaswamy [71.1]												
SP	32	0.038	0.55	1	0.00	5.78	1.38	17.0	35.5	22.6	0.000	0.156
	33	0.038	0.55	1	0.00	7.76	1.03	17.0	39.0	23.2	0.000	0.144
	34	0.038	0.55	1	0.00	7.76	1.03	17.0	25.5	22.6	0.000	0.163
	35	0.038	0.55	1	0.00	4.18	1.92	17.0	14.2	22.8	0.000	0.204
	36	0.038	0.55	1	0.00	2.98	1.92	12.4	17.0	23.7	0.000	0.203
	37	0.038	0.55	3	3.00	2.36	1.92	19.9	31.9	22.5	0.000	0.166
	38	0.038	0.55	2	2.00	0.78	1.92	8.0	28.4	20.5	0.000	0.129
	39	0.038	0.55	3	3.00	1.04	1.92	14.9	31.9	21.5	0.000	0.128

Table C.1

Serie	no.	D	F	n_{sp}	$\frac{t}{d}$	ξ	$\frac{s}{d}$	$\frac{b}{d}$	$\frac{l}{d}$	f_c	ψ	$\frac{\tau}{f_c}$
Ferguson & Krishnaswamy [71.1]												
14S	1	0.038	0.55	2	4.00	1.32	1.92	11.8	26.6	18.7	0.000	0.158
	2	0.038	0.55	2	4.00	1.32	1.92	11.8	31.9	23.1	0.156	0.139
	3	0.038	0.55	2	4.00	1.32	1.92	11.8	17.7	20.8	0.310	0.182
	4	0.038	0.55	2	4.00	1.32	1.92	11.8	17.7	22.1	0.243	0.220
	6	0.038	0.55	2	4.00	1.32	1.92	11.8	21.3	24.6	0.224	0.198
18S	12	0.034	0.55	2	4.00	1.37	1.83	12.0	26.6	21.8	0.000	0.135
	15	0.034	0.55	2	4.00	1.37	1.83	12.0	41.2	17.7	0.000	0.109
	1	0.034	0.55	2	4.00	1.37	1.83	12.0	31.9	18.7	0.184	0.190
	4	0.034	0.55	2	4.00	1.37	1.83	12.0	26.6	27.2	0.379	0.158
	2	0.034	0.55	2	4.00	1.37	1.83	12.0	26.6	18.1	0.228	0.189
	3	0.034	0.55	2	4.00	1.37	1.83	12.0	31.9	32.1	0.037	0.100
	9	0.034	0.55	2	4.00	1.37	1.83	12.0	26.6	20.8	0.324	0.220
	13	0.034	0.55	2	4.00	1.37	1.83	12.0	21.3	23.4	0.287	0.205
SP	40	0.033	0.55	2	4.00	1.37	1.83	12.0	24.0	22.2	0.000	0.139
Ferguson & Briceno [69.1]												
	1	0.038	0.55	2	1.21	0.58	1.92	6.4	60.3	19.3	0.000	0.068
	5	0.038	0.55	2	1.19	0.57	1.92	6.4	60.3	26.9	0.000	0.081
	7	0.038	0.55	2	1.30	0.60	1.92	6.6	40.8	20.1	0.000	0.094
	12	0.038	0.55	2	2.14	0.82	1.92	8.3	46.1	29.3	0.000	0.091
	13	0.038	0.55	2	3.07	1.06	1.92	10.1	31.2	23.3	0.000	0.133
	14	0.038	0.55	2	4.03	1.31	1.92	12.1	23.4	21.0	0.000	0.144
	15	0.038	0.55	2	3.01	1.05	1.92	10.0	46.1	23.0	0.000	0.117
	16	0.038	0.55	2	3.01	0.76	2.63	10.0	31.2	21.1	0.000	0.144
	17	0.038	0.55	2	4.04	1.32	1.92	12.1	35.5	24.5	0.000	0.118
	21	0.038	0.55	2	1.19	0.57	1.92	6.4	60.3	28.9	0.019	0.063
	22	0.038	0.55	2	4.04	1.32	1.92	12.1	35.5	26.9	0.000	0.139
	23	0.038	0.55	2	2.73	0.90	2.08	9.5	51.2	24.8	0.000	0.076
	24	0.038	0.55	2	1.28	0.60	1.92	6.6	46.1	24.9	0.058	0.098
	25	0.038	0.55	3	1.37	0.62	1.92	10.1	30.0	23.0	0.251	0.159
	26	0.038	0.55	3	1.55	0.66	1.92	10.6	30.0	22.1	0.262	0.151
	27	0.038	0.55	3	1.58	0.67	1.92	10.7	30.0	22.5	0.000	0.102
	1a	0.037	0.55	2	2.00	0.60	2.50	8.0	47.0	19.1	0.000	0.098
	2a	0.037	0.55	2	3.00	0.80	2.50	10.0	32.0	27.0	0.000	0.118
	4a	0.037	0.55	2	1.13	1.42	2.50	6.3	42.0	30.0	0.000	0.081

Table C.1

Serie	no.	D	F	n_{sp}	$\frac{t}{d}$	ξ	$\frac{s}{d}$	$\frac{b}{d}$	$\frac{l}{d}$	f_c	ψ	$\frac{\tau}{f_c}$
Thompson et al [79.4]												
	1	0.038	0.55	6	5.33	1.00	3.17	44.0	16.0	25.7	0.000	0.234
	2	0.037	0.55	6	4.00	0.72	3.50	36.0	18.0	32.5	0.000	0.171
	7	0.037	0.55	6	4.00	1.00	2.50	36.0	24.0	21.4	0.000	0.179
	12	0.038	0.55	6	2.84	1.59	1.21	29.0	31.9	24.3	0.000	0.099
	13	0.038	0.55	6	2.84	1.00	1.92	29.0	21.3	19.8	0.000	0.162
	14	0.038	0.55	6	2.84	1.74	1.92	31.8	21.3	23.1	0.000	0.155
	16	0.038	0.55	5	4.26	1.37	1.92	31.3	17.7	27.0	0.000	0.144
	20	0.038	0.55	6	2.84	1.00	1.92	29.0	14.2	22.5	0.231	0.223
	22	0.034	0.55	5	2.38	1.00	1.68	22.2	35.4	19.8	0.000	0.110
	23	0.034	0.55	5	2.38	1.70	1.68	24.5	35.4	22.0	0.000	0.119

Table C.1: *Test data for lap splices.*

Test			Analysis					
Reference	Series	No.	A	B	C	D	E	F
Tepfer [73.1]	732	1	1.062	1.062	1.062	1.062	1.062	1.155
		2	0.911	0.911	0.911	0.911	0.911	0.986
		3	1.010	1.010	1.010	1.010	1.010	1.100
		4	1.018	1.018	1.018	1.018	1.018	1.104
		5	1.128	1.128	1.128	1.128	1.128	1.231
		6	0.939	0.939	0.939	0.939	0.939	1.023
		7	0.776	0.776	0.776	0.776	0.776	0.841
		8	0.788	0.788	0.788	0.788	0.788	0.858
		9	1.196	1.196	1.196	1.196	1.196	1.296
		10	1.121	1.121	1.121	1.121	1.121	1.215
		11	1.140	1.140	1.140	1.140	1.140	1.238
		12	0.886	0.886	0.886	0.919	0.886	0.998
		13	0.906	0.906	0.906	0.906	0.906	0.912
		14	0.949	0.949	0.949	0.949	0.949	0.955
		15	1.053	1.053	1.053	1.053	1.053	1.061
		16	1.009	1.009	1.009	1.009	1.009	1.016
		17	0.987	0.987	0.987	0.987	0.987	0.996
	732	35	1.080	1.080	1.080	1.080	1.080	1.175
		36	0.716	0.716	0.716	0.716	0.716	0.778
		37	0.565	0.565	0.565	0.565	0.565	0.616
		38	1.279	1.279	1.264	1.264	1.264	1.293
		39	1.110	1.110	1.110	1.110	1.110	1.126
		40	1.279	1.279	1.279	1.279	1.279	1.294
		41	1.179	1.179	1.179	1.179	1.179	1.194
		42	1.228	1.228	1.228	1.228	1.228	1.233
		43	0.803	0.803	0.803	0.803	0.803	0.844
		44	0.802	0.802	0.802	0.802	0.802	0.848
		45	0.939	0.939	0.939	0.939	0.939	0.997
		46	1.268	1.190	1.134		1.134	
		47	0.820	0.820	0.820	0.820	0.820	0.892
		48	0.918	0.918	0.918	0.918	0.918	0.999
		49	1.834	1.799	1.767		1.767	
	732	50	1.148	0.897	0.664		0.664	
		51	0.962	0.962	0.962	0.962	0.962	0.994
		52	0.959	0.959	0.959	0.959	0.959	0.993

Table C.2

Test			Analysis					
Reference	Series	No.	A	B	C	D	E	F
Tepfer [73.1]	732	53	0.874	0.874	0.874	0.874	0.874	0.898
		54	0.939	0.939	0.939	0.939	0.939	0.981
		55	0.820	0.820	0.820	0.820	0.820	0.851
		56	1.003	1.003	1.003	1.003	1.003	1.014
		57	1.100	1.100	1.100	1.100	1.100	1.113
		58	0.722	0.719	0.634		0.634	
		59	0.798	0.798	0.798	0.798	0.798	0.869
		60	0.767	0.767	0.767	0.767	0.767	0.806
		61	0.994	0.994	0.994	0.994	0.994	1.004
		62	0.817	0.817	0.817	0.817	0.817	0.818
		63	0.886	0.886	0.886	0.886	0.886	0.932
		64	1.081	1.081	1.081	1.081	1.081	1.162
		65	0.892	0.892	0.892	0.892	0.892	0.971
		66	0.903	0.903	0.903	0.903	0.903	0.984
		67	0.882	0.882	0.882	0.882	0.882	0.886
		68	0.872	0.872	0.872	0.872	0.872	0.881
		69	1.091	1.091	1.091	1.091	1.091	1.106
		70	1.050	1.050	1.050	1.050	1.050	1.070
		71	0.828	0.828	0.828	0.828	0.828	0.894
		72	0.878	0.878	0.878	0.878	0.878	0.943
		73	0.687	0.687	0.687	0.687	0.687	0.733
		74	0.702	0.702	0.702	0.702	0.702	0.738
		75	0.675	0.675	0.675	0.675	0.675	0.701
		76	0.365	0.349	0.349	0.404	0.349	0.415
		77	0.748	0.726	0.726	0.726	0.726	0.747
	732	100	0.887	0.879	0.779		0.779	
		101	0.839	0.834	0.748	0.748	0.748	0.750
		102	0.956	0.953	0.837	0.837	0.837	0.844
		103	0.949	0.945	0.913	0.913	0.913	0.924
		104	0.762	0.763	0.689		0.689	
		105	1.102	1.099	0.971	0.971	0.971	0.972
		106	1.107	1.107	0.976	0.976	0.976	0.985
		107	1.092	1.092	1.052	1.052	1.052	1.064
		108	1.236	1.237	1.038	1.038	1.038	1.027
		109	1.331	1.331	1.069	1.069	1.069	1.074

Table C.2

Test			Analysis					
Reference	Series	No.	A	B	C	D	E	F
Tepfer [73.1]	732	110	1.208	1.207	1.055	1.055	1.055	1.067
		111	1.342	1.339	1.038	1.038	1.038	1.063
		112	0.666	0.649	0.627		0.627	
		113	0.727	0.727	0.710	0.710	0.710	0.708
		114	0.868	0.868	0.809	0.809	0.809	0.813
		115	0.900	0.900	0.900	0.900	0.900	0.906
		116	0.762	0.762	0.737		0.737	
		117	0.749	0.744	0.719	0.719	0.719	0.722
		118	0.739	0.738	0.711	0.711	0.711	0.714
		119	0.892	0.872	0.780	0.780	0.780	0.784
		120	1.646	1.646	0.915		0.915	
		121	1.194	1.191	0.851		0.851	
		122	1.159	1.138	0.917		0.917	
		123	1.502	1.310	0.571		0.571	
		124	0.703	0.703	0.703	0.703	0.703	0.704
		125	0.931	0.931	0.931	0.931	0.931	0.932
	732	126	1.834	1.460	0.631		0.631	
		127	0.785	0.785	0.785	0.785	0.785	0.786
		128	0.525	0.525	0.525	0.525	0.525	0.517
		129	1.502	1.502	1.024		1.024	
		130	1.553	1.548	1.217		1.217	
		131	1.458	1.457	1.256		1.256	
		132	1.333	1.293	0.584		0.584	
		133	0.924	0.921	0.916	0.916	0.916	0.920
		134	0.941	0.941	0.941	0.941	0.941	0.944
		135	1.641	1.435	0.605		0.605	
		136	0.963	0.963	0.963	0.963	0.963	0.959
		137	0.789	0.789	0.789	0.789	0.789	0.786
		138	1.025	1.025	1.025	1.025	1.025	1.027
		139	1.043	1.043	1.043	1.043	1.043	1.046
		140	1.159	1.159	1.159	1.159	1.159	1.160
		141	1.129	1.129	1.129	1.129	1.129	1.132
		142	1.005	1.005	1.005	1.005	1.005	1.007
		143	1.014	1.014	1.014	1.014	1.014	1.015
		144	1.239	1.239	1.239	1.239	1.239	1.240

Table C.2

Test			Analysis					
Reference	Series	No.	A	B	C	D	E	F
Tepfer [73.1]	732	145	1.221	1.221	1.221	1.221	1.221	1.222
		146	0.973	0.973	0.973	0.973	0.973	0.974
		147	1.056	1.056	1.056	1.056	1.056	1.057
		148	1.189	1.189	1.189	1.189	1.189	1.191
		149	1.106	1.106	1.106	1.106	1.106	1.107
		151	0.953	0.953	0.953	0.953	0.953	0.954
		152	1.144	1.144	1.144	1.144	1.144	1.144
		153	1.171	1.171	1.171	1.171	1.171	1.171
		154	0.836	0.836	0.836	0.836	0.836	0.836
		155	0.949	0.949	0.949	0.949	0.949	0.950
		158	0.856	0.856	0.856	0.856	0.856	0.857
		159	0.899	0.899	0.899	0.899	0.899	0.901
		160	1.038	1.038	1.038	1.038	1.038	1.039
	732-L	167	0.974	0.974	0.974	0.974	0.974	1.058
		168	1.294	1.294	1.294	1.294	1.294	1.306
		169	0.964	0.964	0.964	0.964	0.964	1.048
		170	1.244	1.244	1.244	1.244	1.244	1.255
		171	0.999	0.999	0.999	0.999	0.999	1.086
		172	1.225	1.225	1.225	1.225	1.225	1.235
	732-8	176	0.860	0.860	0.860	0.860	0.860	0.922
	747	1	0.844	0.844	0.844	0.844	0.844	0.848
		2	1.039	1.039	1.039	1.039	1.039	1.048
		3	0.963	0.963	0.963	0.963	0.963	0.976
		4	0.857	0.857	0.857	0.857	0.857	0.866
		5	0.934	0.934	0.934	0.934	0.934	0.962
		6	0.880	0.880	0.880	0.880	0.880	0.970
		7	0.687	0.687	0.687	0.687	0.687	0.698
		8	0.812	0.812	0.812	0.812	0.812	0.881
		12					0.900	0.800
		13					0.821	0.787
		14					0.844	0.767
		15					0.791	0.699
		16	0.754	0.754	0.754	0.754	0.754	0.757
		17	0.771	0.771	0.771	0.771	0.771	0.777
		18	0.817	0.817	0.817	0.817	0.817	0.825

Table C.2

Test			Analysis					
Reference	Series	No.	A	B	C	D	E	F
Tepfer [73.1]	123	S1	0.996	0.996	0.996	0.996	0.996	1.048
		2	0.997	0.997	0.997	0.997	0.997	1.070
		3	0.919	0.919	0.919	0.919	0.919	0.996
		4	0.904	0.904	0.904	0.904	0.904	0.987
		7	0.862	0.862	0.862	0.862	0.862	0.949
		8	0.835	0.835	0.835	0.835	0.878	0.833
		9	0.823	0.823	0.823	0.823	0.869	0.860
		10	0.867	0.867	0.867	0.867	0.917	0.922
		13	0.788	0.788	0.788	0.788	0.852	0.802
		14	0.683	0.683	0.683	0.683	0.742	0.709
		19					0.735	0.656
	657	1	0.950	0.950	0.950	0.950	0.950	1.032
		2	0.965	0.965	0.965	0.965	0.965	1.058
		3	0.962	0.962	0.962	0.962	0.962	1.068
		4	0.892	0.892	0.892	0.892	0.892	1.002
		5	0.787	0.787	0.787	0.787	0.841	0.797
		6	0.815	0.815	0.815	0.815	0.875	0.856
		7	0.876	0.876	0.876	0.876	0.942	0.936
		8	0.878	0.878	0.878	0.878	0.945	0.949
		9	0.874	0.874	0.874	0.874	0.913	0.938
		10	0.882	0.882	0.882	0.882	0.955	0.905
		11					0.836	0.820
		12					0.792	0.706
		13	0.907	0.907	0.907	0.907	0.907	0.980
		14	1.081	1.081	1.081	1.081	1.081	1.204
		15	0.932	0.932	0.932	0.932	0.932	1.010
		16	0.829	0.829	0.829	0.829	0.829	0.890
		22	1.068	1.066	0.925		0.925	
		23	1.149	1.149	1.018	1.018	1.018	1.035
		24	1.252	1.252	1.117	1.117	1.117	1.186
		25	1.215	1.212	1.098	1.098	1.098	1.183
		25A	0.967	0.956	0.900	0.900	0.900	0.988
		37	1.057	1.057	0.991		0.991	
		38	0.968	0.968	0.909	0.909	0.909	0.953
		39	1.181	1.178	1.128	1.128	1.128	1.210
		40	1.021	1.013	0.990	0.900	0.990	1.072
		40A	0.927	0.927	0.927	0.927	0.927	1.019

Table C.2

Test			Analysis					
Reference	Series	No.	A	B	C	D	E	F
Tepfer [73.1]	715,56	4					0.917	0.822
		6					0.701	0.614
		7					0.885	0.812
		9					0.817	0.765
		10					0.705	0.633
	715,56	52	1.428	1.425	1.377	1.377	1.377	1.541
		53	1.204	1.204	1.204	1.204	1.204	1.317
		54	0.932	0.932	0.932	0.932	0.932	0.997
		55	0.792	0.792	0.792	0.792	0.792	0.836
		61					0.903	0.798
		64					0.765	0.676
		65					0.731	0.645
		71					0.351	0.344
		72					0.578	0.510
		73					0.657	0.579
Bergholdt [74.2]		9	1.124	1.124	1.124	1.124	1.124	1.129
		12	1.009	1.009	1.009	1.009	1.009	1.013
		13	0.732	0.732	0.732	0.732	0.732	0.734
		14	1.051	1.051	1.051	1.051	1.051	1.053
		15	1.091	1.091	1.091	1.091	1.091	1.093
Chinn et al. [55.1]		D1	1.377	1.377	1.377	1.377	1.377	1.378
		D2	1.152	1.152	1.152	1.152	1.152	1.152
		D3	0.918	0.918	0.918	0.918	0.918	0.916
		D4	0.982	0.982	0.982	0.982	0.982	0.984
		D5	0.993	0.993	0.993	0.993	0.993	0.991
		D6	1.045	1.045	1.045	1.045	1.045	1.043
		D7	1.012	1.012	1.012	1.012	1.012	1.010
		D8	0.993	0.993	0.993	0.993	0.993	0.989
		D9	1.000	1.000	1.000	1.000	1.000	0.996
		D10	0.886	0.886	0.886	0.886	0.886	0.879
		D12	1.009	1.009	1.009	1.009	1.009	1.008
		D13	0.873	0.873	0.873	0.873	0.873	0.873
		D14	1.098	1.098	1.098	1.098	1.098	1.099
		D15	1.383	1.364	1.177	1.177	1.177	1.188

Table C.2

Test			Analysis					
Reference	Series	No.	A	B	C	D	E	F
Chinn et al.[55.1]		D17	1.294	1.294	1.294	1.294	1.294	1.301
		D19	0.919	0.919	0.919	0.919	0.919	0.921
		D20	0.914	0.914	0.914	0.914	0.914	0.908
		D21	0.795	0.795	0.795	0.795	0.795	0.795
		D22	1.033	1.033	1.033	1.033	1.033	1.029
		D23	1.183	1.183	1.183	1.183	1.183	1.190
		D24	0.972	0.961	0.912	0.912	0.912	0.924
		D25	1.044	1.044	1.044	1.044	1.044	1.048
		D26	1.236	1.236	1.236	1.236	1.236	1.251
		D29	0.991	0.991	0.991	0.991	0.991	0.988
		D30	0.941	0.941	0.941	0.941	0.941	0.941
		D31	1.109	1.109	1.109	1.109	1.109	1.107
		D32	0.829	0.829	0.829	0.829	0.829	0.828
		D33	0.924	0.924	0.924	0.924	0.924	0.925
		D34	1.045	1.045	1.045	1.045	1.045	1.042
		D35	1.149	1.149	1.149	1.149	1.149	1.155
		D36	1.153	1.153	1.153	1.153	1.153	1.156
		D38	0.790	0.790	0.790	0.790	0.790	0.788
		D39	0.875	0.875	0.875	0.875	0.875	0.872
		D40	1.146	1.136	1.147	1.147	1.147	1.062
Orr [76.1]		2	1.376	1.376	1.376	1.376	1.376	1.384
		3	1.243	1.243	1.243	1.243	1.243	1.246
		4	1.024	1.024	1.024	1.024	1.024	1.021
Reynolds & Beeby [82.3]		E1	0.837	0.832	0.716	0.716	0.716	0.712
		E2	0.904	0.880	0.880	0.880	0.880	0.882
		E5	0.913	0.898	0.775	0.775	0.775	0.783
Zekany et al. [81.1]		1T	0.785	0.785	0.785	0.785	0.785	0.784
		2B	0.970	0.970	0.970	0.970	0.970	0.969
		3T	0.840	0.840	0.840	0.840	0.840	0.840
		4B	0.972	0.972	0.972	0.972	0.972	0.972
		5B	1.215	1.215	1.215	1.215	1.215	1.215
		6T	0.987	0.987	0.987	0.987	0.987	0.986
		7T	0.995	0.995	0.995	0.995	0.995	0.994
		8B	1.272	1.272	1.272	1.272	1.272	1.271

Table C.2

Test			Analysis					
Reference	Series	No.	A	B	C	D	E	F
Zekany et al. [81.1]		9B	1.237	1.237	1.237	1.237	1.237	1.237
		10T	0.949	0.949	0.949	0.949	0.949	0.948
		11T	0.986	0.986	0.986	0.986	0.986	0.986
		12B	1.126	1.126	1.126	1.126	1.126	1.125
		13T	1.320	1.320	1.320	1.320	1.320	1.320
		14B	1.246	1.246	1.246	1.246	1.246	1.245
		15B	0.974	0.974	0.974	0.974	0.974	0.974
		16T	0.997	0.997	0.997	0.997	0.997	0.996
		17T	0.747	0.747	0.747	0.747	0.747	0.747
		18B	1.063	1.063	1.063	1.063	1.063	1.063
		19B	1.114	1.114	1.114	1.114	1.114	1.114
		20T	0.946	0.946	0.946	0.946	0.946	0.945
		21T	1.077	1.077	1.077	1.077	1.077	1.074
		22B	1.268	1.268	1.268	1.268	1.268	1.264
		23B	1.256	1.256	1.256	1.256	1.256	1.253
		24T	0.889	0.889	0.889	0.889	0.889	0.887
Ferguson & Breen [65.1]	8R	18a	0.964	0.964	0.964	0.964	0.964	0.966
		24a	1.187	1.187	1.187	1.187	1.187	1.197
		30a	1.078	1.078	1.078	1.078	1.078	1.093
	8F	36a	1.085	1.085	1.085	1.085	1.085	1.106
		36b	1.064	1.064	1.064	1.064	1.064	1.084
		39a	1.222	1.222	1.222	1.222	1.222	1.246
		42a	1.220	1.220	1.220	1.220	1.220	1.246
		42b	1.180	1.180	1.180	1.180	1.180	1.206
	8R	42a	1.160	1.160	1.160	1.160	1.160	1.184
		48a	1.177	1.177	1.177	1.177	1.177	1.207
		64a	1.137	1.137	1.137	1.137	1.137	1.174
		80a	1.043	1.043	1.043	1.043	1.043	1.084
	8F	36k	0.962	0.962	0.962	0.962	0.962	0.980
	11R	24a	1.142	1.142	1.142	1.142	1.142	1.156
		30a	1.234	1.230	1.207	1.207	1.207	1.232
		36a	1.076	1.076	1.076	1.076	1.076	1.101
		36b	1.166	1.166	1.166	1.166	1.166	1.193
		42a	1.109	1.109	1.109	1.109	1.109	1.140
		48a	1.261	1.261	1.261	1.261	1.261	1.300
		48b	1.194	1.194	1.194	1.194	1.194	1.229

Table C.2

Test			Analysis					
Reference	Series	No.	A	B	C	D	E	F
Ferguson & Breen [65.1]	11R	48a	1.073	1.073	1.073	1.073	1.073	1.106
		48b	1.108	1.108	1.108	1.108	1.108	1.135
	11F	60a	1.292	1.292	1.292	1.292	1.292	1.338
		60b	1.036	1.036	1.036	1.036	1.036	1.074
	11R	60a	1.298	1.298	1.298	1.298	1.298	1.347
		60b	1.201	1.201	1.201	1.201	1.201	1.242
	BF	30b	0.999	0.999	0.999	0.999	0.999	1.009
		36c	0.978	0.978	0.978	0.978	0.978	0.992
		36d	0.961	0.961	0.961	0.961	0.961	0.973
		36e	1.073	1.073	1.073	1.073	1.073	1.088
		36f	0.979	0.979	0.979	0.979	0.979	0.992
		36g	1.142	1.142	1.142	1.142	1.142	1.157
		36h	0.793	0.793	0.793	0.793	0.793	0.801
		36j	0.933	0.933	0.933	0.933	0.933	0.942
	11R	36a	1.110	1.110	1.110	1.110	1.110	1.123
Champerlin [58.1]		1a	0.662	0.662	0.662		0.662	
		1b	0.662	0.662	0.662		0.662	
		3a	0.944	0.944	0.944	0.944	0.944	0.939
		3b	0.950	0.950	0.950	0.950	0.950	0.945
		3c	0.962	0.962	0.962	0.962	0.962	0.957
		2a	0.744	0.745	0.718		0.718	
		2b	0.779	0.779	0.751		0.751	
		4a	0.770	0.770	0.770	0.770	0.770	0.767
		4b	0.792	0.792	0.792	0.792	0.792	0.789
		4c	0.785	0.785	0.785	0.785	0.785	0.782
Ferguson & Krishnaswarny [71.1]	SP	32	1.427	1.424	1.075	1.075	1.075	1.118
		33	1.637	1.607	1.218	1.218	1.218	1.288
		34	1.619	1.610	1.100	1.100	1.100	1.142
		35	0.900	0.879	0.647	0.647	0.647	0.650
		36	1.050	1.028	0.927	0.927	0.927	0.933
		37	1.531	1.531	1.531	1.531	1.531	1.550
		38	1.368	1.368	1.368	1.368	1.368	1.374
		39	1.325	1.325	1.325	1.325	1.325	1.337

Table C.2

Test			Analysis					
Reference	Series	No.	A	B	C	D	E	F
Ferguson & Krishnaswarny [71.1]	14S	1	1.292	1.292	1.292	1.292	1.292	1.303
		2	1.042	1.042	1.042	1.042	1.042	1.050
		3	0.903	0.903	0.903	0.903	0.903	0.904
		4					0.963	0.964
		6					0.973	0.976
	18S	12	1.278	1.278	1.278	1.278	1.278	1.290
		15	1.136	1.136	1.136	1.136	1.136	1.156
		1	1.337	1.337	1.337	1.337	1.337	1.349
		4	0.947	0.947	0.947	0.947	0.947	0.951
		2	1.173	1.173	1.173	1.173	1.173	1.180
		3	1.141	1.141	1.141	1.141	1.141	1.154
		9					0.964	0.967
		13					0.935	0.937
	SP	40	1.278	1.278	1.278	1.278	1.278	1.288
Ferguson & Briceno [69.1]		1	0.971	0.971	0.971	0.971	0.971	0.978
		5	1.366	1.366	1.366	1.366	1.366	1.375
		7	1.215	1.215	1.215	1.215	1.215	1.220
		12	1.362	1.362	1.362	1.362	1.362	1.376
		13	1.409	1.409	1.409	1.409	1.409	1.421
		14	1.156	1.156	1.156	1.156	1.156	1.163
		15	1.445	1.445	1.445	1.445	1.445	1.465
		16	1.263	1.263	1.263	1.263	1.263	1.268
		17	1.247	1.247	1.247	1.247	1.247	1.263
		21	1.014	1.014	1.014	1.014	1.014	1.020
		22	1.539	1.539	1.539	1.539	1.539	1.559
		23	1.003	1.003	1.003	1.003	1.003	1.017
		24	1.209	1.209	1.209	1.209	1.209	1.214
		25	1.348	1.348	1.348	1.348	1.348	1.350
		26	1.232	1.232	1.232	1.232	1.232	1.234
		27	1.216	1.216	1.216	1.216	1.216	1.220
		1a	1.120	1.120	1.120	1.120	1.120	1.128
		2a	1.230	1.230	1.230	1.230	1.230	1.237
		4a	1.223	1.223	1.223	1.223	1.223	1.225

Table C.2

Test			Analysis					
Reference	Series	No.	A	B	C	D	E	F
Thompson et al. [79.4]		1	1.097	1.097	1.097	1.097	1.097	1.093
		2	1.053	1.053	1.053	1.053	1.053	1.048
		7	1.299	1.299	1.299	1.299	1.299	1.303
		12	1.316	1.316	1.316	1.316	1.316	1.335
		13	1.355	1.355	1.355	1.355	1.355	1.359
		14	1.334	1.334	1.334	1.334	1.334	1.340
		16	1.107	1.107	1.107	1.107	1.107	1.110
		20					0.996	0.995
		22	1.348	1.348	1.348	1.348	1.348	1.362
		23	1.474	1.474	1.474	1.474	1.474	1.492
Mean value			1.041	1.036	1.004	1.017	0.993	1.020
Standard deviation			0.215	0.209	0.198	0.184	0.200	0.198
Number of tests			334	334	334	310	357	333

Table C.2: *Results from various analyses on lap splices.*

Appendix D

Rib Parameters for Reinforcement

In the following table D.1 values for the rib parameters D and F, expression (4.6) and (4.12), respectively, are given for various types of reinforcement. Because information about the width of the ribs, u in figure 4.1, has not been available in all cases this parameter is not included in D and F. Instead a is taken as the distance from midd rib to the midd of the next rib. D is then correct, while F is less than with u.

The values for a and h_d for the Halmstad steel are max and min values, respectively. Hence the values for D and F are as small as possible. In contradistinction to the other steel types the two rib parameters for the Halmstad steel are determined using the real diameter and not the nominal.

Photos have been used to find the values for the rib parameters for Tepfers[73.1] reinforcement. The ASTM A615 is minimum requirements as with the Halmstad steel. The measurements for d, a and h_d are in inches. However the values for the nominal diameter are also shown in mm.

As can be observed in the table the value will in practice be larger than 0.03 for D and 0.5 for F, when u is taken as zero. These values can probably be used in practice as conservative estimations for the parameters if it is not possible to determinate the actual values.

Reference	Type	diameter d		a	h_d	D	F	$\frac{F}{D}$
		nominal	real					
		[mm]	[mm]	[mm]	[mm]			
Halmstad steel	Ks410S	6	5.6	4.9	0.40	0.044	0.57	13.0
		8	7.5	5.9	0.50	0.045	0.57	12.5
		10	9.5	6.5	0.60	0.049	0.56	11.5
		12	11.4	7.8	0.75	0.051	0.57	11.0
		14	13.4	8.8	0.90	0.055	0.57	10.4
		16	15.4	10.0	1.00	0.053	0.57	10.6
		20	19.2	12.0	1.30	0.058	0.57	9.8
		25	24.0	15.0	1.60	0.057	0.57	10.0
		32	30.8	21.0	2.00	0.051	0.57	11.1
	Ks550	8	7.6	5.0	0.56	0.060	0.57	9.5
		10	9.6	5.0	0.60	0.064	0.56	8.8
		12	11.5	6.0	0.72	0.064	0.56	8.8
		14	13.5	7.0	0.84	0.064	0.56	8.8
		16	15.4	8.0	0.96	0.064	0.56	8.8
		18	17.4	9.0	1.08	0.064	0.56	8.8
		20	19.4	10.0	1.20	0.064	0.56	8.8
		25	24.3	12.5	1.50	0.064	0.56	8.8
Tepfers [73.1]	Ks42	10		5.5	0.5	0.048	0.55	11.5
		16		7.9	1.0	0.067	0.56	8.4
	Ks40	8		6.5	0.4	0.032	0.55	17.0
		10		7.7	0.6	0.041	0.56	13.6
		12		8.0	0.9	0.060	0.58	9.5
		16		9.6	1.0	0.055	0.56	10.2
		19		14.5	1.25	0.046	0.57	12.3
		25		18.3	1.7	0.050	0.57	11.5
		32		23.2	3.4	0.081	0.61	7.5
	Ks60	8		5.2	0.7	0.073	0.59	8.0
		10		5.9	0.8	0.073	0.58	7.9
		12		4.9	0.8	0.087	0.57	6.5
		16		6.0	1.0	0.089	0.56	6.4
		19		8.5	1.25	0.078	0.57	7.2
		25		11.7	1.6	0.073	0.56	7.8
	Ks90	16		6.0	1.0	0.089	0.56	6.4
Jensen[82.1]	Ks900	16		8.5	1.1	0.069	0.57	8.2
Rathkjen[72.1]	Kam steel	10		8.0	0.9	0.061	0.59	9.6
		14		10.5	1.2	0.062	0.59	9.4
	Tentor	10		8.5	0.6	0.038	0.56	14.7
		14		11.1	0.9	0.044	0.56	13.0

Reference	Type	diameter d		a	h_d	D	F	$\frac{F}{D}$
		nominal [in]	nominal [mm]	[in]	[in]			
ASTM A615	# 3	0.375	9.5	0.262	0.015	0.030	0.54	18.1
	# 4	0.500	12.7	0.350	0.020	0.030	0.54	18.2
	# 5	0.625	15.9	0.437	0.028	0.033	0.55	16.3
	# 6	0.750	19.1	0.525	0.038	0.038	0.55	14.5
	# 7	0.875	22.2	0.612	0.044	0.038	0.55	14.6
	# 8	1.000	25.4	0.700	0.050	0.037	0.55	14.7
	# 9	1.128	28.7	0.790	0.056	0.037	0.55	14.8
	# 10	1.270	32.3	0.889	0.064	0.038	0.55	14.6
	# 11	1.410	35.8	0.937	0.071	0.038	0.55	14.6
	# 14	1.693	43.0	1.185	0.085	0.038	0.55	14.6
	# 18	2.257	57.3	1.580	0.102	0.034	0.55	14.2

Table D.1: *Values for the rib parameters for various types of reinforcement.*

AFDELINGEN FOR BÆRENDE KONSTRUKTIONER
DANMARKS TEKNISKE HØJSKOLE

Department of Structural Engineering
Technical University of Denmark, DK-2800 Lyngby

SERIE R
(Tidligere: Rapporter)

R 185. NITTEGAARD-NIELSEN, PETER: Elementmetodebaserede bereg-
ningsmodeller for dæmpede konstruktionssvingninger. 1984.
R 186. DAMKILDE, LARS: Beregning af plader af elastisk-plastisk
materiale ved hjælp af elementmetoden. 1984.
R 187. DAMKILDE, LARS: Stability of Plates of Elastic-plastic
Material. 1984.
R 188. NITTEGAARD-NIELSEN, PETER: Elementmetodebaseret bereg-
ningsmodel for dæmpede svingninger i 3-fase kontinuum:
matrixmateriale - væske - luft. 1984.
R 189. Resuméoversigt 1983 - Summaries of Papers 1983. 1984.
R 190. JULIUS SOLNES: Vibration of Suspension Bridges under
Earthquake Loads. 1984.
R 191. MUNCH-ANDERSEN og V. ASKEGAARD: Results from Tests with
Normal and Shear Strees Cells in Medium-Scale Model Silo.
1984.
R 192. DITLEVSEN, OVE: Probabilistic Thinking: An Imperative
in Engineering Modelling. 1984.
R 193. STANG, HENRIK: En Kompositmaterialeteori og dens Anven-
delse til Beskrivelse af Trækpåvirkede Cementkompositter.
1984.
R 194. ARPE, ROBERT: Broers Dynamiske Respons på Trafiklast.
Del 1. Teori. 1984. (Udsolgt), (Out of print).
R 195. ARPE, ROBERT: Broers Dynamiske Respons på Trafiklast.
Del 2. Modelforsøg. 1984.
R 196. GERSTOFT, PETER: Simplified Methods for Dynamic Analysis
of a Guyed Mast. 1984. (Udsolgt), (Out of print).
R 197. DYRBYE, C.: Simulation of Earthquake Ground Motion on a
Microcomputer. 1985.
R 198. ABK Informationsdag 1985.
R 199. RASMUSSEN, KIM: Elastic-Plastic Buckling of Long Plates
in Compression. 1985.
R 200. STANG, HENRIK: Dimensionering af limede konstruktive
samlinger: En litteraturoversigt. 1985.
R 201. Resuméoversigt 1984 - Summaries of Papers 1984. 1985.
R 202. GIMSING, N.J.: Means of Improving the Deformational
Characteristics of Cable Supported Bridges. 1985.
R 203. SOBCZYK, KAZIMIERZ: Stochastic Differential Equations
for Applications. 1985.
R 204. STANG, HENRIK: The Fibre Pull-out Problem; An Analytical
Investigation. 1985.
R 205. STANG, HENRIK: The Fibre Pull-out Problem; An Experi-
mental Investigation. 1985.
R 206. STANG, HENRIK OG RUNE BRINCKER: Udmattelsesforsøg med
limsamlinger mellem stål og glasfiberlaminater. Små
prøver. 1985.
R 207. GOLTERMANN, PER: Samvirken imellem lokal og global sta-
bilitet i tyndvæggede bjælker. 1985.
R 208. MØLLMANN, H.: Theory of Thin-Walled Elastic Beams with
Finite Displacements. 1985.
R 209. HAAHR, HENRIK: Materialeafhængig Stabilitetsopførsel af
Simple Søjler. 1986.
R 210. RIBERHOLT, H.: Glued Bolts in Glulam. 1986.
R 211. Resumeoversigt 1985 - Summaries of Papers 1985. 1986.
R 212. ANDREASEN, BENT og M.P. NIELSEN: Dome Effect in
Reinforced Concrete Slabs. 1986.

R 213. GERSTOFT, PETER: An Assessment of Wind Loading on Tower Shaped Structures. 1986.

R 214. GIMSING, N.J.: Recent and Future Developments of Cable Supported Bridges. 1986.

R 215. LANGE-HANSEN, P.: A Hybrid Upper Bound Theorem for the Limit Load in the Theory of Plasticity. 1986.

R 216. MAGNUSSON, GYLFI: Simulation Algorithms. 1987.

R 217. Resumeoversigt 1986 – Summaries of Papers 1986. 1987.

R 218. DYRBYE, C. Harmonic Vibrations of Plane Frames. 1987.

R 219. WINTERSTEIN, STEVEN R.: Moment-based Hermite Models of Random Vibration. 1987.

R 220. DØSSING, JENS: Stempelproblemer vedrørende cirkulær cylindriske skaller. 1987.

R 221. DØSSING, JENS: Deformerbare dækknudepunkter i offshore stålkonstruktioner. 1987.

R 222. RIBERHOLT, H.: De mekaniske egenskaber af plader oplimet af birkefiner. 1987.

R 223. NIELSEN, LEIF OTTO: Forskydningsspændinger i homogene bjælketværsnit af symmetrisk materiale. 1987.

R 224. LANGE-HANSEN, P. OG SØREN MØLLER NIELSEN: An Improved Upper Bound on the Residual Deflections in Elastic-Plastic Structures Subject to Variable Loading. 1988.

R 225. THORUP, ERIK: User Guide and Documentation on the Program Fatsys (ver.3.0). 1987.

R 226. DITLEVSEN, OVE: Uncertainty and Structural Reliability. Hocus Pocus or Objective Modelling. 1988.

R 227. Resumeoversigt 1987 – Summaries of Papers 1987. 1988.

R 228. RIBERHOLT, H.: Glued Bolts in Glulam. Part 2. 1988.

R 229. RIBERHOLT, H.: Delamineringsprøvning. 1988.

R 230. RIBERHOLT, H.: Woodflanges under tension, 1988.

R 231. HOLKMANN OLSEN, N.: Implementation. 1988.(public. pending

R 232. HOLKMANN OLSEN, N.: Uniaxial. 1988. (public. pending)

R 233. HOLKMANN OLSEN, N.: Anchorage. 1988. " "

R 234. HOLKMANN OLSEN, N.: Heat Induced. 1988. " "

R 235. SCHEEL, HELLE: Rotationskapacitet. 1988." "

R 236. NIELSEN, MONA: Arbejdslinier. 1988. " "

R 237. GANWEI, CHEN: Plastic Analysis of Shear in Beams. Deep Beams and Corbels. 1988.

R 238. ANDREASEN, BENT STEEN: Anchorage of Deformed Reinforcing bars. 1988. (public. pending)

R 239. ANDREASEN, BENT STEEN: Anchorage Tests with Deformed Reinforcing Bars in more than one layer at a Beam Support. 1988. (public. pending)

R 240. GIMSING, N.J.: Cable-Stayed Bridges with Ultra Long Spans. 1988.

R 241. NIELSEN, LEIF OTTO: En Reissner-Mindlin Plade Element Familie. 1989

R 242. KRENK, STEEN og THORUP, ERIK: Stochastic and Concrete Amplitude Fatigue Test of Plate Specimens with a Central Hole. 1989.

R 243. AARKROG, P., THORUP, E., KRENK, S., AGERSKOV, H. and BJØRNBAK-HANSEN, J.: Apparatur til Udmattelsesforsøg. 1989.

R 244. DITLEVSEN, OVE and KRENK, STEEN: Research Workshop on Stochastic Mechanics, September 13-14, 1988.

R 245. ROBERTS, J.B.: Averaging Methods in Random Vibration. 1989.

R 246. Resumeoversigt 1988 – Summaries of Papers 1988. 1989.

Hvis De ikke allerede modtager Afdelingens resumeoversigt ved
udgivelsen, kan Afdelingen tilbyde at tilsende næste års resu-
meoversigt, når den udgives, dersom De udfylder og returnerer
nedenstående kupon.

Returneres til
Afdelingen for Bærende Konstruktioner
Danmarks tekniske Højskole
Bygning 118
2800   Lyngby

Fremtidig tilsendelse af resumeoversigter udbedes af
(bedes udfyldt med blokbogstaver):

Stilling og navn: ....

Adresse: ....

Postnr. og -distrikt: ....

The Department has pleasure in offering to send you a next year's
list of summaries, free of charge. If you do not already receive
it upon publication, kindly complete and return the coupon
below.

To be returned to:
Department of Structural Engineering
Technical University of Denmark
Building 118
DK-2800 Lyngby, Denmark.

The undersigned wishes to receive the Department's
List of Summaries:
(Please complete in block letters)

Title and name ....

Address..

Postal No. and district..............................

Country..